Right-handed Neutrino Production at Finite Temperatures

Radiative Corrections, Soft and Collinear Divergences

Dissertation

by

Frank Glowna

Theoretical Physics of the Early Universe
Physik-Department T70
Technische Universität München

May 2015

Physik-Department der Technischen Universität München

Theoretische Physik des frühen Universums

Right-handed Neutrino Production at Finite Temperatures

Radiative Corrections, Soft and Collinear Divergences

Frank Glowna

Acknowledgments

Contents

Introduction

The study of the fundamental laws of nature and their contribution to the development of the universe is one of the most fascinating chapters of today's basic research in physics. The discovery of the Higgs particle at CERN [1, 2] confirms the Standard Model of particle physics (SM) impressively and with great detail, but it does not explain all particle phenomena. Among these are several observed phenomena that definitely involve physics beyond the SM (BSM):

Based on the standard model of cosmology and according to the results from the Planck mission [3] the known universe contains only 4.9% of ordinary matter. A huge part of the remainder is so-called *dark matter* (DM). Since it is "dark", it does not interact directly, or only very weakly, with the visible sector, but it has huge effects due to gravity. This phenomenon is related to particle physics as it seems difficult to explain these observations on vastly different scales by modifications of gravity.

Extensions of the SM are also motivated by experiments which show *neutrino flavor oscillations*. Due to gauge invariance, the SM neutrinos have to be massless at the renormalizable level and hence the flavor number should be a conserved quantity. This means the observed oscillations indicate that the neutrinos have a mass, and therefore directly relate to new physics beyond the SM.

A third phenomenon, and probably one of the most important open questions in particle physics and cosmology, is the origin of the *baryon asymmetry of the universe* (BAU). The BAU describes the present excess of matter over anti-matter and can be expressed as the baryon-to-photon ratio $\frac{n_B}{n_\gamma} \approx 6 \cdot 10^{-10}$ [4–8]. Theories that explain this excess are collectively called Baryogenesis. Of course the boring answer could be that the universe has always been baryon asymmetric. But, due to symmetry reasons from a theoretical point of view, and also since there is no evidence of large scale detections for the opposite, it is widely believed that the primordial universe was baryon symmetric. See for example [9] for a review.

Sakharov stated three minimal conditions that need to be fulfilled for a successful Baryogenesis in his article [10] from 1967. Those are B violation, C-symmetry and CP-symmetry violation, and interactions out of thermal equilibrium. The first Sakharov condition is mandatory: B is the number of baryons minus anti-baryons, which, if conserved, does not allow for dynamic generation of the baryon asymmetry. C and CP are the charge and charge-parity symmetry, respectively. If C is conserved, for every B violating process a charge conjugated one would exist. Likewise, if CP is conserved, every number of left- and right-handed baryons has to be equal to the number of right- and left-handed anti-baryons such that in total no baryon asymmetry could be generated. The last statement, i.e. thermal non-equilibrium, is necessary for breaking T symmetry. Assuming that B or L-number violating processes are present, the CPT theorem otherwise implies that there are no asymmetries in thermal equilibrium. L is the lepton number.

In the past, Baryogenesis was only thought to be possible by the CP violating decay of some heavy particles of grand unified theories (GUTs). Later, the discovery of sphaleron processes in the SM put GUT particle baryogenesis under pressure. Sphalerons conserve the value $B - L$ but violate $B + L$ [11]. Hence, any primordial baryon asymmetry would have been washed out at the time of electroweak symmetry breaking. Later on, in the year 1986, Fukugita and Yanagida suggested that an asymmetry generated in the leptonic sector could also be converted into a baryon asymmetry by those sphaleron processes [12] and hence explain the BAU without requiring GUT theories. This was the birth of Leptogenesis. See for example [13–15] for recent reviews. In terms of Sakharov conditions, B violation would be realized by the sphaleron process, and C and CP violation are in principle already included in the SM. However, the SM's CP-violating Cabibbo-Kobayashi-Maskawa (CKM) and Dirac phases are much too small to explain the BAU. Particle processes

out of equilibrium were also available in several stages of the early universe, but predicted deviations from thermal equilibrium are too small.

To generate the BAU from a lepton asymmetry, which is converted into a baryon asymmetry via sphaleron processes, models of Leptogenesis have to take place at temperatures above, and typically far above, the electroweak scale. At this stage, the universe cannot simply be described as a weakly interacting dilute plasma. To derive the lepton asymmetry, the time evolution of particle distribution functions has to be considered. However, due to the primordial plasma, it is questionable whether those should be done by semiclassical Boltzmann equations. Therefore, substantial progress was made in the theoretical description of Non-Equilibrium Quantum Field Theory (NEQFT) related to the Closed-Time-Path (CTP) formalism [16–19]. Within the CTP, the time evolution of particle distribution functions can be derived from the Kadanoff-Baym equations, which are related to Boltzmann, Quantum-Boltzmann and Langevin equations [20–28]. Regarding Leptogenesis, particular progress was also made in calculating thermal corrections to the *CP* asymmetry [29–35] and other related questions [36–44].

This thesis contributes on a possible Leptogenesis scenario. Like in most other Leptogenesis models, the SM is extended by a number of right-handed neutrinos (RHN) with Majorana masses. This extension is particularly attractive to the physics community, since the active neutrinos in the SM only come with left-handed chirality. Furthermore, they are the only SM fermions that do not have a right-handed partner. See [45] for a nice review on the phenomenology of RHN. In this framework, the SM neutrinos acquire small masses from mixing through the seesaw mechanism [46–50]. By adding this partner, the resulting theory may also be embedded in a Grand Unified Theory (GUT) such as $SO(10)$ [51–53]. Under restriction to a renormalizable theory, the RHN only interact with the weak sector through Yukawa interactions. Therefore, a possible keV mass right-handed neutrino may provide a natural DM candidate [54, 55]. However, though their masses are in principle unknown and can range between zero and the GUT scale, there are exclusion windows [56]. Hence, the RHN may be able to explain the above questions all at once.

If those neutrinos exist, a lepton asymmetry is most likely generated by out-of-equilibrium decays of heavy RHNs into Higgs bosons and leptons. This is the leading order (*LO*) dominant process in the non-relativistic (NR) limit, i.e. in case the RHNs have masses much larger than the actual temperature at which the decay happens. However, if the RHNs have a mass comparable to the temperature or even smaller up to the ultra-relativistic (UR) limit, the above *LO* process is kinematically suppressed, and radiative corrections become relevant for Leptogenesis. Hence, for a complete calculation of these interactions, ranging from the NR to the UR limit, next-to-leading order effects (*NLO*) must be considered too. The radiative corrections through massless particle exchanges are afflicted by soft and collinear divergences. Recently, those are studied in the NR limit [57, 58], and first calculations regarding RHN production in the UR limit have been performed [59, 60]. In other papers [43, 61–63] radiative corrections have been included by means of modified dispersion relations, i.e. thermal masses. However, those capture only partly the *NLO* effects. Hence, a *NLO* calculation of the RHN production rate is not available in the full range from the non- to the ultra-relativistic limit, so far.[1] This is important in the weak washout regime, in resonant leptogenesis and in ARS-type scenarios, for instance. Related to the issue of the RHN production is the lepton flavor equilibration rate [65–67] and the production of photons in the quark gluon plasma (QGP) [68, 69]. The lepton flavor equilibration rate determines the temperature at which flavor effects become important for calculations of the lepton asymmetry.

The present investigation deals with the production rate of massive and massless RHNs. Based on the two-particle-irreducible (2PI) formulation of the Schwinger-Keldysh or Closed-Time-Path formalism, tools are derived to analytically and numerically calculate thermal production rates and transport coefficients in non-equilibrium QFT. This has the advantage of being a first principle approach that does not rely on semiclassical approximations, and directly providing the correct description of the physical screening in the thermal plasma in terms of resummed propagators. The screening regulates certain divergences that

---

[1] Very recently, [64] contributed on the relativistic regime.

may appear in tree-level scattering diagrams. In this work, the out-of-thermal-equilibrium right-handed neutrinos are described in a thermal equilibrated bath of the other particles. Their differential and total production rate is calculated within several approximations and limits, and are compared to the literature. However, two inconsistencies are found in those calculations that are at least not explained by other authors. The first one appears when "naively" resumming the Higgs self-energy, and a workaround is provided in this thesis. The second inconsistency describes an effect, where actually suppressed processes of nearly massless particles is enhanced by the Bose-Einstein distribution. This enhancement, that appears in perturbative calculations, prohibits the congruence of massless contributions with nearly massless contributions to the RHN production rate.[2]

Outline

The introductory Chapter 1 provides a brief overview of the Schwinger-Keldysh formalism. It explains how the Closed-Time-Path emerges in the path integral formulation of NEQFT, and how the Kadanoff-Baym equations are derived in the 2PI approach. After introducing the Wigner Space and the Gradient Expansion, the tree-level and resummed variants of several 2-point functions are shown and various associated relations are summarized.

In the 2$^{\text{nd}}$ chapter, the SM extension by means of the RHN and the corresponding Feynman rules are shown. The following section discusses renormalization matters in thermal field theory. Afterwards, a method is introduced to easily provide boundary conditions for massive and massless loop integrals. These integrals possibly cannot be solved in dimensional regularization due to the particle distribution functions. The method is exemplified by an analytical calculation of a generic spectral function in thermal equilibrium using tree-level functions. At the end of Chapter 2, the Higgs and lepton self-energies are obtained.

Chapter 3 is devoted to the production rate of the RHN. First the quantum evolution equation for the particle distributions of RHNs is derived. In Section 3.3, the *LO* differential production rate for RHNs in the NR limit is obtained. Section 3.4 addresses the case of massless neutrinos in the UR limit. Furthermore, the *LO* rate is derived within perturbative approximations, but also using resummed Higgs and lepton propagators. Existing results are thereby verified. Section 3.5 concerns the production rate in the intermediate regime between the UR and NR limit, using again the perturbative and resummed methods. The non-relativistic expansion coefficients are derived and fitted to the numerical results at the end of this section.

The considerations used to obtain precise numerical results are described in Chapter 4.

Chapter 5 of this dissertation summarizes the results and provides an outlook to possible further work.

---

[2] Very recently, a similar issue was described in [70].

Conventions

In this thesis, the following conventions are used.

- Planck's constant and the speed of light are set to $\hbar = c = 1$ in natural units.

- The Minkowski metric is fixed by $g_{\mu\nu} = \mathrm{diag}(1, -1, -1, -1)$.

- If not stated otherwise, k^2 always means $k_\mu k^\mu$ for any 4-vector k. Likewise, k^4 is the same as $(k^2)^2$. However, k^0 should be regarded as the zeroth component of k.

- The plasma 4-vector is called u with normalization $u^2 = 1$ and positive u^0. The temperature $T = \beta^{-1}$ is part of the definition of the particle distribution function $f(u \cdot p)$.

- If not stated otherwise, the integrals $\int \mathrm{d}k^0$, $\mathrm{d}|\vec{k}|$ and $\mathrm{d}\cos\angle$ always run from $-\infty \ldots \infty$, $0 \ldots \infty$ and $-1 \ldots 1$, respectively.

1

Schwinger-Keldysh Formalism

The In-Out formalism is the usual method to describe scattering problems in QFT. It is designed to compute S-matrix elements for processes that consider free particles coming in from the infinite past and going out to the infinite future. At some time scale, these particles are thought to "see" each other and hence interact by adiabatically switching on and off their interactions. Adiabatically in this sense means that the initial state vector in the infinite past should be the same as the outgoing state vector in the infinite future. In contrast, this work studies particle production in the early universe at finite density, where not all particles necessarily have to be in equilibrium. Hence, the initial state may be out of equilibrium while the outgoing state should approach equilibrium at some time. For this purpose Schwinger first suggested a framework [16], that was further developed by Keldysh and others [17–19]. This so called Schwinger-Keldysh or In-In formalism is an extension of the In-Out formalism that describes particle production, the energy density, the particle number density and more, in time developing the density matrix of a quantum system from an initial state at time t_i to final time t_f. In the following section, only the main difference of this formalism to the In-Out formalism, the Closed-Time-Path, is derived.

1.1 Closed-Time-Path

The density matrix $\hat{\rho}$ has the physical interpretation of a probability p_n for finding the quantum mechanical system in a state $|\psi_n\rangle$

$$\hat{\rho}(t) = \sum_n p_n |\psi_n(t)\rangle\langle\psi_n(t)|. \tag{1.1}$$

Even if Equation (1.1) is highly compact, p_n is a probability and satisfies

$$\sum_n p_n = 1. \tag{1.2}$$

In quantum mechanics, any observable quantity O is related to an operator $\hat{O}$ in the Heisenberg picture through its expectation value

$$\langle O \rangle = \text{Tr}[\hat{\rho}\,\hat{O}]. \tag{1.3}$$

Equation (1.3) involves the tracing of quantum degrees of freedom, i.e. fluctuations, and statistical degrees of freedom. In QFT, the trace is realized by integrating over all fields at time t at all spatial points[3]. The

---

[3] The spatial dependences are suppressed.

normalization constant $\mathcal{N}$ is absorbed into the definition of the integration measure such that $\langle 1 \rangle = 1$:

$$\langle O(t) \rangle = \int \mathcal{D}\psi_{[t,t]} \langle \psi(t) | \hat{\rho}(t) \hat{O}(t) | \psi(t) \rangle. \tag{1.4}$$

Here, the subscript at the integration measure $\mathcal{D}\psi$ provides the integral support in terms of a closed interval of time slices. This means that modulo the normalization constant, $\mathcal{D}\psi_C$ means

$$\mathcal{D}\psi_C = \prod_{t \in C} \prod_{\forall \vec{x}} \mathrm{d}\psi(t, \vec{x}). \tag{1.5}$$

If the density matrix is only known at some initial time t_i, expectation values can still be evaluated at t by time evolving the corresponding states ($t > t_i$):

$$|\psi(t)\rangle = U(t, t_i)|\psi(t_i)\rangle = U^{\dagger}(t_i, t)|\psi(t_i)\rangle = e^{-i\hat{H}(t-t_i-i\varepsilon)}|\psi(t_i)\rangle \tag{1.6}$$

$$= \int \mathcal{D}\tilde{\psi}_{[t_i,t]} |\tilde{\psi}(t)\rangle e^{i \int_{t_i}^{t} \mathrm{d}x^4 \mathcal{L}(\tilde{\psi}, \dot{\tilde{\psi}}; x)} \underbrace{\langle \tilde{\psi}(t_i) | \psi(t_i) \rangle}_{\prod_{\vec{y}} \delta(\tilde{\psi}(t_i, \vec{y}) - \psi(t_i, \vec{y})) \equiv \delta(\tilde{\psi}(t_i) - \psi(t_i))}. \tag{1.7}$$

The infinitesimal positive ε guaranties the convergence of the time evolution and is absorbed into the time arguments. In this way, one obtains

$$\langle O(t) \rangle = \int \mathcal{D}\psi_{[t_i,t_i]} \langle \psi(t_i) | \hat{\rho}(t_i) U(t_i, t) \hat{O}(t) U(t, t_i) | \psi(t_i) \rangle. \tag{1.8}$$

Note that the state vectors can be evolved to any time t_f as long as the time of measurement t is between t_i and t_f:

$$\langle O(t) \rangle = \int \mathcal{D}\psi_{[t_i,t_i]} \langle \psi(t_i) | \hat{\rho}(t_i) U(t_i, t_f) U(t_f, t) \hat{O}(t) U(t, t_i) | \psi(t_i) \rangle \tag{1.9}$$

$$= \int \mathcal{D}\psi_{[t_i,t_i]} \mathcal{D}\psi^{+}_{[t_i,t]} \langle \psi(t_i) | \hat{\rho}(t_i) U(t_i, t_f) U(t_f, t) \underbrace{\hat{O}(t) | \psi^{+}(t) \rangle}_{|\psi^{+}(t)\rangle O^{+}(t)}$$

$$e^{i \int_{t_i}^{t} \mathrm{d}x^4 \mathcal{L}(\psi^{+}, \dot{\psi}^{+}; x)} \delta\left(\psi^{+}(t_i) - \psi(t_i)\right) \tag{1.10}$$

$$= \int \mathcal{D}\psi_{[t_i,t_i]} \mathcal{D}\psi^{+}_{[t_i,t]} \mathcal{D}\tilde{\psi}^{+}_{[t,t_f]} \mathcal{D}\psi^{-}_{[t_i,t_f]} \langle \psi(t_i) | \hat{\rho}(t_i) | \psi^{-}(t_i) \rangle$$

$$e^{i \int_{t_f}^{t_i} \mathrm{d}x^4 \mathcal{L}(\psi^{-}, \dot{\psi}^{-}; x)} \delta\left(\psi^{-}(t_f) - \tilde{\psi}^{+}(t_f)\right) e^{i \int_{t}^{t_f} \mathrm{d}x^4 \mathcal{L}(\tilde{\psi}^{+}, \dot{\tilde{\psi}}^{+}; x)} \delta\left(\tilde{\psi}^{+}(t) - \psi^{+}(t)\right)$$

$$O^{+}(t) e^{i \int_{t_i}^{t} \mathrm{d}x^4 \mathcal{L}(\psi^{+}, \dot{\psi}^{+}; x)} \delta\left(\psi^{+}(t_i) - \psi(t_i)\right). \tag{1.11}$$

The tilde, plus and minus indices have no real meaning, except to separate the different field variables. After integrating out the deltas, the tilde can be dropped and only plus and minus fields are considered. Consequently, $\langle O(t) \rangle$ is expressed as

$$\langle O(t) \rangle = \int \mathcal{D}\psi^{+}_{[t_i,t_f]} \mathcal{D}\psi^{-}_{[t_i,t_f]} \langle \psi^{+}(t_i) | \hat{\rho}(t_i) | \psi^{-}(t_i) \rangle \delta\left(\psi^{-}(t_f) - \psi^{+}(t_f)\right)$$

$$O^{+}(t) e^{i \int_{t_f}^{t_i} \mathrm{d}x^4 \mathcal{L}(\psi^{-}, \dot{\psi}^{-}; x)} e^{i \int_{t_i}^{t_f} \mathrm{d}x^4 \mathcal{L}(\psi^{+}, \dot{\psi}^{+}; x)}, \tag{1.12}$$

which describes the expectation value of $\hat{O}(t)$ measured by the state $|\psi^{+}(t)\rangle$ in a system prepared at t_i by $\hat{\rho}$. The term

$$\int \mathcal{D}\psi^{+}_{[t_i,t_i]} \mathcal{D}\psi^{-}_{[t_i,t_i]} \langle \psi^{+}(t_i) | \hat{\rho}(t_i) | \psi^{-}(t_i) \rangle \tag{1.13}$$

describes the initial ensemble average. Due to the infinitesimal imaginary part of the time arguments, the $+$ and $-$ fields can be regarded as one field living on $t + i\varepsilon$ and on $t - i\varepsilon$. The time contours can be combined into one contour $C \equiv C_+ \oplus C_-$ called the CTP or Closed-Time-Path contour as sketched in Figure 1.1.
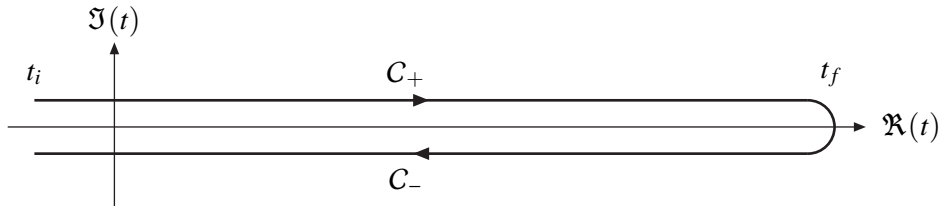
Figure 1.1: CTP contour in the complex t plane.

Then, Equation (1.12) can be written even more compactly. However, first, the general observable $\hat{O}$ must be substituted by time-ordered n-point Green-functions. After removing $\hat{O}$ in (1.4) and adding the current term $i \int_{t_i}^{t_f} \mathrm{d}^4 x J(x)\psi(x)$ to the Lagrangian, the generating functional $\ln Z[J^\pm]$ for time-ordered correlation functions is obtained. Here, time-ordering is meant to be the path-ordering along the CTP. The derivative of $\ln Z[J^\pm]$ with respect to the sources can be written as

$$\langle \mathcal{T}_C \psi(t_1) \dots \psi(t_n) \rangle = \int \mathcal{D}\psi_C \langle \psi^+(t_i)|\hat{\rho}(t_i)|\psi^-(t_i)\rangle \psi^{a_1}(t_1) \dots \psi^{a_n}(t_n) e^{i \int_{t_i}^{t_f} \mathrm{d}x^4 \mathcal{L}(\psi_C, \dot{\psi}_C; x)} . \tag{1.14}$$

$\mathcal{L}(\psi_C, \dots)$ is the short form for $\mathcal{L}(\psi^+, \dots) - \mathcal{L}(\psi^-, \dots)$, and the a_1 to a_n are the CTP indices $\pm$.
The following part focuses on the density matrix. This can be parametrized as

$$\langle \psi^+(t_i)|\hat{\rho}(t_i)|\psi^-(t_i)\rangle = \mathcal{N}_\rho e^{if[\psi_C]} \tag{1.15}$$

with

$$f[\psi_C] = \sum_{n=0}^{\infty} \int_{t_i}^{t_f} \mathrm{d}^4 x_1 \dots \mathrm{d}^4 x_n \sum_{a_1,\dots,a_n=\pm} \alpha^{a_1 \dots a_n}(x_1, \dots, x_n) \psi^{a_1}(x_1) \dots \psi^{a_n}(x_n) . \tag{1.16}$$

$\mathcal{N}_\rho$ is a normalization constant. The α's determine the initial correlations, vanish for any time argument $t \neq t_i$, and have to fulfill $\hat{\rho}$ to be hermitian, because $\hat{\rho}$ must have real eigenvalues. If initial cross correlations between $+$ and $-$ fields are neglected, f can be absorbed into the Lagrangian and hence into the definitions of the sources $J^\pm$, the masses and the couplings. Therefore, the initial conditions formally disappear but re-enter as initial conditions for the n-point Green-functions.
Now the generating functional of time-ordered correlation functions has the usual form

$$W[J^\pm] = i \ln Z[J^\pm] = i \ln \int \mathcal{D}\psi_C e^{i \int_{t_i}^{t_f} \mathrm{d}^4 x \mathcal{L}(\psi_C)} . \tag{1.17}$$

Consequently, the 1PI effective action can be derived by a Legendre transformation with respect to J^+ and J^-. Of course, higher nPI effective actions can be obtained by adding n-point sources to the Lagrangian and the corresponding Legendre transform, as it is known from the vacuum theory.[4] The 2PI effective action especially is the starting point in Section 1.3, where the evolution equations for the 2-point functions are formulated. Therefore, some notational conventions need to be introduced. As a last remark, t_f is set to infinity to include correlation functions for arbitrary large times. However, t_i still should be finite since the system would otherwise have an infinite amount of time to equilibrate until a measurement is done. This means that by setting t_i to $-\infty$, all correlation functions would have their equilibrium forms. Nevertheless, t_i can be set to zero for simplicity.

---

[4] See for example [71] for details.

1.2 2-Point Functions in the CTP

In many cases, it is sufficient to consider only 2-point functions. Their general structure is described in this section. Due to the two time branches of the closed time path, it is possible to construct four different 2-point functions. These are the time-ordered G^{++}, the anti-time-ordered G^{--}, and the "greater" $G^{-+} = G^>$ and "less" $G^{+-} = G^<$ Wightman-functions. They are defined in operator notation, in position space, in terms of a generic charged bosonic field operator ϕ in the Heisenberg picture, that has to obey the equal time commutation relations for canonical quantization

$$\left[\phi(x),\phi^\dagger(y)\right]\Big|_{x^0=y^0} = \left[\dot\phi(x),\dot\phi^\dagger(y)\right]\Big|_{x^0=y^0} = 0 \tag{1.18}$$

$$\left[\phi(x),\dot\phi^\dagger(y)\right]\Big|_{x^0=y^0} = i\delta^{(3)}(\vec{x}-\vec{y})\,, \tag{1.19}$$

through

$$iG_\phi^{++}(x,y) = \langle\mathcal{T}\phi(x)\phi(y)^\dagger\rangle = \theta(x^0-y^0)iG_\phi^>(x,y) + \theta(y^0-x^0)iG_\phi^<(x,y) \tag{1.20}$$

$$iG_\phi^{--}(x,y) = \langle\bar{\mathcal{T}}\phi(x)\phi(y)^\dagger\rangle = \theta(y^0-x^0)iG_\phi^>(x,y) + \theta(x^0-y^0)iG_\phi^<(x,y) \tag{1.21}$$

$$iG_\phi^>(x,y) = \langle\phi(x)\phi(y)^\dagger\rangle \tag{1.22}$$

$$iG_\phi^<(x,y) = \langle\phi(y)^\dagger\phi(x)\rangle\,. \tag{1.23}$$

$\mathcal{T}$ and $\bar{\mathcal{T}}$ are the time-ordering and anti-time-ordering operator. Similar relations hold for a fermion field ψ:

$$\{\psi(x),\psi(y)\}\Big|_{x^0=y^0} = \{\bar\psi(x),\bar\psi(y)\}\Big|_{x^0=y^0} = 0 \tag{1.24}$$

$$\{\psi(x),\bar\psi(y)\}\Big|_{x^0=y^0} = i\delta^{(3)}(\vec{x}-\vec{y})\mathbb{1}\,, \tag{1.25}$$

$$iG_\psi^{++}(x,y) = \langle\mathcal{T}\psi(x)\bar\psi(y)\rangle = \theta(x^0-y^0)iG_\psi^>(x,y) + \theta(y^0-x^0)iG_\psi^<(x,y) \tag{1.26}$$

$$iG_\psi^{--}(x,y) = \langle\bar{\mathcal{T}}\psi(x)\bar\psi(y)\rangle = \theta(y^0-x^0)iG_\psi^>(x,y) + \theta(x^0-y^0)iG_\psi^<(x,y) \tag{1.27}$$

$$iG_\psi^>(x,y) = \langle\psi(x)\bar\psi(y)\rangle \tag{1.28}$$

$$iG_\psi^<(x,y) = -\langle\bar\psi(y)\psi(x)\rangle\,. \tag{1.29}$$

However, even if there are four Wightman functions, only two of them are really independent. This reflects the doubling of the degrees of freedom in thermal non-equilibrium. The two equations that relate those four functions are $G^{++} + G^{--} = G^> + G^<$, which already holds on operator level, and the Kramers-Kronig relation below.

In fact, it can be useful in practical calculations to distinguish between several redefinitions written out explicitly in the following table and shown diagrammatically in Figure 1.2:

hermitian propagator	G^H	$=$	$\frac{1}{2}(G^{++} - G^{--})$	$=$	$\frac{1}{2}(G^R + G^A)$	
anti-hermitian / spectral propagator	$G^{\mathcal{A}}$	$=$	$\frac{1}{2}(iG^> - iG^<)$	$=$	$\frac{1}{2}(iG^R - iG^A)$	
statistical propagator	G^F	$=$	$\frac{1}{2}(G^{++} + G^{--})$	$=$	$\frac{1}{2}(G^> + G^<)$	
retarded propagator	iG^R	$=$	$iG^H + G^{\mathcal{A}}$	$=$	$iG^{++} - iG^<$	$=$ $iG^> - iG^{--}$
advanced propagator	iG^A	$=$	$iG^H - G^{\mathcal{A}}$	$=$	$iG^{++} - iG^>$	$=$ $iG^< - iG^{--}$
"less" propagator	$iG^<$	$=$	$iG^F - G^{\mathcal{A}}$	$=$	$iG^{++} - iG^R$	$=$ $iG^{--} + iG^A$
"greater" propagator	$iG^>$	$=$	$iG^F + G^{\mathcal{A}}$	$=$	$iG^{--} + iG^R$	$=$ $iG^{++} - iG^A$
time-ordered propagator	G^{++}	$=$	$G^F + G^H$	$=$	$G^< + G^R$	$=$ $G^> + G^A$
anti-time-ordered propagator	G^{--}	$=$	$G^F - G^H$	$=$	$G^> - G^R$	$=$ $G^< - G^A$

Table 1.1: Relations between CTP 2-point functions.
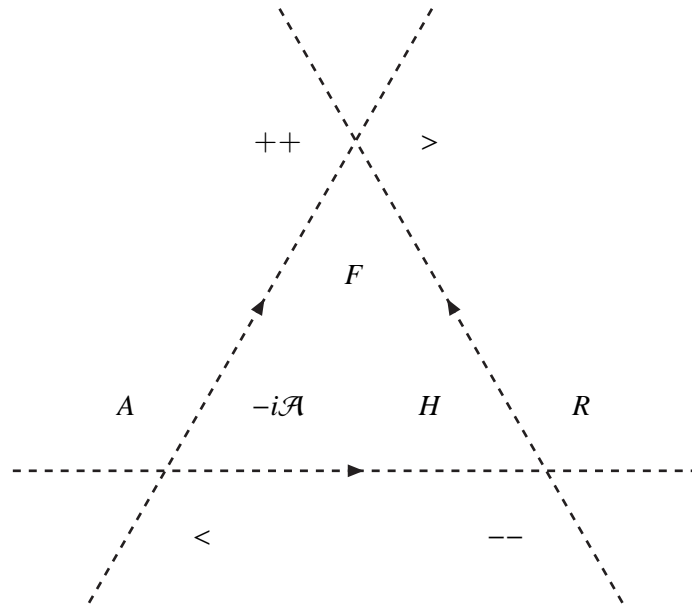
Figure 1.2: This diagram is a possible visualization of the above set of redefinitions. Functions outside of the dashed triangle are calculated via addition or subtraction of the inner ones according to the arrows as explained by the example: $G^H + G^F = G^{++}$ and $G^F - G^H = G^{--}$. Likewise, the inner functions modulo a factor of 2 are calculated from the outside ones: $G^{--} + G^{++} = 2G^F$ and $G^{++} - G^{--} = 2G^H$.

1.3 Kadanoff-Baym Equations in the 2PI Approach

With the record of the general structure of 2-point functions at hand, their evolution equations can be derived. For a generic bosonic field ϕ and a fermionic field ψ with vanishing field expectation values $\langle\phi\rangle = \langle\psi\rangle = 0$, the 2PI effective action has the representation

$$\Gamma^{2\text{PI}}[\Delta, S] = i\text{tr}[\Delta^{(0)-1}\Delta] - i\text{tr}[S^{(0)-1}S] + i\text{tr}\ln\Delta^{-1} - i\text{tr}\ln S^{-1} + \Gamma_2[\Delta, S]. \tag{1.30}$$

Δ and S are dressed 2-point functions for ϕ and ψ respectively, and Γ_2 is the sum of all 2-particle irreducible (2PI) vacuum graphs. $\Delta^{(0)}$ and $S^{(0)}$ are considered to be the tree-level functions.

$\Gamma^{2\text{PI}}[\Delta, S]$ determines the equations of motion for Δ and S by the stationarity conditions

$$\frac{\delta\Gamma}{\delta\Delta} = 0 \quad , \quad \frac{\delta\Gamma}{\delta S} = 0. \tag{1.31}$$

From these, the Kadanoff-Baym-equations for a general bosonic and a fermionic field can be constructed. By evaluating the functional derivatives in (1.31), the stationarity conditions for Δ, and analogously for S, become

$$\frac{\delta\Gamma[\Delta, S]}{\delta\Delta^{ba}(v, u)} = i\Delta^{(0)\,ab-1}(u, v) - i\Delta^{ab-1}(u, v) + \frac{\delta\Gamma_2[\Delta, S]}{\delta\Delta^{ba}(v, u)} = 0 \tag{1.32}$$

in CTP notation and position space. a and b are the CTP indices. The definitions of the bosonic and fermionic self-energy can then be read of modulo conventional signs:

$$\Pi^{ab}(u, v) = iab\frac{\delta\Gamma_2[\Delta, S]}{\delta\Delta^{ba}(v, u)} \tag{1.33}$$

$$\not\Sigma^{ab}(u, v) = -iab\frac{\delta\Gamma_2[\Delta, S]}{\delta\not S^{ba}(v, u)}. \tag{1.34}$$

The additional minus sign in (1.34) compensates the minus that appears when the closed fermionic loop in Γ_2 is opened. Since S and Σ are Dirac vectors, Equation (1.34) is written in a slashed notation. In this convention, $-i$ times the self-energy is the sum of the corresponding diagrams multiplied by a and b. After a convolution of (1.32) with $\Delta^{bc}(v, w)$ and renaming some indices, one obtains

$$(-\partial_u^2 - m_\phi^2)i\Delta^{ab}(u, v) + i\sum_{c=\pm} c\int_0^\infty d^4w\,i\Pi^{ac}(u, w)i\Delta^{cb}(w, v) = a\delta^{ab}i\delta^{(4)}(u - v). \tag{1.35}$$

The fermionic analogon is

$$(i\not\partial_u - m_\psi)i\not S^{ab}(u, v) + i\sum_c c\int_0^\infty d^4w\,i\not\Sigma^{ac}(u, w)i\not S^{cb}(w, v) = a\delta^{ab}i\delta^{(4)}(u - v). \tag{1.36}$$

By adding and subtracting Equation (1.35) for different values of a and b, all $++$ and $--$ functions are substituted by $>$, $<$, retarded and advanced ones. Then, a Schwinger-Dyson equation for the retarded and advanced propagators and an equation for the greater and less propagators can be obtained:

$$(-\partial^2 - m_\phi^2)i\Delta^{R/A} + i\left(i\Pi^{R/A}\odot i\Delta^{R/A}\right) = i\delta^{(4)} \tag{1.37}$$

$$(-\partial^2 - m_\phi^2)i\Delta^{</>} + i\left(i\Pi^R\odot i\Delta^{</>}\right) + i\left(i\Pi^{</>}\odot i\Delta^A\right) = 0. \tag{1.38}$$

Likewise Equation (1.36) can be reduced to

$$(i\slashed{\partial} - m_\psi)i\slashed{S}^{R/A} + i\left(i\slashed{\Sigma}^{R/A} \odot i\slashed{S}^{R/A}\right) = i\delta^{(4)} \tag{1.39}$$

$$(i\slashed{\partial} - m_\psi)i\slashed{S}^{</>} + i\left(i\slashed{\Sigma}^{R} \odot i\slashed{S}^{</>}\right) + i\left(i\slashed{\Sigma}^{</>} \odot i\slashed{S}^{A}\right) = 0 . \tag{1.40}$$

Here, the convolution operator $\odot$ is introduced:

$$A \odot B \equiv \int_0^\infty \mathrm{d}^4 y A(x,y)B(y,z) . \tag{1.41}$$

After replacing the retarded and advanced functions in (1.38) and (1.40) with spectral and hermitian functions, the Kadanoff-Baym equations are obtained:

$$(-\partial^2 - m_\phi^2)\Delta^{</>} - \Pi^H \odot \Delta^{</>} - \Pi^{</>} \odot \Delta^H = C_\phi \equiv \frac{1}{2}\left(\Pi^> \odot \Delta^< - \Pi^< \odot \Delta^>\right) \tag{1.42}$$

$$(i\slashed{\partial} - m_\psi)\slashed{S}^{</>} - \slashed{\Sigma}^H \odot \slashed{S}^{</>} - \slashed{\Sigma}^{</>} \odot \slashed{S}^H = \mathbb{C}_\psi \equiv \frac{1}{2}\left(\slashed{\Sigma}^> \odot \slashed{S}^< - \slashed{\Sigma}^< \odot \slashed{S}^>\right) . \tag{1.43}$$

C_ϕ and $\mathbb{C}_\psi$ are called the collision terms since they vanish in equilibrium.[5]

1.4 Wigner Space and the Gradient Expansion

In equilibrium the 2-point functions $G(x,y)$ depend only on the relative coordinate $x - y$ due to fluctuations that usually take place on microscopic scales. The dependences on the mean coordinate $\frac{x+y}{2}$, on the other hand, typically result from changes on macroscopic scales. These may emerge from a coupling to a slowly varying external bath or a change in the background metric related to inflation. To separate the microscopic scales from the macroscopic ones, a Wigner transformation is performed. This is a Fourier transformation with respect to the relative coordinate:

$$G\left(x + \frac{r}{2}, x - \frac{r}{2}\right) = \int \frac{\mathrm{d}^4 k}{(2\pi)^4} e^{-ik\cdot r}\tilde{G}(k,x) . \tag{1.44}$$

In Wigner space the convolution of 2-point functions reads

$$A \odot B \equiv \int \mathrm{d}^4 y A(x,y)B(y,z) = \tilde{A}\left(k, \frac{x+z}{2}\right) * \tilde{B}\left(k, \frac{x+z}{2}\right) , \tag{1.45}$$

where $*$ is the Moyal star operator

$$\tilde{A}(k,x) * \tilde{B}(k,x) = \tilde{A}(k,x)e^{-i\frac{1}{2}\left(\overleftarrow{\partial}_x \cdot \overrightarrow{\partial}_k - \overleftarrow{\partial}_k \cdot \overrightarrow{\partial}_x\right)}\tilde{B}(k,x) . \tag{1.46}$$

Therefore, the evolution equations for the correlation functions have the following form in Wigner space: convolutions $\odot$ are replaced by the Moyal star $*$, and the derivative with respect to the left variable of the 2-point function $\Delta(u,v)$ in (1.35) and $\slashed{S}(u,v)$ in (1.36) becomes

$$\partial_u \to -ik + \frac{1}{2}\partial_x . \tag{1.47}$$

If $\tilde{A}$ and $\tilde{B}$ do not depend on the mean position x, their Wigner transformation reduces to the Fourier transformation. This reduction can be described by the systematic truncation within the expansion of the exponential

---

[5] See the KMS relations in Equation (1.56).

of the Moyal star, and hence by the number of gradients used to describe the convolution (1.45). This is called the gradient expansion. $e^{r \cdot \partial_x}$ is the translation operator. It can be expanded and truncated for an infinitesimal r, which results in an infinitesimal shift in x. Hence, the gradient expansion is also an expansion in the size of the macroscopic correlation length between A and B in (1.45). This means that if the quantum system that has to be described is close to equilibrium and therefore moving slowly, correlation functions at some mean coordinate x should only depend on the information close to x, but not for example on the conditions far away in the space-time. With the help of the gradient expansion, consequently, the contact to Boltzmann, Langevin and Quantum-Boltzmann equations can be found as explained for example in [21, 72, 73]. In the following investigation, all 2-point functions are assumed to be in Wigner space such that the tilde is dropped.

1.5 Tree-Level Equilibrium Green-Functions

In this chapter, some aspects related to Green-functions are examined. Furthermore, an overview of several relations for the propagators is given. The tree-level functions are solutions of the Klein-Gordon and Dirac equation that can of course be found in the Equations (1.35) and (1.36) by setting all couplings to zero. Those solutions, but also solutions to the full interacting theory, have to obey rules that sometimes are related to thermal equilibrium and sometimes follow from general arguments.

Spectral sum rules: In equilibrium, the Wigner space reduces to the usual Fourier or momentum space. The momentum space spectral propagators have to obey a sum rule that can be deduced from the equal-time canonical commutation relation, as explained for example in [74][6]. In case of bosons with the spacial dependence in momentum space, this reads

$$\left[\phi(t, \vec{k}), \dot{\phi}^\dagger(t', \vec{k}) \right] \Big|_{t=t'} = i \,. \tag{1.48}$$

After writing down the spectral function in operator notation

$$\Delta^{\mathcal{A}}(t, \vec{k}) = \frac{1}{2} \left(\Delta^> - \Delta^< \right)(t, \vec{k}) = \frac{1}{2} \left\langle \left[\phi(t, \vec{k}), \phi^\dagger(0, \vec{k}) \right] \right\rangle , \tag{1.49}$$

taking the time derivative at $t = 0$, and considering the Fourier transformation with respect to t, the following relation is found:

$$-\frac{i}{2} = \dot{\Delta}^{\mathcal{A}}(t = 0, \vec{k}) = \int \frac{\mathrm{d}k^0}{2\pi} (-ik^0) \Delta^{\mathcal{A}}(k) \,. \tag{1.50}$$

Hence, the bosonic spectral sum rule is

$$\int \frac{\mathrm{d}k^0}{\pi} k^0 \Delta^{\mathcal{A}}(k) = 1 \,. \tag{1.51}$$

In an analogous fashion, (Dirac-) fermions have to obey

$$\int \frac{\mathrm{d}k^0}{\pi} S^{0\mathcal{A}}(k) = \int \frac{\mathrm{d}k^0}{\pi} \frac{1}{4} \mathrm{tr}[\gamma^0 \slashed{S}^{\mathcal{A}}(k)] = 1 \,. \tag{1.52}$$

Those rules hold also for an interacting theory and should of course also hold in a similar fashion in non-equilibrium, since they are directly related to the quantization conditions.

---

[6] The spectral propagator in [74] differs by a factor of two compared to the definition in this study.

KMS relations: In thermal equilibrium, the greater- and less- Wightman-functions are in addition related through the Kubo-Martin-Schwinger (KMS) relations which can be inferred, for instance, within the imaginary time formalism. In thermal equilibrium, the density matrix $\hat{\rho}$ can be written as

$$\hat{\rho}_{eq} = Ne^{-\beta\hat{H}}. \tag{1.53}$$

$\hat{H}$ is the Hamiltonian, β is the inverse temperature T, and N is a normalization constant. By comparison with (1.6), $\hat{\rho}_{eq}$ can be regarded as the time evolution operator in imaginary time. Resorting to the cyclicity of the trace in (1.3) and suitably defined Wightman-functions for complex arguments, one can show that in position space the equilibrium bosonic Wightman-functions are related by

$$\Delta^>(t) = \Delta^<(t + i\beta) \tag{1.54}$$

and the fermionic ones by

$$\mathcal{S}^>(t) = -\mathcal{S}^<(t + i\beta). \tag{1.55}$$

In momentum space, those relations give the KMS relations

$$G^>(p) = \mp e^{\beta p^0} G^<(p). \tag{1.56}$$

The upper index is used for fermionic Wightman-functions, and the lower one for bosonic ones.

Thermal equilibrium distributions: Due to the KMS relations in thermal equilibrium, $G^<$ and $G^>$ are completely determined by the spectral function:

$$iG^<(p) = \mp 2f_\pm(p^0)G^\mathcal{A}(p) \tag{1.57}$$
$$iG^>(p) = \pm 2f_\pm(-p^0)G^\mathcal{A}(p). \tag{1.58}$$

f_+, f_-, and the $n_\pm$ in (1.59), are the thermal equilibrium distribution functions for fermions and bosons, i.e. the Fermi-Dirac and the Bose-Einstein distributions, respectively. They read

$$\left\{ \begin{array}{ll} n_\pm(E) & , E>0 \\ \pm 1 - \bar{n}_\pm(|E|) & , E<0 \end{array} \right\} = f_\pm(E) \stackrel{\text{eq.}}{=} \frac{1}{e^{\beta E} \pm 1}. \tag{1.59}$$

Furthermore, they are defined for positive and negative energy corresponding to particles in the initial and final state. The statistical factor $(1 + n_-)$ describes stimulated emission for bosons and the $(1 - n_+)$ results in the Pauli-blocking for fermions. The following rules can be found in thermal equilibrium:

$$f_\pm(E) + f_\pm(-E) = \pm 1, \tag{1.60}$$
$$1 \mp 2f_\pm(E) = -(1 \mp f_\pm(-E)) = \text{sign}(E)(1 \mp 2f_\pm(|E|)), \tag{1.61}$$
$$\lim_{T\to 0} f_\pm(E) = \pm\theta(-E). \tag{1.62}$$

Equation (1.61) in particular is useful for splitting $f_\pm$ into a thermal and a vacuum part. Additionally, Majorana particles fulfill $n_+ = \bar{n}_+$. Therefore, if the right-hand side term of Equation (1.59) is ignored, Equations (1.60) and (1.61) also hold for non-equilibrium distributions.

13

Kramers Kronig relations: Since the retarded function has a pole below the real k^0 axis and is analytic in the closed upper half plane, its real and imaginary parts are related via Cauchy's theorem. This results in the Kramers Kronig relations that relate the hermitian and spectral functions:

$$G^H(p) = -\frac{1}{\pi}\fint dq^0 \frac{q^0}{q^{02} - p^{02}} G^{\mathcal{A}}(q^0, \vec{p}) = -\frac{2}{\pi}\fint_0^\infty dq^0 \frac{q^0}{q^{02} - p^{02}} G^{\mathcal{A}}(q^0, \vec{p}) \tag{1.63}$$

and

$$G^{\mathcal{A}}(p) = \frac{1}{\pi}\fint dq^0 \frac{p^0}{q^{02} - p^{02}} G^H(q^0, \vec{p}) = \frac{2}{\pi}\fint_0^\infty dq^0 \frac{p^0}{q^{02} - p^{02}} G^H(q^0, \vec{p}) \,. \tag{1.64}$$

This also means that in thermal equilibrium, there is only 1 independent 2-point-function. The $\fint$ denotes the Cauchy principal value integral.

By solving the Klein-Gordon equation for the free theory, using the normalization condition (1.51) and the boundary condition (1.56), the bosonic Green-functions in thermal equilibrium and momentum space in their most compact form are given by

$$\Delta^{\mathcal{A}}(k) = \pi\delta(k^2 - m^2)\text{sign}(u \cdot k) \tag{1.65}$$

$$\Delta^H(k) = \mathcal{P}\frac{1}{k^2 - m^2} \,. \tag{1.66}$$

u is the plasma vector and $\mathcal{P}$ denotes that this pole should be integrated in the Cauchy principal value sense. The other functions are obtained from

$$i\Delta^<(k) = 2\Delta^{\mathcal{A}}(k)f_-(u \cdot k) \tag{1.67}$$

$$i\Delta^>(k) = 2\Delta^{\mathcal{A}}(k)(1 + f_-(u \cdot k)) \tag{1.68}$$

$$i\Delta^F(k) = (1 + 2f_-(u \cdot k))\Delta^{\mathcal{A}}(k) \,. \tag{1.69}$$

For completeness, the retarded and advanced functions are also shown:

$$i\Delta^{R/A} = \frac{i}{k^2 - m^2 \pm i\,\text{sign}(u \cdot k)\varepsilon} \,. \tag{1.70}$$

Note that $\text{sign}(u \cdot k) = \text{sign}(k^0)$, since u^2 and u^0 are positive numbers. It is easy to check that Δ^H and $-\Delta^{\mathcal{A}}$ are indeed the real and imaginary parts of Δ^R, and that the Kramers-Kronig relations hold.

Equivalently, by solving the Dirac equation for the free theory and by using the normalization condition (1.52) and the boundary condition (1.56), the fermionic Wightman functions in thermal equilibrium are

$$\mathcal{S}^{\mathcal{A}}(k) = \pi(\slashed{k} + m)\delta(k^2 - m^2)\text{sign}(u \cdot k) \tag{1.71}$$

$$\mathcal{S}^H(k) = \mathcal{P}\frac{\slashed{k} + m}{k^2 - m^2} \tag{1.72}$$

$$i\mathcal{S}^<(k) = 2\mathcal{S}^{\mathcal{A}}(k)(-f_+(u \cdot k)) \tag{1.73}$$

$$i\mathcal{S}^>(k) = 2\mathcal{S}^{\mathcal{A}}(k)(1 - f_+(u \cdot k)) \tag{1.74}$$

$$i\mathcal{S}^F(k) = (1 - 2f_+(u \cdot k))\mathcal{S}^{\mathcal{A}}(k) \tag{1.75}$$

$$i\mathcal{S}^{R/A}(k) = \frac{i(\slashed{k} + m)}{k^2 - m^2 \pm i\,\text{sign}(u \cdot k)\varepsilon} \,. \tag{1.76}$$

Since all unregulated poles that have to be dealt with within this work come from hermitian propagators, the explicit $\mathcal{P}$ is dropped. Those poles are always regarded in the Cauchy principal value sense. The principal value integral is just not mentioned everywhere.

1.6 Resummed Propagators

In Wigner space up to first order in gradients, the Schwinger-Dyson Equations (1.37) for the retarded and advanced propagators read[7]

$$(k^2 + ik \cdot \partial_x - m_\phi^2 - \Pi^{R/A})i\Delta^{R/A} = i \,. \tag{1.77}$$

The zeroth order solution can simply be read off:

$$i\Delta^{R/A} = \frac{i}{k^2 - m_\phi^2 - \Pi^{R/A}} = \frac{i}{k^2 - m_\phi^2 - \Pi^H \pm i\Pi^{\mathcal{A}}} \,. \tag{1.78}$$

Hence, the zeroth order resummed hermitian and spectral propagators are

$$\Delta^H = \frac{k^2 - m_\phi^2 - \Pi^H}{(k^2 - m_\phi^2 - \Pi^H)^2 + (\Pi^{\mathcal{A}})^2} \tag{1.79}$$

$$\Delta^{\mathcal{A}} = \frac{\Pi^{\mathcal{A}}}{(k^2 - m_\phi^2 - \Pi^H)^2 + (\Pi^{\mathcal{A}})^2} \,. \tag{1.80}$$

The hermitian function (1.79) represents a principal value for an infinitesimal $\Pi^{\mathcal{A}}$, and (1.80) has the usual Breit-Wigner form. By taking the formal limit $\Pi^{\mathcal{A}} \to 0$, the resummed spectral function reduces to

$$\Delta^{\mathcal{A}} \to \pi \mathrm{sign}(\Pi^{\mathcal{A}})\delta(k^2 - m_\phi^2 - \Pi^H) \,. \tag{1.81}$$

In case the $\Pi^{\mathcal{A}}$ vanishes at the pole, the standard infinitesimal $\varepsilon \, \mathrm{sign}(k^0)$ term has to be included. Likewise, Equation (1.39) reads

$$\left(\slashed{k} + \frac{1}{2}\slashed{\partial}_x - m_\psi - \slashed{\Sigma}^{R/A} \right) i\slashed{S}^{R/A} = 1 \tag{1.82}$$

in Wigner space and is expanded up to first order in gradients. The zeroth order solution can be read off:

$$i\slashed{S}^{R/A} = \frac{i}{\slashed{k} - m_\psi - \slashed{\Sigma}^{R/A}} = \frac{i}{\slashed{k} - m_\psi - \slashed{\Sigma}^H \pm i\slashed{\Sigma}^{\mathcal{A}}} \,. \tag{1.83}$$

Due to the Dirac structure, the resummed hermitian and spectral functions are slightly different from the scalar one:

$$\slashed{S}^H = \frac{(\slashed{a} + m_\psi)(a^2 - b^2 - m_\psi^2) + \slashed{b}\,2a \cdot b}{(a^2 - b^2 - m_\psi^2)^2 + (2a \cdot b)^2} \tag{1.84}$$

$$\slashed{S}^{\mathcal{A}} = \frac{(\slashed{a} + m_\psi)2a \cdot b - \slashed{b}(a^2 - b^2 - m_\psi^2)}{(a^2 - b^2 - m_\psi^2)^2 + (2a \cdot b)^2} \,, \tag{1.85}$$

with

$$a^\mu = k^\mu - \Sigma^{H\mu} \tag{1.86}$$

$$b^\mu = \Sigma^{\mathcal{A}\mu} \,. \tag{1.87}$$

---

[7] Only gradients in the mean coordinate x are counted, since microscopic fluctuations can still be large. Then, to first order in gradients, the convolution of Π with Δ should include the $\partial_k \cdot \partial_x$ terms. Nevertheless, the rate given by Π is proportional to the change in the macroscopic scale. Therefore, $\Pi\Delta$ is already effectively of first order in gradients.

The dispersion relation is basically given by the zeros of $a^2 - b^2 - m_\psi^2$.[8] If the width $2a \cdot b$ vanishes at one of those poles, a $\varepsilon \delta_0^\mu$ term should be added to b^μ. In the formal limit $b^\mu \to 0$, in the sense of sending couplings to zero, Equation (1.84) reduces to the usual principal value form plus a remainder, which is of higher order in the couplings and therefore vanishes. In addition, the spectral function reduces to the tree-level form

$$\slashed{S}^{\mathcal{A}} \to \pi \mathrm{sign}(a \cdot k)(\slashed{a} + m_\psi)\delta(a^2 - m_\psi^2) \tag{1.88}$$

plus a remainder, but here this remainder vanishes because it becomes $\sim (a^2 - m_\psi^2)\delta(a^2 - m_\psi^2)$.

Finally, if $\Pi^{R/A}$ is constant in x, its resummation into $\Delta^{R/A}$ does not introduce new x dependencies. Hence, the solutions (1.78)-(1.80) to the zeroth order in gradients are also solutions to first order in gradients. The same argument also holds for the fermions.

---

[8] At least in our case, one of those zero's corresponds to a tachyonic pole. This unphysical pole vanishes only if the propagator numerator is not expanded in couplings. See Chapter 4.7 for the lepton dispersion relation.

Extended Standard Model and First Applications of the CTP

2.1 Lagrangian

The temperature relevant for the considered Leptogenesis scenario is much above the electroweak scale, such that the Lagrangian has to be considered in the symmetric electroweak phase and the Higgs doublet ϕ is present in the primordial plasma. Consider the Standard model extended by a number $n : i = 1 \ldots n$ of right-handed neutrinos (RHN) N_i with Majorana masses M_i, that are singlet under the full SM gauge group $\text{SU}_C(3) \times \text{SU}_W(2) \times \text{U}_Y(1)$. Then, the most general renormalizable Lagrangian can only provide new Yukawa interactions Y_{ia} between those neutrinos and the left-handed lepton $\text{SU}(2)$ doublets l_a via

$$\mathcal{L} = \mathcal{L}_{\text{SM}} + \frac{1}{2}\bar{\psi}_{N_i}(i\slashed{\partial} - M_i)\psi_{N_i} - \left(Y_{ia}\bar{\psi}_{N_i}\tilde{\phi}^\dagger P_L \psi_{l_a} + h.c.\right), \qquad (2.1)$$

with $a, b = 1 \ldots N$ and $N = 3$ being the number of generations of lepton doublets. Here, ψ_{N_i} equals $N_i + N_i^c$ with $N^c = C\bar{N}^T$. C is the charge conjugation matrix, such that the Majorana condition $\psi_{N_i} = \psi_{N_i}^c$ is imposed. The tilded Higgs field is defined as $\tilde{\phi} = \epsilon\phi^*$ with ϵ being the antisymmetric tensor in isospin space.

If CP is broken, those interactions lead to the production of right-handed neutrinos and hence generate a lepton number asymmetry for each flavor, too. The lepton number asymmetry can be partly transferred further between the left-handed l_a and right-handed active leptons R_b by the Yukawa couplings h_{ab}:

$$\mathcal{L}_{\text{SM}} \supset -\left(h_{ab}\phi^\dagger \bar{\psi}_{R_a} P_L \psi_{l_b} + h.c.\right). \qquad (2.2)$$

This leads to the decoherence of correlations between different lepton flavors [26].

Gauge boson interactions with Higgs and top-quarks[9] have to be considered at the next order. The first ones are mediated through

$$\mathcal{L}_{\text{SM}} \supset (\mathcal{D}\phi)^\dagger \mathcal{D}\phi, \qquad (2.3)$$

where the covariant derivative of ϕ equals

$$\mathcal{D}_\mu \phi = \left(\partial_\mu + ig_1 Y_\phi B_\mu + ig_2 A^A_\mu t^A\right)\phi \qquad (2.4)$$

---

[9] Its coupling strength is much larger than for the other quarks.

with A_μ^A and B_μ being the SU(2) and the U(1) gauge bosons, respectively. $Y_\phi = \frac{1}{2}$ is the hypercharge, and $t^A = \frac{\sigma^A}{2}$ are the three generators of weak isospin transformations with $A = 1 \ldots 3$. The σ^A are the Pauli matrices.
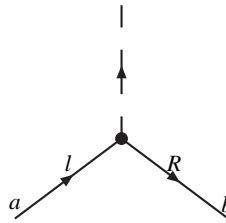
The second ones results through Yukawa interactions with the coupling h_t

$$\mathcal{L}_{\text{SM}} \supset -\left(h_t \bar{\psi}_{t_R} \phi^\dagger P_L \psi_{t_L} + h.c.\right) \tag{2.5}$$

between left-handed top quark SU(2) doublets ψ_{t_L} and right-handed top quark SU(2) singlets t_R. The SU(3) color indices are suppressed during this study.

2.2 Selection of Feynman-Rules

The following section presents the vertices that are relevant for this investigation. Again, a and b are flavor indices, f, g and h are SU(2) doublet indices, and A and B account for the three generators of SU(2) in the fundamental representation. p and k are the 4-momenta flowing in the direction of positive charge flow, which is indicated by the arrow. The color space identity matrix is given by $\mathbb{1}_c$. Each vertex comes with an additional sign corresponding to the $+$ or $-$ CTP branch.

$$-ih_{ba}P_L \tag{2.6}$$

$$-ih_{ba}^\dagger P_R \tag{2.7}$$

$$-iY_{ia}\epsilon^\dagger P_L \tag{2.8}$$

$$-iY_{ia}^\dagger \epsilon P_R \tag{2.9}$$
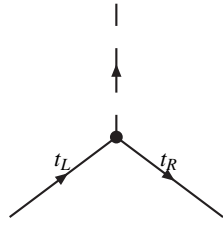
$$-ih_t P_L \mathbb{1}_c \qquad (2.10)$$
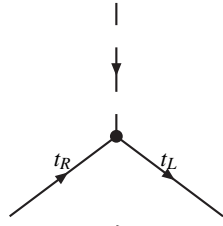
$$-ih_t P_R \mathbb{1}_c \qquad (2.11)$$
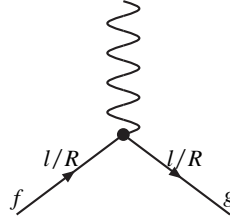
$$\begin{aligned}
&-ig_1\gamma^\mu\left(Y_L P_L + Y_R P_R\right)\delta_{gf} &&, \text{ for } B_\mu \\
&\qquad Y_L = -\tfrac{1}{2} \text{ and } Y_R = -1 \\
&-ig_2\gamma^\mu P_L t^A_{gf} &&, \text{ for } A^A_\mu
\end{aligned} \qquad (2.12)$$
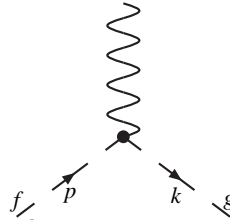
$$\begin{aligned}
&-ig_1 Y_\phi \delta_{gf}(p+k)^\mu &&, \text{ for } B_\mu \\
&\qquad Y_\phi = \tfrac{1}{2} \\
&-ig_2 t^A_{gf}(p+k)^\mu &&, \text{ for } A^A_\mu
\end{aligned} \qquad (2.13)$$
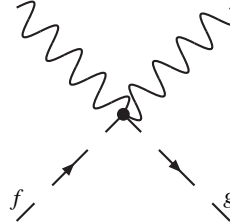
$$\begin{aligned}
&i2g_1^2 Y_\phi^2 \delta_{gf} g^{\mu\nu} &&, \text{ for } B_\mu B_\nu \\
&i\tfrac{1}{2}g_2^2 \delta^{AB}\delta_{gf} g^{\mu\nu} &&, \text{ for } A^A_\mu A^B_\nu
\end{aligned} \qquad (2.14)$$

2.3 Scales and Schemes

The task of this investigation is to calculate production rates relevant for Leptogenesis at high temperatures T. Thereby, T is about $10^9 - 10^{12} GeV$, far above the electroweak scale $\Lambda_{\text{ew}} \approx 246 GeV$, where the SM is unbroken. In this unbroken phase, nearly all particles, except the Higgs and the right-handed neutrino, must have zero tree-level masses due to gauge symmetries. Since the tree-level Higgs mass of about $125 GeV$ is known at zero temperature, the one at high temperature is given by a renormalization group running. The running itself is determined by radiative corrections proportional to small couplings. As a consequence, the tree-level Higgs mass for the theory being defined far above the electroweak scale is still a small number compared to all other relevant scales. Those are for example the temperature T, the still unspecified mass m_N of the right-handed neutrino, and the external momentum of the relevant processes here. If $T \gg m_N$, those external momenta are always of order T, since the phase space prefers large momenta while Bose-Einstein and Fermi-Dirac distributions prefer small momenta. Hence, the dominant contributions to particle processes are at momenta of typically $2 - 3T$. However, if $T \ll m_N$, the temperature is negligible and the only scale that can appear is the RHN mass. In the following pages, this limit is referred to as the "vacuum"-limit, even if T is still much larger than Λ_{ew}. However, the Higgs is always approximately ultra-relativistic and its tree-level mass is set to zero.

To define the meaning of mass and coupling parameters, renormalization conditions have to be imposed. But, as thermal effects are UV finite due to the exponential suppression of the Bose-Einstein and Fermi-Dirac factors, only "vacuum" renormalization conditions are relevant. Thermal effects are treated as quantum effects due to a thermal plasma of particles of a theory defined at scales of the order of the fixed neutrino mass much larger than Λ_{ew}, and the temperature can be varied as a free parameter. In conclusion, the couplings are defined by the renormalization group flow to this fixed scale. By choosing different scales m_N, the couplings may in principle be varied as free parameters too. In this study, several couplings are set to zero to analyze the effect of individual interactions that can be compared to the perturbative results. The other possibility is to choose a set of couplings according to the renormalization group flow to the for-Leptogenesis-relevant scale. Those couplings are given in Table 2.1.

RGE scale	g_1	g_2	g_3	h_t	λ_ϕ	G_l	G_R
10^9 GeV	0.394	0.577	0.689	0.600	-0.049	0.289	0.155
10^{12} GeV	0.414	0.552	0.606	0.526	-0.082	0.271	0.171

Table 2.1: Values of relevant SM couplings taken from [75]. G_l and G_R are defined in (2.82) and (2.83).

Typical schemes are the MS or $\overline{\text{MS}}$ scheme, in vacuum. They are not preferable, because integrations over particle distribution functions have to be taken where dimensional regularization (dim-reg) cannot be considered in a simple way. Nevertheless, all diagrams may be separated into vacuum and thermal contributions within the thermal perturbation theory. For the vacuum ones, dim-reg is suitable.

Another approach is the on-shell scheme. This states that the propagator pole should be at the physical mass scale and should have a residuum of one. This works fine for the right-handed neutrino as long as the limit $m_N \to 0$ is not considered. Since the RHN is a gauge singlet, it is not protected from radiative corrections, which would give rise to ill-defined counter-terms, in this limit. However, these effects are of higher order in the Yukawa coupling Y than what is needed in this work. Hence, the massless limit works in the on-shell scheme as well. Possible conditions on the real part of the neutrino self-energy are

$$\Sigma_N^H(\not{p} = m_N) = 0 \tag{2.15}$$

$$\frac{d}{d\not{p}}\Sigma_N^H(\not{p} = m_N) = 0\,. \tag{2.16}$$

This is not the case for the Higgs. Due to interactions with massless gauge bosons and quarks, the Higgs self-energy is infrared divergent at zero momenta. It is enough to introduce an infinitesimal fictitious infrared regulating gauge boson and top-quark mass at some stages. This regulator is set to zero after the IR divergences have canceled out and before physical observables are calculated. However, in case of the on-shell renormalization for the Higgs, this procedure cancels out IR divergences with UV divergences so that the whole renormalization process gets unnecessarily complicated. Nevertheless, renormalization conditions for the Higgs can be imposed at the unphysical momentum $p^2 = -M^2$ as proposed in [76].

$$\Pi_\phi^{H,vac}(p^2 = -M^2) = 0 \tag{2.17}$$

$$\frac{d}{dp^2}\Pi_\phi^{H,vac}(p^2 = -M^2) = 0. \tag{2.18}$$

This whole vacuum renormalization procedure should be done to get a well-defined meaning of the masses and the couplings. However, this investigation considers only counter-terms to cancel out UV divergences. It is considered case by case whether the remaining finite vacuum renormalizations are effectively be subdominant. The appropriate terms are determined within the perturbative calculation.

2.4 General 1-Loop Spectral Function using Gram Determinants

In this thesis, several cut diagrams are calculated numerically. There is a rich analytic tool set for vacuum diagrams. However, the distribution functions for thermal corrections usually demand numerical integrations. This section introduces a way to easily provide integration domains for massive and massless cut diagrams. In particular, this method is not restricted to a specific type of cut. It can consider loop diagrams with any particles being on-shell. The only assumptions made during this work are $d = 4$ space-time dimensions and Feynman diagrams with maximal d linear independent d-momentum vectors. The method is extendable to non-integer dimensions as well as to diagrams with more than d vectors. However, those cases are not of interest for the present investigation. The technique is not completely new, since special cases can be found for instance in [77, 78]. However, an understanding of the deeper background was not found in the literature. Therefore, the method is considered to be partly new.

The method of gram determinants is introduced by an example in the following. Furthermore, it is necessary to calculate the anti-hermitian part of a general 1-loop 2-point function using tree-level propagators once and for all. The only way to cut such a diagram is through the two internal particles. This means one recovers an integral of the type

$$K_{ab}(p) = \int \frac{\mathrm{d}^4 k}{(2\pi)^4} N(p,k,u)\Delta_1^{\mathcal{A}}(k)\Delta_2^{\mathcal{A}}(p-k)(1 - af_a(k) - bf_b(p-k)) \tag{2.19}$$

multiplied by some constant prefactor. a and b correspond to particle 1 and 2, respectively, and can take the values $+$ and $-$. As usual, a $+$ is used for a fermionic particle while a $-$ indicates a boson. The possible numerator algebra $N(p,k,u)$ can only consist of the vectors p, k and u. Hence, it can always be brought into a form that involves the scalar products p^2, k^2, u^2, $p\cdot k$, $p\cdot u$ and $k\cdot u$.[10] [11] [12] If the $\mathrm{d}^4 k$ is substituted in terms

---

[10] If K_{ab} is a tensor integral, it can be expressed in terms of scalar integrals. Those are obtained via the projection of each tensor index on the vectors p and u. Those integrals only involve the scalar products of p, k and u.

[11] Any convolution with further space-time vectors, momenta or tensors can be expressed as a sum of tensorial K_{ab} folded by the corresponding prefactors.

[12] In case of $d = 3$, the convolution of p, k and u with the Levi-Civita symbol can be expressed in terms of above scalar products: $\epsilon_{\mu\nu\rho}p^\mu k^\nu u^\rho = \sqrt{\mathrm{gd}(p,k,u)}$. gd is the gram determinant given in (2.25).

of Lorentz invariant scalar products, the k^2 and $p \cdot k$ is fixed by the on-shell relations of the internal particles while $k \cdot u$ remains as the integration variable.[13] $k \cdot u$ may only appear in the numerator, if the external particle is a fermion, due to other gauges than Feynman gauge for gauge bosons, or due to non-equilibrated thermal distribution functions. Here, only equilibrium is relevant. However, using tree-level functions with

$$f_a^{eq}(k) = f_a(u \cdot k) = \frac{1}{e^{\beta u \cdot k} + a} , \qquad (2.21)$$

the thermal equilibrium, K_{ab} is expressed as

$$K_{ab} = \int \frac{\mathrm{d}^4 k}{(2\pi)^4} \pi^2 N(u \cdot k) \mathrm{sign}(u \cdot k) \mathrm{sign}(u \cdot (p-k)) \delta(k^2 - m_1^2) \delta((p-k)^2 - m_2^2)$$
$$(1 - a f_a(u \cdot k) - b f_b(u \cdot (p-k))) . \qquad (2.22)$$

The $N(u \cdot k)$ is the same as the $N(p, k, u)$ from above – only k^2 and $p \cdot k$ are replaced by p^2 and the masses via the on-shell delta functions. To obtain dimensionless quantities, all dimensionful factors are rescaled by the temperature $T = \beta^{-1}$. After integrating out the one irrelevant angular direction and the delta functions, one is left with

$$K_{ab} = \frac{\theta(-\mathrm{gd}(p,k))}{2^5 \pi |\vec{p}|} \int_B \mathrm{d}k^0 N(k^0) \mathrm{sign}(k^0) \mathrm{sign}(p^0 - k^0)(1 - a f_a(k^0) - b f_b(p^0 - k^0)) . \qquad (2.23)$$

For simplicity, the plasma frame $\vec{u} = 0$ is chosen, since u is the only 4-vector in (2.22) that definitely has a positive norm.[14] Other reference frames are possible too, but they usually involve one more linear independent 4-vector. The result can easily be extended to any other frame in the end. The $\mathrm{gd}(p, k)$ is the gram determinant of the 4-vectors p and k. It appears in (2.23), since p needs to be such that the peaks of the delta functions in (2.22) are hit:

The method of Gram determinants:

Within a Lorentz invariant description of any space-time integral, gram determinants may serve as an easy way to express the integration domain. A gram matrix is the Hermitian matrix of inner products of a set of vectors $k_1, \ldots, k_n$:

$$\mathrm{Gram}(k_1, \ldots, k_n) = \begin{pmatrix} k_1 \cdot k_1 & \cdots & k_1 \cdot k_n \\ \vdots & \ddots & \vdots \\ k_n \cdot k_1 & \cdots & k_n \cdot k_n \end{pmatrix} . \qquad (2.24)$$

The gram determinant is the determinant of such a matrix.

$$\mathrm{gd}(k_1, \ldots, k_n) = \det \mathrm{Gram}(k_1, \ldots, k_n) \qquad (2.25)$$

Obviously, it vanishes if two of its vectors become linear dependent. This in turn means that if the desired integral contains a number of linear independent space-time vectors, their gram determinants

---

[13] In case the d-vector k only is dotted by p, k or u, the $\mathrm{d}^d k$ can be written as

$$\mathrm{d}^d k = \frac{1}{2} \mathrm{d}\Omega^{d-3}(-\mathrm{gd}(u,p))^{\frac{3-d}{2}} \mathrm{gd}(u,p,k)^{\frac{d-4}{2}} \mathrm{d}(u \cdot k) \mathrm{d}(p \cdot k) \mathrm{d}(k^2) \qquad (2.20)$$

for any appropriate space-time dimension d. The $d - 3$ independent angular directions are integrated out by $\int \mathrm{d}\Omega^{d-3} = \mathrm{Vol}(S^{d-3})$, i.e. the volume of the $d - 3$ sphere.

[14] A general 4-vector r can serve as a reference frame only if it has positive norm. This means that a Lorentz transformation that rotates r into $r^\mu = (r^0, \vec{0})$ must exist.

are non-zero and sometimes need to have a definite sign.[15] In an Euclidean space-time, they represent the volume of the parallelepiped spanned by the corresponding vectors. Hence, they must be positive. However in Minkowski space-time, they have to be positive for an odd number and negative for an even number of vectors k_i, provided that at least one of them has a positive norm $k_1^2 > 0$. This one vector with positive norm is important since it has to serve as a reference frame for parameterizing the integral. It is easy to check that the gram determinant of n linear independent 4-vectors always has the form

$$\mathrm{gd}(k_1, k_2, \ldots, k_n) = -(-1)^n k_1^2 \left|\vec{k_2}\right|^2 \ldots \left|\vec{k_n}\right|^2 \sin^2 \angle(k_2, k_3) \ldots \sin^2 \angle(k_{n-1}, k_n) \tag{2.26}$$

by explicitly parameterizing the spatial $d - 1$ vectors in polar coordinates in the frame of k_1. $\angle(k_i, k_j)$ is the angle between the vectors $\vec{k_i}$ and $\vec{k_j}$. If k_1 is not the frame vector, the simple counterexample $\mathrm{gd}(k_1) = k_1^2 \gtrless 0$ proves the lemma.

Consequently, the determinant $\mathrm{gd}(p, k)$ has to be negative in our case with $k^2 = m_1^2 > 0$ even for negative p^2. Due to the on-shell deltas, this is

$$0 > 4\mathrm{gd}(p, k) = 4\mathrm{gd}(k, p - k) = \begin{vmatrix} 2m_1^2 & p^2 - m_1^2 - m_2^2 \\ p^2 - m_1^2 - m_2^2 & 2m_2^2 \end{vmatrix}. \tag{2.27}$$

The condition $\mathrm{gd}(p, k) < 0$ provides the usual kinematical constraints for $1 \leftrightarrow 2$ processes, which are allowed in a thermal plasma. However, an additional constraint appears in vacuum, since the distribution functions become Heaviside functions.

The general structure of a gram determinant shown in Equation (2.26) states that its sign is preserved. Otherwise, it always vanishes when the boundary of the integration domain B for a corresponding space-time integral $\int_B \mathrm{d}k_2^d \ldots \mathrm{d}k_n^d$ for $n \leq d$ is met. In turn, in the case of (2.23) the domain B can be defined via the sign of all gram determinants that are made of the vectors u, p, k, and that have at least one vector with positive norm. Due to Dodgson's condensation method for determinants, there is a relation between all those determinants, and one can show that a minimal set of conditions is created from

$$B \equiv \{\mathrm{gd}(u) > 0 \wedge \mathrm{gd}(u, p) < 0 \wedge \mathrm{gd}(u, p, k) > 0\}, \tag{2.28}$$

since at least $u^2 = 1$ is positive. Hence, this definition for B also includes the zero masses case. Actually, if one reduces (2.28) in case of $p^2 > 0$, only solution $k_-^0 < k^0 < k_+^0$ can exist if $\mathrm{gd}(p, k) < 0$:

$$k_\pm^0 = \frac{p^0(p^2 + m_1^2 - m_2^2)}{2p^2} \pm \frac{|\vec{p}|}{p^2} \sqrt{-\mathrm{gd}(p, k)}. \tag{2.29}$$

Hence, the θ constraint in (2.23) is already encoded in B. The $\sqrt{-\mathrm{gd}(p, k)}$ in Equation (2.29) is called the Källen function in the literature. The conditions in (2.28) also serve for negative p^2. In this case, the reduction of B results in the two cases $k^0 > k_-^0$ and $k^0 < k_+^0$, if $\mathrm{gd}(p, k) < 0$, and $k^0 \in \mathbb{R}$ if $\mathrm{gd}(p, k) > 0$. However, as long as k^2 or $(p - k)^2$ are positive, the $\mathrm{gd}(p, k)$ must always be negative.

---

[15] Gram determinants of n vectors in d integer dimensions for $n > d$ are zero. This is basically the idea of how to extend the method.

As long as $p^2 > 0$, the $k^0_\pm$ are such that $\text{sign}(k^0)\text{sign}(p^0 - k^0) = \text{sign}(p^2 - m_1^2 - m_2^2)$. Otherwise, the factor $\text{sign}(k^0)\text{sign}(p^0 - k^0)$ is always negative for $p^2 < 0$. Therefore, the sign terms in (2.23) can be put outside the integral. Equation (2.23) becomes

$$K_{ab}(p) = -\frac{1}{2^5\pi|\vec{p}|}\text{sign}(p^2 - m_1^2 - m_2^2)\theta(-\text{gd}(p,k))K(k^0)\left(\Big|_{k^0_-}^{k^0_+} + \theta(-p^2)\Big|_{-\infty}^{\infty}\right), \qquad (2.30)$$

where $K(k^0)$ is the remaining indefinite integral

$$K(k^0) \equiv \int dk^0 N(k^0)\left(1 - af_a(k^0) - bf_b(p^0 - k^0)\right). \qquad (2.31)$$

Up to now, the only used assumption is that the integrand of K_{ab} is a function of p, k and u. In principle, the same calculation also holds for non-equilibrium distributions as long as they can be written as functions of those variables. This would only lead to some other $K(k^0)$ integral. Nevertheless, this integral can always be solved analytically in thermal equilibrium for polynomial $N(k^0)$. In case of $N(k^0) = 1$, the $K(k^0)$ is

$$K(k^0) = k^0 + \ln\left|\frac{b + e^{p^0 - k^0}}{a + e^{k^0}}\right| = k^0 + \ln\left|\frac{f_a(k^0)}{f_b(p^0 - k^0)}\right|. \qquad (2.32)$$

In Chapter 2.6, the case $N(k^0) = k^0$ is relevant. In this case, (2.31) becomes

$$K(k^0) = \Re\left(k^0\ln\left|\frac{a + e^{k^0}}{1 + be^{-p^0 + k^0}}\right| + \text{Li}_2\left(-ae^{k^0}\right) - \text{Li}_2\left(-be^{-p^0 + k^0}\right)\right). \qquad (2.33)$$

Li_2 is the dilogarithm. For negative p^2, the limits $k^0 \to \pm\infty$ are important in Equation (2.30).

This simple example can of course also be evaluated straight forwardly by solving the constraints $|\vec{k}| > 0$ and $|\cos \angle(k, p)| < 1$ for k^0. This is done for a massless diagram in Section 2.5.3. However, the strength of the method becomes clear in the "Vertex Type Contributions" sections, since the delta functions can be solved in terms of its Lorentz invariant scalar products by a simple Gauss elimination, and the gram determinants only involve scalar products. Hence, the reduction of B can to some extent be done without mentioning the explicit way of how the deltas are integrated out. In addition, masses are incorporated easily, since the deltas are always linear in the squared masses.

2.5 Higgs Self-Energy

In the following chapters, the 1-loop hermitian and spectral self-energies of the Higgs ϕ and leptons l are needed. For the Higgs, those are obtained from the "seagull", 4-Higgs, "sunset" and top-loop diagrams.
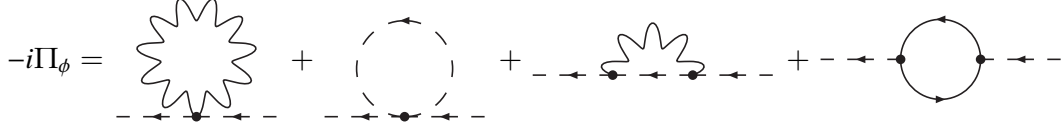
Figure 2.1: Seagull, 4-Higgs, sunset and top-loop diagrams for the Higgs self-energy. Wavy lines correspond to $U(1)$ and $SU(2)$ gauge bosons.

In the following subsections, Π_ϕ accounts for each diagram separately. However, all contributions are added in the end.

2.5.1 Seagull Diagram

Using the Feynman rules from Section 2.2, the hermitian self-energy, i.e. the real part of $i\Pi_\phi$ for the Higgs with a $U(1)$ and a $SU(2)$ gauge boson $\gamma \equiv (B, A^A)$ insertion, is calculated.[16]

$$-i\Pi_\phi^H(p) = -\frac{1}{2}\left(i\Pi_\phi^{++}(p) - i\Pi_\phi^{--}(p)\right) \tag{2.34}$$

$$= iG \int \frac{d^4k}{(2\pi)^4} g^{\mu\nu} \frac{1}{2}\left(i\Delta_{\gamma\mu\nu}^{++}(k) + i\Delta_{\gamma\mu\nu}^{--}(k)\right) \tag{2.35}$$

$$\Pi_\phi^H(p) = -G \int \frac{d^4k}{(2\pi)^4} g^{\mu\nu} i\Delta_{\gamma\mu\nu}^F(k) \tag{2.36}$$

G is the recurring factor

$$\mathbb{1}G = \mathbb{1}Y_\phi^2 g_1^2 + t^A t^A g_2^2 = \mathbb{1}\frac{1}{4}\left(g_1^2 + 3g_2^2\right). \tag{2.37}$$

G depends on g_1 and g_2, i.e. the $U(1)$ and $SU(2)$ gauge couplings, respectively. The plus sign in line (2.35) comes from the minus of the CTP vertex. By replacing the statistical propagator with $\Delta_{\gamma\mu\nu}^F \equiv -g_{\mu\nu}\Delta_\gamma^F$ in Feynman gauge and inserting expressions from Section 1.5, Π_ϕ^H becomes

$$\Pi_\phi^H(p) = G \int \frac{d^4k}{(2\pi)^4} g^{\mu\nu} g_{\mu\nu}\, \pi\delta(k^2)\left(1 + 2f_-(|k^0|)\right) \tag{2.38}$$

in the plasma frame $\vec{u} = 0$. The 1 in $(1 + 2f(|.|))$ corresponds to the vacuum graph, is independent of any scale and therefore would vanish in dimensional regularization (dimreg). If it is not calculated in dimreg, this part would be absorbed by the mass renormalization δm_ϕ^2 as explained below.

$$\Pi_\phi^{H,vac}(p) = 0 \tag{2.39}$$

Therefore only the thermal part is of relevance:

$$\Pi_\phi^{H,T\neq 0}(p) = 4\,G \int \frac{d^4k}{(2\pi)^3}\delta(k^2)f_-(|k^0|) = \frac{1}{3}GT^2\,. \tag{2.40}$$

---

[16] The seagull has a symmetry factor of $\frac{1}{2}$.

The anti-hermitian part of the seagull diagram vanishes, since it cannot be cut, or since non-equal CPT indices would have to be considered at the same vertex:

$$\Pi_\phi^A(p) = \frac{1}{2}\left(i\Pi^> - i\Pi^<\right) = 0. \tag{2.41}$$

2.5.2 4-Higgs Diagram

The hermitian part can be calculated in an analogous way and becomes

$$\Pi_\phi^H(p) = \frac{1}{4}\lambda_\phi T^2. \tag{2.42}$$

The anti-hermitian part vanishes for the same reason as in case of the seagull.

$$\Pi_\phi^{\mathcal{A}}(p) = 0 \tag{2.43}$$

2.5.3 Sunset Diagram

The sunset diagram can be evaluated from

$$-i\Pi_\phi^{ab}(p) = -G\int \frac{\mathrm{d}^4k}{(2\pi)^4}(p+k)^\mu(p+k)^\nu i\Delta_\phi^{ab}(k)i\Delta_{\gamma\mu\nu}^{ab}(p-k) \tag{2.44}$$

$$i\Pi_\phi^H(p) = G\int \frac{\mathrm{d}^4k}{(2\pi)^4}(p+k)^\mu(p+k)^\nu$$
$$\frac{1}{2}\left(i\Delta_\phi^{++}(k)i\Delta_{\gamma\mu\nu}^{++}(p-k) - i\Delta_\phi^{--}(k)i\Delta_{\gamma\mu\nu}^{--}(p-k)\right). \tag{2.45}$$

By replacing $++$ and $--$ propagators with hermitian and statistical propagators and defining $\Delta_{\gamma\mu\nu} \equiv -g_{\mu\nu}\Delta_\gamma$ in Feynman gauge, this equation becomes

$$\Pi_\phi^H(p) = -G\int \frac{\mathrm{d}^4k}{(2\pi)^4}(p+k)^2\left(i\Delta_\phi^F(k)\Delta_\gamma^H(p-k) + \Delta_\phi^H(k)i\Delta_\gamma^F(p-k)\right). \tag{2.46}$$

With help of the tree-level functions from Section 1.5 in the plasma frame,

$$\Pi_\phi^H(p) = -\frac{G}{2}\int \frac{\mathrm{d}^4k}{(2\pi)^3}(p+k)^2\Bigg($$
$$\frac{\delta((p-k)^2 - \lambda^2)}{k^2}\left(1 + 2f_-(|p^0 - k^0|)\right)$$
$$+\frac{\delta(k^2)}{(p-k)^2 - \lambda^2}\left(1 + 2f_-(|k^0|)\right)\Bigg) \tag{2.47}$$

must be calculated. λ is a small mass for the gauge fields to regulate infrared divergences that come from multiple gauge boson scatterings at zero momentum. Later on, before physical observables are calculated, the gauge invariance is recovered by setting λ to zero. This means that the $\ln\lambda$ cancels in the limit $\lambda \to 0$ during the derivation of the RHN production rate. Other regulator prescriptions like for example dimreg are equivalent, but for technical reasons, mass regulation is preferred. Again, the terms proportional to 1 and f in $(1 + 2f(|.|))$ are referred to as vacuum and $T \neq 0$ terms respectively. In the vacuum limit, f becomes a Heaviside theta of minus the argument, see Equation (1.62), and hence it vanishes due to the absolute values.

26

One way to calculate the vacuum term is to calculate $\partial_{p^2}\Pi^{H,vac}$ in the plasma frame. ∂_{p^2} cancels possible UV divergences that would otherwise be absorbed by the mass renormalization $\Pi^{H,vac,ren} = \Pi^{H,vac} + \delta m_\phi^2$.

Since $\Pi^{H,vac}$ is independent of the plasma vector u, the d^4k is equivalent to $4\pi\, dk^0\, d|\vec{k}||\vec{k}|^2$ in this frame. The dk^0 may be integrated via the on-shell delta functions and $d|\vec{k}|$ integrates over the pole. However, the appearing p^2-constant terms are thrown away. Finally, this contribution results in

$$\Pi_\phi^{H,vac}(p) = \frac{G}{(2\pi)^2}p^2\left(\ln\left(\frac{\bar\Lambda}{\sqrt{|p^2-\lambda^2|}}\right) + const\right) + const \tag{2.48}$$

$$\Pi_\phi^{H,vac,ren}(p) = \frac{G}{(2\pi)^2}p^2\ln\left(\frac{\Lambda}{\sqrt{|p^2-\lambda^2|}}\right) \tag{2.49}$$

with $\bar\Lambda$ being an UV cutoff for $|\vec{k}|$. The "*const*" terms and the $\ln(\bar\Lambda)$ are absorbed by the mass and the wave function renormalization. Consequently, Λ is the renormalized finite and renormalization scheme dependent UV cutoff. For comparison, this diagram can also be calculated using dimreg. The same analytical structure then appears, except that $\bar\Lambda$ and Λ are replaced by the renormalization scale μ.

The thermal part is free of IR and UV divergences. Therefore, the fictitious gauge boson mass λ can be set to zero in the beginning. What remains is to evaluate Π in the plasma frame $\vec{u} = 0$. With a shift $k \to p - k$ in the second line of Equation (2.47), $\Pi^{H,T\neq 0}$ can be derived from

$$\Pi^{H,T\neq 0}(p) = -\frac{G}{(2\pi)^2}\int dk^0 d|\vec{k}||\vec{k}|^2 d\cos\angle(k,p)\left(\frac{(2p-k)^2+(p+k)^2}{(p-k)^2}\right)\delta(k^2)f_-(|k^0|). \tag{2.50}$$

$\angle(k,p)$ is the angle between $\vec{k}$ and $\vec{p}$. By integrating dk^0 using the delta function, the $d\cos\angle$ integral can be solved analytically. One ends up with the finite one-dimensional integral

$$\Pi^{H,T\neq 0}(p) = -\frac{1}{12}GT^2 - \frac{G}{(2\pi)^2}\frac{p^2}{|\vec{p}|}\int d|\vec{k}|f_-(|\vec{k}|)\sum_\pm \ln\left|\frac{p^2 \pm 2|\vec{k}|p^0 + 2|\vec{k}||\vec{p}|}{p^2 \pm 2|\vec{k}|p^0 - 2|\vec{k}||\vec{p}|}\right|, \tag{2.51}$$

which is solved numerically. The factor $-\frac{1}{12}$ plus the $\frac{1}{3}$ of the seagull diagram gives $\frac{1}{4}GT^2$, the literature value for the thermal or asymptotic mass of the Higgs in the high temperature limit. See for example [59] for a reference.

The spectral Higgs self-energy through the sunset diagram is given by

$$\Pi_\phi^A(p) = G\int\frac{d^4k}{(2\pi)^4}(p+k)^\mu(p+k)^\nu\frac{1}{2}\left(i\Delta_\phi^>(k)i\Delta_{\gamma\mu\nu}^>(p-k) - i\Delta_\phi^<(k)i\Delta_{\gamma\mu\nu}^<(p-k)\right) \tag{2.52}$$

$$= -G\int\frac{d^4k}{(2\pi)^4}(p+k)^2 2\Delta_\phi^{\mathcal{A}}(k)\Delta_\gamma^{\mathcal{A}}(p-k)\left(1 + f_-(u\cdot k) + f_-(u\cdot(p-k))\right) \tag{2.53}$$

$$= -\frac{G}{2}\int\frac{d^4k}{(2\pi)^2}(p+k)^2\delta(k^2)\delta((p-k)^2 - \lambda^2)\text{sign}(k^0)\text{sign}(p^0-k^0)$$
$$(1 + f_-(u\cdot k) + f_-(u\cdot(p-k))). \tag{2.54}$$

After Equation (2.53) is obtained, the result of Chapter 2.4 could be directly used. There, such an integral is evaluated for the most general case. Here, however, the ordinary way is shown. Again, λ is introduced to regulate infrared divergences – not in $\Pi_\phi^{\mathcal{A}}$ which is finite – but in the right-handed neutrino self-energy later. Using the deltas, $(p+k)^2$ becomes $2p^2 + O(\lambda)$. $d|\vec{k}|$ integrates out the $\delta(k^2)$, and $d\cos\angle(k,p)$ integrates the other delta function. Hence, Π_ϕ^A is obtained from

$$\Pi_\phi^A(p) = -\frac{G}{8\pi}\frac{p^2}{|\vec{p}|}\int_B dk^0\text{sign}(k^0)\text{sign}(p^0-k^0)\left(1 + f_-(k^0) + f_-(p^0-k^0)\right) \tag{2.55}$$

in the plasma frame. B is the induced integration domain

$$B = \{|\cos \angle| \leq 1\} = \left\{ \left| \frac{2p^0 k^0 - p^2 + \lambda^2}{2|\vec{p}|k^0} \right| \leq 1 \right\} \tag{2.56}$$

$$= \begin{cases} k_-^0 \leq k^0 \mathrm{sign}(p^0(p^2 - \lambda^2)) \leq k_+^0 & , p^2 \geq 0 \\ |k_+^0| \leq k^0 \mathrm{sign}p^0 \vee k^0 \mathrm{sign}p^0 \leq -|k_-^0| & , p^2 < 0 \end{cases} \tag{2.57}$$

with

$$k_\pm^0 = \frac{|p^2 - \lambda^2|}{2(|p^0| \mp |\vec{p}|)} = \mathrm{sign}(p^2)\frac{1}{2}(|p^0| \pm |\vec{p}|) + O(\lambda^2). \tag{2.58}$$

The 1 in $(1 + f + f)$ in (2.55) does not represent the vacuum part alone, since the distribution functions do not need to have positive arguments. However, the relation

$$\frac{1}{2} + f_-(E) = \frac{1}{2}\mathrm{sign}(E) + \mathrm{sign}(E)f_-(|E|) \tag{2.59}$$

is found to hold using Equation (1.61), and Equation (2.55) can be decomposed into a thermal and a vacuum part. The latter is

$$\Pi_\phi^{A,vac}(p) = -\frac{G}{16\pi}\frac{p^2}{|\vec{p}|} \int_B dk^0 \left(\mathrm{sign}(k^0) + \mathrm{sign}(p^0 - k^0) \right). \tag{2.60}$$

If p^0 is a fixed positive number, the sign functions are only non-vanishing if $0 \leq k^0 \leq p^0$ such that B reduces to $p^2 \geq \lambda^2$. $p^0 < 0$ exhibits the same B, but with $p^0 \leq k^0 \leq 0$. This is the expected behavior in vacuum, known as the kinematic constraint. Hence, the vacuum part becomes

$$\Pi_\phi^{A,vac}(p) = -\frac{G}{8\pi}\frac{p^2}{|\vec{p}|} \left(k_+^0 - k_-^0 \right) \theta(p^2 - \lambda^2)\mathrm{sign}(p^0) \tag{2.61}$$

$$= -\frac{G}{8\pi}(p^2 - \lambda^2)\theta(p^2 - \lambda^2)\mathrm{sign}(p^0) = -\frac{G}{8\pi}p^2\theta(p^2 - \lambda^2)\mathrm{sign}(p^0) + O(\lambda^2). \tag{2.62}$$

However, if the temperature is non-zero, a particle can take energy from the thermal bath such that a decay, which is kinematically forbidden in vacuum, becomes possible. This can be verified with $\lambda = 0$ by

$$\Pi_\phi^{A,T\neq 0}(p) = -\frac{G}{8\pi}\frac{p^2}{|\vec{p}|} \int_B dk^0 \left(\mathrm{sign}(p^0 - k^0)f_-(|k^0|) + \mathrm{sign}(k^0)f_-(|p^0 - k^0|) \right) \tag{2.63}$$

$$= \frac{G}{4\pi}\frac{p^2}{|\vec{p}|} \left((|k_+^0| - k_-^0) - T\ln\left| \frac{1 - e^{\frac{|k_+^0|}{T}}}{1 - e^{\frac{k_-^0}{T}}} \right| \right) \mathrm{sign}(p^0) \tag{2.64}$$

$$= \begin{cases} \frac{G}{4\pi}\frac{p^2}{|\vec{p}|} \left(\theta(p^0)|\vec{p}| - T\ln\left| \frac{1 - e^{\frac{p^0 + |\vec{p}|}{2T}}}{1 - e^{\frac{p^0 - |\vec{p}|}{2T}}} \right| \right) & , p^2 > 0 \\ \frac{G}{4\pi}\frac{p^2}{|\vec{p}|} \left(p^0 - T\ln\left| \frac{1 - e^{\frac{p^0 + |\vec{p}|}{2T}}}{1 - e^{\frac{-p^0 + |\vec{p}|}{2T}}} \right| \right) & , p^2 < 0 \end{cases}. \tag{2.65}$$

The sum of the Equations $(2.62) + (2.65)$ results in the same as what would be obtained by using the K_{--} from Section 2.4. The $\Pi_\phi^{A,T\neq 0}(p)$ is non-vanishing for positive and negative p^2, and it is anti-symmetric in p^0, which is the expected behavior. At least on-shell, $\Pi_\phi^{\mathcal{A}}$ is proportional to the Higgs's rate of decay. Hence, it should be positive for positive p^0. Here, the off-shell vacuum spectral self-energy as well as the thermal one is negative for positive p^0 and for any positive p^2. However, the leading order spectral Higgs self-energy vanishes at the mass shell $p^2 = 0$.[17]

---

[17] If the Higgs has a non-vanishing tree-level mass, only the vacuum spectral Higgs self-energy obtained from the above diagram vanishes on-shell. Nevertheless, the thermal correction is even negative for positive p^0. Related to this issue are the discussions in the Sections 3.5.2.3 and 3.5.4.

2.5.4 Top-Loop Diagram

The Higgs self-energy via the top-quark loop is given by

$$-i\Pi^{ab}_\phi(p) = h_t^2 \text{tr}_c[\mathbb{1}_c] \int \frac{\mathrm{d}^4 k}{(2\pi)^4} \text{tr}\left[P_L i\mathcal{S}^{ba}_t(-k) P_R i\mathcal{S}^{ab}_t(p-k)\right], \tag{2.66}$$

where tr_c is the color trace and a, b are CTP indices. By defining $g_c = \text{tr}_c[\mathbb{1}_c] = 3$, i.e. the number of colors in SU(3), and extracting the Dirac structure of $\mathcal{S}_t(-k) \equiv -\slashed{k}\Delta_t(k)$, the self-energy can be obtained from

$$-i\Pi^{ab}_\phi(p) = -g_c h_t^2 \int \frac{\mathrm{d}^4 k}{(2\pi)^4} 2(p-k) \cdot k\, i\Delta^{ab}_t(k) i\Delta^{ab}_t(p-k). \tag{2.67}$$

Inserting this into $\Pi^H = \frac{1}{2}(\Pi^{++} - \Pi^{--})$ results in the same workflow as for the sunset diagram. The UV renormalized hermitian Higgs self-energy becomes

$$\Pi^{H,vac,ren}_\phi(p) = -\frac{g_c h_t^2}{2(2\pi)^2} p^2 \ln\left(\frac{2\Lambda}{\sqrt{|p^2 - 4\lambda^2|}}\right) \tag{2.68}$$

$$\Pi^{H,T\neq0}_\phi(p) = \frac{g_c h_t^2}{12} T^2 - \frac{g_c h_t^2}{2(2\pi)^2} \frac{p^2}{|\vec{p}|} \int \mathrm{d}|\vec{k}| f_+(|\vec{k}|) \sum_\pm \ln\left|\frac{p^2 \pm 2|\vec{k}|p^0 + 2|\vec{k}||\vec{p}|}{p^2 \pm 2|\vec{k}|p^0 - 2|\vec{k}||\vec{p}|}\right| \tag{2.69}$$

with λ being a small infrared regulating top-quark mass and Λ being the finite renormalized UV cutoff. λ is set to zero for $T \neq 0$. The spectral self-energy is obtained from (2.67) by

$$\Pi^A_\phi(p) = h_t^2 g_c \int \frac{\mathrm{d}^4 k}{(2\pi)^4} (p-k) \cdot k\, \left(i\Delta^>_t(k) i\Delta^>_t(p-k) - i\Delta^<_t(k) i\Delta^<_t(p-k)\right) \tag{2.70}$$

$$= 4h_t^2 g_c \int \frac{\mathrm{d}^4 k}{(2\pi)^4} (p-k) \cdot k\, \Delta^{\mathcal{A}}_t(k) \Delta^{\mathcal{A}}_t(p-k) \left(1 - f_+(u \cdot k) - f_+(u \cdot (p-k))\right). \tag{2.71}$$

Through comparison with (2.53), note that $(p-k) \cdot k = \frac{1}{2}p^2$ and $(p+k)^2 = 2p^2$, $-G$ can be identified with $\frac{g_c}{2} h_t^2$ under exchange of $f_- \leftrightarrow -f_+$. Consequently, the following calculation can be copied from above. However, the vacuum k^0 boundary conditions are different, since here two particles have the regulating mass λ. The top contribution is given by

$$\Pi^{A,vac}_\phi(p) = g_c \frac{h_t^2}{16\pi} p^2 \theta(p^2 - 4\lambda^2) \text{sign}(p^0) \tag{2.72}$$

$$\Pi^{A,T\neq0}_\phi(p) = -g_c \frac{h_t^2}{8\pi} \frac{p^2}{|\vec{p}|} \left((|k_+^0| - k_-^0) - T\ln\left|\frac{1 + e^{\frac{|k_+^0|}{T}}}{1 + e^{\frac{k_-^0}{T}}}\right|\right) \text{sign}(p^0) \tag{2.73}$$

$$= \begin{cases} -g_c \frac{h_t^2}{8\pi} \frac{p^2}{|\vec{p}|} \left(\theta(p^0)|\vec{p}| - T\ln\left|\frac{1 + e^{\frac{p^0 + |\vec{p}|}{2T}}}{1 + e^{\frac{p^0 - |\vec{p}|}{2T}}}\right|\right) & , p^2 > 0 \\[4mm] -g_c \frac{h_t^2}{8\pi} \frac{p^2}{|\vec{p}|} \left(p^0 - T\ln\left|\frac{1 + e^{\frac{p^0 + |\vec{p}|}{2T}}}{1 + e^{\frac{-p^0 + |\vec{p}|}{2T}}}\right|\right) & , p^2 < 0 \end{cases}. \tag{2.74}$$

This is the same result as what can be found if the K_{++} from Section 2.4 is considered. The $\Pi^{\mathcal{A}}_\phi$ vanishes on-shell at $p^2 = 0$, but for positive p^2 and p^0, both expressions (2.62) and (2.74) are positive.[18]

---

[18] If the Higgs has a non-vanishing tree-level mass, the vacuum and thermal contributions of this diagram still vanish on-shell due to the numerator algebra.

2.5.5 Summary

After adding all contributions together and suppressing the superscript *ren*, the 1-loop Higgs self-energy is

$$\Pi_\phi^{H,vac}(p) = \frac{G}{(2\pi)^2}p^2\ln\left(\frac{\Lambda}{\sqrt{|p^2-\lambda^2|}}\right) - \frac{g_c h_t^2}{2(2\pi)^2}p^2\ln\left(\frac{2\Lambda}{\sqrt{|p^2-4\lambda^2|}}\right) + O\left(\lambda^2\right) \tag{2.75}$$

$$= \frac{G}{(2\pi)^2}p^2\ln\left(\frac{\Lambda}{\lambda}\right) - \frac{g_c h_t^2}{2(2\pi)^2}p^2\ln\left(\frac{\Lambda}{\lambda}\right) + O\left(\frac{p^4}{\lambda^4}\right) + O(\lambda^2) \tag{2.76}$$

$$\Pi_\phi^{H,T\neq0}(p) = \frac{1}{4}GT^2 + \frac{g_c h_t^2}{12}T^2 + \frac{1}{4}\lambda_\phi T^2 - \frac{G}{(2\pi)^2}\frac{p^2}{|\vec{p}|}I_{2-}(p^0,|\vec{p}|) - \frac{g_c h_t^2}{2(2\pi)^2}\frac{p^2}{|\vec{p}|}I_{2+}(p^0,|\vec{p}|) \tag{2.77}$$

$$\Pi_\phi^{A,vac}(p) = -\frac{G}{8\pi}p^2\theta(p^2-\lambda^2)\text{sign}(p^0) + g_c\frac{h_t^2}{16\pi}p^2\theta(p^2-4\lambda^2)\text{sign}(p^0) + O(\lambda^2) \tag{2.78}$$

$$\Pi_\phi^{A,T\neq0}(p) = \begin{cases} \frac{G}{4\pi}\frac{p^2}{|\vec{p}|}\left(\theta(p^0)|\vec{p}| - T\ln\left|\frac{1-e^{\frac{p^0+|\vec{p}|}{2T}}}{1-e^{\frac{p^0-|\vec{p}|}{2T}}}\right|\right) & ,p^2>0 \\ \frac{G}{4\pi}\frac{p^2}{|\vec{p}|}\left(p^0 - T\ln\left|\frac{1-e^{\frac{p^0+|\vec{p}|}{2T}}}{1-e^{\frac{-p^0+|\vec{p}|}{2T}}}\right|\right) & ,p^2<0 \end{cases}$$

$$+ \begin{cases} -g_c\frac{h_t^2}{8\pi}\frac{p^2}{|\vec{p}|}\left(\theta(p^0)|\vec{p}| - T\ln\left|\frac{1+e^{\frac{p^0+|\vec{p}|}{2T}}}{1+e^{\frac{p^0-|\vec{p}|}{2T}}}\right|\right) & ,p^2>0 \\ -g_c\frac{h_t^2}{8\pi}\frac{p^2}{|\vec{p}|}\left(p^0 - T\ln\left|\frac{1+e^{\frac{p^0+|\vec{p}|}{2T}}}{1+e^{\frac{-p^0+|\vec{p}|}{2T}}}\right|\right) & ,p^2<0 \end{cases} \tag{2.79}$$

with the numerical integrals

$$I_{2\pm}(p^0,|\vec{p}|) = \int \text{d}|\vec{k}|f_\pm(|\vec{k}|)\sum_{\pm'}\ln\left|\frac{p^2 \pm' 2|\vec{k}|p^0 + 2|\vec{k}||\vec{p}|}{p^2 \pm' 2|\vec{k}|p^0 - 2|\vec{k}||\vec{p}|}\right|. \tag{2.80}$$

For precise numerics, $I_{2\pm}(p^0,|\vec{p}|)$ may be written as a function of only one argument. Details on this can be found in Chapter 4.1.

2.6 Lepton Self-Energy

At leading order in the gauge couplings, a left-handed lepton l can emit and reabsorb a $SU(2)$ and $U(1)$ gauge boson, while a right-handed lepton R couples only to $U(1)$. Hence, their self-energies up to this order is given by the sunset diagram in Figure 2.2.

$$-i\Sigma_{l/R} = $$

Figure 2.2: Sunset contribution of the lepton self-energy. For leptons of left chirality l, wavy lines indicate $U(1)$ and $SU(2)$ gauge bosons, while for right chirality leptons R, only $U(1)$ has to be considered.

This can be evaluated by following the same steps as in Section 2.5.3 from

$$-i\Sigma_{l/R}^{ab}(p) = -G_{l/R} \int \frac{\mathrm{d}^4 k}{(2\pi)^4} \gamma^\mu P_{L/R} i S_{l/R}^{ab}(p-k) P_{R/L} \gamma^\nu i \Delta_{\mu\nu}^{ab}(k) \tag{2.81}$$

with $G_{l/R}$ being

$$G_l = \mathbb{1} Y_L^2 g_1^2 + t^A t^A g_2^2 = \mathbb{1} \frac{1}{4}(g_1^2 + 3g_2^2) \equiv \mathbb{1} G \tag{2.82}$$

$$G_R = Y_R^2 g_1^2 = g_1^2 \,. \tag{2.83}$$

The $\Sigma_{l/R}$ decomposes into its Lorenz 4-vector via $\Sigma_{l/R} = P_{R/L}\gamma_\mu \Sigma_{l/R}^\mu$. Due to Lorenz invariance, (2.81) can only be proportional to $\slashed{u}$ and $\slashed{p}$. This means that it can be evaluated from the traced self-energies

$$\Sigma^\mu = (p^\mu, u^\mu) \cdot \mathrm{Gram}^{-1}(p, u) \cdot \begin{pmatrix} p \cdot \Sigma \\ u \cdot \Sigma \end{pmatrix} \tag{2.84}$$

$$= \frac{1}{2}(p^\mu, u^\mu) \cdot \mathrm{Gram}^{-1}(p, u) \cdot \begin{pmatrix} \mathrm{tr}[\slashed{p}\Sigma] \\ \mathrm{tr}[\slashed{u}\Sigma] \end{pmatrix}, \tag{2.85}$$

where the inverse Gram matrix of p and u appears and the l/R subscript is omitted for simplicity. The wave-function and mass renormalized vacuum hermitian self-energy with a small gauge boson mass λ can be evaluated as

$$p \cdot \Sigma_{l/R}^{H,vac}(p) = \frac{G_{l/R}}{8\pi^2} p^2 \ln \frac{\sqrt{|p^2 - \lambda^2|}}{\Lambda} \tag{2.86}$$

$$u \cdot \Sigma_{l/R}^{H,vac}(p) = \frac{p \cdot u}{p^2} p \cdot \Sigma_{l/R}^{H,vac}(p) \,, \tag{2.87}$$

but the thermal part needs additional care. For later convenience, $T \neq 0$ needs to be separated into the hard thermal loop (HTL) and a remaining $\overline{T \neq 0}$ part. The term HTL means hard thermal loop momenta, i.e. it refers to the dominant terms in the limit $|\vec{k}| \gg \{T, p^0, |\vec{p}|\}$. This splitting is given by a partial fractioning in $|\vec{k}|$, which, due to k^2 being fixed, is equivalent to a partial fractioning in $p \cdot k$ while holding the partition functions fixed. This is shown for $p \cdot \Sigma^{H,T\neq 0}(p)$ in more detail here.

$$p \cdot \Sigma_{l/R}^{H,T\neq 0}(p) = 4\pi G_{l/R} \int \frac{\mathrm{d}^4 k}{(2\pi)^4} \frac{\delta(k^2)}{(p-k)^2} \left(-p \cdot k f_+(|u \cdot k|) + (p^2 - p \cdot k) f_-(|u \cdot k|)\right) \tag{2.88}$$

$$= G_{l/R} \int \frac{\mathrm{d}^4 k}{(2\pi)^3} \delta(k^2) \left(\underbrace{(f_+(|u \cdot k|) + f_-(|u \cdot k|))}_{HTL} + \underbrace{\frac{p^2}{p^2 - p \cdot k}(-f_+(|u \cdot k|) + f_-(|u \cdot k|))}_{\overline{T \neq 0}} \right) \tag{2.89}$$

By integrating the delta function with dk^0, the $d\cos\angle(k,p)$ integral in the plasma frame can be evaluated:

$$p\cdot\Sigma_{l/R}^{H,T\neq0}(p)=\frac{G_{l/R}}{(2\pi)^2}\left(I_3^{HTL}+\frac{p^2}{4|\vec{p}|}(-I_{2+}+I_{2-})(p^0,|\vec{p}|)\right),\tag{2.90}$$

with

$$I_3^{HTL}=2\int d|\vec{k}|\,|\vec{k}|(f_+(|\vec{k}|)+f_-(|\vec{k}|))=\frac{\pi^2}{2}T^2\,.\tag{2.91}$$

The $I_{2\pm}$ is already defined in (2.80) and account here for the $p\cdot\overline{\Sigma}^{H,T\neq0}(p)$ contribution. Analogously, the other contribution is found to be

$$u\cdot\Sigma_{l/R}^{H,T\neq0}(p)=\frac{G_{l/R}}{8\pi^2|\vec{p}|}\left(\ln\left|\frac{p^0+|\vec{p}|}{p^0-|\vec{p}|}\right|I_3^{HTL}+\overline{I_3}^{T\neq0}(p^0,|\vec{p}|)+p^0 I_{2-}(p^0,|\vec{p}|)\right)\tag{2.92}$$

with

$$\overline{I_3}^{T\neq0}(p^0,|\vec{p}|)=\int d|\vec{k}|\,|\vec{k}|\ln\left|\frac{(2|\vec{k}|)^2-(p^0-|\vec{p}|)^2}{(2|\vec{k}|)^2-(p^0+|\vec{p}|)^2}\right|(f_+(|\vec{k}|)+f_-(|\vec{k}|))\,.\tag{2.93}$$

The integral in (2.93) can be calculated numerically.
The anti-hermitian part is decomposed into

$$p\cdot\Sigma_{l/R}^{\mathscr{A}}(p)=\frac{G_{l/R}}{16\pi}\frac{p^2}{|\vec{p}|}I_0(p^0,|\vec{p}|)\tag{2.94}$$

$$u\cdot\Sigma_{l/R}^{\mathscr{A}}(p)=\frac{G_{l/R}}{8\pi}\frac{1}{|\vec{p}|}I_1(p^0,|\vec{p}|)\,.\tag{2.95}$$

The I integrals are defined as

$$I_0(p^0,|\vec{p}|)=\int_B dk^0\text{sign}(k^0)\text{sign}(p^0-k^0)\left(1-f_+(k^0)+f_-(p^0-k^0)\right)\tag{2.96}$$

$$=(I_0^{vac}+I_0^{T\neq0})(p^0,|\vec{p}|)\tag{2.97}$$

$$I_1(p^0,|\vec{p}|)=\int_B dk^0 k^0\text{sign}(p^0-k^0)\left(1-f_+(k^0)+f_-(p^0-k^0)\right)\tag{2.98}$$

$$=(I_1^{vac}+I_1^{T\neq0})(p^0,|\vec{p}|)=(I_1^{vac}+\overline{I_1}^{T\neq0}+I_1^{HTL})(p^0,|\vec{p}|)\tag{2.99}$$

and evaluate to

$$I_0^{vac}(p^0,|\vec{p}|)=\theta(p^2)|\vec{p}|\text{sign}(p^0)\tag{2.100}$$

$$I_0^{T\neq0}(p^0,|\vec{p}|)=-\theta(p^2)\theta(p^0)2|\vec{p}|-\theta(-p^2)(p^0+|\vec{p}|)+T\ln\left|\frac{1-e^{\frac{p^0+|\vec{p}|}{T}}}{1-e^{\frac{p^0-|\vec{p}|}{T}}}\right|\tag{2.101}$$

$$I_1^{vac}(p^0,|\vec{p}|)=\theta(p^2)\frac{|p^0||\vec{p}|}{2}\tag{2.102}$$

$$\overline{I_1}^{T\neq0}(p^0,|\vec{p}|)=-\theta(p^2)\frac{|p^0||\vec{p}|}{2}-\theta(-p^2)\frac{(p^0)^2}{2}$$
$$+\Re\left[xT\ln\left|\frac{1+e^{\frac{x}{T}}}{1-e^{\frac{x-p^0}{T}}}\right|+T^2\text{Li}_2\left(-e^{\frac{x}{T}}\right)-T^2\text{Li}_2\left(e^{\frac{x-p^0}{T}}\right)\right]\Bigg|_{x=\frac{1}{2}(p^0-|\vec{p}|)}^{x=\frac{1}{2}(p^0+|\vec{p}|)}\tag{2.103}$$

$$I_1^{HTL}(p^0,|\vec{p}|)=\theta(-p^2)\frac{\pi^2}{2}T^2\,.\tag{2.104}$$

The Li_2 is the dilogarithm which was found in Equation (2.33) of Section 2.4.

3

Right-Handed Neutrino Rate

3.1 Preliminaries

In this section, Boltzmann type equations for the right-handed neutrino distribution functions are derived. These can be obtained from the Kadanoff-Baym equations within several approximations. The present model for Leptogenesis delivers close-to-equilibrium properties. First, spatial homogeneity and isotropy can be assumed. Hence, the spatial gradients of (1.43) vanish in Wigner space. Second, all SM particles are assumed to be in thermal equilibrium.[19] For those particles, the time gradients vanish. However, the right-handed neutrinos are gauge singlets and therefore have a much smaller equilibration rate. For them, even a large deviation from thermal equilibrium should only equilibrate slowly, such that including time gradients to first order is assumed to be enough. Expanded up to first order in gradients, the Kadanoff-Baym equations for the right-handed neutrinos are

$$\left(\slashed{k} - m_N - \Sigma_N^H + i \frac{1}{2} \gamma^0 \partial_t \right) \slashed{S}_N^{</>} - \Sigma_N^{</>} \slashed{S}_N^H = \mathcal{C}_N = \frac{1}{2} \left(\Sigma_N^> \slashed{S}_N^< - \Sigma_N^< \slashed{S}_N^> \right) . \tag{3.1}$$

The expression $\Sigma_N^H \slashed{S}_N^{</>}$ is sometimes called the non-local contribution to the mass terms. Hence, this causes dispersive effects. The term $\Sigma_N^{</>} \slashed{S}_N^H$ changes the width of the particles. Finally, the collision term $\mathcal{C}_N$ contains the usual gain and loss terms.

To obtain the production rate for the right-handed neutrinos, the hermitian conjugate is first added:

$$i \frac{1}{2} \partial_t \left\{ \gamma^0, \slashed{S}_N^{</>} \right\} + \left[\slashed{k} - m_N - \Sigma_N^H, \slashed{S}_N^{</>} \right] - \left[\Sigma_N^{</>}, \slashed{S}_N^H \right] = \mathcal{C}_N + \mathcal{C}_N^\dagger . \tag{3.2}$$

Since (3.1) is still a matrix in flavor space, the hermitian conjugation also acts in the flavor space. When substituting the tree-level neutrino propagator (1.73) with some general distribution function[20] [21] for each

---

[19] A small deviation from equilibrium is caused by the Hubble expansion.

[20] They must still respect the fact that the N_i are Majorana particles and hence $f_N(p^0) + f_N(-p^0) = 1$. See the comment for (1.61).

[21] Don't get confused with the different notions for the distribution functions $f_N(t, p)$ and $f_N(t, |\vec{p}|)$. $f_N(t, p)$ equals to $f_N(t, p^0, |\vec{p}|)$ due to homogeneity and isotropy. However, $f_N(t, p^0, |\vec{p}|)$ equals to $f_N(t, |\vec{p}|)$ only if p^0 is fixed at the mass-shell.

flavor, one observes that the time evolution of those can be obtained by

$$-\int \frac{\mathrm{d}p^0}{2\pi}\operatorname{sign}(p^0)\frac{1}{4}\operatorname{tr}_{Dirac}\left[\frac{1}{2}\partial_t\left\{\gamma^0, i\slashed{S}_N^<(p)\right\}\right] = \int \frac{\mathrm{d}p^0}{2\pi}\partial_t 2p^0 f_N(t,p)\pi\delta(p^2 - m_N^2) \tag{3.3}$$

$$= \sum_{p^0 = \pm\sqrt{|\vec{p}|^2 + m_N^2}} \operatorname{sign}(p^0)\frac{1}{2}\partial_t f_N(t,p) \tag{3.4}$$

$$= \partial_t f_N(t, |\vec{p}|). \tag{3.5}$$

Hence, the same procedure has to be applied to the other terms in (3.2). For simplicity, dispersive effects are ignored. Those are caused by the commutator terms. Only the production via scatterings and decay processes is included. The rate is then given by

$$\partial_t f_N(t, |\vec{p}|) = -\frac{1}{4}\int \frac{\mathrm{d}p^0}{2\pi}\operatorname{sign}(p^0)\operatorname{tr}[\mathcal{C}_N(p) + \mathcal{C}_N^\dagger(p)]. \tag{3.6}$$

Under the assumption that possible off-diagonal correlations in the neutrino propagator are negligible and that flavor oscillations are rapid enough to not give coherent contributions, a flavor diagonal basis can be chosen. This is the case if the mass splitting between different neutrino masses corresponding to different flavors is large enough.

Since the medium corrections for the RHN propagator and its self-energy are proportional to $|Y^2|$, tree-level propagators can be inserted for $\slashed{S}_N$ up to this order.

$$\partial_t f_N(t, |\vec{p}|) = \frac{1}{4}\int \frac{\mathrm{d}p^0}{2\pi}\operatorname{sign}(p^0)\operatorname{tr}[i\Sigma_N^>(p)i\slashed{S}_N^<(p) - i\Sigma_N^<(p)i\slashed{S}_N^>(p)] \tag{3.7}$$

$$= \frac{1}{2}\int \frac{\mathrm{d}p^0}{2\pi}\operatorname{sign}(p^0)\operatorname{tr}\left[\left(i\Sigma_N^>(p)(-f_N(t,p)) - i\Sigma_N^<(p)(1 - f_N(t,p))\right)\slashed{S}_N^{\mathcal{A}}(p)\right] \tag{3.8}$$

Lepton and Higgs are assumed to be in thermal equilibrium such that Σ_N satisfies the KMS relation (1.56) and Equations (1.57) and (1.58) can be used:[22]

$$\partial_t f_N(t, |\vec{p}|) = \int \frac{\mathrm{d}p^0}{2\pi}\operatorname{sign}(p^0)\operatorname{tr}[\Sigma_N^{\mathcal{A}}(p)\slashed{S}_N^{\mathcal{A}}(p)]$$
$$\left((1 - f_N^{eq}(p^0))(-f_N(t,p)) + f_N^{eq}(p^0)(1 - f_N(t,p))\right). \tag{3.9}$$

Here, the structure of the collision term in form of gain and loss terms known from Boltzmann equations becomes obvious. With (1.74) the $\mathrm{d}p^0$ integral is solved:

$$\partial_t f_N(t, |\vec{p}|) = -\int \frac{\mathrm{d}p^0}{2\pi}\operatorname{tr}[\slashed{p}\Sigma_N^{\mathcal{A}}(p)]\pi\delta(p^2 - m_N^2)\underbrace{\left(f_N(t,p) - f_N^{eq}(p^0)\right)}_{\delta f_N(t,p)} \tag{3.10}$$

$$= -\sum_{p^0 = \pm\sqrt{\vec{p}^2 + m_N^2}} \frac{1}{4|p^0|}\operatorname{tr}[\slashed{p}\Sigma_N^{\mathcal{A}}(p)]\delta f_N(t,p) \tag{3.11}$$

$$\partial_t f_N(t, |\vec{p}|) = -\frac{1}{2p^0}\operatorname{tr}[\slashed{p}\Sigma_N^{\mathcal{A}}(p)]\delta f_N(t,p)\Big|_{p^0 = \sqrt{|\vec{p}|^2 + m_N^2}}. \tag{3.12}$$

---

[22] Up to order $|Y^2|$ there are only self-energy diagrams that include equilibrated particles. Especially there is no back reaction diagram that contains the right-handed neutrino itself.

The last step uses the symmetry $p^0 \leftrightarrow -p^0$ of f and $\not{\Sigma}$ for Majorana particles N. At this point, it is intuitive to introduce the differential production rate Γ

$$\Gamma_N(|\vec{p}|) = \frac{1}{2|p^0|}\text{tr}\big[\not{p}\Sigma_N^{\mathcal{A}}(p)\big]\Big|_{p^2=m_n^2}. \tag{3.13}$$

Equation (3.12) is a first order differential equation for each mode $|\vec{p}|$ with the solution

$$f_N(t,|\vec{p}|) = \delta f_N(t_0,p)e^{-\Gamma_N(|\vec{p}|)(t-t_0)} + f_N^{eq}(|p^0|)\Big|_{p^2=m_N^2}. \tag{3.14}$$

For ease of comparison with reference [59], the total production rate is defined at zero initial abundance by integrating (3.12) over all $\vec{p}$:

$$\gamma_N = 2\int\frac{\text{d}^3\vec{p}}{(2\pi)^3}\partial_t f_N(t,\vec{p}) = \frac{4}{(2\pi)^2}\int\text{d}|\vec{p}||\vec{p}|^2 f_N^{eq}(p^0)\Gamma_N(|\vec{p}|) \tag{3.15}$$

$$= \frac{2}{(2\pi)^2}\int\text{d}|\vec{p}|\frac{|\vec{p}|^2}{|p^0|}f_N^{eq}(|p^0|)\text{tr}\big[\not{p}\Sigma_N^{\mathcal{A}}(p)\big]\Big|_{p^2=m_N^2}. \tag{3.16}$$

This is approximately the production rate of singlet Majorana neutrinos in the weak washout regime.

3.2 *LO* versus *NLO* in Perturbation Theory and 2PI Formalism

According to (3.16), the differential production rate of right-handed Majorana neutrinos within an equilibrated plasma is proportional to its anti-hermitian self-energy: $\text{tr}\big[\not{p}\Sigma_N^{\mathcal{A}}(p)\big]$. To leading order (*LO*) in perturbation theory, this is given by the processes $N \leftrightarrow l\phi$ and $N \leftrightarrow \bar{l}\bar{\phi}$ to second order in Yukawa couplings Y. However, those are exponentially suppressed for $m_N \ll T$, i.e. the ultra-relativistic regime. Hence, next to leading order (*NLO*) effects should be included. In the ultra-relativistic limit $\frac{m_N}{T} \to 0$ above perturbative *LO* effects vanish and the former *NLO* reduces to the new *LO*.

The perturbative *NLO* is regarded as the sum of 2-loop diagrams that give the wave-function and vertex corrections to the 1-loop case.

The perturbative wave-function corrections contain logarithmically enhanced contributions that diverge for massless neutrinos. Those divergences should be resummed into full propagators, which then also account for the screening induced by the thermal plasma. Hence, at least the 2PI formalism should be used in the ultra-relativistic regime and limit. The perturbative *LO* contribution and the wave-function corrections are then contained within the 2PI *LO*, i.e. the 1-loop RHN self-energy.

The vertex correction however is included in the 2PI *NLO*, i.e. the 2-loop self-energy, or in terms of the effective action at 3-loop order. For a self-consistent description of an effective action up to 3-loop order, the 3PI formalism should be used according to [79]. The 3PI effective action, on the other hand, also includes full 3-vertices. Those 3-point functions are basically determined by a leader resummation [60]. Nevertheless, the present investigation shows numerically that the perturbative 2-loop vertex correction is already finite and does not provide logarithmically enhanced contributions which otherwise would have to be resummed. This does not clarify the question of whether full 3-vertices give sizable corrections to the perturbative case, but at least the perturbative vertex correction does not demand a resummation.

Consequently, the *LO* and *NLO* neutrino production rate is determined by the RHN self-energy which appears in the 2PI approach up to 2-loop order by the following sum of diagrams:

Figure 3.1: 2PI contributions to the neutrino production rate. Particles in the loops are left-handed leptons and Higgs, and the wavy line indicates $U(1)$ and $SU(2)$ gauge bosons. The double lines represent full propagators, and the external legs are understood to be amputated.

Those terms are calculated using several approximations in the next sections. In particular, the full propagators are coupling expanded step by step, as far as non-divergent and physically reasonable results are obtained. This means that the final *LO* and *NLO* results are small coupling results of the 2PI formalism and hence valid in the ultra-relativistic limit up to the non-relativistic limit. Furthermore, for $m_N \gg T$ the results are valid up to *NLO* in perturbation theory.

3.3   Perturbative *LO* Result

As explained in the previous section, the perturbative leading order contribution to the neutrino production rate is given by the interferences of the processes $N \leftrightarrow l\phi$ and $N \leftrightarrow \bar{l}\bar{\phi}$. Via the optical theorem, those are contained in the imaginary part of
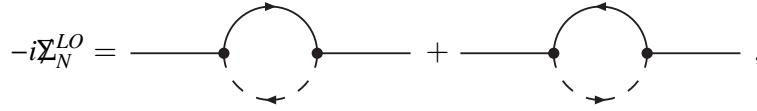
Figure 3.2: The *LO* neutrino self-energy: The particles in the loop are lepton and Higgs doublets.

which, in the CTP formalism, corresponds to the anti-hermitian or spectral part of the RHN self-energy. The tree-level neutrino self-energy can be evaluated from

$$-i\Sigma_N^{LO,ab}(p) = -g_w|Y|^2 \int \frac{\mathrm{d}^4 k}{(2\pi)^4} \left(P_R i \slashed{S}_l^{ab}(k) P_L i \Delta_\phi^{ab}(p-k) + P_L i \slashed{S}_l^{ab}(k) P_R i \Delta_\phi^{ab}(p-k) \right) . \tag{3.17}$$

The factor g_w originates from the isospin-trace $g_w = \mathrm{tr}[\epsilon^\dagger \epsilon]$, while $|Y|^2$ is shorthand for the matrix product $Y^\dagger Y$. Since the leptons are massless, both chirality projectors can be put to one side so that they may be added: $P_L + P_R = 1$. In using the tree-level propagators from Section 1.5, the perturbative *LO* contribution to the production rate can be obtained from

$$\mathcal{H}(p) \equiv \mathrm{tr}[\slashed{p}\Sigma_N^{LO,\mathcal{A}}(p)] = 2g_w|Y|^2 \int \frac{\mathrm{d}^4 k}{(2\pi)^2} p \cdot k\, \delta(k^2) \delta((p-k)^2) \mathrm{sign}(k^0) \mathrm{sign}(p^0 - k^0)$$
$$\left(1 - f_+(k^0) + f_-(p^0 - k^0) \right) \tag{3.18}$$

36

in the plasma frame. This term is called $\mathcal{H}$ for later convenience. The tree-level spectral propagators contain delta distributions at the mass shell. This way, the CTP generates all possible cut diagrams that can be evaluated from Σ_N.

From now on, the calculation for the sunset and top-loop contribution to the Higgs self-energy could be followed, or one simply uses the general result from Section 2.4. Anyway, after splitting the distribution functions into a vacuum and a thermal part, the vacuum distribution functions only allow for the case $p^2 > 0$ such that the vacuum integral becomes

$$\mathcal{H}^{vac}(p) = \frac{g_w |Y|^2}{16\pi} \frac{p^2}{|\vec{p}|} \theta(p^2) \int_{k_-^0}^{k_+^0} dk^0 (\text{sign}(k^0) + \text{sign}(p^0 - k^0)) \tag{3.19}$$

$$= \frac{g_w |Y|^2}{8\pi} p^2 \text{sign}(p^0) \theta(p^2). \tag{3.20}$$

By insertion of $\mathcal{H}^{vac}$ into (3.13) on-shell at $p^2 = m_N^2$ for positive p^0, the known vacuum rate

$$\Gamma_N^{LO,vac} = \frac{g_w |Y|^2}{16\pi} m_N \tag{3.21}$$

is reproduced. The thermal part is obtained from

$$\mathcal{H}^{T \neq 0}(p) = \frac{g_w |Y|^2}{8\pi} \frac{p^2}{|\vec{p}|} \int_B dk^0 \left(-\text{sign}(p^0 - k^0) f_+(|k^0|) + \text{sign}(k^0) f_-(|p^0 - k^0|) \right) \tag{3.22}$$

and evaluates in the usual way to

$$\mathcal{H}^{T \neq 0}(p) = \frac{g_w |Y|^2}{8\pi} \frac{p^2}{|\vec{p}|} \int_B dk^0 \left(-\text{sign}(p^0 - k^0) f_+(|k^0|) + \text{sign}(k^0) f_-(|p^0 - k^0|) \right) \tag{3.23}$$

$$= -\frac{g_w |Y|^2}{8\pi} \frac{p^2}{|\vec{p}|} \left(2(|k_+^0| - k_-^0) - T \ln \left| \frac{1 - e^{\frac{2|k_+^0|}{T}}}{1 - e^{\frac{2k_-^0}{T}}} \right| \right) \text{sign}(p^0) \tag{3.24}$$

$$= \begin{cases} -\frac{g_w |Y|^2}{8\pi} \frac{p^2}{|\vec{p}|} \left(2\theta(p^0)|\vec{p}| - T \ln \left| \frac{1 - e^{\frac{p^0 + |\vec{p}|}{T}}}{1 - e^{\frac{p^0 - |\vec{p}|}{T}}} \right| \right) & , p^2 > 0 \\ -\frac{g_w |Y|^2}{8\pi} \frac{p^2}{|\vec{p}|} \left(2p^0 - T \ln \left| \frac{1 - e^{\frac{p^0 + |\vec{p}|}{T}}}{1 - e^{\frac{-p^0 + |\vec{p}|}{T}}} \right| \right) & , p^2 < 0 \end{cases} \tag{3.25}$$

$\mathcal{H}^{vac} + \mathcal{H}^{T \neq 0}$ is positive for $p^2 > 0$ and $p^0 > 0$. Altogether, the perturbative leading order differential production rate is

$$\Gamma_N^{LO} = \Gamma_N^{LO,vac} \left(-1 + \frac{T}{|\vec{p}|} \ln \left| \frac{1 - e^{\frac{p^0 + |\vec{p}|}{T}}}{1 - e^{\frac{p^0 - |\vec{p}|}{T}}} \right| \right). \tag{3.26}$$

In the non-relativistic limit, the reference to the plasma vector is negligible. Therefore, (3.26) may be evaluated in the limit $|\vec{p}| \to 0$:

$$\Gamma_N^{LO} \bigg|_{\vec{p}=0} = \Gamma_N^{LO,vac} \frac{e^{\frac{m_N}{T}} + 1}{e^{\frac{m_N}{T}} - 1} = \Gamma_N^{LO,vac} \frac{f_-(m_N)}{f_+(m_N)} = \Gamma_N^{LO,vac} (1 + 2f_-(m_N)). \tag{3.27}$$

3.4 *LO* and *NLO* Results in the Ultra-Relativistic Limit

In the ultra-relativistic limit, for $\frac{m_N}{T} \to 0$, the perturbative leading order production rate (3.26) vanishes and loop corrections have to be considered. These are determined by the 2PI expansion, which uses full 2-point functions instead of tree-level ones. If expanded in couplings, the cuts of the 1-loop 2PI diagrams in Figure 3.1 correspond to wave-function corrections to the tree-level process plus the symmetric $1 \leftrightarrow 3$ processes shown in Figure 3.3. Therefore, those are referred to as wave-function type diagrams indicated by a *wv*.
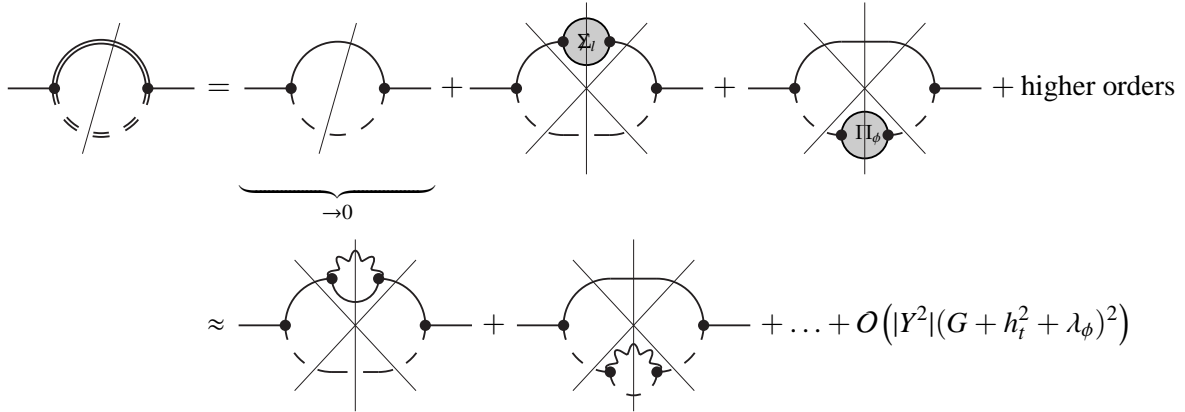
Figure 3.3: This figure shows the cuts of the perturbatively expanded 1-loop 2PI neutrino self-energy. The sums over the cuts and both error directions that indicate the charge flow are implicitly assumed. The dots in the second line represent the other 1-loop Higgs self-energy contributions that are shown in Figure 2.1.

The cuts of the 2-loop 2PI diagrams correspond, with tree-level propagators, to vertex corrections and mixed $1 \leftrightarrow 3$ and $2 \leftrightarrow 2$ processes. They can be found in Figure 3.4.
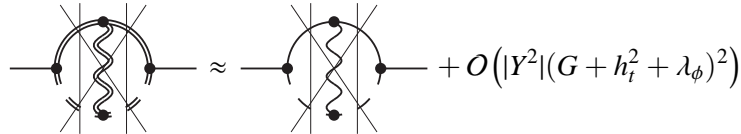
Figure 3.4: This figure shows the cuts of the perturbatively expanded 2-loop 2PI neutrino self-energy. Vertical cuts correspond to vertex corrections, while the diagonal cuts provide the product of mixed type $1 \leftrightarrow 3$ processes. The sums over the cuts and both error directions that indicate the charge flow are implicitly assumed.

They are called vertex-type diagrams in the following, and are indicated by the superscript *vert*. Hence, the RHN self-energy in the massless limit $m_N = 0$ is separated as

$$\Sigma_{N_0}^{LO} = \Sigma_{N_0}^{wv} + \Sigma_{N_0}^{vert}. \tag{3.28}$$

3.4.1 Wave-Function Type Contributions

The *wv* diagram using full propagators has the same structure as Equation (3.17). According to Chapter 1.6, the full propagator for a massless lepton has no scalar part in the numerator such that the left- and right-handed projectors can be put to one side.[23] Hence, the *wv* contribution, including the sum of both chiralities, can be written as

$$i\Sigma_N^{ab,wv}(p) = g_w|Y|^2 \int \frac{\mathrm{d}^4 k}{(2\pi)^4} i\mathcal{S}_l^{ab}(p-k) i\Delta_l^{ab}(k) \,. \tag{3.29}$$

By following the decomposition of any 2-point functions into spectral and statistical propagators, the traced spectral neutrino self-energy is

$$\mathrm{tr}[\not{p}\Sigma_N^{\mathcal{A},wv}(p)] = 2g_w|Y|^2 \int \frac{\mathrm{d}^4 k}{(2\pi)^4} \mathrm{tr}[\not{p}\mathcal{S}_l^{\mathcal{A}}(k)]\Delta_\phi^{\mathcal{A}}(p-k)\left(1 - f_+(u\cdot k) + f_-(u\cdot(p-k))\right) \,. \tag{3.30}$$

Since only the dominant contribution to this process is needed, the tree-level one vanishes in the massless limit, and medium corrections add linearly in G, h_t^2 and λ_ϕ, Equation (3.30) may be decomposed as

$$\mathrm{tr}[\not{p}\Sigma_{N_0}^{\mathcal{A},wv}(p)] \equiv \mathcal{B}_0(p) + \mathcal{F}_0(p) \tag{3.31}$$

with

$$\mathcal{B}_0(p) \equiv \mathrm{tr}\left[\not{p}\Sigma_{N_0}^{\mathcal{A},wv}[\Delta_\phi, \mathcal{S}_l^{(0)}](p)\right] \tag{3.32}$$

$$\mathcal{F}_0(p) \equiv \mathrm{tr}\left[\not{p}\Sigma_{N_0}^{\mathcal{A},wv}[\Delta_\phi^{(0)}, \mathcal{S}_l](p)\right] \tag{3.33}$$

or diagrammatically as

Figure 3.5: Expansion of the *wv* diagram according to Equation (3.31). Double and single lines indicate full and tree-level propagators, respectively. The charge-flow arrows are suppressed, but the sum of both cases is intended.

The index (0) in $\mathcal{S}_l^{(0)}$ and $\Delta_\phi^{(0)}$ denote the tree-level propagators. This means that the $\mathcal{B}$ term involves a full Higgs and a tree-level lepton propagator, while the $\mathcal{F}$ term contains a tree-level Higgs and a full lepton propagator.

The full propagators obtain plasma induced dispersion relations and a width due to their self-energies. Those effects are treated in two manners, which can be compared to each other in the end.

One approach is to neglect Π_ϕ^H and Σ_l^H within the resummed propagators of $\mathcal{B}_0$ and $\mathcal{F}_0$. In particular, those reduced resummed functions are expanded in couplings. The neglected effects are then incorporated by adding the processes $N \leftrightarrow l\phi$ and $N \leftrightarrow \bar{l}\bar{\phi}$, i.e. the perturbative *LO* expression $\mathcal{H}_0$, using tree-level propagators that include the thermal masses.

The second method is to not approximate the resummed propagators in $\mathcal{B}_0$ and $\mathcal{F}_0$ at all. In turn, the integrals have a non-trivial pole structure and can only be evaluated numerically.

---

[23] This argument is repeated in Section 3.4.1.3.

3.4.1.1 Perturbative *LO* Contribution using Thermal Masses

The lepton and Higgs plasma induced dispersion relations are obtained from Σ_l and Π_ϕ, respectively. Hence, the resulting "thermal masses" are momentum dependent even at leading order in the couplings. However, in the ultra-relativistic limit at high temperatures and typical momenta above T, they have to be proportional to T^2, such that only the momentum independent parts are of importance. According to (2.90) and (2.77), the asymptotic thermal masses are[24]

$$(m_l^{th})^2 = \frac{1}{4} G T^2 \tag{3.34}$$

$$(m_\phi^{th})^2 = \frac{1}{4} G T^2 + \frac{g_c}{12} h_t^2 T^2 + \frac{1}{2} \lambda_\phi T^2 . \tag{3.35}$$

Analogously to (3.18), the *LO* neutrino production rate, incorporating above thermal masses in the form of tree-level masses m_l and m_ϕ, can be evaluated from

$$\mathrm{tr}[\not{p}\Sigma_N^{LO,\mathscr{A}}(p)] \equiv \mathcal{H}(p) = 2 g_w |Y|^2 \int \frac{\mathrm{d}^4 k}{(2\pi)^2} p \cdot k\, \delta(k^2 - m_l^2) \delta((p-k)^2 - m_\phi^2)$$
$$\mathrm{sign}(k^0)\mathrm{sign}(p^0 - k^0) \left(1 - f_+(k^0) + f_-(p^0 - k^0)\right) . \tag{3.36}$$

With the help of Section 2.4, the vacuum part of (3.36) becomes

$$\mathcal{H}^{vac}(p) = \frac{g_w |Y|^2}{8\pi} \frac{1}{p^2} \left(p^2 + m_l^2 - m_\phi^2\right) \sqrt{-\left| \begin{matrix} 2m_l^2 & p^2 - m_l^2 - m_\phi^2 \\ p^2 - m_l^2 - m_\phi^2 & 2m_\phi^2 \end{matrix} \right|}$$
$$\mathrm{sign}(p^0)\theta(p^2 - m_l^2 - m_\phi^2) . \tag{3.37}$$

One can easily check that in the limit $m_l, m_\phi \to 0$ the result (3.20) is obtained. Likewise, the thermal part is evaluated in the plasma frame from

$$\mathcal{H}^{T\neq 0}(p) = \frac{g_w |Y|^2}{8\pi} \frac{1}{|\vec{p}|} \left(p^2 + m_l^2 - m_\phi^2\right) \theta\left(-\left| \begin{matrix} 2m_l^2 & p^2 - m_l^2 - m_\phi^2 \\ p^2 - m_l^2 - m_\phi^2 & 2m_\phi^2 \end{matrix} \right|\right)$$
$$\int_{k_-^0}^{k_+^0} \mathrm{d}k^0 \left(\mathrm{sign}(k^0) f_-(|p^0 - k^0|) - \mathrm{sign}(p^0 - k^0) f_+(|k^0|)\right) . \tag{3.38}$$

This becomes for positive p^2

$$\mathcal{H}^{T\neq 0}(p) = \frac{g_w |Y|^2}{8\pi} \frac{1}{|\vec{p}|} \left(p^2 + m_l^2 - m_\phi^2\right) \theta\left(-\left| \begin{matrix} 2m_l^2 & p^2 - m_l^2 - m_\phi^2 \\ p^2 - m_l^2 - m_\phi^2 & 2m_\phi^2 \end{matrix} \right|\right) \tag{3.39}$$
$$\mathrm{sign}(p^2 - m_l^2 - m_\phi^2)\left(-x\,\theta(p^2 - m_l^2 - m_\phi^2)\mathrm{sign}(p^0) + \ln\left|\frac{1 + e^x}{-1 + e^{x-p^0}}\right|\right)\Big|_{x=k_-^0}^{x=k_+^0}$$

with the boundary variables

$$k_\pm^0 = \frac{p^0(p^2 + m_l^2 - m_\phi^2)}{2p^2} \pm \frac{|\vec{p}|}{2p^2} \sqrt{-\left| \begin{matrix} 2m_l^2 & p^2 - m_l^2 - m_\phi^2 \\ p^2 - m_l^2 - m_\phi^2 & 2m_\phi^2 \end{matrix} \right|} . \tag{3.40}$$

In the Equations (3.37) and (3.39) p^2 may be set to m_N^2, such that, as a side-product, a solution for three arbitrary masses $\mathcal{H}(|\vec{p}|; m_N, m_\phi, m_l)$ is found. By setting $m_l = m_\phi = 0$ this can be compared to Equation (3.25).

---

[24] See Section 4.7 for a detailed derivation of the lepton dispersion relation.

For completeness, the limit $p^2 = m_N^2 \to 0$ is taken:

$$\mathcal{H}_0^{T \neq 0}(p) = g_w |Y|^2 \frac{m_\phi^2 - m_l^2}{2^4 \pi} \left[1 + \text{sign}(m_\phi^2 - m_l^2) \frac{2T}{|\vec{p}|} \ln \left| \frac{\cosh \left(\frac{(m_\phi^2 - m_l^2)^2 + 4 m_l^2 |\vec{p}|^2}{8(m_\phi^2 - m_l^2)|\vec{p}|} \right)}{\sinh \left(\frac{(m_\phi^2 - m_l^2)^2 + 4 m_\phi^2 |\vec{p}|^2}{8(m_\phi^2 - m_l^2)|\vec{p}|} \right)} \right| \right]. \tag{3.41}$$

Since the on-shell contribution (3.37) vanishes for $p^2 = m_N^2 = 0$, the effect of the plasma induced thermal masses is calculated from (3.41) alone. In Figures 3.6 and 3.7 those are called "$\mathcal{H}$ using m_ϕ^{th}" and "$\mathcal{H}$ using m_l^{th}". Those m_ϕ^{th} and m_l^{th} are the masses in (3.35) and (3.34).

3.4.1.2 Corrections from the Higgs Boson

Using the assumption $\Pi_\phi^H(p) = 0$, which means neglecting the plasma induced dispersion relation, the resummed Higgs spectral function from Equation (1.80) may be written as

$$\Delta_\phi^{\mathcal{A}}(p) \approx \frac{\Pi_\phi^{\mathcal{A}}(p)}{p^4 + \left(\Pi_\phi^{\mathcal{A}}(p) \right)^2} \approx \frac{\Pi_\phi^{\mathcal{A}}(p)}{p^4} . \tag{3.42}$$

The error that is made by this approximation is investigated in the following. The last term in Equation (3.42) corresponds to the 1-loop correction of the Higgs spectral function within a series expansion to leading order in the couplings G, h_t and λ_ϕ even without neglecting Π_ϕ^H. $\Pi_\phi^{\mathcal{A}}$ is the 1-loop Higgs self-energy from Section 2.5.5, and for the lepton propagator, the massless tree-level spectral function (1.71) may be substituted to Equation (3.30). Then, the scattering correction from the Higgs boson expressed in the plasma frame becomes

$$\mathcal{B}_0(p) = 4 g_w |Y|^2 \int \frac{d^4 k}{(2\pi)^3} p \cdot k \delta(k^2) \text{sign}(k^0) \frac{\Pi_\phi^{\mathcal{A}}(p-k)}{(p-k)^4} \left(1 - f_+(k^0) + f_-(p^0 - k^0) \right) . \tag{3.43}$$

Since $\mathcal{B}_0$ is evaluated on-shell, p^2 can be set to zero. Consequently, after integrating out the delta function, the numerator $2p \cdot k$ decreases the pole degree:

$$\mathcal{B}_0(p) = \frac{g_w |Y|^2}{(2\pi)^2} \int d\cos \angle(k,p) d|\vec{k}| |\vec{k}| \sum_{k^0 = \pm |\vec{k}|} \mp \frac{\Pi_\phi^{\mathcal{A}}(p-k)}{(p-k)^2} \left(f_+(-k^0) + f_-(p^0 - k^0) \right) . \tag{3.44}$$

Since $\Pi_\phi^{\mathcal{A}}(p-k)$ is proportional to $(p-k)^2$, Equation (3.44) is free of divergences and can be calculated straightforwardly.[25] Therefore, the infrared regulating mass λ was set to zero in the beginning. Under restriction to the massless 1-loop spectral Higgs self-energy in vacuum, the constraint $(p-k)^2 > 0$ allows only the negative solution for k^0 if $p^0 = +|\vec{p}|$ is treated as positive. Then Equation (3.44) becomes

$$\mathcal{B}_0^{vac}(p^+) = \left(-G + \frac{g_c h_t^2}{2} \right) \frac{g_w |Y|^2}{2(2\pi)^3} \left(\frac{\pi^2}{12} + \text{Li}_2(e^{-|\vec{p}|}) \right) T^2 . \tag{3.45}$$

Li_2 is the dilogarithm, and p^+ indicates the restriction to positive p^0. In the same way, the thermal spectral Higgs self-energy can be incorporated. When plugging these into (3.16), the total production rate for zero

---

[25] Related to this is the discussion in footnote 33 on page 50.

RHN abundance can be integrated out:

$$\gamma_N[\mathcal{B}_0] \approx \frac{1}{(2\pi)^5} g_w |Y|^2 T^4 \left(\frac{\pi^2}{12}\right)^2 \left(\underbrace{\frac{13}{10}\left(-G + \frac{g_c h_t^2}{2}\right)}_{\text{using } \Pi_\phi^{\mathcal{A},vac}} + \underbrace{5.8595(7 \pm 6)G + 1.2213(6 \pm 2)\frac{g_c h_t^2}{2}}_{\text{using } \Pi_\phi^{\mathcal{A},T \neq 0}} \right) \quad (3.46)$$

$$\approx g_w |Y^2| T^4 \left(3.1496(4 \pm 6) \cdot 10^{-4} G + 8.7084(7 \pm 7) \cdot 10^{-5} g_c h_t^2\right). \quad (3.47)$$

In case of the the Standard Model values $g_w = 2$ and $g_c = 3$, the numerical coefficient in front of the top Yukawa coupling is $5.2250(8 \pm 4) \cdot 10^{-4}$. This is in good agreement to the $5.22 \cdot 10^{-4}$ of [60]. These numbers are published with less accuracy in [75] and correspond to the lines "$\mathcal{O}(G)$" and "$\mathcal{O}(h_t^2)$" in the Figures 3.6 and 3.7. The G in [75] is defined as the $g_w G$ of here.

The more realistic $\mathcal{B}_0$ is obtained with

$$\Delta_\phi^{\mathcal{A}}(p) \approx \frac{\Pi_\phi^{\mathcal{A}}(p)}{p^4 + \left(\Pi_\phi^{\mathcal{A}}(p)\right)^2} \quad (3.48)$$

or

$$\Delta_\phi^{\mathcal{A}}(p) = \frac{\Pi_\phi^{\mathcal{A}}(p)}{\left(p^2 - \Pi_\phi^H(p)\right)^2 + \left(\Pi_\phi^{\mathcal{A}}(p)\right)^2}, \quad (3.49)$$

and in consequence γ_N can only be calculated numerically by fixing the couplings. The results using Equations (3.48) and (3.49) are given in Table 3.1 for several couplings. In Figures 3.6 and 3.7, they are referred to as "$\Pi_\phi^H = 0$" and "full", respectively. Checked is the range $10^{-6} \le G \le 10^{-0.1}$ and $10^{-3} \le h_t \le 10^{-0.05}$, using 60 points per scan. The "full" result is obtained by splitting the integration region into a "pole" and a "non-pole" part. These are the lines (a) and (b) in the plots. Details on the numerics can be found in Chapter 4.4.

	γ_N using eq. (3.48)	γ_N using eq. (3.49)
RGE scale 10^9	$3.58(6 \pm 4) \cdot 10^{-4} |Y|^2 T^4$	$-2.63(7 \pm 8) \cdot 10^{-4} |Y|^2 T^4$
RGE scale 10^{12}	$3.05(1 \pm 4) \cdot 10^{-4} |Y|^2 T^4$	$-2.01(1 \pm 7) \cdot 10^{-4} |Y|^2 T^4$
$G = 10^{-1}$	$3.07(9 \pm 5) \cdot 10^{-4} |Y|^2 T^4 2G$	$-3.0(3 \pm 1) \cdot 10^{-4} |Y|^2 T^4 2G$
$G = 10^{-2}$	$3.14(7 \pm 5) \cdot 10^{-4} |Y|^2 T^4 2G$	$-2.6(4 \pm 1) \cdot 10^{-4} |Y|^2 T^4 2G$
$G = 10^{-3}$	$3.14(9 \pm 5) \cdot 10^{-4} |Y|^2 T^4 2G$	$-2.3(7 \pm 1) \cdot 10^{-4} |Y|^2 T^4 2G$
$G = 10^{-4}$	$3.15(0 \pm 5) \cdot 10^{-4} |Y|^2 T^4 2G$	$-2.2(6 \pm 1) \cdot 10^{-4} |Y|^2 T^4 2G$
$G = 10^{-5}$	$3.15(0 \pm 5) \cdot 10^{-4} |Y|^2 T^4 2G$	$-2.2(2 \pm 1) \cdot 10^{-4} |Y|^2 T^4 2G$
$G = 10^{-6}$	$3.15(0 \pm 5) \cdot 10^{-4} |Y|^2 T^4 2G$	$-2.2(0 \pm 1) \cdot 10^{-4} |Y|^2 T^4 2G$
$h_t = 10^{-1}$	$5.22(5 \pm 4) \cdot 10^{-4} |Y|^2 T^4 h_t^2$	$1.55(1 \pm 1) \cdot 10^{-3} |Y|^2 T^4 h_t^2$
$h_t = 10^{-2}$	$5.22(5 \pm 4) \cdot 10^{-4} |Y|^2 T^4 h_t^2$	$1.59(0 \pm 2) \cdot 10^{-3} |Y|^2 T^4 h_t^2$
$h_t = 10^{-3}$	$5.22(5 \pm 4) \cdot 10^{-4} |Y|^2 T^4 h_t^2$	$1.59(3 \pm 2) \cdot 10^{-3} |Y|^2 T^4 h_t^2$

Table 3.1: Numerical results for $\gamma_N[\mathcal{B}_0]$ of massless right-handed neutrinos in different approximations. The RGE scale couplings are summarized in Table 2.1. The other cases are calculated for comparison and use only the mentioned coupling while the others are set to zero.
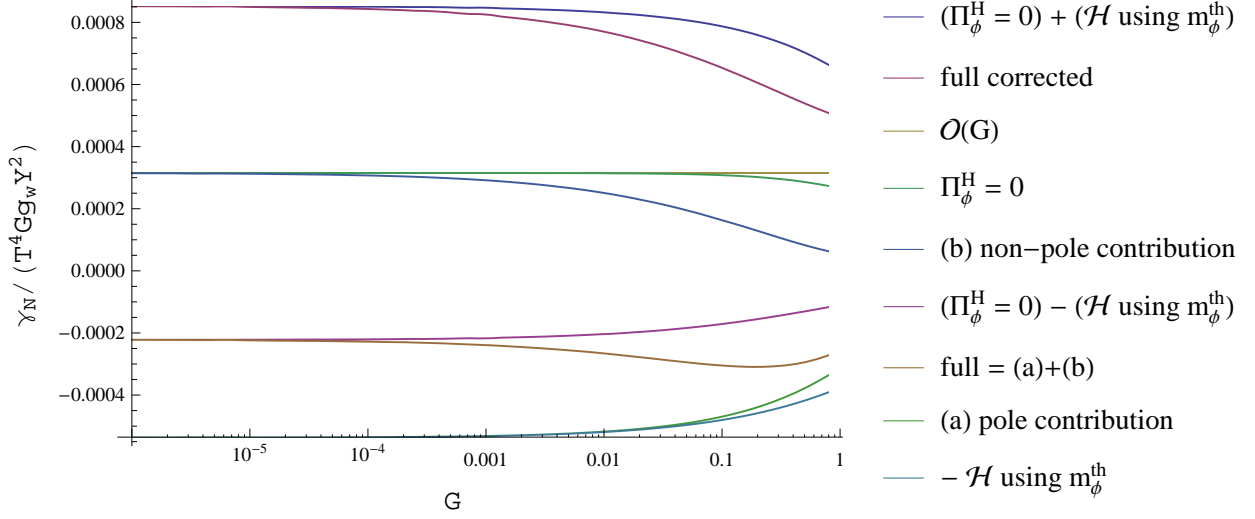
Figure 3.6: The figure shows contributions to $\gamma_N[\mathcal{B}_0](G)$ using $h_t = \lambda_\phi = 0$. The "$\Pi_\phi^H = 0$" line is the rate calculated with (3.48), while "full" means the rate calculated with (3.49). "$\mathcal{H}$ using m_ϕ^{th}" is the rate obtained by (3.41).
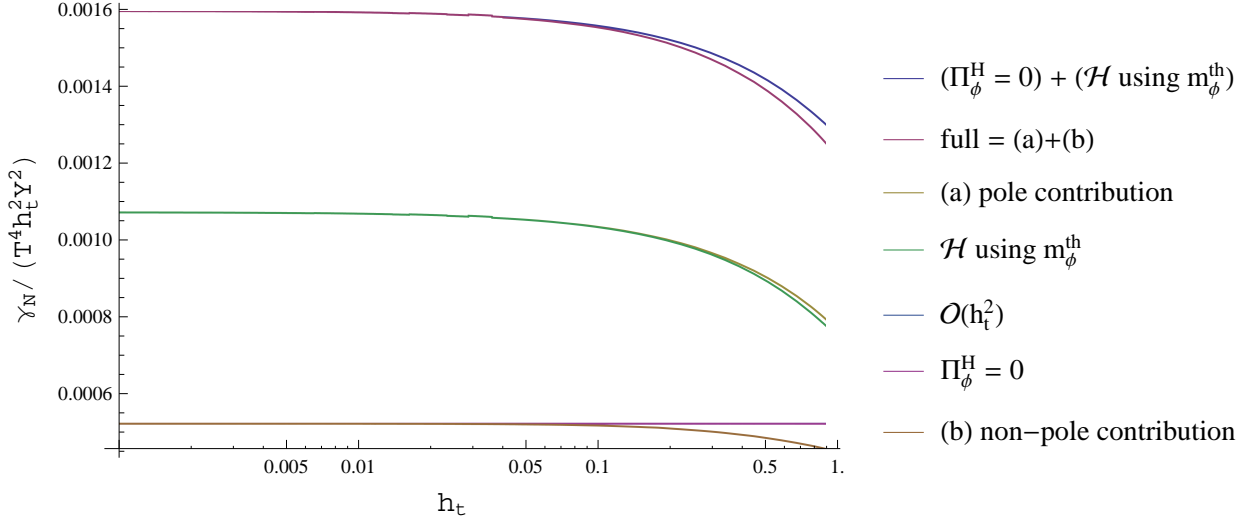
Figure 3.7: The figure shows contributions to $\gamma_N[\mathcal{B}_0](h_t)$ using $G = \lambda_\phi = 0$. The "$\Pi_\phi^H = 0$" line is the rate calculated with (3.48), while "full" means the rate calculated with (3.49). "$\mathcal{H}$ using m_ϕ^{th}" is the rate obtained by (3.41). The "$O(h_t^2)$" line is covered by "$\Pi_\phi^H = 0$" in the plot.

In the case of the gauge interactions, approximation (3.42) compared to (3.48) is valid up to percent accuracy for $G < 0.1$. Furthermore, in the case of the top quark interaction, the difference is smaller than the numerical error. However, approximation (3.48) compared to the full case of (3.49) loses the information of the thermal masses of the Higgs and the lepton. In the ultra-relativistic regime, this thermal mass becomes important since it regularizes the infrared divergences. Hence, it should be included even though the ultra-relativistic limit appears to be finite without a thermal mass. Both figures show that the thermal mass effect can be incorporated into (3.48) approximately by adding or subtracting the $1 \leftrightarrow 2$ tree-level process, i.e. the $\mathcal{H}_0$ term, with tree-level masses $m_N = m_l = 0$ and $m_\phi = m_\phi^{th}$. This approximation then resembles the full result for $G < 10^{-4}$ and $h_t < 10^{-1}$ separately within percent accuracy.

In the case of the top-quark interaction shown in Figure 3.7, $\mathcal{H}_0$ is added. This results in a positive contribution to the neutrino production rate. However, in the case of the gauge boson interactions in Figure 3.6,

the subtraction of $\mathcal{H}_0$ is at first glance strange. It even turns out to be wrong. The discussion of this sign is postponed to Chapter 3.5.2.3. For now, only the following short answer is given: The on-shell spectral function can be recovered according to (1.81) by taking the small coupling limit. This assumes that the relation $\text{sign}(\Pi_\phi^{\mathcal{A}}(p)) = \text{sign}(p^0)$ holds on-shell. However, this is not true for the $\Pi_\phi^{\mathcal{A},(\gamma)}$ from Section 2.5. The $\mathcal{H}_0$ should only be added. Hence, one may ask whether approach (3.48) plus two times $\mathcal{H}_0$ including m_ϕ^{th} approximates the true "full" result better or not. This question is discussed in Section 3.5.4 in detail. There, a correction of the gauge boson resummed spectral Higgs propagator is formulated. The resulting corrected rate is plotted in Figure 3.6 and indicated as "full corrected".

3.4.1.3 Corrections from the Lepton

The contributions from the lepton can be calculated in nearly the same way as in the last section. The full spectral function of a massless lepton is (1.85):

$$P_L \mathcal{S}_l^{\mathcal{A}}(p) = P_L \frac{\gamma \cdot a\, 2a \cdot b - \gamma \cdot b \left(a^2 - b^2\right)}{\left(a^2 - b^2\right)^2 + \left(2a \cdot b\right)^2} P_R \quad , \quad a^\mu = p^\mu - \Sigma_l^{H\mu} \quad , \quad b^\mu = \Sigma_l^{\mathcal{A}\mu}. \quad (3.50)$$

The Σ_l^μ is defined in Section 2.6 via $\Sigma_l = P_L \gamma \cdot \Sigma_l$ without chiral projectors. Therefore, the explicit notation $\gamma \cdot a$ and $\gamma \cdot b$ is preferred in place of $\slashed{a}$ and $\slashed{b}$. $\mathcal{S}_l^{\mathcal{A}}$ clearly can be defined without projectors. When Equation (3.50) is inserted into (3.17), the projectors sum up. The resulting $\mathcal{F}_0$ term is

$$\mathcal{F}_0(p) = \frac{2g_w |Y|^2}{(2\pi)^2} \int_B dk^0 d|\vec{k}| \frac{|\vec{k}|}{|\vec{p}|} p \cdot S_l^{\mathcal{A}}(k) \text{sign}(p^0 - k^0) \left(f_+(-k^0) + f_-(p^0 - k^0)\right). \quad (3.51)$$

According to (2.84) any appearing scalar products can be expressed by known functions, such that (3.51) can be evaluated numerically.

An approximation as similar to Equation (3.42) for the Higgs case is only possible for large spatial momenta $|\vec{k}|$. The 1-loop correction to the lepton propagator introduces an infrared divergence in the t-channel exchange of a massless lepton in the processes $Nl \to \phi\gamma$ and $N\gamma \to \phi l$. This divergence can be regularized by giving the neutrino a mass or resumming the 1-loop lepton self-energy to all orders, which dynamically introduces a thermal mass for the lepton. By using the resummed lepton, the coupling G can effectively be regarded as the regulator. Therefore, for a small G, the rate can be expected to be constituted by G, but also by $G \ln(G)$ from the t-channel. The error is then of the order $G^2 \ln(G)$.

In the next step, Equation (3.51) is solved numerically up to an relative error of 10^{-3} for each mode $|\vec{p}|$ separately.[26] The evaluated parameter range is $10^{-1} \le G \le 1$ using 11 points[27] and $10^{-3} \le |\vec{p}| \le 10^{1.5}$ using 46 points[28] both on a logarithmic scale. The result is interpolated and shown in the Figures 3.8 and 3.9. From those, the differential rate Γ_{N_0} can be obtained and integrated to give the total rate γ_{N_0}. The latter is plotted in Figure 3.10.

---

[26] See Chapter 4.7 for details on the numerics.

[27] According to Table 2.1, this is approximately the relevant interval for realistic gauge couplings important for Leptogenesis.

[28] When the total rate is calculated, higher $|\vec{p}|$ modes are suppressed by the exponential of the distribution function. Since the neutrinos have a Fermi-Dirac distribution, the lower cutoff is allowed due to suppression by the $|\vec{p}|$ factor from the integral measure $\frac{d^3\vec{p}}{2p^0}$. In the case of Bose-Einstein distributions, a smaller $|\vec{p}|$ could be important.
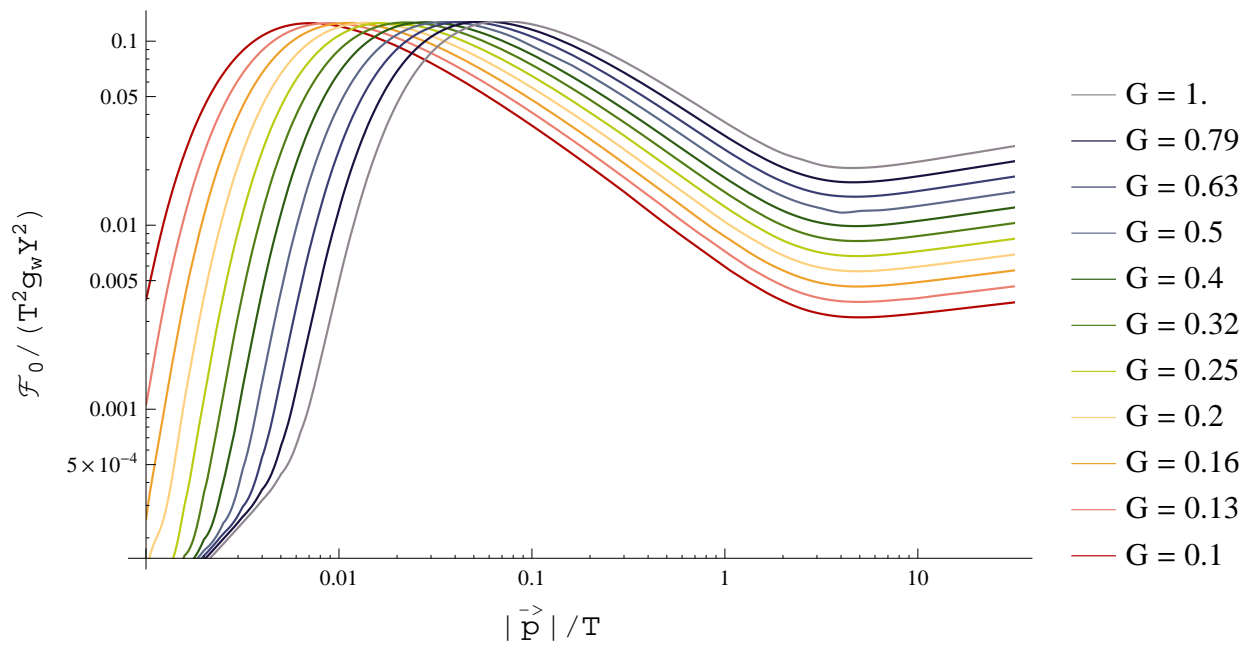
Figure 3.8: This figure shows the contribution to the neutrino rate due to gauge boson radiation from the lepton for different couplings G.
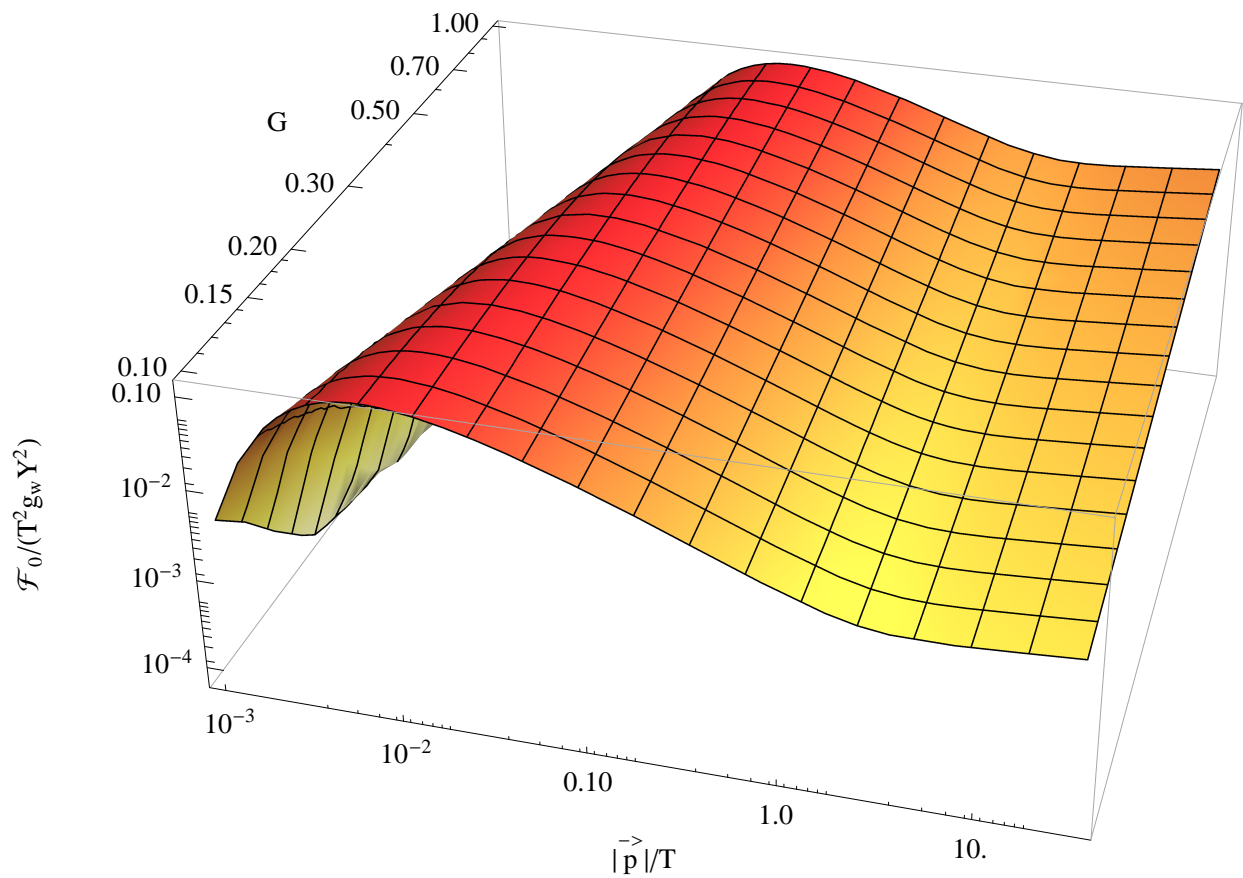
Figure 3.9: The same as Figure 3.8, but with G interpolated.
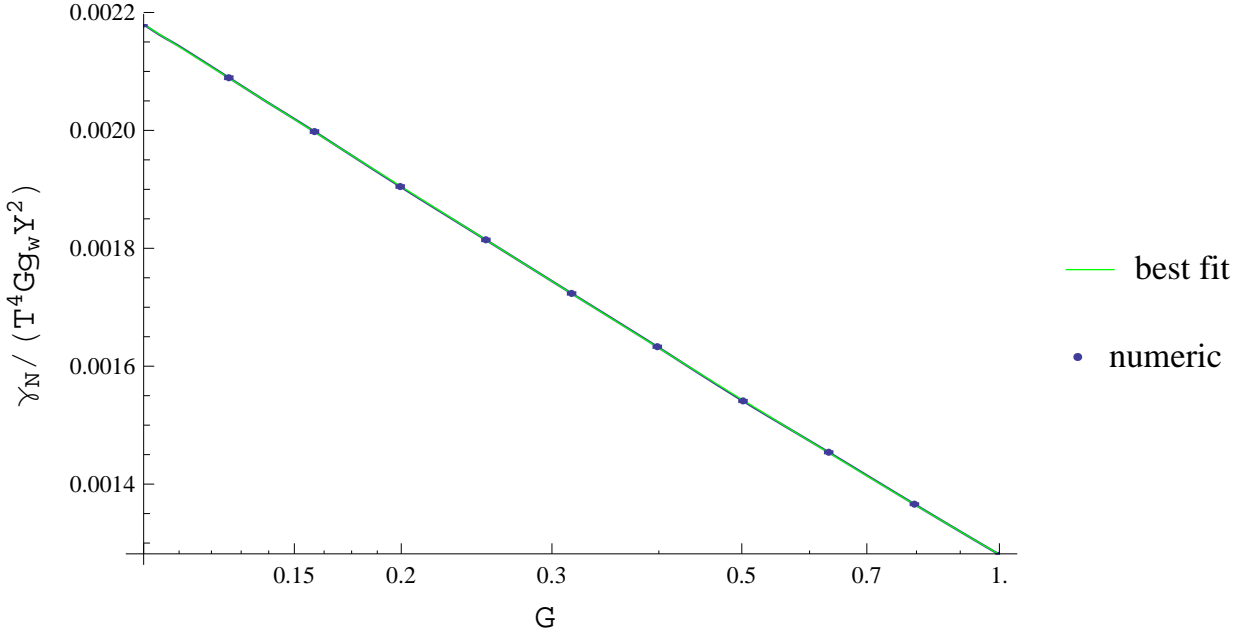
Figure 3.10: The figure shows the contribution to $\gamma_N[\mathcal{F}_0](G)$ and the fit (3.52). There is a blue line behind the green one that is the total rate obtained by integrating the differential rate from the interpolation in Figure 3.9 for all plot points.

Figure 3.10 shows γ_{N_0} divided by G in a logarithmic-linear style, such that the expected $G + G\ln(G)$ dependence becomes a straight line. From this the leading coefficients are extracted by a fit:

$$\gamma_{N_0}[\mathcal{F}_0] \approx \Big(1.28(19 \pm 6)G - 0.39(24 \pm 4)G\ln(G) + 0.02(8 \pm 3)G^2\ln(G)\Big) \cdot 10^{-3} g_w |Y^2| T^4 \qquad (3.52)$$

$$= \Big(1.544(4 \pm 4)(2G) - 0.39(64 \pm 6)(2G)\ln(2G)$$

$$+ 0.00(89 \pm 7)(2G)^2\ln(2G)\Big) \cdot 10^{-3} |Y^2| T^4 \,. \qquad (3.53)$$

In (3.53) the higher order term $G^2\ln(G)$ is included to obtain an error estimate for the lower orders. The numbers in (3.53) assume the group factor $g_w = 2$ and are arranged such that they can be compared directly to earlier results published in [75].[29]

3.4.2 Vertex Type Contributions

Also the vertex type contributions $\Sigma_{N_0}^{vert}$, corresponding to the cuts in Figure 3.4, give a sizable contribution to the neutrino production rate. Those cuts can be calculated along the lines of Chapter 3.5.6, but in the plasma frame. This was done in [75]. Their result is quoted for later comparison:

$$\gamma_{N_0}[\mathcal{J}_0] = 3.15 \cdot 10^{-4} g_w |Y^2| G T^4 \,. \qquad (3.54)$$

The $\mathcal{J}_0 = \mathrm{tr}[\not{p}\Sigma_{N_0}^{\mathcal{A},vert}(p)]$ is introduced in accordance with the notation of later chapters.

---

[29] The numeric here is done independently from [75].

3.5 *NLO* **Results in the Non-Relativistic to the Ultra-Relativistic Regime**

The goal of the following section is to find the transition from the ultra-relativistic limit at high temperatures to the non-relativistic limit at low temperatures compared to the neutrino mass. The non-relativistic limit is dominated by the tree-level processes $N \leftrightarrow l\phi$ and $N \leftrightarrow \bar{l}\bar{\phi}$. Those are calculated in Chapter 3.26 perturbatively. However, the ultra-relativistic limit is dominated by radiative corrections to the tree-level processes that have to be resummed. This was calculated in the previous chapter. The intermediate regime should render the crossover from one limit to the other one and therefore should be calculated using the approach that applies for both regions. Hence, the 2PI resummation is used. Nevertheless, it is instructive to verify that the perturbation theory is well-defined up to some point without resorting to a resummation.

For non-vanishing neutrino masses, the tree-level process is included in the 2PI 1-loop diagram for the neutrino self-energy. Therefore, it may be expanded for simplicity according to Figure 3.11:

Figure 3.11: Expansion of the *wv* diagram valid for a RHN mass ranging from the non-relativistic to the ultra-relativistic regime. Double and single lines indicate full and tree-level propagators, respectively. The charge-flow arrows are suppressed, but the sum of both cases is intended.

The first two diagrams on the right-hand side were called the wave-function type contributions in the last sections. In the following sections, this terminology is maintained even if the tree-level process $\mathcal{H}$ is included as well. The last term subtracts the overcounted $\mathcal{H}$, which is already obtained in Equation (3.26). In case of the 2-loop 2PI diagram, i.e. the vertex type contribution, the expansion shown in Figure 3.12 remains:
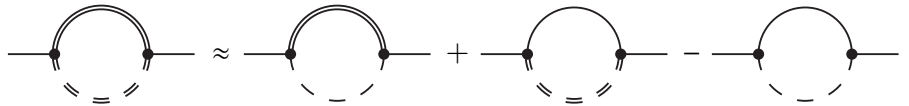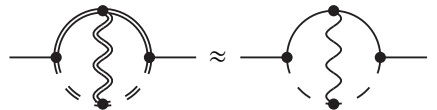

Figure 3.12: Perturbative expansion of the *vert* diagram valid for a RHN mass ranging from the non-relativistic to the ultra-relativistic regime. The sum over both charge flow directions is implicitly assumed.

Those terms are derived in the following sections.

3.5.1 Wave-Function Type Contributions - Perturbative Thermal Mass Insertion

In the non-relativistic limit, *NLO* corrections to the neutrino rate are given by the coupling expansion of the corresponding diagrams to second order in the Yukawas Y and h_t, to second order in the gauge couplings g_1 and g_2, which means first order in G, and to first order in the Higgs quartic interaction λ_ϕ. The lepton and Higgs receive 1-loop corrections from a gauge boson exchange. Furthermore, the Higgs obtains corrections from a top quark and a Higgs loop. To this order, the full Higgs and lepton propagators may be expanded as

$$\Delta_\phi \approx \Delta_\phi^{(0)} + \Delta_\phi^{(1)} \tag{3.55}$$

$$\mathcal{S}_l \approx \mathcal{S}_l^{(0)} + \mathcal{S}_l^{(1)}, \tag{3.56}$$

where a (0) again corresponds to the tree-level function and a (1) to the 1-loop correction. Hence, the perturbative *NLO* corrections from Figure 3.11 are given by $\Delta_\phi^{(1)}$ and $\mathcal{S}_l^{(0)}$, and vice versa by $\Delta_\phi^{(0)}$ and $\mathcal{S}_l^{(1)}$.[30] Here and in all following subsections, those terms are referred to by $\mathcal{B}$ and $\mathcal{F}$ terms, respectively. They again correspond to the bosonic and fermionic contributions:

$$\mathcal{B}^{O(G,h_t^2,\lambda_\phi)}(p) \equiv \mathrm{tr}\left[\not{p}\Sigma_N^{\mathcal{A},(\phi)}(p)\right] \equiv \mathrm{tr}\left[\not{p}\Sigma_N^{\mathcal{A},wv}[\Delta_\phi^{(1)},\mathcal{S}_l^{(0)}](p)\right] \tag{3.57}$$

$$\mathcal{F}^{O(G)}(p) \equiv \mathrm{tr}\left[\not{p}\Sigma_N^{\mathcal{A},(l)}(p)\right] \equiv \mathrm{tr}\left[\not{p}\Sigma_N^{\mathcal{A},wv}[\Delta_\phi^{(0)},\mathcal{S}_l^{(1)}](p)\right]. \tag{3.58}$$

Especially for the comparison with the resummed approach, the specific perturbative expansion order is mentioned explicitly. However, in the following subsections this is dropped for notational simplicity. $\Delta_\phi^{(1)}$ and $\mathcal{S}_l^{(1)}$ are the sum of spectral and hermitian self-energies. Since the spectral self-energy is the sum of all cuts of the corresponding diagrams, those terms result in corrections from $2 \leftrightarrow 2$ scatterings and $1 \leftrightarrow 3$ decays and inverse decays in the present case. Likewise, the terms proportional to the hermitian self-energy are regarded as wave-function type corrections to the $1 \leftrightarrow 2$ process of N, l and ϕ. Those are responsible for the perturbative inclusion of the thermal mass effects. Therefore, the $\mathcal{B}$ and $\mathcal{F}$ terms can be split further into a "*sca*" and a "*wv*" contribution: $\mathcal{B} = \mathcal{B}^{sca} + \mathcal{B}^{wv}$ and $\mathcal{F} = \mathcal{F}^{sca} + \mathcal{F}^{wv}$. In order to derive them, the 1-loop corrections $\Delta_\phi^{(1)}$ and $\mathcal{S}_l^{(1)}$ are consistently expressed by retarded and advanced functions, since those rely on the Schwinger-Dyson equations:

$$i\Delta_\phi^{(1),R/A}(p) = i\Delta_\phi^{(0),R/A}(p)(-i)\Pi_\phi^{R/A}(p)i\Delta_\phi^{(0),R/A}(p), \tag{3.59}$$

and the likewise one for $\mathcal{S}_l^{(1)}$. The Π_ϕ here is the perturbative 1-loop Higgs self-energy from Section 2.5. Only the spectral part of $\Delta_\phi^{(1)}$ is needed:

$$\Delta_\phi^{(1),\mathcal{A}} = \frac{1}{2}\left(i\Delta_\phi^{(1),R} - i\Delta_\phi^{(1),A}\right) \tag{3.60}$$

$$= -\frac{1}{2}\left(\left[\left(i\Delta_\phi^{(0),R}\right)^2 - \left(i\Delta_\phi^{(0),A}\right)^2\right]i\Pi_\phi^H + \left[\left(i\Delta_\phi^{(0),R}\right)^2 + \left(i\Delta_\phi^{(0),A}\right)^2\right]\Pi_\phi^{\mathcal{A}}\right). \tag{3.61}$$

In the same way, the leptonic correction $\mathcal{S}_l^{(1),\mathcal{A}}$ can be evaluated as

$$i\mathcal{S}_l^{(1),R/A}(p) = i\mathcal{S}_l^{(0),R/A}(-i)\Sigma_l^{R/A}i\mathcal{S}_l^{(0),R/A} = -\not{p}\,i\Sigma_l^{R/A}\not{p}\left(i\Delta_l^{(0),R/A}\right)^2 \tag{3.62}$$

$$\mathcal{S}_l^{(1),\mathcal{A}}(p) = -\frac{1}{2}\left(\left[\left(i\Delta_l^{(0),R}\right)^2 - \left(i\Delta_l^{(0),A}\right)^2\right]\not{p}\,i\Sigma_l^H\not{p} + \left[\left(i\Delta_l^{(0),R}\right)^2 + \left(i\Delta_l^{(0),A}\right)^2\right]\not{p}\Sigma_l^{\mathcal{A}}\not{p}\right). \tag{3.63}$$

---

[30] The *LO* term $\mathcal{H}$ in Figure 3.11 is obtained from $\Delta_\phi^{(0)}$ and $\mathcal{S}_l^{(0)}$.

Again, Δ_l is the scalar or non-Dirac part of $\mathcal{S}_l$, i.e. $\mathcal{S}_l(p) = \not{p}\Delta_l(p)$. The difference between retarded and advanced scalar tree-level propagators can be evaluated using Cauchy's integral formula:

$$\partial_z^n f(z) = \frac{n!}{2\pi i} \oint \frac{f(\zeta)}{(\zeta - z)^{1+n}} d\zeta. \tag{3.64}$$

The retarded and advanced propagators have poles above and below the real axis

$$i\Delta^{R/A}(p) = \frac{i}{p^2 - m^2 \pm i\varepsilon \operatorname{sign}(p^0)}, \tag{3.65}$$

determined by an infinitesimal positive $\varepsilon = 0^+$. In the limit $\varepsilon \to 0$, they become the same function

$$i\Delta^{R/A}(p) \xrightarrow{\varepsilon \to 0} \frac{i}{(z_+ - p^0)(z_- - p^0)}, \qquad z_\pm \equiv \pm\sqrt{\vec{p}^2 + m^2}, \tag{3.66}$$

but the integral contour has to change to preserve causality. Hence, one may evaluate for some appropriate test function f

$$\int_{-\infty}^{\infty} dk^0 f(k^0) \left[\left(i\Delta^{(0),R}\right)^2 - \left(i\Delta^{(0),A}\right)^2\right](k) = \int_{-\infty}^{\infty} dk^0 f(k^0) \left(i\Delta^{(0),R}\right)^2 + \int_{\infty}^{-\infty} dk^0 f(k^0) \left(i\Delta^{(0),A}\right)^2. \tag{3.67}$$

The poles are moved onto the real axis by setting ε to zero. However, the integration contour of Equation (3.67) changes according to Figure 3.13.
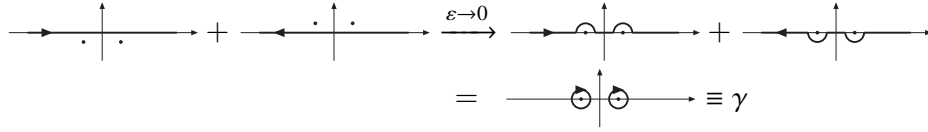
Figure 3.13: Shown is the integration contour in the complex k plane. Thick arrows indicate the direction of integration, and the dots represent the poles of retarded and advanced $\Delta^{(0)}(k)$.

Therefore, Equation (3.67) evaluates to

$$\oint_\gamma dk^0 f(k^0) \frac{i^2}{(k^2 - m^2)^2} = \sum_{z_\pm} 2\pi i \partial_{z_\pm} \left(\frac{f(z_\pm)}{(z_\mp - z_\pm)^2}\right) \tag{3.68}$$

$$= 2\pi i \sum_\pm \left(\frac{\partial_{z_\pm} f(z_\pm)}{4z_\pm^2} - \frac{f(z_\pm)}{4z_\pm^3}\right) \tag{3.69}$$

$$= \int_{-\infty}^{\infty} dk^0 \sum_\pm \delta\left(k^0 \pm \sqrt{\vec{k}^2 + m^2}\right) \frac{i\pi}{2k^{0 2}} \left(\partial_{k^0} - \frac{1}{k^0}\right) f(k^0). \tag{3.70}$$

By comparing (3.67) with (3.70), the relation

$$\left[\left(i\Delta^{(0),R}\right)^2 - \left(i\Delta^{(0),A}\right)^2\right](k) = \sum_\pm \delta\left(k^0 \pm \sqrt{\vec{k}^2 + m^2}\right) \frac{i\pi}{2k^{0 2}} \left(\partial_{k^0} - \frac{1}{k^0}\right) \tag{3.71}$$

can be found to hold under integration, provided the test function is holomorphic within a neighborhood of $k^2 = m^2$. Regarding the present perturbative wave-function type contributions, the only terms that may spoil the holomorphicity are the sign function and the delta distribution of the corresponding tree-level

propagator.[31] Nevertheless, the sign is not problematic, because as long as $m_N \neq 0$, a neighborhood of the pole where the sign is fixed always exists. However, the derivative in Equation (3.71) acts on an on-shell delta function, which leads to a term of the form $\int \mathrm{d}x f(x)\delta(x-y)\partial_x\delta(x-z)$. While such an integral can be solved by a partial integration in a symmetric fashion, while always checking for possible consequences on the integration bounds, it is easier to integrate out all deltas before solving the Cauchy integral. In following the same calculation starting from

$$\int \mathrm{d}k^0 \mathrm{d}|\vec{k}| f(k^0, |\vec{k}|)\delta(|\vec{k}| - (m_N \pm k^0))\left[\left(i\Delta^{(0),R}\right)^2 - \left(i\Delta^{(0),A}\right)^2\right](k),\tag{3.72}$$

this rule can be found:

$$\delta(|\vec{k}| - (m_N \pm k^0))\left[\left(i\Delta^{(0),R}\right)^2 - \left(i\Delta^{(0),A}\right)^2\right](k) = \tag{3.73}$$
$$\delta\left(|\vec{k}| - \frac{m_N^2 - m^2}{2m_N}\right)\delta\left(k^0 \pm \frac{m_N^2 + m^2}{2m_N}\right)\frac{i\pi}{2m_N^2}\left(\partial_{k^0} \pm \partial_{|\vec{k}|}\right).$$

In the case of $m = 0$, both rules act the same way on k^2.[32] This is of importance for [80] to show the cancellation of infrared divergences in the wave-function type corrections, as they use the relation (3.71). To circumvent the $\delta\partial\delta$ term, Equation (3.73) is used thereafter.

Likewise, the sum of retarded and advanced functions squared can be showed to correspond to a Cauchy principal value under certain conditions:

$$\left[\left(i\Delta^{(0),R}\right)^2 + \left(i\Delta^{(0),A}\right)^2\right](k) = -2\mathcal{P}\frac{1}{(k^2 - m^2)^2}.\tag{3.74}$$

Relation (3.74) alone is not well-defined. It holds only together with an appropriate test function that renders the principal value finite under integration.

What remains is to clarify why retarded and advanced functions are not simply converted to hermitian and spectral functions like $(i\Delta^{(0),R/A})^2 = (i\Delta^{(0),H} \pm \Delta^{(0),\mathcal{A}})^2$. The answer to this goes back to footnote 31. $\Delta^{(0),H}$ and $\Delta^{(0),\mathcal{A}}$ are the real and imaginary parts of some meromorphic functions $\Delta^{(0),R/A}$ that include the finite ε term. In the limit $\varepsilon \to 0^+$, those become complex distributions. A product of distributions cannot be defined without further input, such as the causality prescription obtained from the infinitesimal ε term or the explicit mentioned integration contour above. In other words, an expression like $(i\Delta^{(0),H} \pm \Delta^{(0),\mathcal{A}})^2$ would involve undefined products of distributions, such as a delta function squared or terms like $\delta(x)\mathcal{P}\frac{1}{x}$.[33]

In principle, thermal equilibrium may be assumed too, as it applies to this case. However practically, this assumption can be relaxed: Since the 2PI formulation assumes a full propagator, which is described by the resummation of all self-energy insertions, at two and higher loops, products of retarded and advanced propagators appear. In the limit $\varepsilon \to 0$, their poles above and below the real axis lead to the so called pinch singularities. These terms only disappear if, for example for the scalar case, the corresponding distribution function f satisfies $fi\Pi^> - (1 + f)i\Pi^< = 0$ [73], which is another form of the KMS relation. Hence, f should take its equilibrium form. However, a resummation of all loop insertions removes the pinch

---

[31] Even though the complex tree-level propagators should be meromorphic functions, their real and imaginary parts must not be meromorphic. The sign and delta functions are a consequence of restricting k^0 to the real axis.

[32] ... if $|\vec{k}| = m_N \pm k^0$

[33] The squared distribution $\left(\mathcal{P}\frac{1}{(p-k)^2}\right)^2$ was already found in Equation (3.43). In fact, (3.43) is well-defined, since $\Pi_\phi^{\mathcal{A}}(p-k)$ cancels one of those distributions. However, if the "consistent" result for $\Pi_\phi^{\mathcal{A}}$ from Section 3.5.4 is used within Equation (3.43), the terms do not cancel. In Equation (3.43) this would become manifest by a logarithmic divergence in $(p-k)^2$, which would be ascribed to an inconsistent expansion of the resummed spectral function at the right-hand side of Equation (3.42): There, a function is expanded perturbatively in couplings, and consequently an ill-defined product of distributions is obtained.

singularities, and only equilibrium contributions remain in the propagator in [81]. This is a result of the Fourier transform, which removes any time dependence such that only equilibrium is possible. Nevertheless, in Wigner space, the non-equilibrium contributions take their intuitively expected resummed form to all orders in a gradient expansion, showing that no equilibrium assumptions have to be done [73].

This statement is supported by the following argument: The pinch singularities are a consequence of an undefined limit $\varepsilon \to 0$. Nevertheless, in the top down 2PI approach, the full propagators have a width such that the ε can safely be set to zero. Hence, the ill-defined product of distributions in perturbation theory becomes a well-defined product of full propagators, such that no pinch singularities are present. The perturbative expansion of the full 2PI functions may involve products of distributions, but the correct treatment of those is determined by the expansion manner and has to be well-defined at all stages.

The next step is to evaluate the $\mathcal{B}$ and $\mathcal{F}$ terms for a massive on-shell RHN. Hence, p^2 is set to $m_N^2 > 0$, such that the Lorentz frame $\vec{p} = 0$ can be chosen. This is of particular importance for some terms, which can then easily be integrated out analytically. An analogous calculation in the plasma frame should be possible too, but in the non-relativistic limit the neutrino frame is appropriate. Since $\mathrm{tr}[\not{p}\Sigma_N^{\mathcal{A}}(p)]$ is anti-symmetric in $p^0 \leftrightarrow -p^0$, the calculation may be further restricted to $p^0 = +m_N$ for simplicity.

Lorentz transformations made easy:

Since only three linearly independent 4-momenta have to be considered, i.e. the plasma vector u, the neutrino vector p and the loop momentum k, their important components in the p-frame are related to the one in the u-frame via their scalar products. From now on, the index p or u is used to specify the frame of the corresponding 4-momenta explicitly. Using the definition $\tilde{p}_p^\mu \equiv m_N u_p^\mu$, the scalar products of u, p and k read

$$p_u^0 = u_u \cdot p_u = u_p \cdot p_p = u_p^0 m_N \equiv \tilde{p}_p^0 \tag{3.75}$$

$$k_u^0 = u_u \cdot k_u = u_p \cdot k_p = \frac{1}{m_N}\tilde{p}_p \cdot k_p = \frac{1}{m_N}\left(\tilde{p}_p^0 k_p^0 - |\vec{\tilde{p}}_p||\vec{k}_p|\cos \angle(k_p, \tilde{p}_p)\right) \tag{3.76}$$

$$p_u \cdot k_u = p_p \cdot k_p = m_N k_p^0. \tag{3.77}$$

Likewise, one finds

$$|\vec{p}_u|^2 = p_u^{0\,2} - p_u^2 = \tilde{p}_p^{0\,2} - \tilde{p}_p^2 = |\vec{\tilde{p}}_p|^2 \tag{3.78}$$

$$|\vec{k}_u|^2 = k_u^{0\,2} - k_u^2 = k_u^{0\,2} - k_p^2. \tag{3.79}$$

The angle between $\vec{k}_u$ and $\vec{p}_u$ is given by

$$\cos \angle(k_u, p_u) = \frac{k_u^0 p_u^0 - p \cdot k}{|\vec{k}_u||\vec{p}_u|} \tag{3.80}$$

with the right-hand side expressed in the p-frame variables from above. The $\tilde{p}_p$ equals to p_u at least in the zeroth component and the absolute value of its space-like vector. By demanding that $\tilde{p}_p = p_u$, the Lorentz transformation is completely fixed.

Hence, the p_u dependence of $\mathcal{B}$ and $\mathcal{F}$ calculated in the u-frame can be rearranged to a $\tilde{p}_p$ dependence of $\mathcal{B}$ and $\mathcal{F}$ calculated in the p-frame and vice versa. Note that the momenta in the self-energies of Section 2.5 are u-frame momenta. For the rest of this section, all momenta are thought to be in the frame of p, if not explicitly stated otherwise.

3.5.1.1 Corrections from the Higgs Boson

Taking Equations (3.29) and (3.57), the $\mathcal{B}$ term for $p^0 = +m_N$ is given by

$$\mathcal{B}(\tilde{p}) = g_w|Y|^2 \frac{1}{2} \int \frac{d^4k}{(2\pi)^4} \text{tr}\left[\slashed{p}\, i\mathcal{S}_l^{(0),>}(p-k)i\Delta_\phi^{(1),>}(k) - \slashed{p}\, i\mathcal{S}_l^{(0),<}(p-k)i\Delta_\phi^{(1),<}(k)\right] \tag{3.81}$$

$$= g_w|Y|^2 2 \int \frac{d^4k}{(2\pi)^4} \text{tr}\left[\slashed{p}\, \mathcal{S}_l^{(0),\mathcal{A}}(p+k)\right]\Delta_\phi^{(1),\mathcal{A}}(k)\left(f_-(u\cdot k) + f_+(u\cdot(p+k))\right). \tag{3.82}$$

The sign change of k from Equation (3.81) to (3.82) is just for convenience and not important. After the insertion of (3.61) the wave-function correction becomes

$$\mathcal{B}^{wv}(\tilde{p}) = -\frac{g_w|Y|^2 2}{(2\pi)^3} \int d^4k\, \delta((p+k)^2)\left[\left(i\Delta_\phi^{(0),R}\right)^2 - \left(i\Delta_\phi^{(0),A}\right)^2\right](k)$$
$$\text{sign}(m_N + k^0)(p^2 + p\cdot k)i\Pi_\phi^H(k)\left(f_-(u\cdot k) + f_+(u\cdot(p+k))\right) \tag{3.83}$$

$$= -\frac{g_w|Y|^2}{(2\pi)^2} \int dk^0 d|\vec{k}|d\cos\measuredangle(k,u) \sum_\pm \delta(|\vec{k}| \pm (m_N + k^0))\left[\left(i\Delta_\phi^{(0),R}\right)^2 - \left(i\Delta_\phi^{(0),A}\right)^2\right](k)$$
$$|\vec{k}|m_N|m_N + k^0|i\Pi_\phi^H(k)\left(f_-(u\cdot k) + f_+(u\cdot(p+k))\right). \tag{3.84}$$

This k^0 integral may be split into one running from $-\infty$ to $-m_N$ and one running from $-m_N$ to ∞ in order to fix the term $\text{sign}(m_N + k^0)$. In using the $\delta(|\vec{k}| \pm (m_N + k^0))$, the retarded minus advanced functions only have one pole at $k^0 = -\frac{m_N}{2}$. This allows only for the minus sign in $\sum_\pm$ and chooses the k^0 contour $k^0 \geq -m_N$. The pole of $f_-(u\cdot k)$ does not interfere with $k^0 = -\frac{m_N}{2}$, since the zero of $u\cdot k$ occurs at $k^0 = \frac{|\vec{p}|m_N \cos\measuredangle}{\tilde{p}^0 - |\vec{p}|\cos\measuredangle} > -\frac{m_N}{2}$ for $|\vec{p}| > 0$. Therefore, a neighborhood can always be found to circle $k^0 = -\frac{m_N}{2}$, such that the Cauchy integral can be evaluated as in (3.73). $\mathcal{B}^{wv}$ then is

$$\mathcal{B}^{wv}(\tilde{p}) = \frac{g_w|Y|^2}{2^3\pi} \int dk^0 d|\vec{k}|d\cos\measuredangle(k,u)\delta\left(|\vec{k}| - \frac{m_N}{2}\right)\delta\left(k^0 + \frac{m_N}{2}\right)\left(\partial_{k^0} + \partial_{|\vec{k}|}\right)$$
$$\left(\frac{|\vec{k}|(m_N + k^0)}{m_N}\Pi_\phi^H(k)\left(f_-(u\cdot k) + f_+(u\cdot(p+k))\right)\right). \tag{3.85}$$

By further defining the recurring integral measure

$$dF^{\mathcal{B}}(\tilde{p}, k^0, |\vec{k}|) \equiv d\cos\measuredangle(k,u)\left(f_-(u\cdot k) + f_+(u\cdot(p+k))\right), \tag{3.86}$$

$\mathcal{B}^{wv}$ can be written as

$$\mathcal{B}^{wv}(\tilde{p}) = \frac{g_w|Y|^2}{2^3\pi}\left.\left(\left(\partial_{k^0} + \partial_{|\vec{k}|}\right)\left(\frac{|\vec{k}|(m_N + k^0)}{m_N}\int \Pi_\phi^H(k)dF^{\mathcal{B}}(\tilde{p}, k^0, |\vec{k}|)\right)\right)\right|_{\substack{|\vec{k}| = \frac{m_N}{2} \\ k^0 = -\frac{m_N}{2}}}. \tag{3.87}$$

If the self-energy Π_ϕ^H evaluates to zero at $k^2 = 0$, the derivatives in (3.87) can only act on Π_ϕ^H. Since the vacuum term $\Pi_\phi^{H,vac}$ does not depend on u, $\int dF^{\mathcal{B}}$ can be evaluated and becomes

$$F^{\mathcal{B}}(\tilde{p}, k^0, |\vec{k}|) \equiv \int dF^{\mathcal{B}} = \frac{m_N T}{|\vec{k}||\vec{p}|}\ln\left|\frac{f_-\left(\frac{k^0\tilde{p}^0 - |\vec{k}||\vec{p}|}{m_N}\right)f_+\left(\frac{(k^0+m_N)\tilde{p}^0 + |\vec{k}||\vec{p}|}{m_N}\right)}{f_-\left(\frac{k^0\tilde{p}^0 + |\vec{k}||\vec{p}|}{m_N}\right)f_+\left(\frac{(k^0+m_N)\tilde{p}^0 - |\vec{k}||\vec{p}|}{m_N}\right)}\right|. \tag{3.88}$$

In the limit $T \to 0$, the vacuum part of $F^{\mathcal{B}}$ reads

$$F^{\mathcal{B},vac}(k^0) = \text{sign}(k^0) - \text{sign}(m_N + k^0)\,, \tag{3.89}$$

such that $F^{\mathcal{B}}$ can be separated into a vacuum and a thermal contribution as well:

$$F^{\mathcal{B}} \equiv F^{\mathcal{B},vac} + F^{\mathcal{B},T\neq0}\,. \tag{3.90}$$

Using (3.82), (3.61) and (3.74), the scattering part of $\mathcal{B}$ is given by

$$\mathcal{B}^{sca}(\tilde{p}) = 4g_w|Y|^2 m_N \int \frac{\mathrm{d}^4k}{(2\pi)^3}(m_N + k^0)\delta((p+k)^2)\text{sign}(m_N+k^0)$$
$$\frac{1}{(k^2)^2}\Pi^{\mathcal{A}}_\phi(k)\left(f_-(u\cdot k) + f_+(u\cdot(p+k))\right) \tag{3.91}$$

$$= 2g_w|Y|^2 m_N \int \frac{\mathrm{d}^3k}{(2\pi)^3}\sum_{k^0=-m_N\pm|\vec{k}|}\frac{1}{(k^2)^2}\Pi^{\mathcal{A}}_\phi(k)\left(f_-(u\cdot k)+f_+(u\cdot(p+k))\right) \tag{3.92}$$

$$= \frac{2g_w|Y|^2}{(2\pi)^2}\int \mathrm{d}|\vec{k}||\vec{k}|^2 \sum_{k^0=-m_N\pm|\vec{k}|}\frac{1}{(m_N\mp 2|\vec{k}|)k^2}\Pi^{\mathcal{A}}_\phi(k)\mathrm{d}F^{\mathcal{B}}(\tilde{p},k^0,|\vec{k}|)\,. \tag{3.93}$$

$\Pi^{\mathcal{A}}$ is proportional to k^2. It cancels one of the k^2 in the denominator, and only one principal value integrable singularity at $|\vec{k}| = \frac{m_N}{2}$ is left.

In the next step, $\mathcal{B}$ is split like $\Pi^{\mathcal{A}}_\phi$ and inherits its superscripts as in Equation (3.94). In addition, $\mathcal{B}$ contains thermal and vacuum contributions from the exterior distribution functions $f_- + f_+$. Later on, these are separated too, as shown in Equation (3.95):

$$\mathcal{B}^{wv/sca} = \mathcal{B}^{wv/sca,vac} + \mathcal{B}^{wv/sca,T\neq0} \tag{3.94}$$

$$= \mathcal{B}^{wv/sca,vac,vac} + \mathcal{B}^{wv/sca,vac,T\neq0} + \mathcal{B}^{wv/sca,T\neq0}\,. \tag{3.95}$$

Contributions using vacuum self-energies:

The contributions with the vacuum self-energies from (2.76) and (2.78) are

$$\mathcal{B}^{wv,vac}(\tilde{p}) = \frac{g_w|Y|^2 m_N^2}{2^6\pi^3}\left(G - \frac{g_c h_t^2}{2}\right)\ln\left(\frac{\lambda}{\Lambda}\right)F^{\mathcal{B}}\left(\tilde{p}, -\frac{m_N}{2}, \frac{m_N}{2}\right) + O(\lambda^2) \tag{3.96}$$

$$\mathcal{B}^{sca,vac\pm}(\tilde{p}) = \frac{2g_w|Y|^2}{(2\pi)^2}\int \mathrm{d}|\vec{k}||\vec{k}|^2 \frac{G\theta\left(\left(\frac{m_N}{2} - \frac{\lambda^2}{2m_N}\right)\mp|\vec{k}|\right) - \frac{g_c h_t^2}{2}\theta\left(\left(\frac{m_N}{2} - \frac{2\lambda^2}{m_N}\right)\mp|\vec{k}|\right)}{8\pi(m_N\mp 2|\vec{k}|)}$$
$$F^{\mathcal{B}}(\tilde{p}, -m_N\pm|\vec{k}|, |\vec{k}|) + O(\lambda^2)\,. \tag{3.97}$$

The sum over $\pm$ in $\mathcal{B}^{sca,vac}$ is replaced by $\mathcal{B}^{sca,vac+} + \mathcal{B}^{sca,vac-}$. The second term $\mathcal{B}^{sca,vac-}$ is finite in the infrared, such that λ can be set to zero. In $\mathcal{B}^{sca,vac+}$, a partial integration leads to a $\ln(\lambda)$, which cancels the one in $\mathcal{B}^{wv,vac}$.

$$\mathcal{B}^{sca,vac+}(\tilde{p}) = \frac{g_w|Y|^2}{2^5\pi^3}\Bigg($$
$$\frac{m_N^2}{4}\left(G\ln\left|\frac{Tm_N}{\lambda^2}\right| - \frac{g_c h_t^2}{2}\ln\left|\frac{Tm_N}{4\lambda^2}\right|\right)F^{\mathcal{B}}\left(\tilde{p}, -\frac{m_N}{2}, \frac{m_N}{2}\right)$$
$$+\left(G - \frac{g_c h_t^2}{2}\right)\int_0^{\frac{m_N}{2}}\mathrm{d}|\vec{k}||\vec{k}|\ln\left|\frac{m_N - 2|\vec{k}|}{T}\right|\partial_{|\vec{k}|}\left(|\vec{k}|^2 F^{\mathcal{B}}(\tilde{p}, -m_N+|\vec{k}|, |\vec{k}|)\right)$$
$$+ O(\lambda^2)\Bigg) \tag{3.98}$$

By redefining

$$\mathcal{B}^{vac-}(\tilde{p}) \equiv \mathcal{B}^{sca,vac-}(\tilde{p}) \tag{3.99}$$

$$= \frac{g_w|Y|^2}{2(2\pi)^3}\left(G - \frac{g_c h_t^2}{2}\right)\int d|\vec{k}||\vec{k}|^2\frac{1}{(m_N + 2|\vec{k}|)}F^{\mathcal{B}}(\tilde{p}, -m_N - |\vec{k}|, |\vec{k}|) \tag{3.100}$$

and

$$\mathcal{B}^{vac,\Lambda} + \mathcal{B}^{vac+} \equiv \mathcal{B}^{wv,vac} + \mathcal{B}^{sca,vac+}, \tag{3.101}$$

such that $\mathcal{B}^{vac,\Lambda}$ contains the renormalization scheme Λ dependence, the resulting functions are free of the regulating mass λ, which therefore can safely be set to zero.

$$\mathcal{B}^{vac,\Lambda}(\tilde{p}) = \frac{g_w|Y|^2}{2^7\pi^3}m_N^2\left(G\ln\left|\frac{Tm_N}{\Lambda^2}\right| - \frac{g_c h_t^2}{2}\ln\left|\frac{Tm_N}{4\Lambda^2}\right|\right)F^{\mathcal{B}}\left(\tilde{p}, -\frac{m_N}{2}, \frac{m_N}{2}\right) \tag{3.102}$$

$$\mathcal{B}^{vac+}(\tilde{p}) = \frac{g_w|Y|^2}{2^5\pi^3}\left(G - \frac{g_c h_t^2}{2}\right)\int_0^{\frac{m_N}{2}}d|\vec{k}|\ln\left|\frac{m_N - 2|\vec{k}|}{T}\right|\partial_{|\vec{k}|}\left(|\vec{k}|^2 F^{\mathcal{B}}(\tilde{p}, -m_N + |\vec{k}|, |\vec{k}|)\right) \tag{3.103}$$

The pure vacuum part, i.e. $\mathcal{B}^{vac\pm}$ using $F^{\mathcal{B},vac}$, can be evaluated analytically:

$$\mathcal{B}^{vac+,vac} = -\frac{g_w|Y|^2}{2^5\pi^3}\left(G - \frac{g_c h_t^2}{2}\right)$$
$$\int_0^{\frac{m_N}{2}}d|\vec{k}|\ln\left|\frac{m_N - 2|\vec{k}|}{T}\right|\partial_{|\vec{k}|}\left(|\vec{k}|^2\left(\text{sign}(|\vec{k}|) + \text{sign}(m_N - |\vec{k}|)\right)\right) \tag{3.104}$$

$$= -\frac{g_w|Y|^2}{2^3\pi^3}\left(G - \frac{g_c h_t^2}{2}\right)\int_0^{\frac{m_N}{2}}d|\vec{k}|\ln\left|\frac{m_N - 2|\vec{k}|}{T}\right||\vec{k}| \tag{3.105}$$

$$= -\frac{g_w|Y|^2}{2^7\pi^3}\left(G - \frac{g_c h_t^2}{2}\right)m_N^2\left(-3 + 2\ln\left(\frac{m_N}{T}\right)\right) \tag{3.106}$$

$$\mathcal{B}^{vac-,vac} = \frac{g_w|Y|^2}{2(2\pi)^3}\left(G - \frac{g_c h_t^2}{2}\right)\int d|\vec{k}||\vec{k}|^2\frac{1}{(m_N + 2|\vec{k}|)}F^{\mathcal{B},vac}(-m_N - |\vec{k}|) \tag{3.107}$$

$$\sim \int d|\vec{k}||\vec{k}|^2\frac{1}{(m_N + 2|\vec{k}|)}\left(\text{sign}(|\vec{k}|) - \text{sign}(m_N + |\vec{k}|)\right) = 0. \tag{3.108}$$

To obtain $\mathcal{B}^{vac+,T\neq0}$ and $\mathcal{B}^{vac-,T\neq0}$ from Equations (3.103) and (3.100) respectively, the $F^{\mathcal{B}}$ is replaced by $F^{\mathcal{B},T\neq0}$:

$$\mathcal{B}^{vac+,T\neq0}(\tilde{p}) = \frac{g_w|Y|^2}{2^5\pi^3}\left(G - \frac{g_c h_t^2}{2}\right)$$
$$\int_0^{\frac{m_N}{2}}d|\vec{k}|\ln\left|\frac{m_N - 2|\vec{k}|}{T}\right|\partial_{|\vec{k}|}\left(|\vec{k}|^2 F^{\mathcal{B},T\neq0}(\tilde{p}, -m_N + |\vec{k}|, |\vec{k}|)\right) \tag{3.109}$$

$$\mathcal{B}^{vac-,T\neq0}(\tilde{p}) = \frac{g_w|Y|^2}{2(2\pi)^3}\left(G - \frac{g_c h_t^2}{2}\right)$$
$$\int d|\vec{k}||\vec{k}|^2\frac{1}{(m_N + 2|\vec{k}|)}F^{\mathcal{B},T\neq0}(\tilde{p}, -m_N - |\vec{k}|, |\vec{k}|). \tag{3.110}$$

Contributions using thermal self-energies:

Left over are the terms $\mathcal{B}^{wv,T\neq0}$ and $\mathcal{B}^{sca,T\neq0}$. Since $\Pi_\phi^{H,T\neq0}(k)$ has a k-constant part[34] and a term proportional to k^2, $\mathcal{B}^{wv,T\neq0}$ results from two different contributions:

$$\mathcal{B}^{wv,T\neq0,1}(\tilde{p}) = \frac{g_w|Y|^2}{2^3\pi}\Pi_\phi^{H,T\neq0}(k^2=0)$$
$$\left.\left(\left(1+\frac{m_N}{4}\left(\partial_{k^0}+\partial_{|\vec{k}|}\right)\right)F^\mathcal{B}(\tilde{p},k^0,|\vec{k}|)\right)\right|_{\substack{|\vec{k}|=\frac{m_N}{2}\\k^0=-\frac{m_N}{2}}} \tag{3.111}$$

$$\mathcal{B}^{wv,T\neq0,2}(\tilde{p}) = \frac{g_w|Y|^2m_N^2}{2^6\pi^3}\left(\int\frac{1}{|\vec{k_u}|}\left(GI_{2-}(k_u^0,|\vec{k_u}|)+\frac{g_ch_t^2}{2}I_{2+}(k_u^0,|\vec{k_u}|)\right)\right.$$
$$\left.\left.\mathrm{d}F^\mathcal{B}(\tilde{p},k^0,|\vec{k}|)\right)\right|_{\substack{|\vec{k}|=\frac{m_N}{2}\\k^0=-\frac{m_N}{2}}} . \tag{3.112}$$

Since $\mathrm{sign}(k_u^0)$ equals to $\mathrm{sign}(k^0)$ and k^2 is a Lorentz scalar, $I_{2\pm}$ can be simplified further in the limit $k_u^0 \to -|\vec{k_u}|$. The second part then reduces to

$$\mathcal{B}^{wv,T\neq0,2}(\tilde{p}) = \frac{g_w|Y|^2m_N^2}{2^6\pi^3}\int\mathrm{d}\cos\sphericalangle\mathrm{d}|\vec{q}|\left(\frac{1}{|\vec{k_u}|}\left(f_-(-|\vec{k_u}|)+f_+(\tilde{p}^0-|\vec{k_u}|)\right)\right.$$
$$\left.\left.\left(Gf_-(|\vec{q}|)+\frac{g_ch_t^2}{2}f_+(|\vec{q}|)\right)\ln\left|\frac{|\vec{q}|-|\vec{k_u}|}{|\vec{q}|+|\vec{k_u}|}\right|\right)\right|_{|\vec{k_u}|=\frac{\tilde{p}^0+|\vec{p}|\cos\sphericalangle}{2}} . \tag{3.113}$$

The remaining scattering contribution is

$$\mathcal{B}^{sca,T\neq0}(\tilde{p}) = \frac{2g_w|Y|^2}{(2\pi)^2}\int\mathrm{d}|\vec{k}||\vec{k}|^2\sum_{k^0=-m_N\pm|\vec{k}|}\frac{1}{(m_N\mp2|\vec{k}|)k^2}\Pi_\phi^{\mathcal{A},T\neq0}(k)\mathrm{d}F^\mathcal{B}(\tilde{p},k^0,|\vec{k}|) . \tag{3.114}$$

The Equations (3.113) and (3.114) can be evaluated numerically.

3.5.1.2 Numerical Solution

Figure 3.14 provides an overview of all existing $\mathcal{B}$ terms in this expansion, their splittings and the equation indices. Those functions are evaluated numerically with the tools from Chapter 4.5 within a relative error of 10^{-3}. The evaluated parameter space is spanned by $10^{-4} \leq m_N \leq 10^2$ using 61 points on a logarithmic scale, and $10^{-3} \leq |\vec{p}| \leq 10^{1.5}$ using 46 points on a logarithmic scale. For comparison with later results, h_t and λ_ϕ are set to zero. Also for ease of comparison, the total rate γ_N is calculated using the various contributions to $\mathcal{B}$ separately by integrating over $|\vec{p}|$ from $10^{-3}T$ to $10^{1.5}T$. In particular, the parameter space for $|\vec{p}|$ is chosen such that γ_N can be evaluated within a relative error of 10^{-3}. The results are presented in Figure 3.15. As mentioned, the additional "$O(G)$" index indicates the perturbative expansion in the gauge couplings.

---

[34] The thermal mass of the Higgs is $(m_\phi^{th})^2 \equiv \Pi^{H,T\neq0}(k^2=0) = \frac{1}{4}GT^2 + \frac{g_ch_t^2}{12}T^2 + \frac{1}{4}\lambda_\phi T^2$.
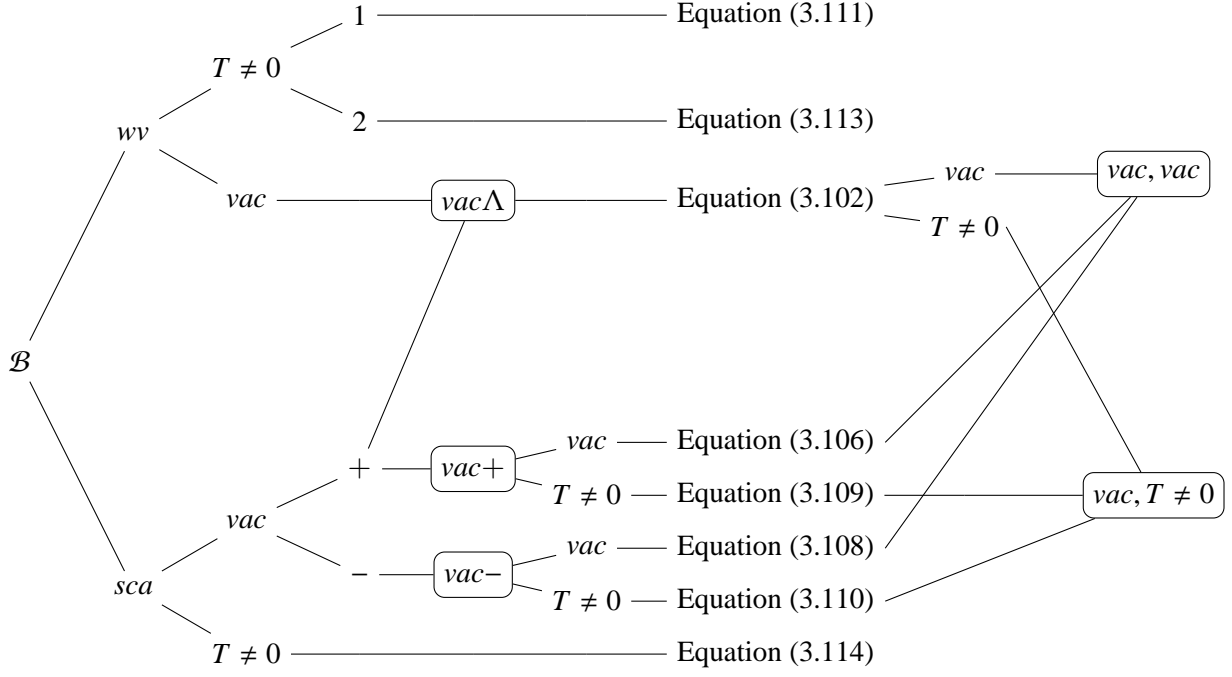
Figure 3.14: Splitting of $\mathcal{B}^{O(G,h_t^2,\lambda_\phi)}$ by notion of its superscripts. The first separation into vacuum and thermal contributions corresponds to a separation of the Higgs self-energy into a vacuum and thermal part. The second one splits the exterior distribution functions, i.e. $F^{\mathcal{B}}$. A boxed node means that the whole branch is renamed as this node.
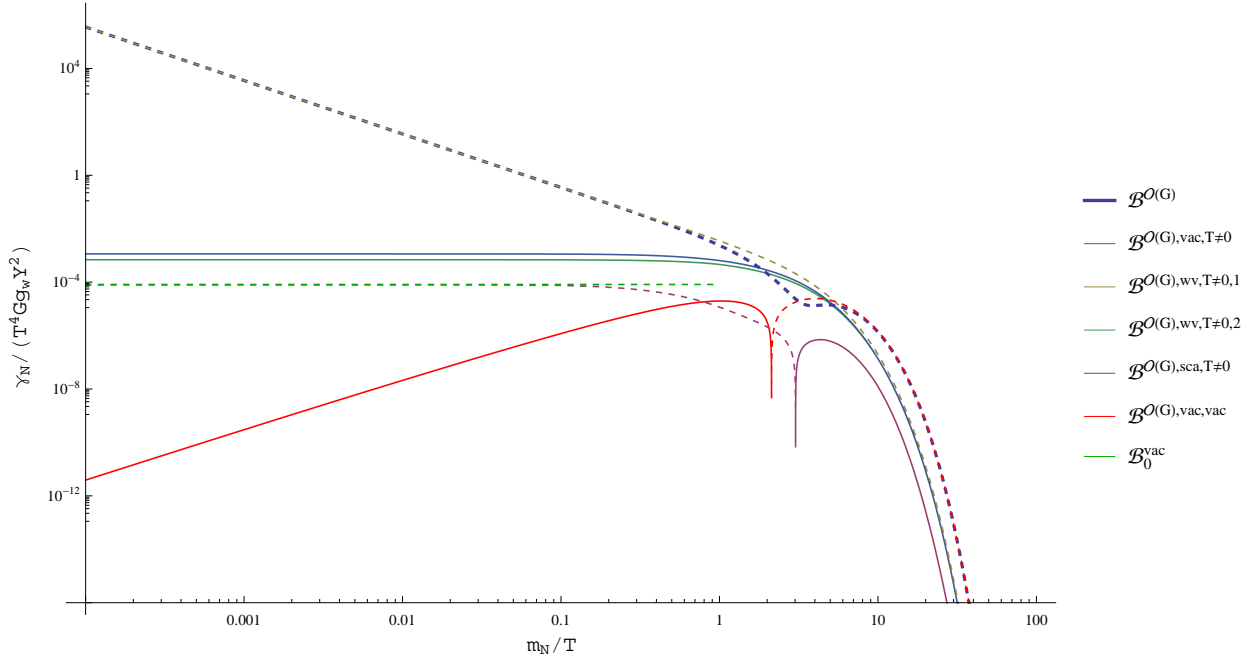
Figure 3.15: Plot of $\gamma_N\left[\mathcal{B}^{O(G)}\right](m_N)$ for various contributions of $\mathcal{B}^{O(G)}$ and $\Lambda = T$. $\mathcal{B}_0^{vac}$ corresponds to the Higgs contribution using the $\Pi_\phi^{\mathcal{A},vac}$ in the massless limit. Solid and dashed lines respectively correspond to positive and negative values.

As can be seen, the pure vacuum terms summed up in $B^{vac,vac}$, i.e. the red line, become unimportant in the ultra-relativistic limit. However, they dominate the $O(G)$ correction to the rate $\gamma[\mathcal{B}^{O(G)}]$, i.e. the thick blue line, in the non-relativistic limit.

A logarithmic and a power divergence is found for small $\frac{m_N}{T}$. This results from the Bose-Einstein distribution in the $B^{wv,T\neq0,1}$ term, which is one of the terms that perturbatively include the thermal mass. In the $\frac{m_N}{T} \to 0$ limit, the divergent terms can be evaluated analytically:

$$\gamma_N\left[B^{wv,T\neq0,1}(m_N \ll T)\right]_{\text{div}} = g_w|Y|^2 G T^4 \frac{1}{2^5\pi^3}\left(\ln\left(\frac{2m_N}{T}\right) - 3\zeta(3)\left(\frac{T}{m_N}\right)^2\right), \qquad (3.115)$$

where ζ is the Riemann zeta function. This divergent behavior is no surprise, since the perturbative coupling expansion is expected to break down for massless Higgs propagator momenta of the order of T. These momenta correlate to the neutrino mass and the temperature via the Bose-Einstein distribution. In particular, the Bose-Einstein pole is regulated by $\frac{m_N}{T}$. Hence, for small $\frac{m_N}{T}$ values, the loop integral is dominated by small Higgs propagator momenta. At this point, effects from the plasma become important. Those screen the enhancement in $B^{wv,T\neq0,1}$ by inducing a thermal mass non-perturbatively. Conversely, the perturbative expansion breaks down. The physical screening from the thermal plasma is incorporated by using resummed propagators as suggested by the 2PI formalism. This is done in Section 3.5.2.

Nevertheless, contact of the scattering terms with the perturbatively expanded result (3.43) should be found in the ultra-relativistic limit. When all terms that include only the vacuum spectral Higgs self-energy are added together, the contribution to the total rate for the smallest evaluated neutrino mass is

$$\gamma_N\left[\mathcal{B}^{O(G),vac}\right](m_N = 10^{-4}T) \approx -1.29(95 \pm 13)\frac{1}{(2\pi)^5}\left(\frac{\pi^2}{12}\right)^2 g_w|Y|^2 G T^4 . \qquad (3.116)$$

This is in good agreement to the exact factor $-1.3G$ of $\gamma_N[\mathcal{B}_0]$ in Equation (3.46), which is called $\mathcal{B}_0^{vac}$ in Figure 3.15. $\gamma_N[\mathcal{B}^{O(G),vac}]$ corresponds to the line $\mathcal{B}^{O(G),vac,T\neq0}$, since $\mathcal{B}^{O(G),vac,vac}$ and the $\mathcal{B}^{O(G),vac,\Lambda}$ for a fixed Λ vanish in the massless limit.

Likewise, the contributions that include only the thermal part of the spectral Higgs self-energy should coincide with the factor 5.8596 in Equation (3.46). This is the $\mathcal{B}^{O(G),sca,T\neq0}$ term from Equation (3.114). In fact, one can show that by tracing back in the calculation, up to the point where Equation (3.114) is completely written in terms of Lorentz invariant scalar products and setting $m_N = 0$, this is exactly the same equation as (3.43). However, the numerical result is

$$\gamma_N\left[\mathcal{B}^{O(G),sca,T\neq0}\right](m_N = 10^{-4}T) \approx 17.8(6 \pm 2)\frac{1}{(2\pi)^5}\left(\frac{\pi^2}{12}\right)^2 g_w|Y|^2 G T^4 . \qquad (3.117)$$

The reason for this mismatch is that the cancellation of the propagator pole in (3.43) with the numerator algebra works only when m_N is set to zero. To investigate this further, Equation (3.114) can be rewritten as

$$\mathcal{B}^{O(G),sca,T\neq0}(\tilde{p}) = \frac{2g_w|Y|^2}{(2\pi)^2}\int d|\vec{k}|\frac{|\vec{k}|}{2}\sum_{k^0=-m_N\pm|\vec{k}|}(\mp)\left(\underbrace{\frac{1}{(a)}}_{} - \underbrace{\frac{m_N}{m_N \mp 2|\vec{k}|}}_{(b)}\right)\frac{\Pi_\phi^{\mathcal{A},T\neq0}(k)}{k^2}d\mathcal{F}^{\mathcal{B}}(\tilde{p},k^0,|\vec{k}|), \quad (3.118)$$

where part (b) is the one that was set to zero in the ultra-relativistic calculation. A numerical check of part (a) evaluates to

$$\gamma_N[\text{Equation (3.118)}(a)](m_N = 10^{-4}T) \approx 5.85(957 \pm 586)\frac{1}{(2\pi)^5}\left(\frac{\pi^2}{12}\right)^2 g_w|Y|^2 G T^4 , \qquad (3.119)$$

57

which fits perfectly to the massless result even for more digits than estimated by the error. However, the (b) part of (3.118) does not vanish under the integral for small m_N, numerically checked up to $m_N = 10^{-4}T$.

$$\gamma_N[\text{Equation (3.118)}(b)](m_N = 10^{-4}T) \approx 12.0(0 \pm 3)\frac{1}{(2\pi)^5}\left(\frac{\pi^2}{12}\right)^2 g_w|Y|^2 GT^4 \qquad (3.120)$$

This non-zero value originates from an interference of three enhancements coming from the Bose-Einstein distributions within $\Pi^{\mathcal{A}}$, the Bose-Einstein distribution in $\mathrm{d}\mathcal{F}^{\mathcal{B}}$, and the principal value at $|\vec{k}| = \frac{m_N}{2}$.

One possible explanation for the non-vanishing (b) part is that $m_N = 10^{-4}T$ may be not small enough. The (b) term could be evaluated for even smaller masses, and eventually one would find another limit. However, there is a likewise simple counter-argument: Within the perturbative calculation and after $|\vec{p}|$ is integrated out, the only remaining scales are m_N and T. Therefore, modifications of the corresponding physics are found at approximately $m_N \approx T$. Nevertheless, there is no physical reason for a change below $m_N < 10^{-4}T$. Another explanation is that the non-vanishing (b) term partly captures the missing thermal mass effects of (3.43): According to Section 3.4.1.2, the missing order G correction to Equation (3.43) is given by the $1 \leftrightarrow 2$ processes $N \leftrightarrow l\phi$ and $N \leftrightarrow \bar{l}\bar{\phi}$, including a thermal tree-level mass for the Higgs. In the small coupling limit, this is approximately

$$\gamma_N[\mathcal{H}(m_\phi = m_\phi^{th})][m_N = 0, G \ll 1] \approx 7.75(2 \pm 1)\frac{1}{(2\pi)^5}\left(\frac{\pi^2}{12}\right)^2 g_w|Y|^2 GT^4. \qquad (3.121)$$

in comparison to the factor 12.0 of Equation (3.120).

On the other hand, arguments over whether this result in the ultra-relativistic limit is physically correct or not are useless. The logarithmic and power divergence for small $\frac{m_N}{T}$ shows the breakdown of perturbation theory, which states that mathematically a resummation and physically screening processes at $m_N = 0$ are needed. This breakdown happens theoretically at latest at – but practically above – the thermal mass scale $m_N \approx m_\phi^{th}$. This means that the resummation introduces a new mass scale where the physics changes. Above that point, the non-vanishing (b) term is acceptable and physically correct, but below it, (b) does not describe the correct processes.

3.5.1.3 Corrections from the Lepton

The same steps can be applied on the lepton side. First, the $\mathcal{S}_l^{(1),\mathcal{A}}$ is written as retarded and advanced functions, i.e. the expression in Equation (3.63). The $\mathcal{F}$-terms proportional to Σ^H are called the *wv* terms, and the one proportional to $\Sigma^{\mathcal{A}}$ are referred to by the *sca* terms. When (3.63) is included in

$$\mathcal{F}(\tilde{p}) = g_w|Y|^2 2 \int \frac{\mathrm{d}^4k}{(2\pi)^4} \mathrm{tr}\left[\not{p}\mathcal{S}_l^{(1),\mathcal{A}}(k)\right]\Delta_\phi^{(0),\mathcal{A}}(k-p)\left(f_-(u\cdot(k-p)) + f_+(u\cdot k)\right), \qquad (3.122)$$

the Dirac trace together with (2.84) gives

$$\frac{1}{4}\mathrm{tr}\left[\not{p}\not{k}\not{\Sigma}\not{k}\right] = 2p\cdot k\, k\cdot\Sigma - k^2\, p\cdot\Sigma \qquad (3.123)$$

$$= \left(-k^2, 2p\cdot k\right)\cdot\begin{pmatrix} p\cdot k & p\cdot u \\ k^2 & k\cdot u \end{pmatrix}\cdot\mathrm{Gram}^{-1}(k,u)\cdot\begin{pmatrix} k\cdot\Sigma \\ u\cdot\Sigma \end{pmatrix} \qquad (3.124)$$

for a general Lorentz vector $\Sigma(k,u) = c_1 k + c_2 u$ with corresponding scalar coefficients c_1 and c_2. In the case of vacuum self-energies $\Sigma^{vac}(k) = c_1 k$, the trace can be reduced to

$$\frac{1}{4}\mathrm{tr}\left[\not{p}\not{k}\Sigma^{vac}\not{k}\right] = p\cdot k\, k\cdot\Sigma^{vac}. \qquad (3.125)$$

58

First, the abbreviation

$$dF^{\mathcal{F}}\left(\tilde{p},k^0,|\vec{k}|\right) \equiv d\cos \angle(k,u)\left(f_-\left(u\cdot(k-p)\right)+f_+\left(u\cdot k\right)\right) \tag{3.126}$$

$$\int dF^{\mathcal{F}}\left(\tilde{p},k^0,|\vec{k}|\right) = F^{\mathcal{F}}\left(\tilde{p},k^0,|\vec{k}|\right) = \frac{m_N T}{|\vec{k}||\vec{p}|}\ln\left|\frac{f_-\left(\frac{(m_N-k^0)\tilde{p}^0+|\vec{k}||\vec{p}|}{m_N}\right)f_+\left(\frac{-k^0\tilde{p}^0-|\vec{k}||\vec{p}|}{m_N}\right)}{f_-\left(\frac{(m_N-k^0)\tilde{p}^0-|\vec{k}||\vec{p}|}{m_N}\right)f_+\left(\frac{-k^0\tilde{p}^0+|\vec{k}||\vec{p}|}{m_N}\right)}\right| \tag{3.127}$$

$$F^{\mathcal{F},vac}(k^0) = \text{sign}(k^0-m_N) - \text{sign}(k^0) \tag{3.128}$$

is introduced. Then, the *wv*-vacuum expression is derived:

$$\mathcal{F}^{wv,vac}(\tilde{p}) = g_w|Y|^2\frac{1}{\pi^2}\int dk^0 d|\vec{k}|\text{sign}(k^0-m_N)\frac{1}{2}\left(\delta(|\vec{k}|+k^0-m_N)+\underbrace{\delta(|\vec{k}|-k^0+m_N)}_{\to 0}\right)$$

$$\delta(k^0-\frac{m_N}{2})\frac{\pi}{4m_N^2}\left(\partial_{k^0}-\partial_{|\vec{k}|}\right)\left(|\vec{k}|\,p\cdot k\,k\cdot\Sigma_l^{H,vac}dF^{\mathcal{F}}\left(\tilde{p},k^0,|\vec{k}|\right)\right) \tag{3.129}$$

$$= -g_w|Y|^2\frac{1}{2^3\pi m_N^2}\int dk^0 d|\vec{k}|\,\delta\left(|\vec{k}|-\frac{m_N}{2}\right)\delta\left(k^0-\frac{m_N}{2}\right)$$

$$\left(\partial_{k^0}-\partial_{|\vec{k}|}\right)\left(|\vec{k}|\,p\cdot k\,k\cdot\Sigma_l^{H,vac}dF^{\mathcal{F}}\left(\tilde{p},k^0,|\vec{k}|\right)\right)\,. \tag{3.130}$$

Even if it is the same for this case, one may need to ensure that $\delta((k-p)^2)$ is separated into two deltas with a factor of $\frac{1}{2|\vec{k}|}$ and not $\frac{1}{2|k^0-m_N|}$. A possible difference could arise due to the derivatives. During the construction of (3.73), the delta distribution was integrated out by $d|\vec{k}|$ while dk^0 became the Cauchy integral. Therefore, $\frac{1}{2|\vec{k}|}$ is definitely the right choice.

One of the delta functions vanishes, since it is never solved together with the $k^2 = 0$ condition from the Cauchy integral of $S_l^{(1),\mathcal{A}}$. Since $k\cdot\Sigma_l^{H,vac}(k)$ is proportional to k^2, the derivatives can only act on this k^2. Otherwise the resulting expression would vanish after integrating over the delta distributions. Consequently,

$$\mathcal{F}^{wv,vac}(\tilde{p}) = -g_w|Y|^2\frac{m_N}{2^5\pi}\int dk^0 d|\vec{k}|dF^{\mathcal{F}}\left(\tilde{p},\frac{m_N}{2},\frac{m_N}{2}\right)\delta\left(|\vec{k}|-\frac{m_N}{2}\right)\delta\left(k^0-\frac{m_N}{2}\right)\left(\partial_{k^0}-\partial_{|\vec{k}|}\right)k\cdot\Sigma_l^{H,vac} \tag{3.131}$$

$$= -g_w|Y|^2\frac{Gm_N^2}{2^7\pi^3}\ln\frac{\lambda}{\Lambda}F^{\mathcal{F}}\left(\tilde{p},\frac{m_N}{2},\frac{m_N}{2}\right) \tag{3.132}$$

is obtained. $\mathcal{F}^{wv,vac}$ contains a "finite" part and a part originating from the collinear divergence of the $l\to l\gamma$ scattering, which is regulated by the fictitious gauge boson mass λ. The $\ln(\lambda)$-dependent part and the remainder are called $\mathcal{F}^{wv,vac,col}(\tilde{p})$ and $\mathcal{F}^{wv,vac,fin}$, respectively.[35]

$$\mathcal{F}^{wv,vac,fin}(\tilde{p}) = g_w|Y|^2\frac{Gm_N^2}{2^7\pi^3}\ln\frac{\Lambda}{T}F^{\mathcal{F}}\left(\tilde{p},\frac{m_N}{2},\frac{m_N}{2}\right) \tag{3.133}$$

$$\mathcal{F}^{wv,vac,col}(\tilde{p}) = -g_w|Y|^2\frac{Gm_N^2}{2^7\pi^3}\ln\frac{\lambda}{T}F^{\mathcal{F}}\left(\tilde{p},\frac{m_N}{2},\frac{m_N}{2}\right) \tag{3.134}$$

Likewise, $\mathcal{F}^{sca,vac}$ is found to be

$$\mathcal{F}^{sca,vac}(\tilde{p}) = \frac{g_w|Y|^2}{(2\pi)^2}\int d|\vec{k}|\,|\vec{k}|\sum_{k^0=m_N\pm|\vec{k}|}\pm\frac{m_N^2+k^2}{k^4}k\cdot\Sigma_l^{\mathcal{A},vac}(k)dF^{\mathcal{F}}\left(\tilde{p},k^0,|\vec{k}|\right)\,. \tag{3.135}$$

---

[35] The introduced $\ln(.)$ can take any scale. However, since the Λ in the numerics is set to T, the scale T is chosen for convenience.

Since $k \cdot \Sigma_l^{\mathcal{A},vac}(k)$ is proportional to k^2, the part that arises from the k^2 in the numerator is finite, while the part that arises from the m_N^2 contains a collinear divergence. Hence, those are referred to in the usual way.

$$\mathcal{F}^{sca,vac,fin}(\tilde{p}) = \frac{g_w|Y|^2 G}{2^6 \pi^3} \int \mathrm{d}|\vec{k}|\,|\vec{k}| \sum_{k^0 = m_N \pm |\vec{k}|} \pm \theta(k^2)\mathrm{sign}(k^0)\mathrm{d}F^{\mathcal{F}}\left(\tilde{p}, k^0, |\vec{k}|\right) \tag{3.136}$$

$$= \frac{g_w|Y|^2 G}{2^6 \pi^3} \int \mathrm{d}|\vec{k}|\,|\vec{k}| \sum_{\pm} \pm \theta(m_N \pm 2|\vec{k}|) F^{\mathcal{F}}\left(\tilde{p}, m_N \pm |\vec{k}|, |\vec{k}|\right) \tag{3.137}$$

$$\mathcal{F}^{sca,vac,col}(\tilde{p}) = \frac{g_w|Y|^2 G}{2^6 \pi^3} \int \mathrm{d}|\vec{k}|\,|\vec{k}| \sum_{k^0 = m_N \pm |\vec{k}|} \pm \frac{m_N^2}{k^2} \theta(k^2 - \lambda^2)\mathrm{sign}(k^0) F^{\mathcal{F}}\left(\tilde{p}, k^0, |\vec{k}|\right) \tag{3.138}$$

$\mathcal{F}^{sca,vac,col}$ should be split further into $\mathcal{F}^{sca,vac,col\pm}$ corresponding to the sum, since the fictitious gauge boson mass λ can be set to zero in $\mathcal{F}^{sca,vac,col+}$.

$$\mathcal{F}^{sca,vac,col+}(\tilde{p}) = \frac{g_w|Y|^2 G}{2^6 \pi^3} \int \mathrm{d}|\vec{k}| \frac{m_N}{m_N + 2|\vec{k}|} |\vec{k}| F^{\mathcal{F}}\left(\tilde{p}, m_N + |\vec{k}|, |\vec{k}|\right) \tag{3.139}$$

In $\mathcal{F}^{sca,vac,col-}$, a partial integration analogous to the case for $\mathcal{B}^{sca,vac+}$ reveals a $\ln(\lambda)$ term that cancels the $\ln(\lambda)$ in $\mathcal{F}^{wv,vac,col}$:

$$\mathcal{F}^{sca,vac,col-}(\tilde{p}) = -\frac{g_w|Y|^2 G}{2^6 \pi^3} \int_0^{\frac{m_N^2 - \lambda^2}{2m_N}} \mathrm{d}|\vec{k}| \frac{m_N}{m_N - 2|\vec{k}|} |\vec{k}| F^{\mathcal{F}}\left(\tilde{p}, m_N - |\vec{k}|, |\vec{k}|\right) \tag{3.140}$$

$$= \frac{g_w|Y|^2 G m_N}{2^7 \pi^3} \ln\left(\frac{m_N - 2|\vec{k}|}{T}\right) |\vec{k}| F^{\mathcal{F}}\left(\tilde{p}, m_N - |\vec{k}|, |\vec{k}|\right)\Bigg|_0^{\frac{m_N^2 - \lambda^2}{2m_N}} \tag{3.141a}$$

$$- \frac{g_w|Y|^2 G m_N}{2^7 \pi^3} \int_0^{\frac{m_N}{2}} \mathrm{d}|\vec{k}| \ln\left(\frac{m_N - 2|\vec{k}|}{T}\right) \partial_{|\vec{k}|}\left(|\vec{k}| F^{\mathcal{F}}\left(\tilde{p}, m_N - |\vec{k}|, |\vec{k}|\right)\right). \tag{3.141b}$$

Equation (3.141b) is called $\mathcal{F}^{sca,vac,col-,2}$. It is finite and it can be calculated numerically. Equation (3.141a), i.e. $\mathcal{F}^{sca,vac,col-,1}$, added to $\mathcal{F}^{wv,vac,col}$ results in

$$\mathcal{F}^{vac,col-,1} \equiv -\frac{g_w|Y|^2 G m_N^2}{2^8 \pi^3} \ln\left(\frac{m_N}{T}\right)\left(F^{\mathcal{F}}\left(\tilde{p}, \frac{m_N}{2}, \frac{m_N}{2}\right) + 2\frac{T}{|\vec{p}|}\ln\left|\frac{\tilde{p}^0 - |\vec{p}|}{\tilde{p}^0 + |\vec{p}|}\right|\right) + O(\lambda^2) \tag{3.142}$$

$$= \frac{g_w|Y|^2 G m_N^2}{2^7 \pi^3} \ln\left(\frac{m_N}{T}\right)\frac{T}{|\vec{p}|}\ln\left|\frac{\tilde{p}^0 + |\vec{p}|}{\tilde{p}^0 - |\vec{p}|} \frac{f_-\left(\frac{\tilde{p}^0 - |\vec{p}|}{2}\right)f_+\left(\frac{-\tilde{p}^0 + |\vec{p}|}{2}\right)}{f_-\left(\frac{\tilde{p}^0 + |\vec{p}|}{2}\right)f_+\left(\frac{-\tilde{p}^0 - |\vec{p}|}{2}\right)}\right| + O(\lambda^2), \tag{3.143}$$

such that λ can safely be set to zero.

All that remains is to write down the thermal contributions. Those can be split into a $\overline{T \neq 0}$ and a HTL part as derived in Chapter 2.6. While the $\overline{T \neq 0}$ contributions are perfectly finite, the HTL terms also involve an infrared divergence from the t-channel exchange of a massless lepton. Therefore, a fictitious lepton mass m_l is introduced, such that only a collinear divergence regulated by m_l has to be dealt with. Whenever possible, m_l is set to zero.

The *sca* contributions can be simplified using the $\delta((k-p)^2)$ from $\Delta_\phi^{(0),\mathcal{A}}$. However, in the case of the *wv* contributions, the derivative has to be considered first. With $k \cdot u = k_u^0$ and

$$\delta(|\vec{k}| + k^0 - m_N)\mathrm{tr}\left[\not{p}\not{S}_l^{(1),\mathcal{A}}\right]\Big|^{wv} = \delta(|\vec{k}| - \frac{m_N}{2} + \frac{m_l^2}{2m_N})\delta(k^0 - \frac{m_N}{2} - \frac{m_l^2}{2m_N})\frac{\pi}{m_N^2}\left(\partial_{k^0} - \partial_{|\vec{k}|}\right) \tag{3.144}$$

$$\frac{1}{|\vec{k}_u|^2}\left((|\vec{k}_u|^2 + k_u^{0^2})p \cdot k - k^2 k_u^0\, p \cdot u,\, k^2(k^2 p \cdot u - k_u^0\, p \cdot k)\right) \cdot \left(\begin{array}{c} k \cdot \Sigma_l^H \\ u \cdot \Sigma_l^H \end{array}\right)$$

$$= \delta\left(|\vec{k}| - \frac{m_N}{2} + \frac{m_l^2}{2m_N}\right)\delta\left(k^0 - \frac{m_N}{2} - \frac{m_l^2}{2m_N}\right)\pi \tag{3.145}$$

$$\left(\frac{m_N^2 + 2k_u^0(k_u^0 - p \cdot u)}{m_N k_u^{0^2}} + \left(\partial_{k^0} - \partial_{|\vec{k}|}\right), -\frac{m_N}{k_u^0}\right) \cdot \begin{pmatrix} k \cdot \Sigma_l^H \\ u \cdot \Sigma_l^H \end{pmatrix} + O(m_l^2),$$

the thermal *wv* and *sca* terms, including m_l, read

$$\mathcal{F}^{wv}(\tilde{p}) = -\frac{g_w|Y|^2}{2^3\pi}\int dk^0 d|\vec{k}|\delta\left(k^0 - \frac{m_N}{2} - \frac{m_l^2}{2m_N}\right)\delta\left(|\vec{k}| - \frac{m_N}{2} + \frac{m_l^2}{2m_N}\right) \tag{3.146}$$

$$\left(\frac{m_N^2 + 2k_u^0(k_u^0 - p \cdot u)}{m_N k_u^{0^2}} + \left(\partial_{k^0} - \partial_{|\vec{k}|}\right), -\frac{m_N}{k_u^0}\right) \cdot \left[|\vec{k}|dF^{\mathcal{F}}\left(\tilde{p}, k^0, |\vec{k}|\right)\begin{pmatrix} k \cdot \Sigma_l^H \\ u \cdot \Sigma_l^H \end{pmatrix}\right] + O(m_l^2)$$

$$\mathcal{F}^{sca}(\tilde{p}) = \frac{g_w|Y|^2}{2\pi^2}\int d|\vec{k}| \sum_{k^0 = M\pm|\vec{k}|} \pm\frac{1}{(k^2 - m_l^2)^2}|\vec{k}|dF^{\mathcal{F}}\left(\tilde{p}, k^0, |\vec{k}|\right) \tag{3.147}$$

$$\left(2p \cdot k + \frac{k^2}{|\vec{k}_u|^2}\left(p \cdot k - k \cdot u\, p \cdot u\right), \frac{k^2}{|\vec{k}_u|^2}\left(k^2 p \cdot u - k \cdot u\, p \cdot k\right)\right) \cdot \begin{pmatrix} k \cdot \Sigma_l^{\mathcal{A}} \\ u \cdot \Sigma_l^{\mathcal{A}} \end{pmatrix}.$$

The expression proportional to $k \cdot \Sigma_l^{H,HTL}(k)$ is finite at $m_l = 0$. The one proportional to $u \cdot \Sigma_l^{H,HTL}(k)$ contains the collinear divergence regulated by m_l. Therefore, those are split into *fin* and *col* terms.

$$\mathcal{F}^{wv,HTL,fin}(\tilde{p}) = -\frac{g_w|Y|^2 GT^2}{2^6\pi m_N}\int dk^0 d|\vec{k}|\delta\left(k^0 - \frac{m_N}{2}\right)\delta\left(|\vec{k}| - \frac{m_N}{2}\right)$$

$$\left(\frac{m_N^2 + 2k_u^0(k_u^0 - p \cdot u)}{k_u^{0^2}} + m_N\left(\partial_{k^0} - \partial_{|\vec{k}|}\right)\right)\left[|\vec{k}|dF^{\mathcal{F}}\left(\tilde{p}, k^0, |\vec{k}|\right)\right] \tag{3.148}$$

The finite *sca* part vanishes, since $k \cdot \Sigma_l^{\mathcal{A},HTL} = 0$:

$$F^{sca,HTL,fin}(\tilde{p}) = 0. \tag{3.149}$$

The collinear divergent *wv* part contains the $\ln(m_l)$:

$$\mathcal{F}^{wv,HTL,col}(\tilde{p}) = \frac{g_w|Y|^2 GT^2 m_N^2}{2^5\pi}\int\frac{\ln\left(\frac{\tilde{p}^0 - |\vec{p}|\cos\angle(k,u)}{m_l}\right)}{\left(\tilde{p}^0 - |\vec{p}|\cos\angle(k,u)\right)^2}dF^{\mathcal{F}}\left(\tilde{p}, \frac{m_N}{2}, \frac{m_N}{2}\right) + O\left(m_l^2\right). \tag{3.150}$$

This $\ln(m_l)$ cancels the one in $F^{sca,HTL,col-,1}$. The derivation starts with

$$F^{sca,HTL,col}(\tilde{p}) = \frac{g_w|Y|^2 GT^2}{2^5\pi}\int d|\vec{k}| \sum_{k^0 = M\pm|\vec{k}|} \pm\frac{1}{k^2 - m_l^2}|\vec{k}|dF^{\mathcal{F}}\left(\tilde{p}, k^0, |\vec{k}|\right)$$

$$\frac{1}{|\vec{k}_u|^3}\left(k^2 p \cdot u - k \cdot u\, p \cdot k\right)\theta(-k^2 - m_l^2) + O\left(m_l^2\right) \tag{3.151}$$

including the fictitious lepton mass m_l. The minus part is

$$F^{sca,HTL,col-}(\tilde{p}) = \frac{g_w|Y|^2 GT^2}{2^6\pi m_N}\int_{\frac{m_N^2 + m_l^2}{2m_N}}^{\infty} d|\vec{k}|\frac{1}{|\vec{k}| - \frac{m_N^2 - m_l^2}{2m_N}}|\vec{k}|dF^{\mathcal{F}}\left(\tilde{p}, m_N - |\vec{k}|, |\vec{k}|\right)$$

$$\frac{1}{|\vec{k}_u|^3}\left(k^2 p \cdot u - k \cdot u\, p \cdot k\right)\Big|_{k^0 = m_N - |\vec{k}|} + O\left(m_l^2\right), \tag{3.152}$$

61

which equals, due to a partial integration, the sum of

$$F^{sca,HTL,col-,1}(\tilde{p}) = \frac{g_w|Y|^2 GT^2}{2^6\pi m_N}\int \ln\left(\frac{|\vec{k}|-\frac{m_N^2-m_l^2}{2m_N}}{T}\right)|\vec{k}|\mathrm{d}F^{\mathcal{F}}\left(\tilde{p}, m_N - |\vec{k}|, |\vec{k}|\right)$$

$$\left.\frac{1}{|\vec{k}_u|^3}\left(k^2 p\cdot u - k\cdot u\, p\cdot k\right)\right|_{k^0=m_N-|\vec{k}|}\Bigg|_{\frac{m_N^2+m_l^2}{2m_N}}^{\infty} \tag{3.153}$$

and

$$F^{sca,HTL,col-,2}(\tilde{p}) = -\frac{g_w|Y|^2 GT^2}{2^6\pi m_N}\int_{\frac{m_N}{2}}^{\infty}\mathrm{d}|\vec{k}|\ln\left(\frac{|\vec{k}|-\frac{m_N}{2}}{T}\right)\partial_{|\vec{k}|}\Bigg[|\vec{k}|\mathrm{d}F^{\mathcal{F}}\left(\tilde{p}, m_N - |\vec{k}|, |\vec{k}|\right)$$

$$\left.\frac{1}{|\vec{k}_u|^3}\left(k^2 p\cdot u - k\cdot u\, p\cdot k\right)\right|_{k^0=m_N-|\vec{k}|}\Bigg]. \tag{3.154}$$

In $F^{sca,HTL,col-,2}$, the mass m_l can be set to zero. $F^{sca,HTL,col-,1}$ becomes

$$F^{sca,HTL,col-,1}(\tilde{p}) = \frac{g_w|Y|^2 GT^2 m_N^2}{2^6\pi}\int \frac{\ln\left(\frac{m_l^2}{m_N T}\right)}{\left(\tilde{p}^0 - |\vec{p}|\cos\angle(k,u)\right)^2}\mathrm{d}F^{\mathcal{F}}\left(\tilde{p}, \frac{m_N}{2}, \frac{m_N}{2}\right) + O\left(m_l^2\right), \tag{3.155}$$

and with $F^{HTL,col-,1} \equiv F^{sca,HTL,col-,1} + F^{wv,HTL,col}$,

$$F^{HTL,col-,1} = \frac{g_w|Y|^2 GT^2 m_N^2}{2^6\pi}\int \frac{\ln\left(\frac{\left(\tilde{p}^0-|\vec{p}|\cos\angle(k,u)\right)^2}{m_N T}\right)}{\left(\tilde{p}^0 - |\vec{p}|\cos\angle(k,u)\right)^2}\mathrm{d}F^{\mathcal{F}}\left(\tilde{p}, \frac{m_N}{2}, \frac{m_N}{2}\right) + O\left(m_l^2\right) \tag{3.156}$$

is free of the regulator. From now on, m_l is set to zero. The remaining terms are finite and are summarized in the following. Due to the θ function, $F^{sca,HTL,col+}$ vanishes:

$$F^{sca,HTL,col+}(\tilde{p}) = 0. \tag{3.157}$$

The other terms are

$$\mathcal{F}^{wv,\overline{T\neq0}}(\tilde{p}) = -\frac{g_w|Y|^2}{2^3\pi m_N}\int \mathrm{d}k^0\mathrm{d}|\vec{k}|\delta\left(k^0-\frac{m_N}{2}\right)\delta\left(|\vec{k}|-\frac{m_N}{2}\right) \tag{3.158}$$

$$\left(\frac{m_N^2 + 2k_u^0(k_u^0 - p\cdot u)}{k_u^{02}} + m_N\left(\partial_{k^0}-\partial_{|\vec{k}|}\right), -\frac{m_N^2}{k_u^0}\right)\cdot\left[|\vec{k}|\mathrm{d}F^{\mathcal{F}}\left(\tilde{p},k^0,|\vec{k}|\right)\begin{pmatrix} k\cdot\Sigma_l^{H,\overline{T\neq0}} \\ u\cdot\Sigma_l^{H,\overline{T\neq0}} \end{pmatrix}\right]$$

and

$$F^{sca,\overline{T\neq0}}(\tilde{p}) = \frac{g_w|Y|^2}{2\pi^2}\int \mathrm{d}|\vec{k}|\sum_{k^0=M\pm|\vec{k}|}\pm\frac{1}{k^4}|\vec{k}|\mathrm{d}F^{\mathcal{F}}\left(\tilde{p},k^0,|\vec{k}|\right) \tag{3.159}$$

$$\left(2p\cdot k + \frac{k^2}{|\vec{k}_u|^2}\left(p\cdot k - k\cdot u\, p\cdot u\right), \frac{k^2}{|\vec{k}_u|^2}\left(k^2 p\cdot u - k\cdot u\, p\cdot k\right)\right)\cdot\begin{pmatrix} k\cdot\Sigma_l^{\mathcal{A},\overline{T\neq0}} \\ u\cdot\Sigma_l^{\mathcal{A},\overline{T\neq0}} \end{pmatrix}.$$

3.5.1.4 Numerical Solution

See Figure 3.16 for an overview of the final expressions. Those terms are evaluated numerically in the same parameter range as the Higgs contribution. Details on the numerics can be found in Chapter 4.5. The results are presented in Figures 3.17 and 3.18. In the second one, the *wv* and *sca* contributions as well as the *col* and *fin* terms, are summed together for simplicity. However, the distribution functions $F^{\mathcal{F}}$ are separated into a vacuum and a thermal part to study their individual effects.
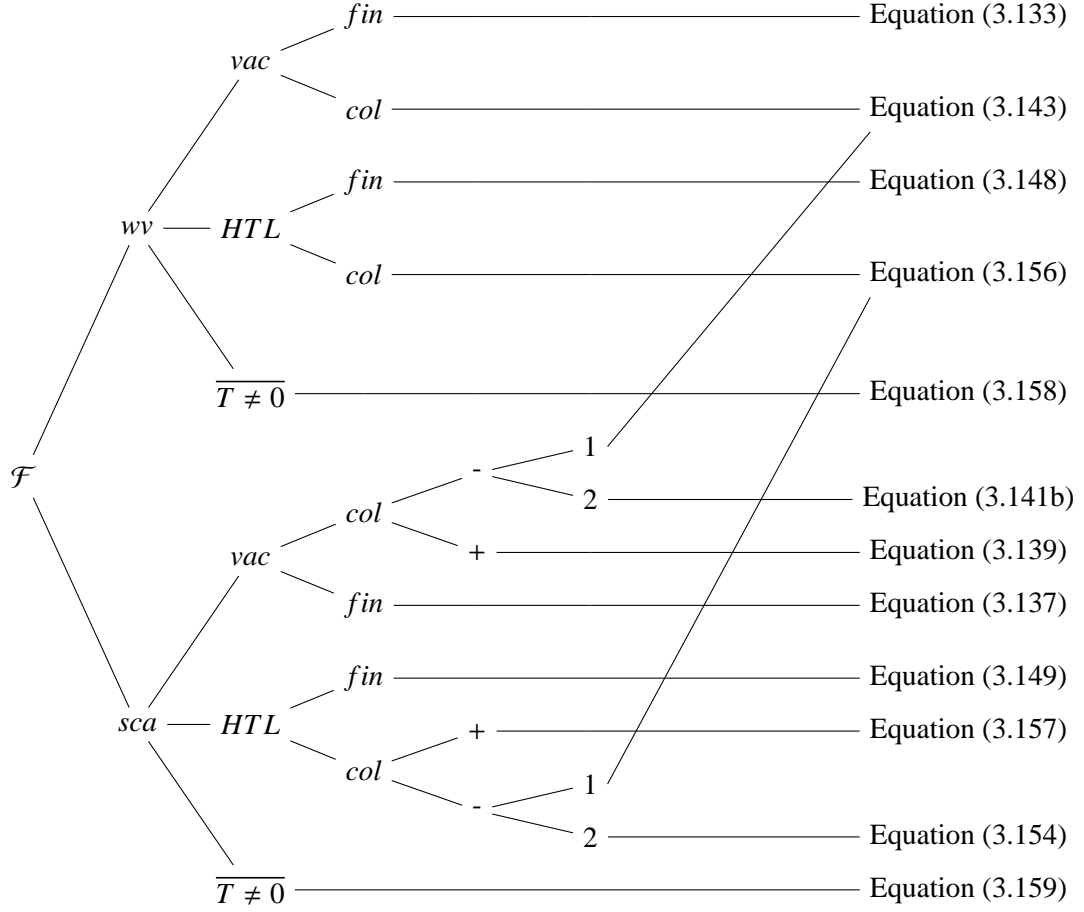
Figure 3.16: Splitting of $\mathcal{F}^{O(G)}$ by notion of its superscripts. The separation into vacuum, thermal and HTL contributions corresponds to a separation of the lepton self-energy. For the numerics, a splitting with respect to the exterior distribution functions, i.e. $F^{\mathcal{F}}$, is performed too.
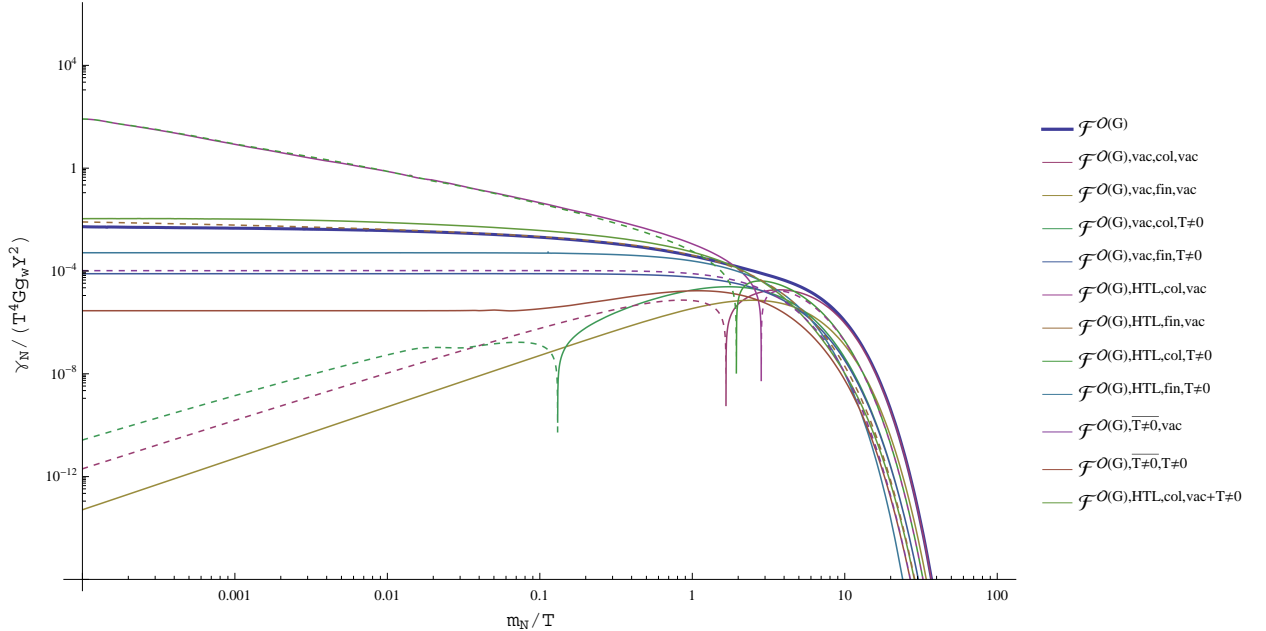
Figure 3.17: Plot of $\gamma_N\big[\mathcal{F}^{O(G)}\big](m_N)$ for various contributions of $\mathcal{F}^{O(G)}$ and $\Lambda = T$. Solid and dashed lines respectively correspond to positive and negative values.
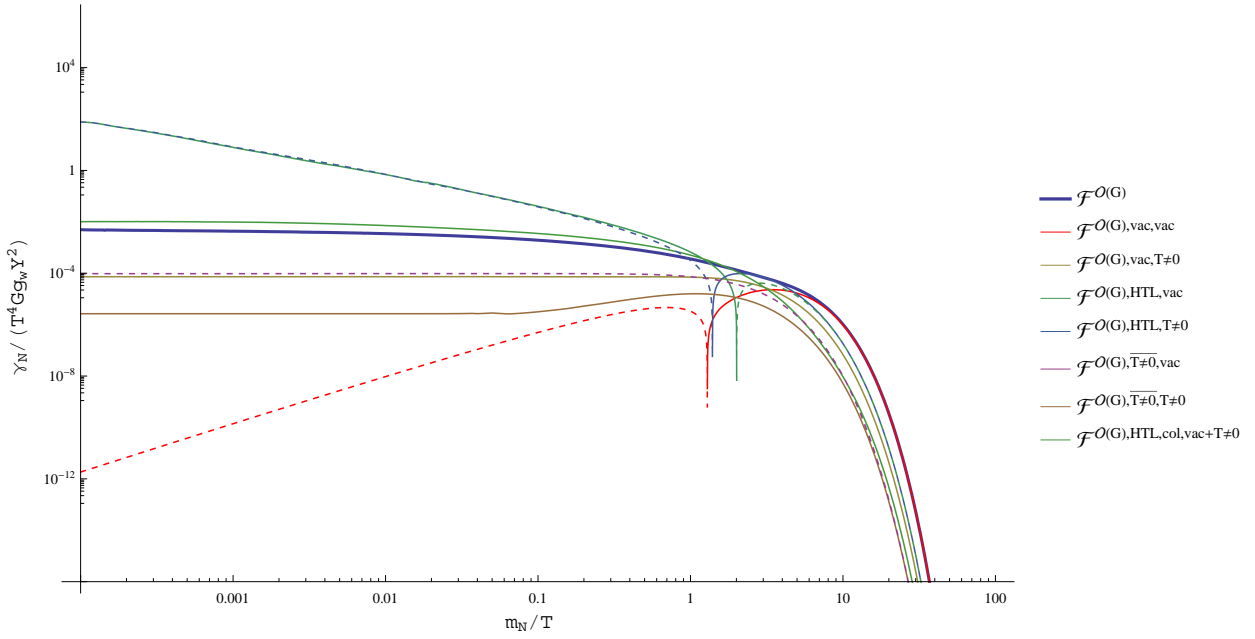
Figure 3.18: The same as Figure 3.17, except that *wv* and *sca* as well as *col* and *fin* contributions are added. Solid and dashed lines respectively correspond to positive and negative values.

In the non-relativistic limit, the $\mathcal{F}^{O(G)}$ contribution to the rate is dominated by $\mathcal{F}^{O(G),vac,vac}$. In the ultra-relativistic limit, it is obtained via a cancellation of mainly three contributions: The $\mathcal{F}^{O(G),HTL,col,vac}$ correction cancels the $\mathcal{F}^{O(G),HTL,col,T\neq0}$ contribution at high temperature. Therefore, those terms are reevaluated together within one integral. The sum of both is indicated by $\mathcal{F}^{O(G),HTL,col,vac+T\neq0}$. This one cancels a sizable contribution from $\mathcal{F}^{O(G),HTL,fin,vac}$. Altogether, the high temperature limit of the perturbative $\mathcal{F}^{O(G)}$ is dominated by $\mathcal{F}^{O(G),vac,fin,T\neq0}$, and hence by the vacuum Higgs self-energy. The other thermal contributions cancel or are too small to contribute sizably. This non-intuitive behavior could be interpreted as the breakdown of the perturbation theory, since according to Section 3.4.1.3 the ultra-relativistic limit should be non-perturbative.

To obtain the validity range of this approach, the $\mathcal{F}$ contribution to the RHN rate should also be obtained via the resummed lepton propagator. This is done in the following section.

64

3.5.2 Wave-Function Type Contributions - Resummed Self-Energies

The perturbative coupling expansion of the full propagators that was utilized in the last two sections, is valid only in a certain parameter range including the non-relativistic limit $m_N \gg T$. In the intermediate regime $m_N \approx T$, and especially when $m_N \approx m_\phi^{th}$ or $m_N \approx m_l^{th}$, the perturbative expansion is assumed to break down. In addition, the $G \ln(G)$ enhanced part, known from the ultra-relativistic result, could dominate the perturbative $\mathcal{F}$ contributions and consequently lower the validity range. To check this, a computation using full 2-point functions has to be done.

Analog to the massless neutrino case, the complexity of the computation is restricted to a 1-loop resummed propagator for the Higgs, while for the lepton a tree-level propagator is used, and vice versa. The corresponding $\mathcal{B}$ term reads in the p-frame

$$\mathcal{B}(\tilde{p}) = g_w |Y|^2 2 \int \frac{\mathrm{d}^4 k}{(2\pi)^4} \mathrm{tr} \left[\slashed{p} \slashed{\mathcal{S}}_l^{(0),\mathcal{A}}(p+k) \right] \Delta_\phi^{\mathcal{A}}(k) \left(f_-(u \cdot k) + f_+(u \cdot (p+k)) \right) \tag{3.160}$$

$$= g_w |Y|^2 \frac{2}{(2\pi)^2} m_N \int \mathrm{d}|\vec{k}| \, |\vec{k}|^2 \sum_{k^0 = -m_N \pm |\vec{k}|} \frac{\Pi_\phi^{\mathcal{A}}}{\left(k^2 - \Pi_\phi^H \right)^2 + \left(\Pi_\phi^{\mathcal{A}} \right)^2} \mathrm{d}F^{\mathcal{B}}(\tilde{p}, k^0, |\vec{k}|) \tag{3.161}$$

similar to Equation (3.82). The $\mathrm{d}F^{\mathcal{B}}$ is the reduced integral measure defined in (3.86). Details on the numerical evaluation of (3.161) can be found in Chapter 4.6.

In contrast to the $\mathcal{B}^{O(G,h_t^2,\lambda_\phi)}$ of Equation (3.82), however, the $\mathcal{B}$ here includes the *LO* processes as well. The same applies to $\mathcal{F}$.

Likewise, the $\mathcal{F}$ term corresponding to (3.122) could be evaluated in the p-frame. However, the lepton has a complex dispersion relation, which is only known analytically in the HTL approximation in the plasma frame. As explained in the numerics Chapter 4.7, knowing the position of the poles is of particular importance for the numerical stability, when the pole width is small. Therefore, it is preferable to calculate $\mathcal{F}$ in the u-frame and to boost the arguments back to the p-frame for comparison with (3.122). The corresponding representation of $\mathcal{F}$ was already obtained in Equation (3.51), and it is copied here for completeness:

$$\mathcal{F}(p_u) = \frac{2 g_w |Y|^2}{(2\pi)^2} \int_B \mathrm{d}k_u^0 \mathrm{d}|\vec{k}_u| \frac{|\vec{k}_u|}{|\vec{p}_u|} p \cdot S_l^{\mathcal{A}}(k) \mathrm{sign}(p_u^0 - k_u^0) \left(f_+(-k_u^0) + f_-(p_u^0 - k_u^0) \right). \tag{3.162}$$

Nevertheless, a deeper insight to the resummation approach needs to be gained before these integrals can be evaluated.

3.5.2.1 Resummation of Vacuum Self-Energies

In the present case, there are processes that definitely need to be resummed: The perturbative correction of the $\mathcal{B}$ term possesses a m_N power divergence in the ultra-relativistic limit. Physically, this is regulated by thermal plasma screening effects, and technically, it is described via the resummed Higgs propagator. While $\mathcal{F}$ does not have such a divergence, the perturbative form of $\mathcal{F}$ in (3.162) exhibits logarithmic divergences from the zero momentum exchange of a lepton in the t-channel. This divergence occurs precisely due to the HTL part of the spectral lepton self-energy. After resummation, those processes contribute parametrically of order $G \ln G$.

However, one question in the context of self-energy resummation is served by the infrared divergences of the vacuum self-energy and their cancellation. Both the $\Pi_\phi^{H,vac}$ and $\Sigma_l^{H,vac}$ from Section 2.5 and 2.6 contain infrared divergences from massless particle exchanges. In the present case, those are regulated by a fictitious mass parameter λ. This λ shifts the branch cut of the complex self-energy, and hence, it reappears in the kinematical constraint expressed as the Heaviside theta that is contained in the spectral self-energy. For the derivation of physical observables, those λ terms have to cancel such that λ can be set to zero.

65

In vacuum, this cancellation is guaranteed by the Kinoshita-Lee-Nauenberg (KLN) theorem: It states that the IR divergences cancel to all orders in perturbation theory within "real" and "virtual" contributions under the integral. This cancellation to all orders has not been proven so far for finite temperature. However, the cancellation of the $\ln \lambda$ terms is shown up to a specific coupling order. Therefore, the thermal perturbation theory, i.e. the "perturbative thermal mass insertion", is free of IR divergences: The $\mathcal{B}^{vac,+}$ and the $\mathcal{F}^{vac,col-}$ terms are independent of λ, such that λ can be set to zero.

The resummed case behaves differently. When the vacuum self-energies are resummed into Δ_ϕ and $\mathcal{S}_l$, the corresponding dispersion relation is modified by a $\ln(\lambda)$ term. On the other side, the λ within the spectral self-energy can safely be set to zero.[36] Therefore, the corresponding $\mathcal{B}$ and $\mathcal{F}$ do not necessarily have to be independent of λ.[37]

The λ dependency does not mean that the thermal perturbation theory is not IR-finite above some coupling order. It only states that the type of resummation that has been done does not include effects to all coupling orders. In fact, the full propagators of the theory are unknown. However, those are approximated by the resummation of self-energies obtained up to 1-loop order in thermal perturbation theory. Even back reaction effects are not – but maybe must be – included. In particular, the full theory also provides plasma induced thermal masses for the gauge bosons. Those thermal masses replace the regulator mass λ and physically regulate the IR divergence in $\Pi_\phi^{H,vac}$ and $\Sigma_l^{H,vac}$.

In the literature, the vacuum parts of the hermitian self-energies are usually ignored during resummation in the ultra-relativistic limit. See for example [59, 60, 64]. It is assumed that vacuum effects are dominated by thermal ones in this limit, as is the case here: For $m_N \ll T$, the RHN rate is dominated by thermal effects.[38]

The hermitian vacuum self-energy, or at least the infrared logarithm, is technically absorbed by a vacuum counter term. In addition to the ultra-relativistic limit, this counter term can be justified also for RHN masses within the ultra-relativistic regime up to some point in the non-relativistic regime. Since the thermal perturbation theory is finite in the intermediate and the non-relativistic regime up to some fixed order, the counter term should be at least parametrically of higher perturbative order. However, a vacuum counter term having the same perturbative order as the hermitian vacuum self-energy, must be included. This means that in order to justify the counter term for all m_N, the effects of the hermitian vacuum self-energy have to be parametrically of higher perturbative order:

The $\Pi^{H,vac}$ is a vacuum wave function renormalization. This contributes proportional to m_N^2: See Equations (3.96) and (3.132). Since thermal effects contribute of orders $m_N T$ and T^2, vacuum wave function renormalizations are suppressed above $T > m_N$ – even in thermal perturbation theory.

In the resummed approach, the convolution of a resummed propagator has to be analyzed. Therefore, a generic coupling c and a full spectral propagator Δ is introduced. The $\text{sign}(x \cdot u)$ and the spatial components of x^μ are not important for the argumentation. x is just the energy component. Furthermore, Δ is modeled by a Breit-Wigner form originating from the resummation:

$$\Delta(x) \sim \frac{c\Gamma}{(x^2 - m_0^2 - c(ax^2 + b))^2 + (c\Gamma)^2}. \tag{3.163}$$

The peak position and the width are determined by the renormalized and IR finite hermitian and spectral self-energies. Close to the pole, their generic form

$$\Pi^H \sim c(ax^2 + b), \qquad\qquad \Pi^{\mathcal{A}} \sim c\Gamma \tag{3.164}$$

is assumed. a, b and Γ are appropriate constants. If Δ is convoluted with some other full spectral propagator χ, the following two extrema are possible. The width of χ may be much smaller than the one of Δ. χ

---

[36] The finiteness of those integrals can be checked numerically.

[37] The λ dependence is checked numerically too.

[38] Vacuum processes of massless particles are kinematically suppressed. In the case of $m_N = 0$, they are kinematically forbidden. Such processes can be ignored and do not need to be resummed.

then can be approximated by a delta function. Hence, the convolution $\Delta \odot \chi$ results in Δ evaluated at the χ particles pole y.[39] If it is expanded in couplings, the Breit-Wigner width appears at the first coupling order, while the hermitian self-energy is multiplied by the width and appears within the second coupling order.

$$\Delta \odot \chi \sim \frac{c\Gamma}{(y - m_0^2 - c(ay + b))^2 + (c\Gamma)^2} = c\frac{\Gamma}{(y - m_0^2)^2} + 2c^2\Gamma\frac{ay + b}{(y - m_0^2)^3} + O(c^3) \tag{3.165}$$

Such a form of χ is relevant in particular in the non-relativistic regime. Therefore, as long as Δ has a Breit-Wigner form, non-relativistic effects due to the hermitian self-energy are effectively of higher order in the coupling.

However, at least in the intermediate and ultra-relativistic regime, χ obtains additional continuum contributions ζ from multi-particle exchanges and thermal particle distributions. The explicit form of ζ does not need to be specified. At some point, its effective support is much larger than the width of Δ. Hence, Δ can be approximated by a delta distribution, which feeds its peak position into ζ during integration. Since the width $c\Gamma$ can be neglected, effects of the peak position and hence the hermitian self-energy are superior to effects of the spectral one. This argument tells us that the thermal mass, as a consequence of the hermitian self-energy, dominates the physics at high temperature. However, effects of the hermitian vacuum self-energy are exponentially suppressed in the ultra-relativistic regime up to some point in the intermediate regime. Hence, in order to also guarantee the validity of the last argument in the full intermediate regime, this specific point needs to be evaluated by a comparison of the perturbative and the resummed approach. As long as there is a region of agreement, the above argumentation for thermal perturbation theory also justifies the resummed approach in this range. Such regions for $\mathcal{B}$ and $\mathcal{F}$ can be found in Section 3.5.5. Those are the blue areas in the Figures 3.25c and 3.26c, respectively.

In total, this means that during resummation, the effects of $\Pi^{H,vac}$ and $\Sigma^{H,vac}$, and analogously the vacuum counter terms are effectively suppressed. Those effects are neglected in the following numerics. However, the unproblematic $\Pi^{\mathcal{A},vac}$ and $\Sigma^{\mathcal{A},vac}$ terms are included for resummation.

This argumentation only holds if the resummed propagator Δ really has the Breit-Wigner form. In particular for $m_N \gg T$, in the small coupling limit, Δ reduces to the ordinary tree-level delta distribution $\Delta^{(0)}$. In this case, the above counter term is not parametrically suppressed and may modify the renormalization of $\Delta^{(0)}$ in comparison to the one of the $\Delta^{(0)}$ used for the thermal perturbation theory. Hence, both approaches only agree in this limit, if the renormalization scheme itself provides the correct counter term for the resummation and for the perturbation theory. Nevertheless, the mentioned range, where both approaches agree, may be used to switch between the resummation and the perturbation theory. In this way, the full RHN mass range is covered within any renormalization scheme.

3.5.2.2 Numerical Solution

The numerical results for $\mathcal{B}$ and $\mathcal{F}$, respecting the gauge boson and top-quark contributions individually, are presented in Figures 3.19, 3.20 and 3.21. The integrals are calculated within a relative error of 10^{-3} for the neutrino masses $m_N = 10^{-4} \ldots 10^2 T$ divided into 61 points and for each neutrino momentum $|\vec{p}_u| = 10^{-3} \ldots 10^{1.5} T$ using 46 points. In addition, in the case of $\mathcal{B}$, the couplings are varied in the range $G = 10^{-6} \ldots 10^0$ and $h_t = 10^{-3} \ldots 10^0$, both divided into 61 points. In the case of $\mathcal{F}$, the corresponding range is $G = 10^{-4} \ldots 10^0$ using 41 points. All variations are regarded logarithmically.

The figures show the contributions to the total neutrino production rate by logarithmic plots. Positive and negative contributions are indicated respectively by red/yellow and blue. The green lines that are printed at $\frac{m_N}{T} = 10^{-4}$, show the corresponding ultra-relativistic limits that were obtained in Sections 3.4.1.2 and 3.4.1.3.

---

[39] Due to the trilinear interaction in $\mathcal{B}$ and $\mathcal{F}$, the third particle carries additional 4-momentum p. Hence, y is a function of p and the mass of χ.

Figure 3.19: This figure shows $\gamma_N[\mathcal{B}](m_N, G)$ for $h_t = \lambda_\phi = 0$. Red/yellow and blue areas correspond to positive and negative values, respectively. The green line shows the $m_N = 0$ result.
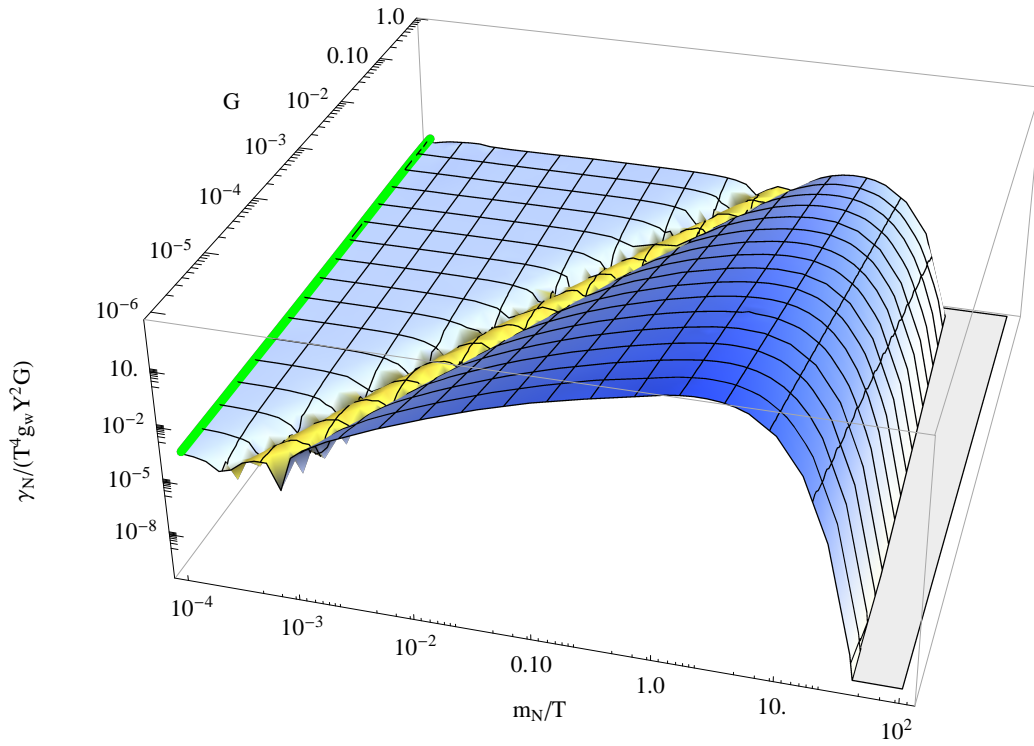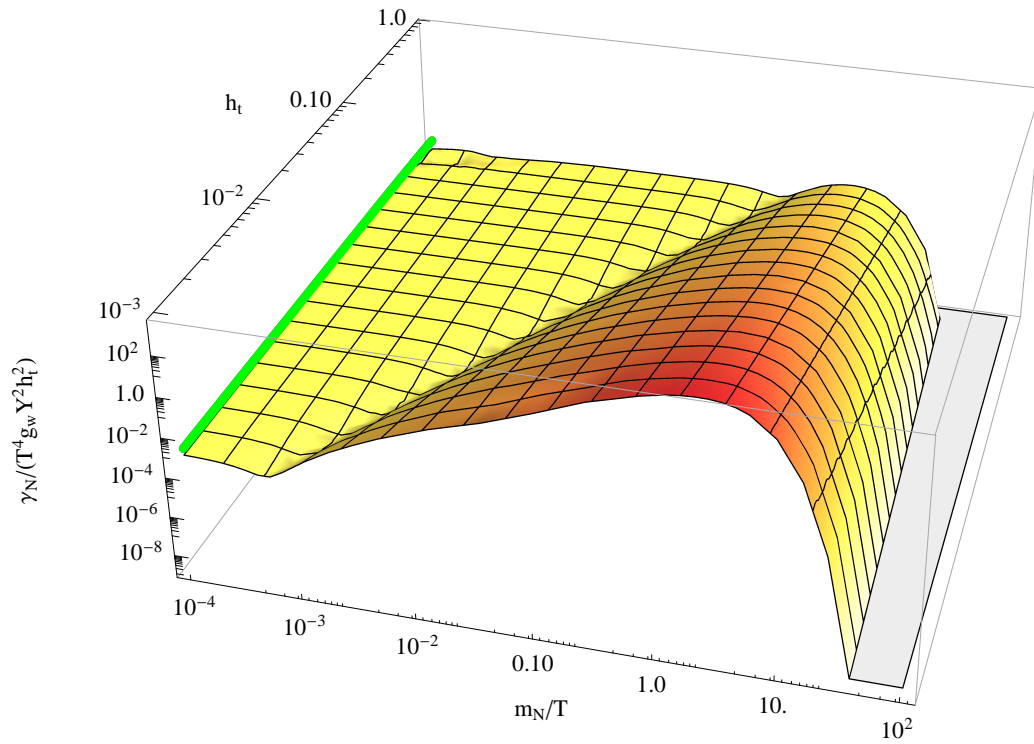

Figure 3.20: This figure shows $\gamma_N[\mathcal{B}](m_N, h_t)$ for $G = \lambda_\phi = 0$. Red/yellow and blue areas correspond to positive and negative values, respectively. The green line shows the $m_N = 0$ result.
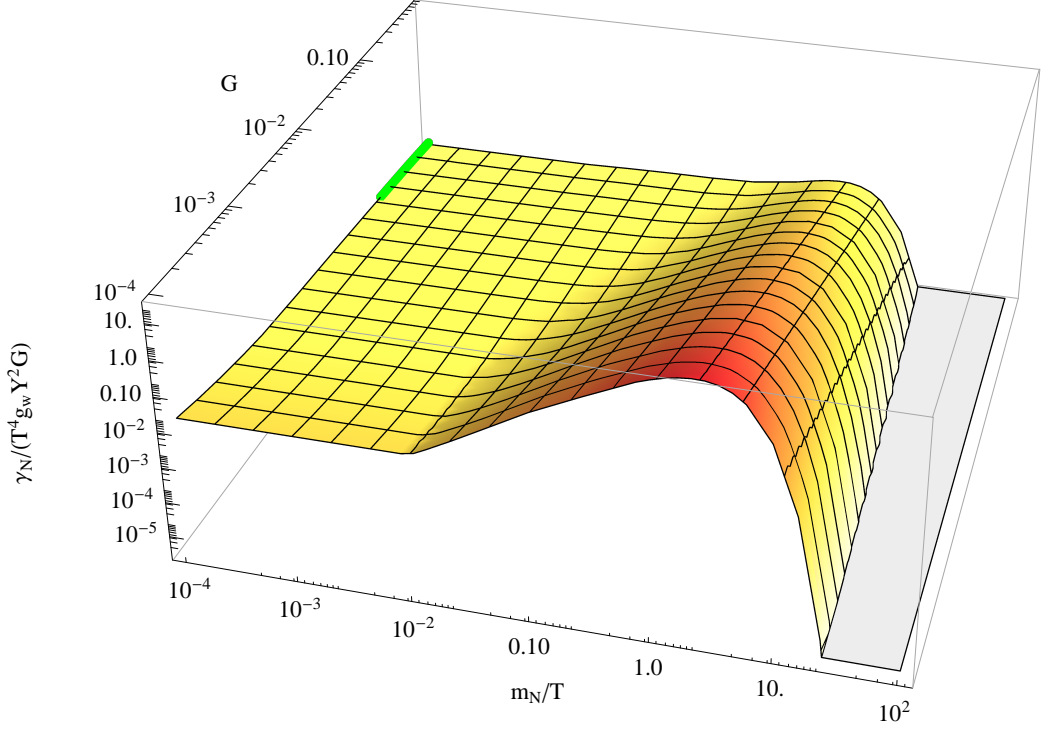
Figure 3.21: This figure shows $\gamma_N[\mathcal{F}](m_N, G)$. Red/yellow and blue areas correspond to positive and negative values, respectively. The green line shows the $m_N = 0$ result.

The plots possess a kink at the corresponding thermal mass and at $m_N \approx \pi T$. The kink at $m_N \approx \pi T$ is where the decay of RHNs into the plasma particles becomes most effective. Far above that mass scale, the RHN is too heavy to be influenced by the plasma. Below this scale, the RHN decay stops until the plasma decays into the RHNs. This is the point of the kink at the thermal mass. If $m_N > m_\phi^{th}$ and likewise $m_N > m_l^{th}$, the decay of the RHNs into Higgs and leptons is allowed. Otherwise, the Higgs and leptons decay into the right-handed neutrinos. In the ultra-relativistic regime, good agreement with the $m_N = 0$ result is found. Furthermore, the contributions $\gamma_N[\mathcal{B}](m_N, h_t)$ and $\gamma_N[\mathcal{F}](m_N, G)$ are positive on the full parameter range. In contrast, and as expected from Figure 3.6, the values of $\gamma_N[\mathcal{B}](m_N, G)$ are negative in the ultra-relativistic regime and for a certain reason also in the non-relativistic regime, except for a small range around $m_N^2 = (m_\phi^{th})^2 = \frac{GT^2}{4}$. The small range in Figure 3.19 with a positive rate is correct up to *NLO*. However, the negative rate is wrong. The reason for this is clarified in the following pages. Finally, Section 3.5.4 resolves this matter and identifies the correct way of calculating the rate up to *NLO*.

3.5.2.3 Causality Violation through Resummation

The negative contribution to the neutrino rate that is obtained in the last section by using the resummed Higgs propagator and gauge boson interactions, cannot be correct. If $\mathcal{B}$ were the only contribution, a negative rate would directly indicate unitarity violation of the theory. One possible thought about this is the following: The negative sign appears only when the radiative corrections from gauge interactions are included to the Higgs. However, the rate calculated from $\mathcal{B}$ is only one contribution to the full physical rate. Due to gauge invariance, the leptons have to interact with the gauge bosons as well. Hence, summing the wave-function type contributions $\mathcal{B} + \mathcal{F}$ together with the vertex-type contributions and subtracting the overcounted tree-level process should cure the negative rate. In fact, a positive rate can be found in the ultra-relativistic regime already from the sum of $\mathcal{B} + \mathcal{F} - \mathcal{H}$. However, this is a coincidence likely only because of the $G \ln G$ enhancement in the lepton sector. For large neutrino masses, and in particular in the

non-relativistic limit for small G, where perturbation theory should be valid, this sum is still negative and in addition approximately minus the *LO* rate. The correct answer to this issue resorts only to the Higgs and its self-energy:

If the other interactions are switched off, the spectral Higgs self-energy up to 1-loop order is determined by the sunset diagram: It was calculated in Chapter 2.5 using a tree-level gauge boson and a tree-level

Figure 3.22: Sunset diagram from Chapter 2.5. The 2PI formalism demands the use of the full Higgs propagator within Π_ϕ.

Higgs propagator. This is already an approximation, i.e. an expansion up to order G. Without this approximation, the 2PI formalism demands the use of the resummed Higgs propagator within the calculation of the self-energy. That including this kind of back reaction should solve the issue can be understood in the following way:

By using the tree-level Higgs propagator, one obtains a self-energy $\Pi_\phi^{\mathcal{A}}(p)$ that is negative for positive p^0, p^2 but vanishes on-shell at $p^2 = 0$. Likewise, a non-vanishing mass shift is also generated by Π_ϕ^H. When resumming both, a Green-function is obtained that has a pole approximately at the thermal mass $p^2 = (m_\phi^{th})^2 > 0$. There, the sign of $\Pi_\phi^{\mathcal{A}}(p)$ is negative for positive energy and also for arbitrary small m_ϕ^{th}. Consequently, the retarded and advanced resummed propagators have their poles on the wrong side in the complex p^0 plane. Hence, the resummation violates causality. Of course, causality should be guaranteed by the infinitesimal $i\varepsilon$ term. However, as long as the mass shift does not vanish, the $\Pi_\phi^{\mathcal{A}}$ does not vanish on-shell and therefore always dominates ε. This shows that the resummation of the tree-level self-energy has a vanishing convergence radius in the coupling: Since the mass shift is proportional to G, G must not be larger than of order of the infinitesimal ε. Nevertheless, a causal solution to the Schwinger-Dyson equations and non-infinitesimal G should be possible.[40]

These arguments also explain why the resummed lepton propagator does not have such a problem even for the same type of self-energy diagram. According to (1.88), the lepton propagator $\mathcal{S}_l^{\mathcal{A}}$ obtains its sign from the on-shell value of $p \cdot \Sigma_l^{\mathcal{A}}(p)$. This value is positive for positive p^0.

One possibility to circumvent solving a Schwinger-Dyson type equation and still conserving causality is to include other interactions for the Higgs. The considered Lagrangian also contains Yukawa interactions of the Higgs with the quarks. Those contribute to $\Pi_\phi^{\mathcal{A}}$, such that the G-convergence radius raises proportional to h_t^2. However, within the physical relevant coupling range given in Table 2.1, the gauge couplings are still much too large for this ansatz. One could also try to partially include the back reaction by using a Higgs tree-level propagator with at a thermal mass within the derivation of the Higgs self-energy. Such a massive integral is again easily solved in terms of the K_{ab} of Section 2.4. However, this does not resolve the issue for this case.

---

[40] Likewise, it is possible to argue that in the limit of small G, the resummed spectral propagator calculated from the 1-loop $O(G)$ self-energy reduces according to (1.81) to the negative tree-level function. However, the negative tree-level Higgs propagator gives the previously obtained spectral self-energy times minus one. Therefore, iteratively calculating the self-energy from the resummed propagator and vice versa are two competing processes. The only solution is to solve both self-consistently.

3.5.3 Frequency Sums Revisited

In the light of the wave-function type contributions and the issues found in the last sections, the spectral sum rules (1.51) and (1.52) should be checked. At tree-level those can be verified easily. For example, the bosonic case is

$$\int \frac{\mathrm{d}k^0}{\pi} k^0 \Delta^{\mathcal{A}}(k) = \int \frac{\mathrm{d}k^0}{\pi} k^0 \pi \mathrm{sign}(k^0) \delta\left(k^2 - m^2\right) \tag{3.166}$$

$$= \int \mathrm{d}k^0 \frac{1}{2} \sum_{\pm} \delta\left(k^0 \pm \sqrt{\vec{k}^2 + m^2}\right) = 1 . \tag{3.167}$$

The fermionic analogon does not give any new insight. More interesting is the vacuum 1-loop correction using Higgs spectral function. This involves Section 3.5.1. Furthermore, only the gauge boson interactions are included.

The Δ_ϕ function is split into a tree-level part $\Delta_\phi^{(0)}$ and a 1-loop correction $\Delta_\phi^{(1)}$. Since $\Delta_\phi^{(0),\mathcal{A}}$ already results in 1, the correction term should give zero in the spectral sum. This is

$$\int \frac{\mathrm{d}k^0}{\pi} \Delta_\phi^{(1),\mathcal{A}}(k) = \int \frac{\mathrm{d}k^0}{\pi} \frac{1}{2} \left(\sum_{\pm} \delta\left(k^0 \pm |\vec{k}|\right) \frac{\pi}{2k^{0^2}} \left(\partial_{k^0} - \frac{1}{k^0} \right) k^0 \Pi_\phi^H(k) + \frac{2k^0}{k^4} \Pi_\phi^{\mathcal{A}}(k) \right) \tag{3.168}$$

using the perturbative Higgs self-energy Π_ϕ from Section 2.5.5. The term proportional to Π_ϕ^H corresponds to virtual corrections while the term proportional to $\Pi_\phi^{\mathcal{A}}$ can be identified with real corrections to the tree-level propagator. The former one evaluates in vacuum to

$$\frac{1}{(2\pi)^2} G \ln\left(\frac{\Lambda}{\lambda}\right) . \tag{3.169}$$

The Higgs mass renormalization $\Pi_\phi^H \rightarrow \Pi_\phi^H + \delta m^2$ does not contribute to the spectral sum up to this order since the derivative in k^0 cancels the fraction $\frac{1}{k^0}$. However, the wave-function renormalization δZ_ϕ occurs with a factor k^2, and Λ is the renormalization scheme dependent finite scale.

In contrast, the term proportional to $\Pi_\phi^{\mathcal{A}}$ is UV divergent for the perturbatively calculated vacuum $\Pi_\phi^{\mathcal{A}}$. By introducing an other UV regulator Λ' for k^0, this part becomes

$$-\frac{1}{(2\pi)^2} G \int_0^{\Lambda'} \mathrm{d}k^0 k^0 \frac{1}{k^2} \theta(k^2 - \lambda^2) = -\frac{1}{(2\pi)^2} G \ln\left(\frac{\Lambda'}{\lambda}\right) . \tag{3.170}$$

Hence, the cancellation of infrared divergences can be found in the sum of virtual and real corrections, i.e. the $\ln \lambda$ vanishes. However, the infinite Λ' should somehow cancel the finite Λ. This UV issue is no surprise since the Kramers-Kronig relations (1.63) for $\Pi^{H,vac}$ and $\Pi^{\mathcal{A},vac}$ are also not fulfilled. Indeed, both are non-analytic functions due to the absolute value and the Heaviside theta that appear in the perturbative calculation of the self-energy. Assuming that (1.63) is fulfilled,

$$\int \frac{\mathrm{d}k^0}{\pi} \frac{k^0}{k^4} \Pi_\phi^{\mathcal{A}}(k) = \left[\partial_{\mu^2} \int \frac{\mathrm{d}k^0}{\pi} \frac{k^0}{k^2 - \mu^2} \Pi_\phi^{\mathcal{A}}(k^0, |\vec{k}|) \right]\Bigg|_{\mu^2=0} \tag{3.171}$$

$$= -\left[\partial_{\mu^2} \Pi_\phi^H\left(\sqrt{|\vec{k}|^2 + \mu^2}, |\vec{k}| \right) \right]\Bigg|_{\mu^2=0} \tag{3.172}$$

$$= -\frac{1}{(2\pi)^2} G \ln\left(\frac{\Lambda}{\lambda}\right) \tag{3.173}$$

can be evaluated. The first order correction then adds a zero to the spectral sum rule.

Even though the spectral sum seems to be violated, this issue does not spoil the perturbative calculation of the neutrino production rate. In the derivation of (3.106) and (3.108), the UV finiteness is guaranteed by the bounded phase space support in vacuum, and also due to the exponential suppression of the thermal equilibrium distribution functions at finite temperature.

Finally, the case of a generic resummed propagator is mentioned. When solving the Kadanoff-Baym equations up to first order in gradients, the retarded and advanced functions of a scalar field have the form

$$i\Delta^{R/A}(p) = \frac{i}{p^2 - m^2 - \Pi^{R/A}(p)} \, . \tag{3.174}$$

Both are meromorphic functions[41] in p^0, that have, if causality is conserved, respectively, poles below and above the real axis. Therefore, for these the Kramers-Kronig relations and their spectral sums have to hold. In order to evaluate the spectral sum of the full spectral function, Cauchy's integral formula may be used. Therefore, the retarded and advanced self-energies are decomposed within Equation (3.174) as $\Pi^H \mp i\Pi^{\mathcal{A}}$, and one obtains the Breit-Wigner type form of $\Delta^{\mathcal{A}}$:

$$\Delta^{\mathcal{A}}(p) = \frac{\Pi^{\mathcal{A}}}{\left(p^2 - m^2 - \Pi^H\right)^2 + \Pi^{\mathcal{A}2}} \, . \tag{3.175}$$

Even though this expression contains two poles above and two poles below the real p^0 axis, Cauchy's theorem is not applicable since Π^H and $\Pi^{\mathcal{A}}$ are the real and imaginary parts of one meromorphic function. However, in the quasi-particle approximation, i.e. $m^2 + \Pi^H \equiv \mu^2$ and $\frac{1}{p^0}\Pi^{\mathcal{A}} \equiv \Gamma$ are replaced by their value at the pole.[42] Then, a meromorphic integrand is recovered that vanishes for large $\mathcal{R}(p^0)$ at least like $\frac{1}{|p^0|^4}$. The integration contour can be closed by a semicircle at infinity, such that the two poles above the real axis are encircled. Cauchy's integral formula leads to

$$\oint \frac{\mathrm{d}k^0}{\pi} k^0 \frac{k^0 \Gamma}{(k^0 - \omega^+)(k^0 + \omega^+)(k^0 - \omega^-)(k^0 + \omega^-)} = \mathrm{sign}(\Gamma) \tag{3.176}$$

with

$$\omega^\pm = \sqrt{\mu^2 + \frac{1}{2}\Gamma(-\Gamma \pm \sqrt{\Gamma^2 - 4\mu^2})} \, . \tag{3.177}$$

Hence, the quasi-particle approximation shows the trend that can be expected for more general self-energies: The spectral sum equals $+1$ only if Γ is positive and likewise, if the Δ^R and Δ^A are causal. This is the case for the Higgs propagator with a resummed top quark loop. Therefore, the positive rate plotted in Figure 3.20 is obtained. However, in case of the gauge bosons, the spectral Higgs self-energy is negative at the thermal mass shell. In fact, the spectral sum can be checked numerically to be approximately -1 for typical parameters.[43] Every deviation from $+1$ indicates an inconsistency of the treatment of the physical model.

---

[41] This implies that the self-energies too are solved consistently with the Kadanoff-Baym equations.

[42] If $i\Pi^{\mathcal{A}}$ vanishes at the pole, it must be replaced by the usual $i\varepsilon$ prescription for the retarded and advanced functions.

[43] For this numerical evaluation, a UV-cutoff far away from the pole needs to be assumed, since the spectral sum up to infinity diverges for the same reason it does above for the perturbative correction. A consistent self-energy resummation should include back reaction effects, as is explained in the next section. Those self-screenings suppress UV divergences, since the integral support of the self-energy diagrams is bounded in vacuum and otherwise exponentially suppressed via thermal distribution functions. Nevertheless, the UV-cutoff in the spectral sum mimics the exponential suppression of the thermal distributions that occurs for the evaluation of the RHN production rate.

3.5.4 Restoration of Causality

The spectral sum of about -1 that is found in the last section, explains the negative unphysical rate in Figures 3.6 and 3.19, why the rate equals approximately minus the *LO* result in the non-relativistic regime, and why the pole contribution in the ultra-relativistic regime and limit coincides with minus the $\mathcal{H}$ term including the thermal mass. Hence, this demands for solving the full system of the resummed Higgs propagator and its self-energy self-consistently.

This section inspects the consequence of such a self-consistent resummation and provides a workaround to the wrong resummation. First, a simplified version of the Schwinger-Dyson equation for the spectral Higgs propagator is analyzed and solved in vacuum. Furthermore, only the problematic interactions of the Higgs with the gauge bosons is considered.

The resummed form of $\Delta_\phi^{\mathcal{A}}$ is known from Equation (1.80). This assumes that the self-energies $\Pi_\phi^{\mathcal{A}}$ and Π_ϕ^{H} are correct and consistent. Consequently, these self-energies are in principle functional of all other consistent n-point functions. Up to 2PI 1-loop order only the gauge boson and the consistent Higgs propagator in question are needed:

$$\Delta_\phi^{\mathcal{A}}(p) = \frac{\Pi^{\mathcal{A}}[\Delta_\phi, \Delta_\gamma](p)}{\left(p^2 - \Pi_\phi^{H}[\Delta_\phi, \Delta_\gamma](p)\right)^2 + \left(\Pi_\phi^{\mathcal{A}}[\Delta_\phi, \Delta_\gamma](p)\right)^2} \ . \tag{3.178}$$

As is known from the last chapters, Π_ϕ^{H} does not spoil the causality. It only modifies the dispersion relation and therefore is responsible for the thermal particle mass. Hence, only a sub-leading modification of the physics is expected from this term, and Equation (3.178) is approximated by $\Pi_\phi^{H}[\Delta_\phi, \Delta_\gamma](p) = \left(m_\phi^{th}\right)^2$. The problematic part is $\Pi_\phi^{\mathcal{A}}$. At the perturbative 1-loop order, this term vanishes at the zero mass shell and becomes negative at any positive mass shell. However, the 2PI 1-loop $\Pi^{\mathcal{A}}[\Delta_\phi, \Delta_\gamma]$ is given by

$$\Pi_\phi^{\mathcal{A}}[\Delta_\phi, \Delta_\gamma](p) = -2G \int \frac{\mathrm{d}^4 k}{(2\pi)^4} (p+k)^2 \Delta_\phi^{\mathcal{A}}(k) \Delta_\gamma^{\mathcal{A}}(p-k) \left(1 + f_-(u \cdot k) + f_-(u \cdot (p-k))\right) \tag{3.179}$$

$$= -2m_N G \int \frac{\mathrm{d}k^0 \mathrm{d}\cos(k, u)}{(2\pi)^2} k^0 (m_N - k^0) \Delta_\phi^{\mathcal{A}}(k)$$

$$\left(1 + f_-(u \cdot k) + f_-(u \cdot (p-k))\right)\Big|_{|\vec{k}|=|m_N - k^0|} \tag{3.180}$$

in the p-frame. For simplicity, the tree-level gauge boson propagator $\Delta_\gamma^{\mathcal{A}}$ is used. The Equations (3.178) and (3.180) form a non-linear system of integro-differential functional equations. When Equation (3.178) is inserted into (3.180), $\Pi_\phi^{\mathcal{A}}$ is solved numerically, for example with the help of spectral methods[44]. The solution can be plugged into (3.178), such that finally the propagator can be obtained.[45]

For simplicity, and as a first hint to the full solution, $\Pi_\phi^{\mathcal{A},vac}$ is solved in vacuum. Since the plasma vector u is unimportant in vacuum, Equation (3.180) can be simplified such that the 2-point functions only depend on one parameter p^2 or k^2:

$$\Pi_\phi^{\mathcal{A},vac}(p^2) = -\frac{G}{2^3 \pi^2 p^2} \int_{-p^2}^{p^2} \mathrm{d}k^2 (p^4 - k^4) \Delta_\phi^{\mathcal{A},vac}(k^2) \tag{3.181}$$

$$= -\frac{G}{2^3 \pi^2 p^2} \int_{-p^2}^{p^2} \mathrm{d}k^2 (p^4 - k^4) \frac{\Pi_\phi^{\mathcal{A},vac}(k^2)}{(k^2 - m^2)^2 + \left(\Pi_\phi^{\mathcal{A},vac}(k^2)\right)^2} \ . \tag{3.182}$$

---

[44] In a nutshell, this means that the searched function is parameterized by an appropriate fit function like, for example, a polynomial, a Fourier series, or a Legendre or Chebyshev series. The corresponding parameters are then fitted to the equation system.

[45] Likewise, the propagator could directly be solved too, but the pole shape of the solution complicates the numerical treatment.

In the following pages, this equation is solved for $\Pi_\phi^{\mathcal{A},vac}(p^2)$, with $-0.05 \leq p^2 \leq 1.00$ for a fixed coupling $G = 0.1$, and optionally with $m = 0$ and $m = m_\phi^{th}$.

(a) $m^2 = 0$, spectral sum = 0.9763

(b) $m^2 = 0$

(c) $m^2 = 0$

(d) $m^2 = 0$

(e) $m^2 = \frac{1}{4}GT^2$, spectral sum = 0.9654

(f) $m^2 = \frac{1}{4}GT^2$

(g) $m^2 = \frac{1}{4}GT^2$

(h) $m^2 = \frac{1}{4}GT^2$

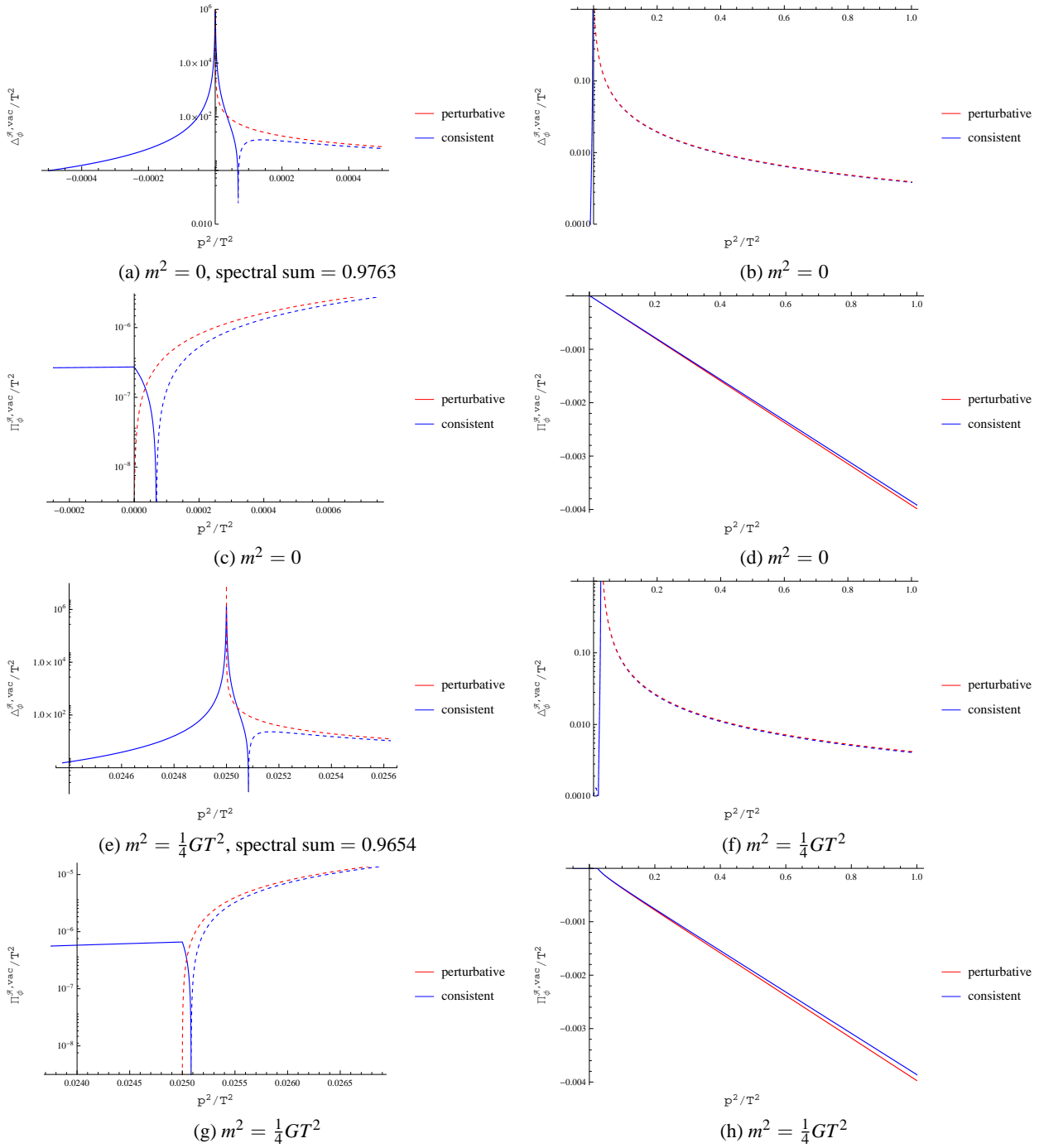Figure 3.23: Comparison of the resummed Higgs propagators which are obtained from the perturbative $\Pi_\phi^{\mathcal{A},vac}$ of Section 2.5 (red line) and from Equation (3.182) (blue line). The coupling is fixed by $G = 0.1$, and the consequences of a thermal mass are shown. The spectral sums are obtained from the consistent propagators. Regular and dashed lines correspond to positive and negative values, respectively.

The plots in Figure 3.23 present the resulting consistent spectral vacuum Higgs propagators and self-energies in comparison to the incorrectly resummed ones. One can observe a significant change in the pole structure. In particular, the sign change in the propagators of Figures 3.23a and 3.23e reflects the small positive value for the self-energies of the Figures 3.23c and 3.23g close to the mass-shell. This ensures causality. The improved consistency of the resummation is proved by the spectral sum values of approximately $+1$. Away from the mass-shell, the convergence of the consistent and incorrect propagators and likewise of the self-energies is observable in the graphs one the left-hand side. However, far away from the mass-shell, in the figures on the right-hand side, the propagators and self-energies differ due to the previously mentioned self-screening in the UV.

Regarding the negative rate contribution $\gamma_N[\mathcal{B}](m_N, G)$ in Figure 3.19, the consistent thermal spectral Higgs propagator should be solved next to recalculate the $\mathcal{B}(m_N, G)$ term. In principle, this should also be done for all couplings G, h_t and λ_ϕ. Nevertheless, from the above solution and the spectral sums, one can learn how to correct the wrong resummed spectral Higgs function.

The resummed spectral Higgs propagator using the 1-loop self-energies $\Pi_\phi^{\mathcal{A}}(p)$ and $\Pi_\phi^{H}(p)$ from Section 2.5 can be corrected by switching its sign locally at the mass shell. Away from the pole, the true resummed propagator is well modeled by the inconsistent resummation. In other words, the tree-level propagator with an appropriate tree-level mass may be added to the inconsistent resummed propagator two times to obtain the approximated, but causality and spectral sum conserving, resummed spectral propagator:

$$\Delta_\phi^{\mathcal{A},corr}(p) \equiv \frac{\Pi_\phi^{\mathcal{A}}(p)}{\left(p^2 - \Pi_\phi^{H}(p)\right)^2 + \left(\Pi_\phi^{\mathcal{A}}(p)\right)^2} + 2\pi \mathrm{sign}(p^0)\delta(p^2 - \Pi_\phi^{H}(p)) \tag{3.183}$$

$$\approx \frac{\Pi_\phi^{\mathcal{A}}(p)}{\left(p^2 - \Pi_\phi^{H}(p)\right)^2 + \left(\Pi_\phi^{\mathcal{A}}(p)\right)^2} + 2\pi \mathrm{sign}(p^0)\delta(p^2 - (m_\phi^{th})^2) . \tag{3.184}$$

This form is in accordance with the observation in the ultra-relativistic limit, Section 3.4.1.2, Figure 3.6. There, it was found that only the "pole contribution" appears to have the wrong sign. This is corrected by (3.184). Nevertheless, the "non-pole contribution" that accounts for the continuum effects far away from the pole is perfectly fine and unmodified by (3.184).

As stated above, the Π_ϕ^{H} here is of course only the thermal part $\Pi_\phi^{H,T\neq0}$. Therefore, the tree-level mass shell is approximated by m_ϕ^{th} in Equation (3.184). This has the advantage that the numerical result of $\mathcal{B}(m_N, |\vec{p}|, G)$, Section 3.5.2.2, Figure 3.19, may be corrected without a recalculation by simply adding two times the massive $\mathcal{H}$ term of Section 3.4.1.1. The $\mathcal{B}$ contains plus the continuum contributions and minus the pole contribution. $\mathcal{H}$ contains only the pole contribution, since this is derived with tree-level propagators:

$$\mathcal{B}^{corr}(|\vec{p}|; m_N, G) = \mathcal{B}(|\vec{p}|; m_N, G) + 2\mathcal{H}\left(|\vec{p}|; m_N, m_\phi = \frac{1}{2}\sqrt{G}T, m_l = 0\right) . \tag{3.185}$$

This separation into pole and continuum part in the ultra-relativistic regime coincides with the separation into *LO* and *NLO* effects in the non-relativistic and perturbative regime. For large $m_N \gg m_\phi^{th}$, the incorrect resummed propagator contains at *LO* minus the $1 \leftrightarrow 2$ processes and at *NLO* the symmetric $1 \leftrightarrow 3$ processes. Perturbatively, the *NLO* effects are determined by two Higgs propagators and one Higgs self-energy. While the wrong resummation uses a perturbatively well-defined self-energy, the two Higgs propagators at *NLO* are the ones with the wrong pole sign. Since those propagators have the same momentum, the sign squares and the perturbative *NLO* effects are consequently correct implemented. This observation explains the small strip in Figure 3.19, where the rate is positive. Since $\mathcal{H}\left(|\vec{p}|; m_N, m_\phi = \frac{1}{2}\sqrt{G}T, m_l = 0\right)$ vanishes for $m_N = m_\phi$, the resummed *LO* $1 \leftrightarrow 2$ effect vanishes and the positive *NLO* rate contribution is directly found. Therefore, $\mathcal{B}^{corr}$ is regarded as correct to *NLO* globally within the validity range of the resummation. Using (3.185) the corrected bosonic wave-function type contribution is obtained up to *NLO*:
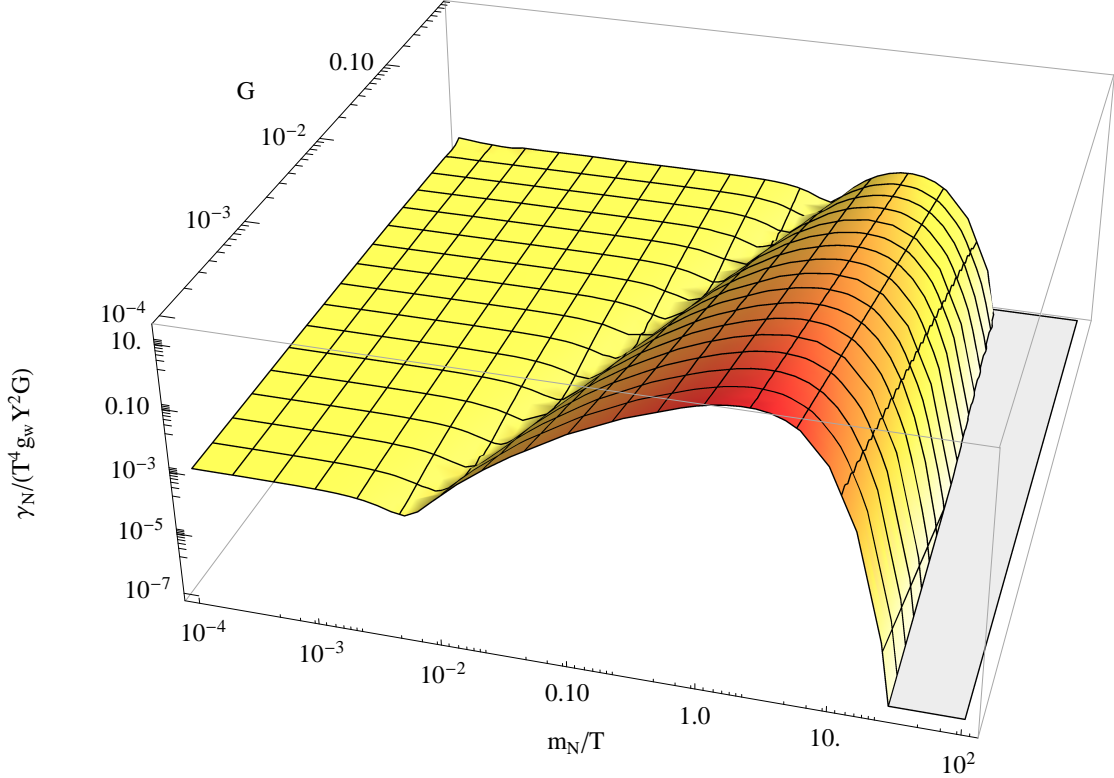

Figure 3.24: This figure shows $\gamma_N[\mathcal{B}](m_N, G)$ for $h_t = \lambda_\phi = 0$. Red/yellow and blue areas correspond to positive and negative values, respectively.

3.5.5 Perturbative Thermal Mass Insertion vs Resummation

The two methods for obtaining the next-to-leading order contributions to the neutrino production rate should be comparable at some stage. Since both approaches differ significantly in the amount of numerical effort, what is the most practical solution for a given task?

The perturbative method of Section 3.5.1 is valid in the non-relativistic limit up to some point in the intermediate regime, while the resummation of thermal corrections is only relevant within the intermediate regime up to the ultra-relativistic limit. In the intermediate regime, where the RHN mass is of order of the temperature, vacuum effects become less dominant. Therefore, the perturbative wave-function type contribution, i.e. $\mathcal{H}(m_l = m_\phi = 0) + \mathcal{B}^{O(G)}$, may directly be compared to the corrected $\mathcal{B}^{corr}(G)$ term in Figure 3.25.
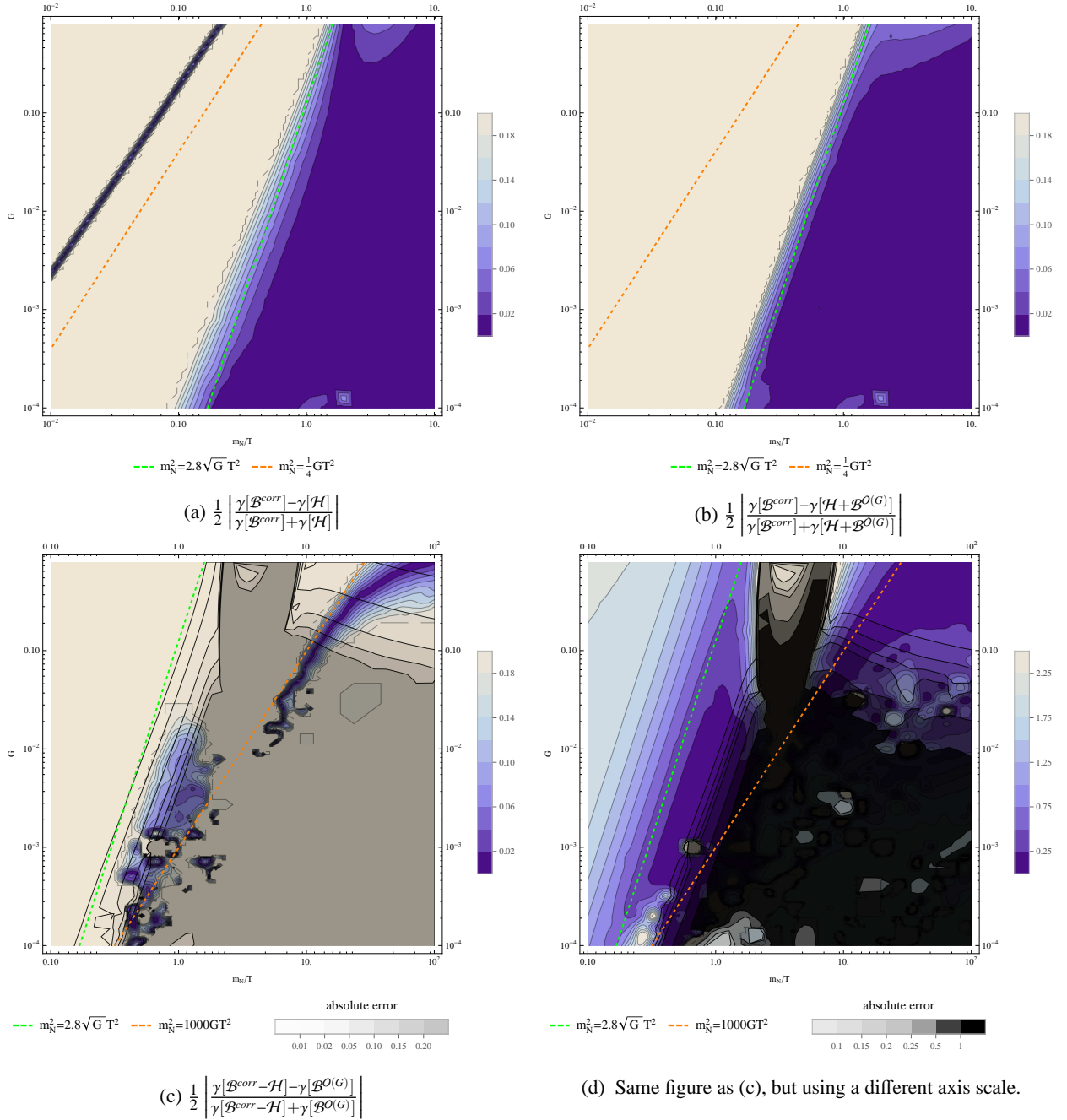
$\text{(a)} \quad \frac{1}{2} \left| \frac{\gamma[\mathcal{B}^{corr}] - \gamma[\mathcal{H}]}{\gamma[\mathcal{B}^{corr}] + \gamma[\mathcal{H}]} \right|$

$\text{(b)} \quad \frac{1}{2} \left| \frac{\gamma[\mathcal{B}^{corr}] - \gamma[\mathcal{H} + \mathcal{B}^{O(G)}]}{\gamma[\mathcal{B}^{corr}] + \gamma[\mathcal{H} + \mathcal{B}^{O(G)}]} \right|$

$\text{(c)} \quad \frac{1}{2} \left| \frac{\gamma[\mathcal{B}^{corr} - \mathcal{H}] - \gamma[\mathcal{B}^{O(G)}]}{\gamma[\mathcal{B}^{corr} - \mathcal{H}] + \gamma[\mathcal{B}^{O(G)}]} \right|$

(d) Same figure as (c), but using a different axis scale.

Figure 3.25: Comparison of the perturbative and resummation approach to $\mathcal{B}^{corr}$. The blue color gradient presents the relative difference of the contributions to the total RHN production rate as indicated by the captions. The overlaid gray shaded areas encompass the absolute error of the relative differences due to the numerical error of the results. The relative difference and the absolute error plots are clipped off below and above the range provided by the legends. Figure 3.25a compares the resummed to the perturbative *LO* approach, while 3.25b compares the resummed to the perturbative *LO + NLO*. Figures 3.25c and 3.25d compare the *NLO* parts.

The agreement of the resummed approach $\mathcal{B}^{corr}$ to the perturbative *LO* term $\mathcal{H}$ is found in Figure 3.25a above $m_N^2 \gtrsim 2.8 \sqrt{G} T^2$. The $\sqrt{G}$ factor results due to the term (3.115) is resummed into $\mathcal{B}^{corr}$. In thermal perturbation theory, this term diverges in the ultra-relativistic limit like $|Y|^2 G T^4 \left(\frac{T}{m_N} \right)^2$. Furthermore, $\gamma_N[\mathcal{H}]$ behaves for small m_N like $|Y|^2 T^4 \left(\frac{m_N}{T} \right)^2$. Equating those results in the observed $m_N^2 \sim \sqrt{G} T^2$ dependence.

The thin line below $m_N < m_\phi^{th}$ is an intersection point of the two terms. This provides no information about the validity of the perturbative approach.

In comparison to Figure 3.25a, including the perturbative *NLO* slightly improves the agreement with $\mathcal{B}^{corr}$ for smaller m_N. As can be seen in Figure 3.25b, in the small coupling range $G < 0.1$, the "2%" threshold shifts closer to the green $m_N^2 = 2.8\sqrt{G}T^2$ line. However, the worse agreement for $G > 0.1$ may be a coincidence, since even though the order G^2 corrections are wrong, they are included in $\mathcal{B}^{corr}$ too.

Figures 3.25c and 3.25d provide the comparison of the order G corrections. The shown relative differences have a large error, since the evaluation of $\mathcal{B}^{corr}$ in the non-relativistic regime for small couplings is dominated by the *LO*. The resummed sub-leading order is obtained by subtracting the *LO* $\mathcal{H}$ term from $\mathcal{B}^{corr}$. Hence, if two large numbers are subtracted from each other, the small remainder may be smaller than the small relative error of the large numerical number. Therefore, the plots are overlaid by a transparent gray shaded color gradient related to the absolute numerical error of the relative differences. Yet one finds two special lines. The first one, $m_N^2 \gtrsim 2.8\sqrt{G}T^2$, that is already discussed above, is relevant in the small coupling range below $G < 10^{-2}$. Above that range, between the intermediate and the non-relativistic regime, the thermal higher order corrections inside of $\mathcal{B}^{corr}$ spoil the agreement below the mass scale of about $m_N^2 \lesssim 1000GT^2$. Assuming that the order G^2 correction is thermally enhanced due to Bose-Einstein distributions, a dimensional analysis suggests that those contributions behave like $|Y|^2 G^2 T^4 \times \frac{m_N}{T} K_1\left(\frac{m_N}{T}\right)$. The factor $\frac{m_N}{T} K_1\left(\frac{m_N}{T}\right)$ appears from the $d|\vec{p}|$ integral in $\gamma_N[1]$ for $m_N \gtrsim 5T$. $K_n(z)$ is the modified Bessel function of the second kind. From Figure 3.15, it is apparent that above $m_N \gtrsim \pi T$ the $\mathcal{B}^{O(G)}$ term is determined by the pure vacuum parts $\mathcal{B}^{O(G),vac,vac}$. Since $\gamma_N[\mathcal{B}^{O(G),vac,vac}]$ performs like $|Y|^2 G T^4 \left(\frac{m_N}{T}\right)^3 K_1\left(\frac{m_N}{T}\right)$, equating both relations explains the $m_N^2 \sim GT^2$ boundary. This analysis also explains the crossover at $G = 10^{-2}$: At $m_N \approx \sqrt{1000 \times 10^{-2}}T \approx \pi T$ the $\mathcal{B}^{O(G)}$ term switches between $\mathcal{B}^{O(G),vac,vac}$ and $\mathcal{B}^{O(G),wv,T\neq0,1}$ domination. The latter is responsible for the mentioned ultra-relativistic divergence.

Finally, the range above $m_N \gtrsim 10^{1.4}T$ is considered, where the numerical error is below 5%. Since this regime is purely non-relativistic, a declining agreement of both approaches is found for small couplings. In the small coupling limit, the resummed Higgs propagator reduces to the ordinary tree-level propagator. As explained in Section 3.5.2.1, this means that the arguments for neglecting the hermitian vacuum self-energy do not hold anymore. Since neglecting $\Pi_\phi^{H,vac}$ and setting the renormalization scheme $\Lambda = T$ do not arise out of the same renormalization conditions, the approaches have to differ at *NLO* in this limit. Only a common renormalization scheme for both approaches, that is valid in vacuum and the high temperature limit,[46] would lead to a perfect agreement. Nevertheless, the crossover between the vacuum renormalization and the high temperature renormalization specified region can directly be read off in Figure 3.25c. This is given by the 2% agreement area at approximately the orange line. Consequently, while the resummed approach is in principle valid in the full m_N mass range, the perturbative approach breaks down for masses below $m_N^2 \lesssim 2.8\sqrt{G}T^2 = 5.8 m_\phi^{th}T$.[47] On the right-hand side, the threshold is expressed coupling independently. This allows for the following statement: Since this limit arises from the $\mathcal{B}^{wv,T\neq0,1}$ term in Equation (3.111) and since $\mathcal{B}^{wv,T\neq0,1}$ diverges for $m_N \to 0$ independently of $\Pi_\phi^{H,T\neq0}(k)\big|_{k^2=0} = (m_\phi^{th})^2$, including the top quark and Higgs self-interaction does not or only slightly modifies this statement on the part of the resummed approach.

---

[46] For example with help of the aforementioned thermal gauge boson mass, the vacuum Higgs self-energy is IR finite and can be resummed.

[47] For typical perturbatively acceptable couplings $G < 1$, this threshold is much larger than the thermal Higgs mass.

In the following pages, the equivalent analysis for the $\mathcal{F}$ term is performed.
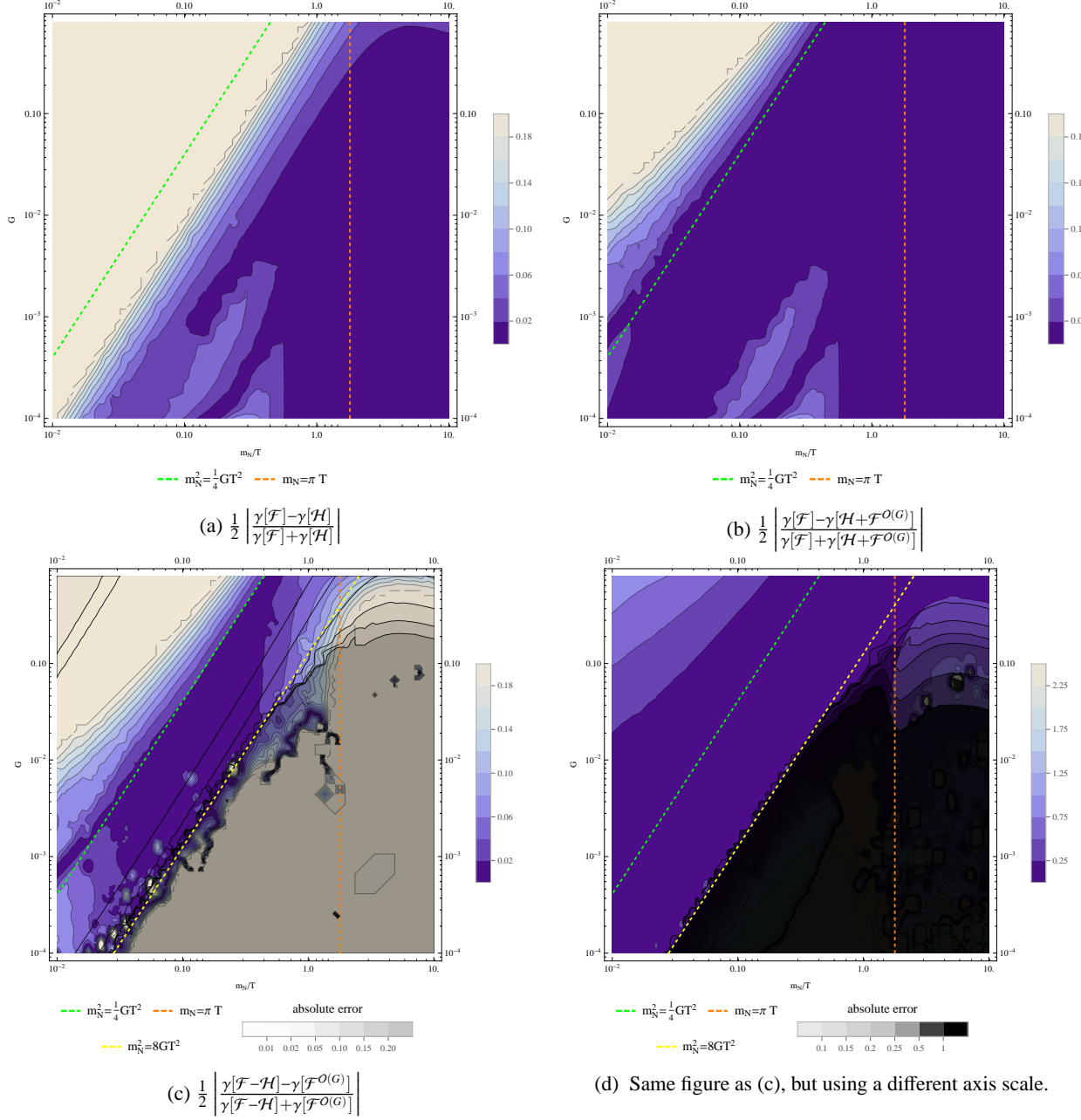

(a) $\frac{1}{2}\left|\frac{\gamma[\mathcal{F}]-\gamma[\mathcal{H}]}{\gamma[\mathcal{F}]+\gamma[\mathcal{H}]}\right|$

(b) $\frac{1}{2}\left|\frac{\gamma[\mathcal{F}]-\gamma[\mathcal{H}+\mathcal{F}^{O(G)}]}{\gamma[\mathcal{F}]+\gamma[\mathcal{H}+\mathcal{F}^{O(G)}]}\right|$

(c) $\frac{1}{2}\left|\frac{\gamma[\mathcal{F}-\mathcal{H}]-\gamma[\mathcal{F}^{O(G)}]}{\gamma[\mathcal{F}-\mathcal{H}]+\gamma[\mathcal{F}^{O(G)}]}\right|$

(d) Same figure as (c), but using a different axis scale.

Figure 3.26: The same as Figure 3.25, but relating to $\mathcal{F}$.

Figure 3.26a provides the comparison of the resummed approach for $\mathcal{F}$ to the perturbative *LO* $\mathcal{H}$ term. Both terms agree within 4% up to some mass scale of order $m_N^2 \sim GT^2$. This may be related only to the thermal lepton mass $(m_l^{th})^2 = \frac{1}{4}GT^2$, since, in contrast to $\mathcal{B}^{O(G)}$, the perturbative $\mathcal{F}^{O(G)}$ is finite in the ultra-relativistic limit. In adding the *NLO* contribution $\mathcal{F}^{O(G)}$ within Figure 3.26b, the 2% boundary moves across the thermal mass threshold, i.e. the green line. For $m_N < m_l^{th}$, the $G\ln G$ enhancement from resumming the IR t-channel divergences of the massless lepton exchange dominates the perturbative order G correction.[48] Hence, the perturbative approach breaks down below $m_N < m_l^{th}$.

---

[48] See Chapter 3.4.1.3.

The remaining plots, Figure 3.26c - 3.26d, show the comparison of the *NLO* contributions. In particular, Figure 3.26c shows the same disagreement for masses below $m_N < m_l^{th}$.

In the perturbative small coupling range, a large numerical error of the resummed *NLO* contributions is found. Above $m_N > \pi T$ for the coupling $G > 0.15$, this error drops down below 10% while the relative difference stays above 18%. This means that a discrepancy of both approaches is found in the non-relativistic regime. Of course, above $G > 0.15$ order G^2 corrections can be important too. However, since the difference grows for small couplings and the perturbative *NLO* correction obtains sizable corrections from the vacuum Higgs self-energy, the influence of the vacuum renormalization scheme Λ is visible even in the intermediate regime.[49] Therefore, this disagreement is related to the different renormalization schemes.

For the same reason, the approaches supposedly disagree in the small coupling intermediate regime, even though the large numerical error forbids a strict statement. By going to smaller neutrino masses m_N, at some point in the perturbatively accessible intermediate regime, the $\Pi_\phi^{H,vac}$ becomes irrelevant and both approaches have to agree. This crossover is given by the yellow line at $m_N^2 \approx 8GT^2$.

The small deviation up to 8% at $m_N \lesssim 10^{-1.8}$ and $G < 10^{-3}$ may only be related to numerical issues.

Finally, one can conclude: The resummed approach to $\mathcal{F}$ is valid in the full RHN mass range, while the perturbative approach breaks down at $m_N < m_l^{th}$. At *LO*, the numerical agreement of both approaches is obtained within the perturbative accessible region. However, due to different renormalization schemes, the *NLO* rate contributions differ above $m_N^2 \gtrsim 8GT^2$. In between those limits, i.e. $(m_l^{th})^2 < m_N^2 \lesssim 8GT^2$, a numerical agreement of both approaches is found up to *NLO*.

---

[49] See Chapter 3.5.1.3 for the details.

3.5.6 Vertex Type Contributions

This section handles the 2-loop correction to the right-handed neutrino production rate shown in Figure 3.1. This contribution is called the $\mathcal{J}$ term and is defined by

$$\mathcal{J}(p) \equiv \mathrm{tr}[\not{p} \Sigma_N^{\mathcal{A},vert}(p)] = -\frac{1}{2f_+(u\cdot p)}\mathrm{tr}[\not{p}\,i\Sigma_N^{<,vert}(p)]. \tag{3.186}$$

Since all internal particles are in equilibrium, the KMS relation (1.57) is utilized at the second equality. This step reduces the number of terms to consider. However, the extraction of the vacuum and the thermal part becomes unintuitive. The 2-loop correction to the right-handed neutrino self-energy can be parametrized as

$$-i\Sigma^{ab,vert}(p) = -\int \frac{\mathrm{d}^4k}{(2\pi)^4}\frac{\mathrm{d}^4q}{(2\pi)^4}\left(g_1^2 Y_L Y_\phi \mathrm{tr}[\epsilon^\dagger\epsilon] + g_2^2\mathrm{tr}[\epsilon^\dagger t^A \epsilon(t^A)^\dagger]\right)(P_L + P_R)(2(p-k)-q)^\nu$$

$$|Y|^2 \sum_{c,d} cd\, i\mathcal{S}_l^{ac}(k+q)\gamma^\mu i\mathcal{S}_l^{cb}(k)i\Delta_{\gamma\mu\nu}^{cd}(q)i\Delta_\phi^{ad}(p-k-q)i\Delta_\phi^{db}(p-k) \tag{3.187}$$

$$= g_w|Y|^2 \frac{1}{4}\underbrace{\left(g_1^2+3g_2^2\right)}_{G}\int \frac{\mathrm{d}^4k}{(2\pi)^4}(2(p-k)-q)^\nu \sum_{c,d} cd\, i\mathcal{S}_l^{ac}(k+q)\gamma^\mu i\mathcal{S}_l^{cb}(k)$$

$$i\Delta_{\gamma\mu\nu}^{cd}(q)i\Delta_\phi^{ad}(p-k-q)i\Delta_\phi^{db}(p-k). \tag{3.188}$$

This already includes the sum of both chiralities. While the 2PI formalism demands resummed 2-point functions, one may start easy and write down $\mathcal{J}$ with tree-level propagators.

$$\mathcal{J}(p) = -\frac{g_w|Y|^2 G}{2f_+(u\cdot p)}\int \frac{\mathrm{d}^4k}{(2\pi)^4}\frac{\mathrm{d}^4q}{(2\pi)^4}(2(k-p)+q)^\nu \mathrm{tr}\Big[\not{p}$$

$$\sum_{c,d} cd\, i\mathcal{S}_l^{+c}(k+q)\gamma^\mu i\mathcal{S}_l^{c-}(k)i\Delta_{\gamma\mu\nu}^{cd}(q)i\Delta_\phi^{+d}(p-k-q)i\Delta_\phi^{d-}(p-k)\Big] \tag{3.189}$$

The next step is to replace all time- and anti-time-ordered propagators $++$ and $--$ by hermitian and statistical functions H and F. By shifting the momenta $k+q \to k$ and $q \to -q$ within the terms proportional to $\mathcal{S}^H(k+q)$ and $\mathcal{S}^F(k+q)$, and taking into account the relation $\Delta_{\mu\nu}^{+-}(-q) = \Delta_{\mu\nu}^{-+}(q)$, the following symmetrized form is obtained:

$$\mathcal{J}(p) = -\frac{2g_w|Y|^2 G}{2f_+(u\cdot p)}\int \frac{\mathrm{d}^4k}{(2\pi)^4}\frac{\mathrm{d}^4q}{(2\pi)^4}(2(k-p)+q)^\nu \mathrm{tr}\Big[\not{p}\Big\{$$

$$i\mathcal{S}_l^H(k)\gamma^\mu i\mathcal{S}_l^<(k+q)i\Delta_{\gamma\mu\nu}^F(q)i\Delta_\phi^<(p-k-q)i\Delta_\phi^H(p-k) \tag{3.190}$$

$$+ i\mathcal{S}_l^H(k)\gamma^\mu i\mathcal{S}_l^<(k+q)i\Delta_{\gamma\mu\nu}^H(q)i\Delta_\phi^<(p-k-q)i\Delta_\phi^F(p-k) \tag{3.191}$$

$$+ i\mathcal{S}_l^F(k)\gamma^\mu i\mathcal{S}_l^<(k+q)i\Delta_{\gamma\mu\nu}^H(q)i\Delta_\phi^<(p-k-q)i\Delta_\phi^H(p-k) \tag{3.192}$$

$$+ i\mathcal{S}_l^H(k)\gamma^\mu i\mathcal{S}_l^<(k+q)i\Delta_{\gamma\mu\nu}^>(q)i\Delta_\phi^H(p-k-q)i\Delta_\phi^<(p-k) \tag{3.193}$$

$$+ i\mathcal{S}_l^F(k)\gamma^\mu i\mathcal{S}_l^<(k+q)i\Delta_{\gamma\mu\nu}^F(q)i\Delta_\phi^<(p-k-q)i\Delta_\phi^F(p-k) \tag{3.194}$$

$$- i\mathcal{S}_l^F(k)\gamma^\mu i\mathcal{S}_l^<(k+q)i\Delta_{\gamma\mu\nu}^>(q)i\Delta_\phi^F(p-k-q)i\Delta_\phi^<(p-k) \tag{3.195}$$

$$\Big\}\Big]. \tag{3.196}$$

The statistical, greater and less Wightman-functions are on-shell while the hermitian functions are purely off-shell propagators. All summands with two and four on-shell delta functions vanish such that only six different cases remain. The lines (3.190) - (3.192) and (3.194) are two-particle cuts with one and three of

the remaining particles being on-shell. The lines (3.193) and (3.195) correspond to three-particle cuts with zero and two of the remaining particles being on-shell.

However, (3.194) and (3.195) vanish due to the vanishing phase-space since all internal particles are massless: The vectors u, p, k and q form a linear independent base of 4-vectors for this diagram. Therefore, there are seven nontrivial integrations for the integration with respect to $\mathrm{d}^4 k$ and $\mathrm{d}^4 q$. Hence, the five delta functions leave only two of them. The integration variables of those two non-trivial integrals can be chosen to be $\mathrm{d}k_u^0$ and $\mathrm{d}q_u^0$. The integral boundary conditions for them are given by $\mathrm{gd}(u, p, k) > 0$ and $\mathrm{gd}(u, p, k, u) < 0$.[50] The first condition is the usual $\frac{1}{2}(p_u^0 - |\vec{p}_u|) < k_u^0 < \frac{1}{2}(p_u^0 + |\vec{p}_u|)$ for positive p^2 and all internal particles being massless. However, the second condition is simply $0 > 4\mathrm{gd}(u, p, k, u) = (q_u^0)^2 p^2$, which has no real solution for q_u^0. In the case of massive internal particles, this must not necessarily be true.

What remains are the terms proportional to three delta functions. Line (3.193) corresponds to the interference of the $1 \leftrightarrow 3$ (inverse-) decay process in Figure 3.27a and between the three $2 \leftrightarrow 2$ scatterings in the Figure 3.27b and 3.27d. This constibution is denoted by $\mathcal{J}^{sca}$, even if the term "scattering" does not strictly apply. The other lines (3.190)-(3.192) are interferences of the 1-loop vertex corrections, with one of the internal particles being on-shell, with the tree-level amplitude. See Figures 3.27e and 3.27g. These terms are called $\mathcal{J}^{vert,1}$, $\mathcal{J}^{vert,2}$ and $\mathcal{J}^{vert,3}$, respectively.

(a)

(b) $t - t$
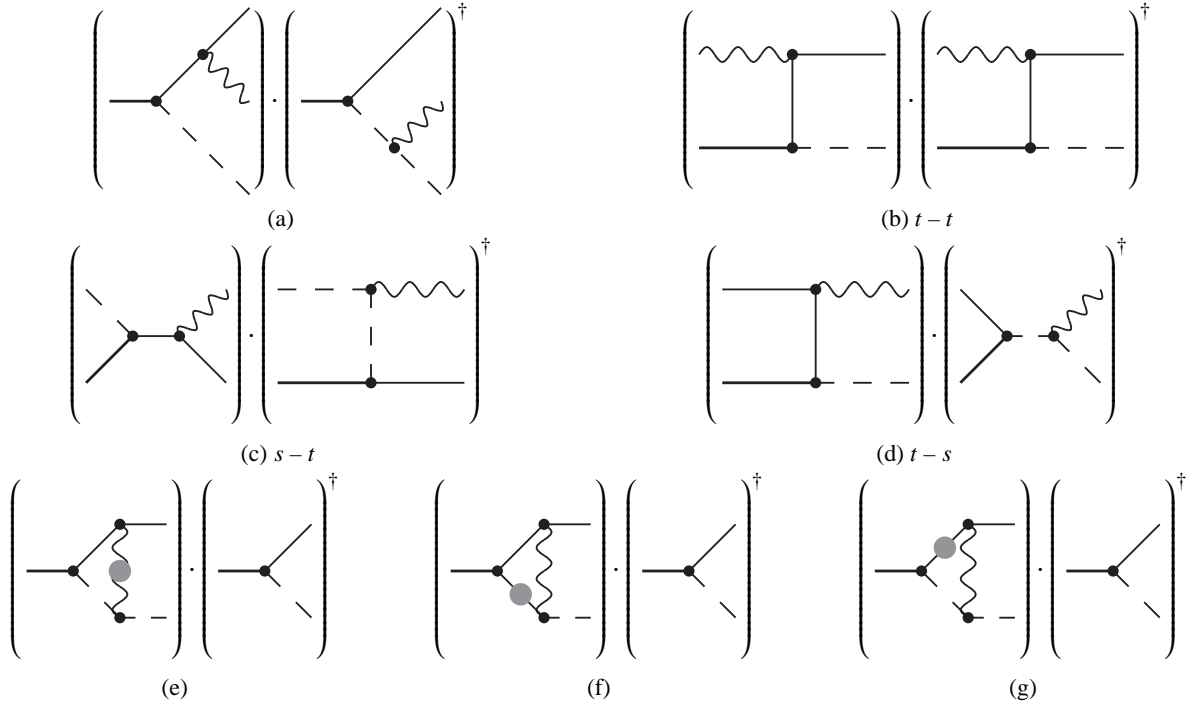
(c) $s - t$

(d) $t - s$

(e)

(f)

(g)

Figure 3.27: Interferences related to the 3-particle cut of the vertex diagram. The thick and thin lines, respectively, correspond to the RHN and the lepton. The gray blob indicates that this particle is on-shell.

Each of those four contributions obey IR divergences when the hermitian propagators are on-shell. Since only the sum of them has to be IR-finite and numerical limits of some regulators going to zero are technically undesirable, an appropriate way has to be found to parametrize the integrands such that all divergent pieces cancel. The IR divergences are naturally regulated by the masses of the corresponding particles. Therefore, setting these masses to zero means that the IR divergences are located at the boundary of the integration domain. After integrating out the delta distributions, these domains must not be unique for different cuts and of course depend on the specific parametrization. With three delta functions, there are four non-trivial

---

[50] See Chapter 2.4 for details.

integrations left. Their integration variables are chosen to be $\mathrm{d}x$, $\mathrm{d}y$ and two angular integrations.[51] x and y are the two inverse hermitian propagators of those contributions. All of the four individual contributions then may have a pole structure of the type $\frac{1}{x}$, $\frac{1}{y}$ or $\frac{1}{xy}$ and different integration domains of the type $x > 0 \wedge y > 0 \wedge \ldots$ for appropriately signed x and y. This strategy indeed works out in vacuum, if all those contributions are add, split and fold along $x = 0$ and $y = 0$ such that x and y are always positive. All collinear and mass divergences then cancel such that the integrand becomes IR-finite in vacuum. However, for the vertex corrections $\mathcal{J}^{vert,2}$ and $\mathcal{J}^{vert,3}$ the integration domains allow for a principal value integration at one of the hermitian propagators. This gives no IR-divergence but is at the same time evaluated by means of the $x \leftrightarrow -x$ and $y \leftrightarrow -y$ symmetrization. Only the Bose-Einstein distributions can cause trouble when the particle momenta become collinear to the plasma vector. They explicitly depend on the mentioned angles, which are therefore symmetrized too. This strategy works best if the same momentum parametrization is chosen in each of above vertex corrections. The choice of the momentum parametrization for the scattering term compared to the vertex terms is unimportant. Nevertheless, the same one may be chosen. The derivation of the vacuum part then also simplifies. If the angles are symmetrized, the integrand is IR-finite also for $T \neq 0$.

After all these considerations, this method still has one subtlety. Even if all IR divergences have canceled, a symmetric cancellation scheme is introduced like the one used for principal values.[52] On the other hand, a specific scheme is already given by the limit masses $\to 0$. Therefore, a correction term has to be added to account for the difference of both schemes. To be precise, the lines (3.190) - (3.193) are divergent and ill-defined. Only the sum of them is finite. To be able to integrate out the delta distributions in each term separately, individual finite and well-defined contributions are important. By introducing a fictitious mass λ for the gauge bosons, the divergences are already regulated and the individual contributions are made finite. The separate terms can be rearranged working in the limit $\lambda \to 0$, such that they can be added under one integral. λ is then set to zero.

The third point to mention is the following: Even if (3.196) is IR-finite, there are still UV-divergences in the vacuum part of (3.196). Those have to be renormalized using the Yukawa coupling Y. The vacuum expression and consequently the renormalization can be derived analytically. Hence, only IR and UV finite thermal contribution with possible principal value integrable singularities need to be evaluated numerically. The possibility of simplifying the integrand in this way is one of the basic features of the diagram, since it is symmetric under exchange of the two lepton propagators while also exchanging the two Higgs propagators. Other diagrams of this topology can consist of more terms. Nevertheless, the method described above should apply to them too. Further considerations would be required, only if there are less non-trivial integration variables than hermitian propagators. To continue, the shift $k \to p - q$, $q \to k + q - p$ is applied to the whole (3.196). This simplifies the integration over the deltas in the end.

$$\mathcal{J}(p) = -\frac{2g_w|Y|^2 G}{2f_+(u \cdot p)} \int \frac{\mathrm{d}^4 k}{(2\pi)^4} \frac{\mathrm{d}^4 q}{(2\pi)^4} (k - q - p)^\nu \mathrm{tr}\Big[\not{p} \Big\{$$

$$i\slashed{S}_l^H(p-q)\gamma^\mu i\slashed{S}_l^<(k) i\Delta_{\gamma_{\mu\nu}}^F(k+q-p) i\Delta_\phi^<(p-k) i\Delta_\phi^H(q) \tag{3.197}$$

$$+ i\slashed{S}_l^H(p-q)\gamma^\mu i\slashed{S}_l^<(k) i\Delta_{\gamma_{\mu\nu}}^H(k+q-p) i\Delta_\phi^<(p-k) i\Delta_\phi^F(q) \tag{3.198}$$

$$+ i\slashed{S}_l^F(p-q)\gamma^\mu i\slashed{S}_l^<(k) i\Delta_{\gamma_{\mu\nu}}^H(k+q-p) i\Delta_\phi^<(p-k) i\Delta_\phi^H(q) \tag{3.199}$$

$$+ i\slashed{S}_l^H(p-q)\gamma^\mu i\slashed{S}_l^<(k) i\Delta_{\gamma_{\mu\nu}}^>(k+q-p) i\Delta_\phi^H(p-k) i\Delta_\phi^<(q) \tag{3.200}$$

$$\Big\} \Big] \tag{3.201}$$

---

[51] In vacuum, those integrals decouple from the plasma vector. Hence, only the two integrations with respect to x and y are non-trivial.

[52] After applying the substitution $x \to 2x$, for instance to the scattering contribution, the IR divergent poles still cancel those from the vertex parts. Nevertheless, the integral value changes.

3.5.6.1 Vertex Corrections with on-shell Gauge Boson

The vertex correction from Equation (3.201) with the on-shell gauge boson is given by

$$\mathcal{J}(p)^{vert,1} = -\frac{g_w|Y|^2 G}{f_+(u\cdot p)} \int \frac{\mathrm{d}^4 k}{(2\pi)^4} \frac{\mathrm{d}^4 q}{(2\pi)^4} (k-q-p)^\nu \mathrm{tr}\left[\slashed{p}\, i\slashed{S}_l^H(p-q)\gamma^\mu i\slashed{S}_l^<(k)\right]$$

$$i\Delta^F_{\gamma_{\mu\nu}}(k+q-p)i\Delta^<_\phi(p-k)i\Delta^H_\phi(q) \tag{3.202}$$

$$= -\frac{g_w|Y|^2 G}{2(2\pi)^5 f_+(u\cdot p)} \int \mathrm{d}^4 k\,\mathrm{d}^4 q (k-q-p)^\nu \mathrm{tr}\left[\slashed{p}\,(\slashed{p}-\slashed{q})\gamma_\nu \slashed{k}\right] \frac{1}{(p-q)^2 q^2}$$

$$\delta\left(k^2\right)\delta\left((k+q-p)^2 - \lambda^2\right)\delta\left((p-k)^2\right)\mathrm{sign}(u\cdot k)\mathrm{sign}(u\cdot(k+q-p))\mathrm{sign}(u\cdot(p-k))$$

$$(-f_+(u\cdot k))(1 + 2f_-(u\cdot(k+q-p)))f_-(u\cdot(p-k)). \tag{3.203}$$

$\mathrm{d}^3\vec{k}$ is parametrized in polar coordinates with respect to $\vec{u}$, such that the one free angular parameter in the p-frame is the azimuthal angle going from 0 to 2π. The polar angle is one of the non-trivial angular integrations. However, there is still q. Hence, to really have (3.201) free of this azimuthal angle, polar coordinates need to be used for $\mathrm{d}^3\vec{q}$ with respect to $\vec{k}$.[53] The volume element then is

$$\mathrm{d}^4 k\,\mathrm{d}^4 q = \mathrm{d}k^0\,\mathrm{d}q^0\,\mathrm{d}|\vec{k}|\,\mathrm{d}|\vec{q}|\,\mathrm{d}\cos\angle(k,u)\,\mathrm{d}\phi_k^u\,\mathrm{d}\cos\angle(q,k)\,\mathrm{d}\phi_q^k\,|\vec{k}|^2|\vec{q}|^2. \tag{3.204}$$

The $\mathrm{d}\phi_k^u$ simply integrates to 2π. Since the p-frame is chosen, the only way to switch from $(p-q)^2 q^2$ to xy is via the variables q^0 and $|\vec{q}|$. Therefore, $\delta\left(k^2\right)$ should be integrated with help of $\mathrm{d}|\vec{k}|$, $\delta\left((p-k)^2\right)$ gets integrated using $\mathrm{d}k^0$, and $\delta\left((k+q-p)^2 - \lambda^2\right)$ is integrated with $\mathrm{d}\cos\angle(q,k)$. The Jacobian of this integration becomes

$$\mathrm{d}^4 k\,\mathrm{d}^4 q\,\delta\left(k^2\right)\delta\left((k+q-p)^2 - \lambda^2\right)\delta\left((p-k)^2\right) = \mathrm{d}q^0\,\mathrm{d}|\vec{q}|\,\mathrm{d}\cos\angle(k,u)\,\mathrm{d}\phi_q^k\frac{\pi|\vec{q}|}{2^2 m_N}. \tag{3.205}$$

The invariant scalar products are

$$u\cdot p = \tilde{p}^0 \tag{3.206}$$

$$u\cdot k = u^0 k^0 - |\vec{u}||\vec{k}|\cos\angle(k,u) = \frac{1}{m_N}\left(\tilde{p}^0 k^0 - |\vec{p}||\vec{k}|\cos\angle(k,u)\right) \tag{3.207}$$

$$u\cdot q = \frac{1}{m_N}\left(\tilde{p}^0 q^0 - |\vec{p}||\vec{q}|\left(\cos\angle(k,u)\cos\angle(q,k) - \cos(\phi_q^k)\sin\angle(k,u)\sin\angle(q,k)\right)\right) \tag{3.208}$$

$$p^2 = m_N^2 \tag{3.209}$$

$$p\cdot k = m_N k^0 = \frac{m_N^2}{2} \tag{3.210}$$

$$p\cdot q = m_N q^0 \tag{3.211}$$

$$k^2 = 0 \tag{3.212}$$

$$q^2 = (q^0)^2 - |\vec{q}|^2 \tag{3.213}$$

$$k\cdot q = \frac{\lambda^2 - q^2 + 2p\cdot q}{2} \tag{3.214}$$

together with

$$k^0 = |\vec{k}| = \frac{m_N}{2} \tag{3.215}$$

$$\cos\angle(q,k) = \frac{q^2 - \lambda^2 - 2p\cdot q + 2k^0 q^0}{2|\vec{k}||\vec{q}|}. \tag{3.216}$$

---

[53] The explicit parametrization can be found in (3.217).

For $u \cdot q$, the explicit parametrization

$$p = \begin{pmatrix} m_N \\ 0 \\ 0 \\ 0 \end{pmatrix} \qquad u = \begin{pmatrix} u^0 \\ 0 \\ 0 \\ |\vec{u}| \end{pmatrix} \qquad k = R_3(\theta_k^u)\begin{pmatrix} k^0 \\ 0 \\ 0 \\ |\vec{k}| \end{pmatrix} \qquad q = R_3(\theta_k^u)R_4(\phi_q^k)R_3(\theta_q^k)\begin{pmatrix} q^0 \\ 0 \\ 0 \\ |\vec{q}| \end{pmatrix} \tag{3.217}$$

modulo the irrelevant ϕ_k^u dependence is used.[54] Hence, the goal of parametrizing $\mathcal{J}^{vert,1}$ in terms of the inverse hermitian propagators is obtained by defining

$$q^2 \equiv 2m_N x \tag{3.218}$$

$$(p-q)^2 = m_N(m_N - 2q^0) + q^2 \equiv 2m_N y. \tag{3.219}$$

The additional factor $2m_N$ is for convenience, since the integration variables in the scattering part then do not need to be rescaled later on. Therefore, the transformation rules are

$$|\vec{q}| = \sqrt{\left(\frac{m_N}{2} + x - y\right)^2 - 2m_N x} \tag{3.220}$$

$$q^0 = \frac{m_N}{2} + x - y \tag{3.221}$$

$$\mathrm{d}q^0\,\mathrm{d}|\vec{q}| = -\frac{m_N}{|\vec{q}|}\mathrm{d}x\,\mathrm{d}y. \tag{3.222}$$

Altogether, the $\mathcal{J}^{vert,1}$ contribution becomes

$$\mathcal{J}(p)^{vert,1} = -\frac{g_w|Y|^2 G}{2^4(2\pi)^4 f_+(u \cdot p)} \int_{V_1} \mathrm{d}\cos\angle(k,u)\,\mathrm{d}\phi_q^k\,\mathrm{d}x\,\mathrm{d}y\frac{\lambda^2 + m_N^2 - m_N(2x+y)}{xy}$$
$$f_+(u \cdot k)(1 + 2f_-(|u \cdot (k+q-p)|))f_-(u \cdot (p-k)). \tag{3.223}$$

Since $\mathrm{sign}(u \cdot k) = \mathrm{sign}(k^0) = 1 = \mathrm{sign}(u \cdot (p-k))$, the integration is exponentially suppressed due to the $f_+(u \cdot k)f_-(u \cdot (p-k))$. Hence, only the 1 in $1 + 2f_-(|u \cdot (k+q-p)|)$ can give rise to UV-divergences. This term is called the vacuum part. $\mathcal{J}(p)^{vert,1}$ is split into

$$\mathcal{J}(p)^{vert,1,vac} = \frac{g_w|Y|^2 G}{2^4(2\pi)^4 f_+(u \cdot p)} \int_{V_1} \mathrm{d}\cos\angle(k,u)\,\mathrm{d}\phi_q^k\,\mathrm{d}x\,\mathrm{d}y\frac{\lambda^2 + m_N^2 - m_N(2x+y)}{xy}$$
$$(-f_+(u \cdot k))f_-(u \cdot (p-k)) \tag{3.224}$$

and

$$\mathcal{J}(p)^{vert,1,T\neq 0} = \frac{g_w|Y|^2 G}{2^3(2\pi)^4 f_+(u \cdot p)} \int_{V_1} \mathrm{d}\cos\angle(k,u)\,\mathrm{d}\phi_q^k\,\mathrm{d}x\,\mathrm{d}y\frac{\lambda^2 + m_N^2 - m_N(2x+y)}{xy}$$
$$f_-(|u \cdot (k+q-p)|)(-f_+(u \cdot k))f_-(u \cdot (p-k)). \tag{3.225}$$

The $\mathrm{sign}(u \cdot k)\mathrm{sign}(u \cdot (p-k))(-f_+(u \cdot k))f_-(u \cdot (p-k))$ is just the quantum statistical factor for the vertex correction generated by the CTP. Otherwise, the true vacuum part[55] of $\mathcal{J}^{vert,1}$ can be separated too, as it is done for the wave-function type contribution. However, one would then need to calculate $\mathcal{J} \propto \Sigma_N^{\mathcal{A}}$ out of $\Sigma_N^> - \Sigma_N^<$. The term $(-f_+(u \cdot k))f_-(u \cdot (p-k))$ would have to be replaced by

---

[54] R_3 and R_4 are rotation matrices for a spacial rotation around the 3rd and 4th axis, and θ_x^y is shorthand for $\angle(x,y)$. As can be observed, if the k and q are defined with an additional $R_4(\phi_k^u)$ factor, the scalar products $u \cdot k$, $u \cdot q$ and $k \cdot q$ are independent of ϕ_k^u.

[55] i.e. the temperature-independent part.

$1 - f_+(u \cdot k) + f_-(u \cdot (p - k)) = \theta(k^0) + \theta(k^0 - m_N) - f_+(|u \cdot k|) + f_-(|u \cdot (p - k))|$. Consequently, vacuum-thermal mixing terms would be obtained too, which complicates the expressions.[56]

The next step is to determine the integration domain V_1. Since the Dirac deltas are integrated out by k^0, $|\vec{k}|$ and $\cos \angle(q, k)$, all of them constitute conditions to V_1. Nevertheless, these integrations do not involve any knowledge of u. $\vec{k}$ was parametrized with respect to $\vec{u}$, but θ_k^u could have been set to any value and still lead to the same integral over the deltas. The conclusion is that the p-frame integration domain given by $\mathrm{gd}(p) > 0 \wedge \mathrm{gd}(p, k) < 0 \wedge \mathrm{gd}(p, k, q) > 0 \wedge \mathrm{gd}(p, k, q, u) < 0$, which is equivalent to $|\vec{k}|, |\vec{q}| > 0$ and $|\cos \angle(k, u)|, |\cos \angle(q, k)| < 1$, reduces to $\mathrm{gd}(p) > 0 \wedge \mathrm{gd}(p, k) < 0 \wedge \mathrm{gd}(p, k, q) > 0$ and $|\cos \angle(k, u)| < 1$. Therefore, after integration over the deltas, only the conditions generated by $\mathrm{gd}(p, k)$ and $\mathrm{gd}(p, k, q)$ get affected. The first one is $\mathrm{gd}(p, k) = -\frac{m_N^4}{4} < 0$. This is fulfilled trivially. The second one is

$$V_1 \equiv \left\{ \frac{4\mathrm{gd}(p, k, q)}{m_N^2} = -\left(\lambda^4 + 4m_N^2 xy + \lambda^2 m_N (m_N - 2(x + y)) \right) > 0 \right\}. \tag{3.226}$$

Obviously, the domain V_1 is given by $xy < 0$ in the limit $\lambda \to 0$. This is of course the same condition that one would find by working out the Boolean algebra directly from the conditions $|\vec{k}| > 0$ and $|\cos \angle(q, k)| < 1$. Figure 3.28 shows a plot of V_1. On the left side, λ is set to zero, and on the right one $\lambda = 0.4m_N$ is used.

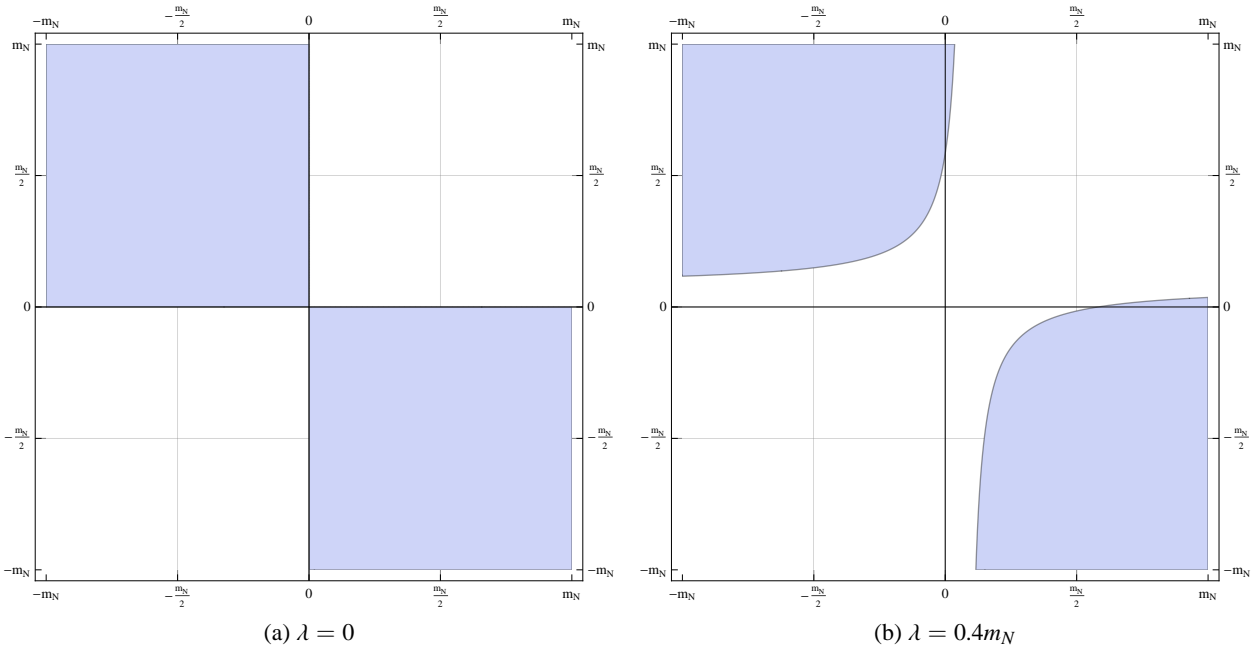(a) $\lambda = 0$

(b) $\lambda = 0.4m_N$

Figure 3.28: Plot of integration domain V_1. The two separate areas correspond to the two energy solutions when integrating over the delta distribution of the blobbed particle in Figure 3.27e.

For completeness, one may check that $\mathrm{gd}(p, k, q, u) < 0$ is always true: After insertion of all variable substitutions this determinant equals to

$$\mathrm{gd}(p, k, q, u) = (\cos^2 \angle(k, u) - 1)|\vec{p}|^2 \sin^2(\phi_q^k) \frac{\mathrm{gd}(p, k, q)}{m_N^2} < 0. \tag{3.227}$$

Since $\mathrm{gd}(p, k, q)$ has to be positive, this directly infers $\cos^2 \angle(k, u) < 1$, as expected.

---

[56] See Section 3.5.6.6 for the evaluation of the vacuum part.

3.5.6.2 Vertex Corrections with on-shell Higgs

The vertex correction with the on-shell Higgs boson is given by

$$\mathcal{J}(p)^{vert,2} = -\frac{g_w |Y|^2 G}{f_+(u \cdot p)} \int \frac{\mathrm{d}^4 k}{(2\pi)^4} \frac{\mathrm{d}^4 q}{(2\pi)^4} (k - q - p)^\nu \mathrm{tr}\left[\not{p} i \not{S}_l^H (p-q) \gamma^\mu i \not{S}_l^< (k)\right]$$
$$i\Delta_{\gamma_{\mu\nu}}^H (k + q - p) i\Delta_\phi^< (p - k) i\Delta_\phi^F (q) \tag{3.228}$$

$$= -\frac{g_w |Y|^2 G}{2(2\pi)^5 f_+(u \cdot p)} \int \mathrm{d}^4 k\, \mathrm{d}^4 q\, (k - q - p)^\nu \mathrm{tr}\left[\not{p}(\not{p} - \not{q})\gamma_\nu \not{k}\right] \frac{1}{(p-q)^2((k+q-p)^2 - \lambda^2)}$$
$$\delta\left(k^2\right)\delta\left((p-k)^2\right)\delta\left(q^2\right)\mathrm{sign}(u \cdot k)\mathrm{sign}(u \cdot (p-k))\mathrm{sign}(u \cdot q)$$
$$(-f_+(u \cdot k))f_-(u \cdot (p-k))(1 + 2f_-(u \cdot q)). \tag{3.229}$$

Since the same parametrization as for $\mathcal{J}^{vert,1}$ is used, $\delta\left((p-k)^2\right)$ needs to be integrated via $\mathrm{d}k^0$, $\delta\left(k^2\right)$ is integrated with the help of $\mathrm{d}|\vec{k}|$, and $\delta\left(q^2\right)$ is integrated for instance with $\mathrm{d}|\vec{q}|$. Hence, the switch from $(p-q)^2((k+q-p)^2 - \lambda^2)$ to xy has to be done via the variables q^0 and $\cos \angle(q,k)$. The Jacobian of this integration becomes

$$\mathrm{d}^4 k\, \mathrm{d}^4 q\, \delta\left(k^2\right)\delta\left((p-k)^2\right)\delta\left(q^2\right) = \mathrm{d}q^0\, \mathrm{d}\cos\angle(q,k)\, \mathrm{d}\cos\angle(k,u)\, \mathrm{d}\phi_q^k \frac{\pi|\vec{k}||\vec{q}|}{2^2 m_N}. \tag{3.230}$$

In terms of invariant scalar products, this means

$$u \cdot p = \tilde{p}^0 \tag{3.231}$$

$$u \cdot k = u^0 k^0 - |\vec{u}||\vec{k}| \cos\angle(k,u) = \frac{1}{m_N}\left(\tilde{p}^0 k^0 - |\vec{p}||\vec{k}| \cos\angle(k,u)\right) \tag{3.232}$$

$$u \cdot q = \frac{1}{m_N}\left(\tilde{p}^0 q^0 - |\vec{p}||\vec{q}|\left(\cos\angle(k,u)\cos\angle(q,k) - \cos(\phi_q^k)\sin\angle(k,u)\sin\angle(q,k)\right)\right) \tag{3.233}$$

$$p^2 = m_N^2 \tag{3.234}$$

$$p \cdot k = m_N k^0 = \frac{m_N^2}{2} \tag{3.235}$$

$$p \cdot q = m_N q^0 \tag{3.236}$$

$$k^2 = q^2 = 0 \tag{3.237}$$

$$k \cdot q = k^0 q^0 - |\vec{k}||\vec{q}| \cos\angle(q,k) \tag{3.238}$$

together with

$$k^0 = |\vec{k}| = \frac{m_N}{2} \tag{3.239}$$

$$|\vec{q}| = |q^0|. \tag{3.240}$$

x and y are defined to be the invariant momentum squares of the hermitian propagators:

$$(p-q)^2 = p^2 - 2p \cdot q \equiv 2m_N x \tag{3.241}$$

$$(k+q-p)^2 - \lambda^2 = 2k \cdot q - 2p \cdot q - \lambda^2 \equiv 2m_N y. \tag{3.242}$$

Therefore, the transformation rules are

$$q^0 = \frac{m_N}{2} - x \tag{3.243}$$

$$\cos\angle(q,k) = \frac{-2\lambda^2 - m_N^2 + 2m_N(x - 2y)}{m_N|m_N - 2x|} \tag{3.244}$$

$$\mathrm{d}q^0 \, \mathrm{d}\cos \angle(q,k) = \frac{2}{|\vec{q}|} \mathrm{d}x \, \mathrm{d}y \,. \tag{3.245}$$

Altogether, the $\mathcal{J}^{vert,2}$ contribution becomes

$$\mathcal{J}(p)^{vert,2} = -\frac{g_w |Y|^2 G}{2^4 (2\pi)^4 f_+(u \cdot p)} \int_{V_2} \mathrm{d}\cos \angle(k,u) \, \mathrm{d}\phi_q^k \, \mathrm{d}x \, \mathrm{d}y \frac{\lambda^2 + m_N(m_N - x + 2y)}{xy}$$
$$f_+(u \cdot k) f_-(u \cdot (p-k))(1 + 2f_-(|u \cdot q|)) \,. \tag{3.246}$$

Here, the same quantum statistical factor is obtained as above, since it corresponds to the same 2-particle cut and it has the same parametrization. $\mathcal{J}^{vert,2}$ is split according to

$$\mathcal{J}(p)^{vert,2,vac} = \frac{g_w |Y|^2 G}{2^4 (2\pi)^4 f_+(u \cdot p)} \int_{V_2} \mathrm{d}\cos \angle(k,u) \, \mathrm{d}\phi_q^k \, \mathrm{d}x \, \mathrm{d}y \frac{\lambda^2 + m_N(m_N - x + 2y)}{xy}$$
$$(-f_+(u \cdot k)) f_-(u \cdot (p-k)) \tag{3.247}$$

$$\mathcal{J}(p)^{vert,2,T\neq 0} = \frac{g_w |Y|^2 G}{2^3 (2\pi)^4 f_+(u \cdot p)} \int_{V_2} \mathrm{d}\cos \angle(k,u) \, \mathrm{d}\phi_q^k \, \mathrm{d}x \, \mathrm{d}y \frac{\lambda^2 + m_N(m_N - x + 2y)}{xy}$$
$$f_-(|u \cdot q|)(-f_+(u \cdot k)) f_-(u \cdot (p-k)) \,. \tag{3.248}$$

The integration domain V_2 is again only given by $\mathrm{gd}(p,k) = -\frac{m_N^4}{4} < 0$ and $\mathrm{gd}(p,k,q) > 0$:

$$V_2 \equiv \left\{ \frac{4}{m_N^2} \mathrm{gd}(p,k,q) > 0 \right\} = \left\{ \left(\lambda^2 + 2m_N y \right) \left(\lambda^2 + m_N(m_N - 2x + 2y) \right) < 0 \right\} \,. \tag{3.249}$$

In the limit $\lambda \to 0$, the domain V_2 is given by $y = 0$ and $x = \frac{m_N}{2} + y$. This means that the pole at $x = 0$ has to be evaluated in the principal value sense and is finite. Figure 3.29 shows a plot of V_2.
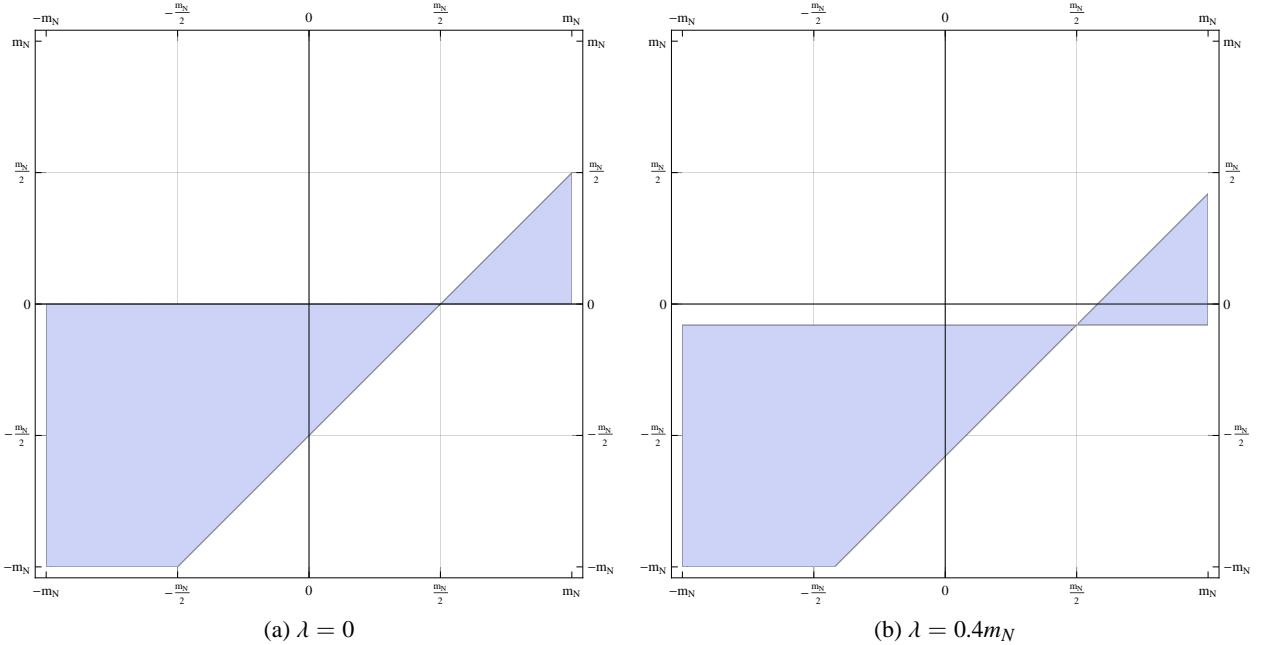

Figure 3.29: Plot of integration domain V_2. The two separate areas correspond to the two energy solutions when integrating over the delta distribution of the blobbed particle in Figure 3.27f.

3.5.6.3 Vertex Corrections with on-shell Lepton

The vertex correction with the on-shell lepton is given by

$$
\mathcal{J}(p)^{vert,3} = -\frac{g_w |Y|^2 G}{f_+(u \cdot p)} \int \frac{\mathrm{d}^4 k}{(2\pi)^4} \frac{\mathrm{d}^4 q}{(2\pi)^4} (k - q - p)^\nu \mathrm{tr} \left[\not{p} \, i \mathcal{S}_l^F(p - q) \gamma^\mu i \mathcal{S}_l^<(k) \right]
$$
$$
i \Delta_{\gamma_{\mu\nu}}^H (k + q - p) i \Delta_\phi^<(p - k) i \Delta_\phi^H(q) \tag{3.250}
$$
$$
= -\frac{g_w |Y|^2 G}{2(2\pi)^5 f_+(u \cdot p)} \int \mathrm{d}^4 k \, \mathrm{d}^4 q (k - q - p)^\nu \mathrm{tr} \left[\not{p} \, (\not{p} - \not{q}) \gamma_\nu \not{k} \right] \frac{1}{((k + q - p)^2 - \lambda^2) q^2}
$$
$$
\delta \left((p - q)^2 \right) \delta \left(k^2 \right) \delta \left((p - k)^2 \right) \mathrm{sign}(u \cdot (p - q)) \mathrm{sign}(u \cdot k) \mathrm{sign}(u \cdot (p - k))
$$
$$
(1 - 2 f_+(u \cdot (p - q))) (-f_+(u \cdot k)) f_-(u \cdot (p - k)) . \tag{3.251}
$$

In this parametrization, $\delta \left((p - k)^2 \right)$ should be integrated using $\mathrm{d}k^0$. $\delta \left(k^2 \right)$ is integrated with the help of $\mathrm{d}|\vec{k}|$, and $\delta \left((p - q)^2 \right)$ can be integrated for instance with $\mathrm{d}|\vec{q}|$. Hence, one may switch from $((k + q - p)^2 - \lambda^2) q^2$ to xy via the variables q^0 and $\cos \angle(q, k)$. The Jacobian of this integration is

$$
\mathrm{d}^4 k \, \mathrm{d}^4 q \, \delta \left((p - q)^2 \right) \delta \left(k^2 \right) \delta \left((p - k)^2 \right) = \mathrm{d}q^0 \, \mathrm{d} \cos \angle(q, k) \, \mathrm{d} \cos \angle(k, u) \, \mathrm{d}\phi_q^k \frac{\pi |\vec{k}| |\vec{q}|}{2^2 m_N} . \tag{3.252}
$$

The scalar products are

$$
u \cdot p = \tilde{p}^0 \tag{3.253}
$$
$$
u \cdot k = u^0 k^0 - |\vec{u}| |\vec{k}| \cos \angle(k, u) = \frac{1}{m_N} \left(\tilde{p}^0 k^0 - |\vec{p}| |\vec{k}| \cos \angle(k, u) \right) \tag{3.254}
$$
$$
u \cdot q = \frac{1}{m_N} \left(\tilde{p}^0 q^0 - |\vec{p}| |\vec{q}| \left(\cos \angle(k, u) \cos \angle(q, k) - \cos(\phi_q^k) \sin \angle(k, u) \sin \angle(q, k) \right) \right) \tag{3.255}
$$
$$
p^2 = m_N^2 \tag{3.256}
$$
$$
p \cdot k = m_N k^0 = \frac{m_N^2}{2} \tag{3.257}
$$
$$
p \cdot q = m_N q^0 \tag{3.258}
$$
$$
k^2 = 0 \tag{3.259}
$$
$$
q^2 = 2 p \cdot q - p^2 \tag{3.260}
$$
$$
k \cdot q = k^0 q^0 - |\vec{k}| |\vec{q}| \cos \angle(q, k) \tag{3.261}
$$

together with

$$
k^0 = |\vec{k}| = \frac{m_N}{2} \tag{3.262}
$$
$$
|\vec{q}| = |m_N - q^0| . \tag{3.263}
$$

x and y are defined by

$$
q^2 \equiv 2 m_N x \tag{3.264}
$$
$$
(k + q - p)^2 - \lambda^2 = 2 k \cdot q - 2 p \cdot k - \lambda^2 \equiv 2 m_N y . \tag{3.265}
$$

Hence, the transformation rules are

$$q^0 = \frac{m_N}{2} + x \tag{3.266}$$

$$\cos \measuredangle(q, k) = \frac{-2\lambda^2 - m_N^2 + 2m_N(x - 2y)}{m_N|m_N - 2x|} \tag{3.267}$$

$$\mathrm{d}|\vec{q}|\mathrm{d}\cos \measuredangle(q, k) = \frac{2}{|\vec{q}|}\mathrm{d}x\mathrm{d}y. \tag{3.268}$$

Altogether, the $\mathcal{J}^{vert,2}$ contribution becomes

$$\mathcal{J}(p)^{vert,3} = -\frac{g_w|Y|^2 G}{2^4 (2\pi)^4 f_+(u \cdot p)} \int_{V_3} \mathrm{d}\cos \measuredangle(k, u) \mathrm{d}\phi_q^k \mathrm{d}x \mathrm{d}y \frac{\lambda^2 + m_N(m_N - 2x + 2y)}{xy}$$
$$(1 - 2f_+(|u \cdot (p - q)|))f_+(u \cdot k)f_-(u \cdot (p - k)), \tag{3.269}$$

which is the sum of

$$\mathcal{J}(p)^{vert,3,vac} = \frac{g_w|Y|^2 G}{2^4 (2\pi)^4 f_+(u \cdot p)} \int_{V_3} \mathrm{d}\cos \measuredangle(k, u) \mathrm{d}\phi_q^k \mathrm{d}x \mathrm{d}y \frac{\lambda^2 + m_N(m_N - 2x + 2y)}{xy}$$
$$(-f_+(u \cdot k))f_-(u \cdot (p - k)) \tag{3.270}$$

and

$$\mathcal{J}(p)^{vert,3,T \neq 0} = -\frac{g_w|Y|^2 G}{2^3 (2\pi)^4 f_+(u \cdot p)} \int_{V_3} \mathrm{d}\cos \measuredangle(k, u) \mathrm{d}\phi_q^k \mathrm{d}x \mathrm{d}y \frac{\lambda^2 + m_N(m_N - 2x + 2y)}{xy}$$
$$f_+(|u \cdot (p - q)|)(-f_+(u \cdot k))f_-(u \cdot (p - k)). \tag{3.271}$$

Since it is the same 2-particle cut as for the other vertex corrections, V_3 is again only given by $\mathrm{gd}(p, k, q) > 0$:

$$V_3 \equiv \left\{ \left(\lambda^2 + 2m_N y\right)\left(\lambda^2 + m_N(m_N - 2x + 2y)\right) < 0 \right\}. \tag{3.272}$$

Obviously, V_3 is the same as V_2, since both corresponding cuts are topologically symmetric under exchange of the on-shell Higgs with the lepton, i.e. the diagrams in Figure 3.27f and 3.27g.

3.5.6.4 Scatterings

Finally, the scattering part is given by

$$\mathcal{J}(p)^{sca} = -\frac{g_w |Y|^2 G}{f_+(u \cdot p)} \int \frac{\mathrm{d}^4 k}{(2\pi)^4} \frac{\mathrm{d}^4 q}{(2\pi)^4} (k - q - p)^\nu \mathrm{tr} \left[\not{p} i \mathcal{S}_l^H (p - q) \gamma^\mu i \mathcal{S}_l^< (k) \right]$$
$$i\Delta_{\gamma\mu\nu}^> (k + q - p) i \Delta_\phi^H (p - k) i \Delta_\phi^< (q) \tag{3.273}$$

$$= -\frac{g_w |Y|^2 G}{(2\pi)^5 f_+(u \cdot p)} \int \mathrm{d}^4 k \, \mathrm{d}^4 q (k - q - p)^\nu \mathrm{tr} \left[\not{p} (\not{p} - \not{q}) \gamma_\nu \not{k} \right] \frac{1}{(p - q)^2 (p - k)^2}$$
$$\delta \left(k^2 \right) \delta \left((k + q - p)^2 - \lambda^2 \right) \delta \left(q^2 \right) \mathrm{sign}(u \cdot k) \mathrm{sign}(u \cdot (k + q - p)) \mathrm{sign}(u \cdot q)$$
$$(-f_+(u \cdot k))(1 + f_-(u \cdot (k + q - p))) f_-(u \cdot q) . \tag{3.274}$$

If one does not want to deal with a sum of several solutions, $\delta \left(k^2 \right)$ is best integrated by $\mathrm{d}|\vec{k}|$. For the same reason, $\delta \left(q^2 \right)$ should be integrated by $\mathrm{d}|\vec{q}|$. However, since $(p - q)^2 (p - k)^2$ is substituted by xy in the end, k^0 and q^0 should be left unchanged. Hence, the remaining $\delta \left((k + q - p)^2 - \lambda^2 \right)$ should only be integrated by $\mathrm{d}\cos \angle(q, k)$. The Jacobian of this integration is

$$\mathrm{d}^4 k \, \mathrm{d}^4 q \, \delta \left(k^2 \right) \delta \left((k + q - p)^2 - \lambda^2 \right) \delta \left(q^2 \right) = \frac{\pi}{2^2} \mathrm{d}\cos \angle(k, u) \, \mathrm{d}\phi_q^k \, \mathrm{d}k^0 \, \mathrm{d}q^0 . \tag{3.275}$$

The scalar products are

$$u \cdot p = \tilde{p}^0 \tag{3.276}$$

$$u \cdot k = u^0 k^0 - |\vec{u}||\vec{k}| \cos \angle(k, u) = \frac{1}{m_N} \left(\tilde{p}^0 k^0 - |\vec{p}||\vec{k}| \cos \angle(k, u) \right) \tag{3.277}$$

$$u \cdot q = \frac{1}{m_N} \left(\tilde{p}^0 q^0 - |\vec{p}||\vec{q}| \left(\cos \angle(k, u) \cos \angle(q, k) - \cos(\phi_q^k) \sin \angle(k, u) \sin \angle(q, k) \right) \right) \tag{3.278}$$

$$p^2 = m_N^2 \tag{3.279}$$

$$p \cdot k = m_N k^0 \tag{3.280}$$

$$p \cdot q = m_N q^0 \tag{3.281}$$

$$k^2 = q^2 = 0 \tag{3.282}$$

$$k \cdot q = \frac{\lambda^2 - p^2}{2} + p \cdot k + p \cdot q \tag{3.283}$$

together with

$$|\vec{k}| = |k^0| \tag{3.284}$$

$$|\vec{q}| = |q^0| \tag{3.285}$$

$$\cos \angle(q, k) = \frac{-\lambda^2 + p^2 - 2p \cdot k - 2p \cdot q + 2k^0 q^0}{2|\vec{k}||\vec{q}|} . \tag{3.286}$$

x and y are defined by

$$(p - k)^2 = m_N (m_N - 2k^0) \equiv 2m_N x \tag{3.287}$$

$$(p - q)^2 = m_N (m_N - 2q^0) \equiv 2m_N y . \tag{3.288}$$

This results in

$$k^0 = \frac{m_N}{2} - x \tag{3.289}$$

$$q^0 = \frac{m_N}{2} - y \tag{3.290}$$

$$|\vec{k}| = \left| \frac{m_N}{2} - x \right| \tag{3.291}$$

$$|\vec{q}| = \left| \frac{m_N}{2} - y \right| \tag{3.292}$$

$$\cos \sphericalangle(q,k) = \frac{p^2 - \lambda^2 - p \cdot k - p \cdot q + 2k^0 q^0}{2|\vec{k}||\vec{q}|} \tag{3.293}$$

and consequently $\mathcal{J}^{sca}$ becomes

$$\mathcal{J}^{sca}(\tilde{p}) = \frac{g_w |Y|^2 G}{2^3 (2\pi)^4 f_+(u \cdot p)} \int_S \mathrm{d}\cos \sphericalangle(k,u) \mathrm{d}\phi_q^k \mathrm{d}x \mathrm{d}y \frac{\lambda^2 + M^2 - 2Mx - My - 2xy}{xy} \tag{3.294}$$
$$\operatorname{sign}\left(\frac{m_N}{2} - x \right) \operatorname{sign}(-x-y) \operatorname{sign}\left(\frac{m_N}{2} - y \right) (-f_+(u \cdot k))(1 + f_-(u \cdot (k+q-p))) f_-(u \cdot q) \,.$$

Since $\mathcal{J}$ is not calculated out of $\Sigma_N^> - \Sigma_N^<$, the vacuum part cannot be found by a trivial limit $T \to 0$.[57] Hence, the vacuum part should be known by assumption, or the KMS relation should not be used in the beginning. Without the KMS relation, the statistical factor of this diagram is modulo global sign factors: $(1 - f_+(u \cdot k)) f_-(u \cdot (k+q-p))(1 + f_-(u \cdot q)) - (-f_+(u \cdot k))(1 + f_-(u \cdot (k+q-p))) f_-(u \cdot q)$. Hence, the trivial limit $T \to 0$ reduces the integral support to the area

$$\operatorname{supp}_{vac} = x < \frac{m_N}{2} \wedge y < \frac{m_N}{2} \wedge x + y > 0 \,. \tag{3.295}$$

Consequently, the vacuum part of $\mathcal{J}^{sca}$ is Equation (3.294) restricted to $\operatorname{supp}_{vac}$. To cancel the IR divergences within the sum of the scattering and vertex parts at the integrand level, the statistical factor $\operatorname{sign}(u \cdot k)\operatorname{sign}(u \cdot (k+q-p))\operatorname{sign}(u \cdot q)(-f_+(u \cdot k))(1 + f_-(u \cdot (k+q-p))) f_-(u \cdot q)$ has to be replaced by the factor $\operatorname{sign}(E_1)\operatorname{sign}(E_2)(-f_+(E_1)) f_-(E_2)$ from the vacuum vertex corrections. E_1 and E_2 are respectively the $u \cdot k$ and $u \cdot (p-k)$ from the vertex corrections:

$$\mathcal{J}^{sca,vac}(\tilde{p}) = \frac{g_w |Y|^2 G}{2^3 (2\pi)^4 f_+(u \cdot p)} \int_{S \wedge \operatorname{supp}_{vac}} \mathrm{d}\cos \sphericalangle(k,u) \mathrm{d}\phi_q^k \mathrm{d}x \mathrm{d}y \frac{\lambda^2 + M^2 - 2Mx - My - 2xy}{xy}$$
$$(-f_+(E_1)) f_-(E_2) \,. \tag{3.296}$$

Whether this is the "true" vacuum part or not is unimportant. Only the cancellation of the IR divergences has to work. Furthermore, this vacuum part can be evaluated analytically. Afterwards, the thermal part can be obtained by the subtraction:

$$\mathcal{J}^{sca,T \neq 0}(\tilde{p}) = \mathcal{J}^{sca}(\tilde{p}) - \mathcal{J}^{sca,vac}(\tilde{p}) \,. \tag{3.297}$$

---

[57] In this limit, the internal distribution functions restrict the integral phase space to zero while the external $\frac{1}{f_+(u \cdot p)}$ grows to infinity for positive p^0.

The integration domain S is again determined by $\mathrm{gd}(p,k)$ and $\mathrm{gd}(p,k,q)$. The first one evaluates to

$$\mathrm{gd}(p,k) = -\frac{m_N^2}{4}(m_N - 2x)^2 < 0,\qquad(3.298)$$

which is trivially fulfilled. The second one gives

$$S \equiv \left\{ \frac{4\mathrm{gd}(p,k,q)}{m_N^2} = \left(4xy - \lambda^2\right)\left(\lambda^2 + m_N^2 - 2m_N(x+y)\right) > 0 \right\}.\qquad(3.299)$$

If λ is set to zero, the boundary is composed of the problematic lines $x = 0$ and $y = 0$, and $x + y = \frac{m_N}{2}$. Figure 3.30 shows a plot of S with and without a non-zero λ. In vacuum, only region I of Figure 3.30 is allowed.

(a) $\lambda = 0$ (b) $\lambda = 0.4 m_N$
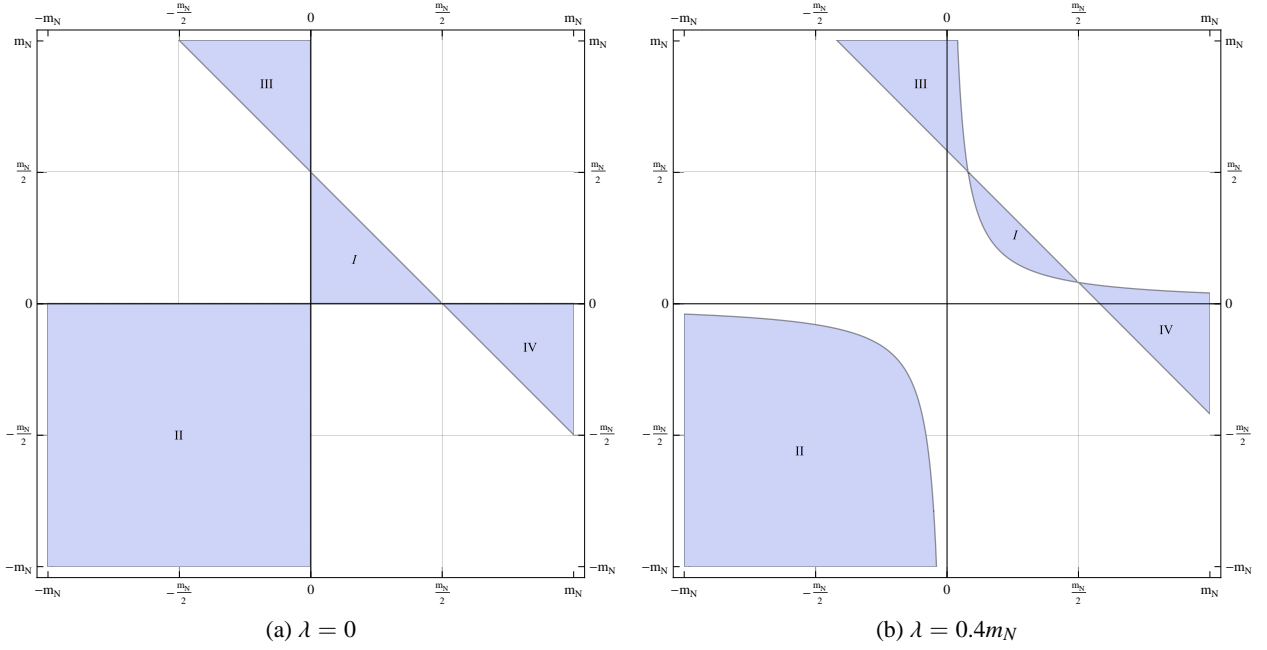
Figure 3.30: This is a plot of integration domain S. Region I is known as the Dalitz plot for $1 \leftrightarrow 3$ scatterings. Hence, this area reflects the process of Figure 3.27a. Likewise, regions II-IV are easily related to the $2 \leftrightarrow 2$ processes of Figures 3.27b and 3.27d, respectively.

3.5.6.5 The IR and UV finite Integrand

In order to add the thermal scattering and vertex corrections to one finite integrand, the symmetrization operator O is introduced. This has the intuitive definition

$$O(r) \int_A \psi \equiv \int_{A_1} \psi + \int_{r[A_2]} r[\psi]\qquad(3.300)$$

for some test integrand ψ and the symmetrization rule r. The integration area $A = A_1 \oplus A_2$ is split according to r into disjunct A_1 and A_2, such that $r[A_2]$ is the integration area of $r[\psi]$. In this way, the IR and UV finite integrand is compactly written:

$$\mathcal{J}^{T\neq 0} = O(\cos \angle(k,u) \to -\cos \angle(k,u)) O(\phi_q^k \to \pi + \phi_q^k) O(x \leftrightarrow y) O(y \to -y) O(x \to -x)$$
$$\left(\mathcal{J}^{vert,1,T\neq 0} + \mathcal{J}^{vert,2,T\neq 0} + \mathcal{J}^{vert,3,T\neq 0} + \mathcal{J}^{sca,T\neq 0} \right).\qquad(3.301)$$

93

Equation (3.301) still carries the λ dependence within the integrand and the integration domain boundaries. Since (3.301) is IR finite, λ can be set to zero within the integrand and the boundaries.[58] However, an IR finite correction term $\mathcal{J}^{T\neq0,corr}$ has to be added to account for the correct limit $\lambda \to 0$:

$$\lim_{\lambda\to0}\mathcal{J}^{T\neq0} = \mathcal{J}^{T\neq0,\lambda=0} + \mathcal{J}^{T\neq0,corr}\,. \tag{3.302}$$

In $\mathcal{J}^{T\neq0,\lambda=0}$ the λ is set to zero even within the boundaries. Therefore, the x-y domains $V_1,\ldots,V_3$ and S after the symmetrization consist only of the lines $x = 0$, $x = y$, $x + y = \frac{m_N}{2}$ and $x - y = \frac{m_N}{2}$.[59] The remaining total x-y area is shown in Figure 3.31. The IR finiteness of $\mathcal{J}^{T\neq0,\lambda=0}$ can be verified by the limit

$$\lim_{y\to0} y\,\mathcal{J}^{T\neq0,\lambda=0}(x,y,\ldots) = 0\,, \tag{3.303}$$

while the UV finiteness is ensured by the exponential suppression of the distribution functions.
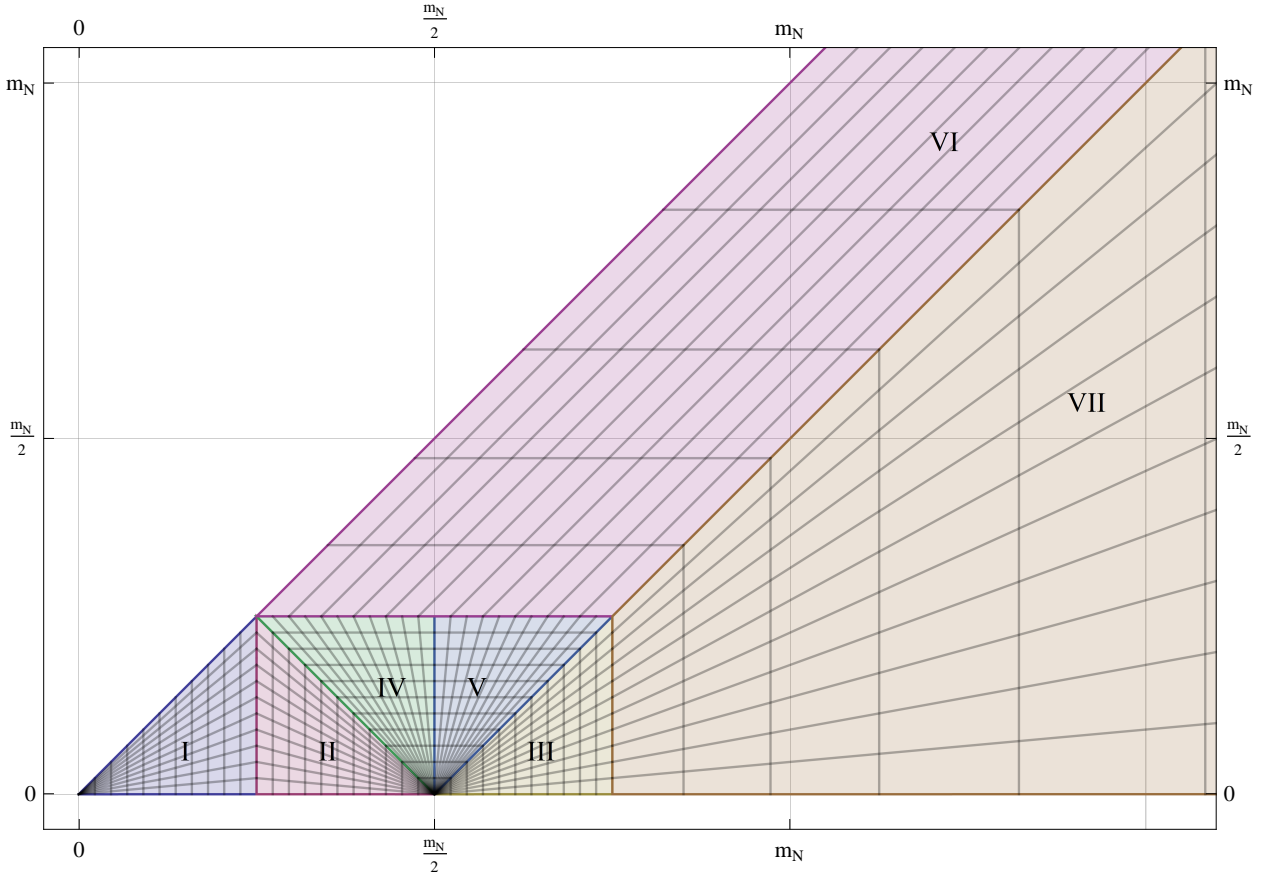
Figure 3.31: This plot shows the $x-y$ integration domain for $\mathcal{J}^{T\neq0,\lambda=0}$ after all symmetrizations are done. Since the integrand is the sum of three different $2\leftrightarrow2$ scatterings and one $1\leftrightarrow3$ process, the corresponding supports shown in Figures 3.28-3.30 generate discontinuities at $x+y=\frac{m_N}{2}$ and $x-y=\frac{m_N}{2}$. The additional splittings are done for numerical convenience. I - VI is phase space suppressed in the ultra-relativistic limit.

To obtain the correction term, the correct limit $\lambda \to 0$ relative to $\lambda = 0$ has to be evaluated. In the limit $\lambda \to 0$, all the λ dependence in (3.301) can be reduced to the boundaries of x and y. All integrand terms are split into pieces proportional to $\frac{1}{y}$ and remainders. Within the $\frac{1}{y}$ terms, a partial integration with respect

---

[58] Since $\mathcal{J}^{T\neq0}$ is IR finite, this would otherwise only give corrections of the order λ and $\lambda\ln\lambda$. Those vanish in the limit $\lambda \to 0$.

[59] Hence, the sector spanned by $0 < x \wedge 0 < y < x$ is chosen.

to y is performed, such that the $\frac{1}{y}$ pole becomes a $\ln(y)$.[60] The boundary term of the partial integration obtains the λ dependence, and the remainder becomes sub-leading in λ. The limit $\lambda \to 0$ can then be performed analytically, and only the dx and the angle integrals are left behind. In the following pages, this procedure is shown in more detail. Here, the notion of the dependence on the remaining variables is dropped for notational simplicity. The functions $\psi_i(y)$ represent the terms of the fully symmetrized integrand of (3.301) multiplied by y, such that they have no pole at $y = 0$. The index i reflects the corresponding integration boundaries given by $y_-^i(\lambda) < y < y_+^i$. The $y_-^i(\lambda)$ are the lower bound of y with the property $\lim_{\lambda \to 0} y_-^i(\lambda) = 0$. This means that only the boundaries i are considered, which reduce to $y = 0$ for $\lambda = 0$. To have well-defined finite integrals in intermediate steps, another function y_- is chosen such that it fulfills $0 < y_- < |y_-^i|$ for all i. Hence, y_- should also vanish smoothly for small λ. In the following, the notion of i for the irrelevant upper bound y_+^i is dropped too, since one aims for only the correction term. Within $\mathcal{J}^{T \neq 0}$, one then has to calculate

$$\mathcal{J}^{T \neq 0} \sim \sum_i \int_{y_-^i(\lambda)}^{y_+} \mathrm{d}y \frac{\psi_i(y)}{y} = \underbrace{\int_{y_-(\lambda)}^{y_+} \mathrm{d}y \sum_i \frac{\psi_i(y)}{y}}_{\sim \mathcal{J}^{T \neq 0, \lambda = 0}} + \underbrace{\sum_i \int_{y_-^i(\lambda)}^{y_-(\lambda)} \mathrm{d}y \frac{\psi_i(y)}{y}}_{\sim \mathcal{J}^{T \neq 0, corr}} . \tag{3.304}$$

Since the $\frac{1}{y}$ poles are poles of hermitian propagators, in the case of negative $y_-^i(\lambda)$, the integral in the correction term should be regarded as a principal value integral. This is

$$\sum_i \int_{y_-^i(\lambda)}^{y_-(\lambda)} \mathrm{d}y \frac{\psi_i(y)}{y} = \sum_i \ln(|y|) \psi_i(y) \Big|_{y_-^i(\lambda)}^{y_-(\lambda)} - \sum_i \underbrace{\int_{y_-^i(\lambda)}^{y_-(\lambda)} \mathrm{d}y \ln(|y|) \, \partial_y \psi_i(y)}_{\propto \lambda \ln(\lambda) \to 0} . \tag{3.305}$$

The remainder is suppressed for small λ, since $\partial_y \psi_i(y)$ is smooth at $y = 0$. In addition, the upper bound of the boundary term in (3.305) has to vanish under the sum in the limit $\lambda \to 0$, since otherwise $\mathcal{J}^{T \neq 0, \lambda = 0}$ would not be IR finite and (3.303) would be untrue. Therefore, one obtains

$$\lim_{\lambda \to 0} \int_{y_-(\lambda)}^{y_+} \mathrm{d}y \sum_i \frac{\psi_i(y)}{y} = \int_0^{y_+} \mathrm{d}y \sum_i \frac{\psi_i(y)}{y} \sim \mathcal{J}^{T \neq 0, \lambda = 0} \tag{3.306}$$

and

$$\lim_{\lambda \to 0} \sum_i \ln(y_-(\lambda)) \psi_i(y_-(\lambda)) = 0 . \tag{3.307}$$

The next step is to perform the limit $\lambda \to 0$ of the sum of the boundary terms of (3.305) analytically, which is finite too. In fact, $\mathcal{J}^{T \neq 0, corr}$ can be written down in short form as

$$\mathcal{J}^{T \neq 0, corr} = - \int_0^1 \mathrm{d}\cos \angle(k, u) \int_0^\pi \mathrm{d}\phi_q^k \int_0^\infty \mathrm{d}x \lim_{\lambda \to 0} \sum_i \ln(|y_-^i(\lambda)|) \psi_i(y_-^i(\lambda)) . \tag{3.308}$$

$\mathcal{J}^{T \neq 0, \lambda = 0}$ and $\mathcal{J}^{T \neq 0, corr}$ can be calculated numerically without the need of a numerical limit procedure. The solutions are presented in Section 3.5.6.7.

---

[60] The $\frac{1}{x}$ pole is phase space suppressed for small y due to the symmetrization in $x \leftrightarrow y$.

3.5.6.6 The Vacuum Part

The thermal part of $\mathcal{J}$ was shown to be IR and UV finite, and it must be calculated numerically. However, the vacuum part can be obtained analytically. Using $E_{1/2} = \frac{1}{2}\left(\tilde{p}^0 \mp |\vec{p}|\cos \angle(k,u)\right)$, the common factor

$$A \equiv -\frac{1}{2f_+(u \cdot p)}\frac{g_w|Y|^2 G}{2^6\pi^4}\int \mathrm{d}\cos\angle(k,u)\mathrm{d}\phi_q^k(-f_+(E_1))f_-(E_2) \tag{3.309}$$

$$= \frac{1}{32\pi^3}\left(1 + \frac{T}{|\vec{p}|}\ln\left(\frac{f_-(\tilde{p}^0 - |\vec{p}|)}{f_-(\tilde{p}^0 + |\vec{p}|)}\right)\right) \tag{3.310}$$

can be extracted. The scattering contribution in Equation (3.296) becomes

$$\mathcal{J}^{sca,vac} = -A\int_{\frac{\lambda^2}{2m_N}}^{\frac{m_N}{2}}\mathrm{d}x\int_{\frac{\lambda^2}{2m_N}}^{\frac{m_N}{2}+\frac{\lambda^2}{2m_N}-x}\mathrm{d}y\,\frac{m_N^2 + \lambda^2 - m_N(2x+y) - 2xy}{xy} \tag{3.311}$$

$$= Am_N^2\left(-\frac{11}{4} + \frac{\pi^2}{6} - 3\ln\left(\frac{\lambda}{m_N}\right) - 2\ln^2\left(\frac{\lambda}{m_N}\right)\right) + O(\lambda). \tag{3.312}$$

Likewise, the vertex contributions from Equations (3.224), (3.247) and (3.270) are calculated. However, those are UV divergent. In order to verify the cancellation of the IR divergent $\ln(\lambda)$, an UV cutoff that is common to all three contributions must be introduced.[61] x and y cannot simply be restricted by some Λ: $|x|, |y| < \Lambda$, since they are differently defined for each term. Nevertheless, q^0 is a common variable and can be restricted:

$$|q^0| < \Lambda. \tag{3.313}$$

Then, the corresponding UV bound for x and y can be obtained. This leads to

$$\mathcal{J}^{vert,1,vac} = Am_N^2\left(-\frac{3}{2} + \ln(2)^2 - \ln\left(\frac{2\lambda}{m_N}\right) + 2\ln^2\left(\frac{\lambda}{m_N}\right) - \ln\left(\frac{\lambda}{m_N}\right) + 4\ln\left(\frac{2\Lambda}{m_N}\right)\right.$$
$$\left. - (1 - \ln(4))\ln\left(\frac{\Lambda}{m_N}\right) + \ln^2\left(\frac{\Lambda}{m_N}\right)\right) + O(\lambda) \tag{3.314}$$

$$\mathcal{J}^{vert,2,vac} = Am_N^2\left(-\frac{\pi^2}{12} - \frac{1}{2}\ln^2(2) - \ln(2)\ln\left(\frac{\Lambda}{m_N}\right) - \frac{1}{2}\ln^2\left(\frac{\Lambda}{m_N}\right)\right.$$
$$\left. + \left(1 + 2\ln\left(\frac{\lambda}{m_N}\right)\right)\ln\left(\frac{2\Lambda}{m_N}\right)\right) + O(\lambda), \tag{3.315}$$

and

$$\mathcal{J}^{vert,3,vac} = Am_N^2\left(2 - \frac{\pi^2}{12} - \frac{1}{2}\ln^2(2) - \ln(2)\ln\left(\frac{\Lambda}{m_N}\right) - \frac{1}{2}\ln^2\left(\frac{\Lambda}{m_N}\right)\right.$$
$$\left. + 2\ln\left(\frac{\lambda}{m_N}\right)\left(2 + \ln\left(\frac{2\Lambda}{m_N}\right)\right) - \ln\left(\frac{2\Lambda}{m_N}\right)\right) + O(\lambda). \tag{3.316}$$

The sum of them gives in total

$$\mathcal{J}^{vac} = -Am_N^2\left(\frac{9}{4} + \ln\left(\frac{2\Lambda}{m_N}\right)\right), \tag{3.317}$$

which is IR finite. This means that λ can be set to zero in the vacuum expressions too. The remaining UV divergent $\ln\Lambda$ can be absorbed into the vertex counter term of the Yukawa coupling Y by some particular renormalization scheme.

---

[61] Any UV cutoff in x and y regulates the integrals. However, λ then has to be absorbed into those cutoffs during renormalization. One would have to cancel IR with UV divergences.

3.5.6.7 Numerical Solution

The following section presents the numerical results of $\mathcal{J}$. Figure 3.32 shows the total rate obtained via the several contributions of $\mathcal{J}$.
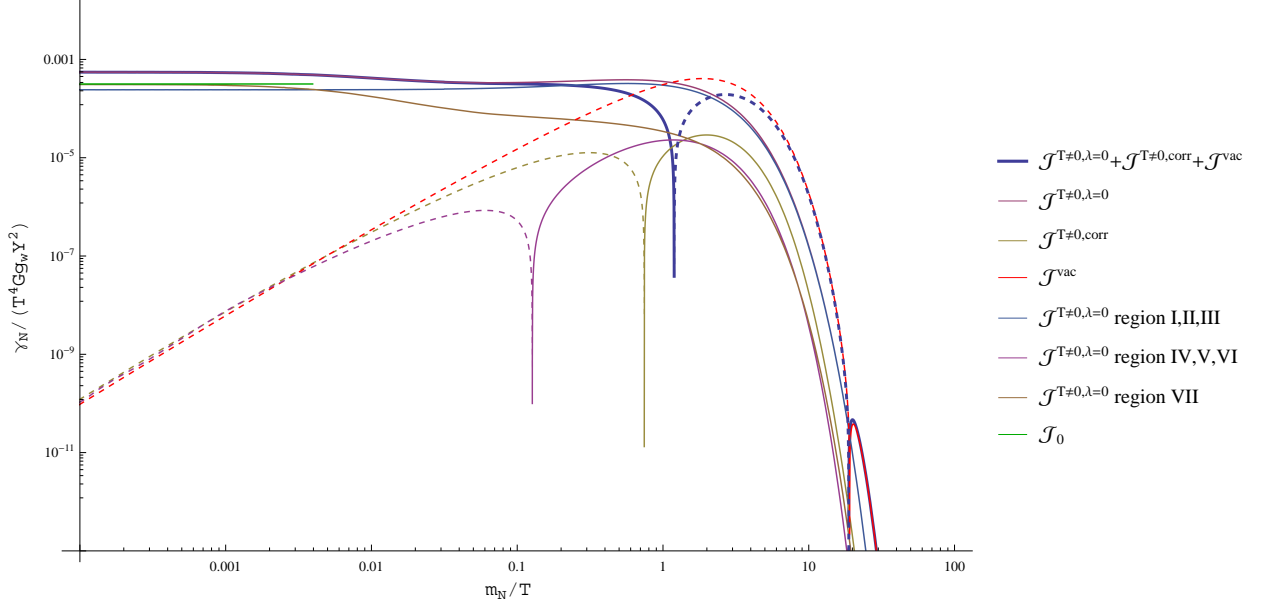

Figure 3.32: This figure shows $\gamma_N[\mathcal{J}](m_N)$ for various contributions of $\mathcal{J}$. Solid and dashed lines respectively correspond to positive and negative values. The corresponding integration regions can be found in Figure 3.31. For $\mathcal{J}^{vac}$, the UV regulator equals $\Lambda = T$.

One question discussed in the literature is, whether the vertex diagram with tree-level functions is divergent for small RHN masses compared to the temperature or not. Such a divergence would indicate the need of full propagators as suggested by the 2PI formalism. Regarding the numerical results from Figure 3.32, no evidence for a divergent behavior is found for small RHN masses. Hence, one can expect that the use of resummed propagators would only give higher order corrections. Nevertheless, the vertex diagram is a 2-loop diagram resulting from a 3-loop vacuum bubble. For a 3-loop complete theory, the 3PI formalism that introduces full vertices is needed. In 2PI, such full vertices are resembled in form of vertex resummations. A particular vertex resummation is the ladder resummation, which in the present case sums up the contributions of an arbitrary number of gauge boson exchanges between the lepton and the Higgs.

$$(3.318)$$

Figure 3.33: The vertex function indicated by the blob represents an infinite amount of gauge boson insertions. Since crossed type insertions are typically suppressed, the resummation can be reduced to the ladder resummation.

Those exchanges may become important at gauge boson momenta of the order $\sqrt{G}T$, such that all ladder diagrams could contribute equally to the neutrino rate. Here, the size of the ladder resummation effect cannot be answered. However, the cancellation of infrared divergences is also shown numerically in the ultra-relativistic limit up to $\frac{m_N}{T} = 10^{-4}$. Since there are no other scales than m_N and T relevant for $\gamma_N[\mathcal{J}]$, a

significant change for smaller values of $\frac{m_N}{T}$ is not expected.

Nevertheless, the result for $\gamma_0[\mathcal{J}_0]$ from Equation 3.54 for a massless neutrino is not obtained in the ultra-relativistic limit. The reason is comparable to the issues found in Equation (3.118) for the ultra-relativistic limit of the $\mathcal{B}$ term. It appears that the limit $m_N \to 0$ does not equal $m_N = 0$. The poles of the integrand of $\mathcal{J}$ within region I, II and III are enhanced by the interference with the Bose-Einstein distributions of the Higgs and gauge bosons. The enhancement appears mainly for the $1 \leftrightarrow 3$ processes but also part of the $2 \leftrightarrow 2$ processes phase space close to the mass divergences at $(x,y) = (0,0)$, $(0,\frac{m_N}{2})$ and $(\frac{m_N}{2},0)$. Therefore, the differential production rate of nearly massless neutrinos appears to have additional sizable contributions compared to the $2 \leftrightarrow 2$ scatterings of perfectly massless neutrinos. The numerical values are:

$$\gamma_N^{vertex}[\mathcal{J}^{T\neq 0, \lambda=0, \text{VII}}](m_N = 10^{-4}T) \approx 3.06(4 \pm 4) \cdot 10^{-4} T^4 g_w G |Y^2| \tag{3.319}$$

$$\gamma_N^{vertex}[\mathcal{J}^{T\neq 0, \lambda=0, \text{I-III}}](m_N = 10^{-4}T) \approx 2.39(6 \pm 3) \cdot 10^{-4} T^4 g_w G |Y^2|. \tag{3.320}$$

Hence, only the limit value obtained from region VII fits to the massless result from Section 3.4.2. However, even if phase space suppressed, the rates from the regions I-III still are as large as the one from region VII. Since $\mathcal{J}^{vac}$ and $\mathcal{J}^{T\neq 0, corr}$ vanish for $m_N \to 0$, the total contribution to the rate obtained from the vertex diagram in the ultra-relativistic limit is

$$\gamma_N^{vertex}[\mathcal{J}](m_N = 10^{-4}T) \approx 5.46(2 \pm 6) \cdot 10^{-4} T^4 g_w G |Y^2|. \tag{3.321}$$

While for the wave-function type contribution $\mathcal{B}$ the disagreement of the $m_N = 0$ and $m_N \to 0$ case may or may not be related to the breakdown of perturbation theory, the vertex type contribution is finite even in the massless limit. Since the RHN mass is not protected by symmetries of the Lagrangian, the massless calculation itself has to fit the massless limit. In this regard, the disagreement only means that the RHN mass must not be set to zero under the integral, i.e. integration and limit is not exchangeable.

3.5.7 Non-Relativistic Limit

In the following, $\mathcal{B}^{O(G,h_t^2,\lambda_\phi)}$, $\mathcal{F}^{O(G)}$ and $\mathcal{J}^{T\neq0}$ is verified in the non-relativistic limit $m_N \gg T$. Using the redefinitions $z = \frac{\pi T}{m_N}$ and $s = \frac{|\vec{p}|}{m_N}$, the $\mathcal{B}^{O(G,h_t^2,\lambda_\phi)}$ terms are expanded up to the order $m_N^2 O\left(z^6, s^4, e^{-\frac{m_N}{2T}}\right)$, while $\mathcal{F}^{O(G)}$ and $\mathcal{J}^{T\neq0}$ are expanded up to the order $m_N^2 O\left(z^6, s^2, e^{-\frac{m_N}{2T}}\right)$ for simplicity.[62] The recurring factor A is defined as $A = \frac{g_w|Y|^2 m_N^2}{\pi^3}$.

3.5.7.1 Expansion Coefficients of $\mathcal{B}^{O(G,h_t^2,\lambda_\phi)}$

The series expansion of $\mathcal{B}^{O(G,h_t^2,\lambda_\phi)}$ for each contribution separately is

$$\mathcal{B}^{vac,\Lambda,vac} = A\frac{1}{64}\ln\left(\frac{\Lambda^2}{Tm_N}\right)\left(G - \frac{3}{2}\ln(2)h_t^2\right) \tag{3.322}$$

$$\mathcal{B}^{vac,+,vac} = A\frac{1}{27}\left(3 + 2\ln\left(\frac{T}{m_N}\right)\right)\left(G + \frac{3}{2}h_t^2\right) \tag{3.323}$$

$$\mathcal{B}^{vac,-,vac} = 0 \tag{3.324}$$

$$\mathcal{B}^{vac,\Lambda,T\neq0} = 0 \tag{3.325}$$

$$\mathcal{B}^{vac,+,T\neq0} = Az^3\left(\frac{3}{16}\zeta(3) + \frac{7}{480}z + \frac{45}{4}\zeta(5)z^2\right)\left(G + \frac{3}{2}h_t^2\right) \tag{3.326}$$

$$\mathcal{B}^{vac,-,T\neq0} = Az^3\left(-\frac{3}{16}\zeta(3) + \frac{7}{480}z - \frac{45}{4}\zeta(5)z^2\right)\left(G + \frac{3}{2}h_t^2\right) \tag{3.327}$$

$$\mathcal{B}^{sca,T\neq0} = A\left(\frac{1}{24}z^2 G + \frac{1}{96}z^2 h_t^2\right) \tag{3.328}$$

$$\mathcal{B}^{wv,T\neq0,1} = -A\frac{1}{16}z^2\left(G + h_t^2 + \lambda_\phi\right) \tag{3.329}$$

$$\mathcal{B}^{wv,T\neq0,2} = Az^2\left(\left(\frac{1}{24} + \frac{1}{45}z^2\right)G + \left(\frac{1}{32} + \frac{7}{240}z^2\right)h_t^2\right). \tag{3.330}$$

ζ is the Riemann zeta function. Altogether, the following series coefficients are obtained for $\mathcal{B}^{O(G,h_t^2,\lambda_\phi)}$ in the non-relativistic limit:

$$\mathcal{B}^{O(G,h_t^2,\lambda_\phi),NR} = \frac{g_w|Y|^2 m_N^2}{\pi^3}\left(G\left(\frac{3}{128} + \frac{1}{32}\ln\left(\frac{\Lambda}{m_N}\right) + \frac{1}{48}z^2 + \frac{37}{720}z^4\right)\right.$$
$$+ h_t^2\left(\frac{9}{256} - \frac{1}{48}z^2 + \frac{7}{96}z^4 + \frac{3}{128}\left((-1 + \ln(2))\ln\left(\frac{m_N}{T}\right) - 2\ln(2)\ln\left(\frac{\Lambda}{T}\right)\right)\right)$$
$$\left. - \lambda_\phi\frac{1}{16}z^2\right) + m_N^2 O(z^6, s^4, e^{-\frac{m_N}{2T}}). \tag{3.331}$$

The thermal expansion coefficients, i.e. $\frac{1}{48}z^2 + \frac{37}{720}z^4$ proportional to G and $-\frac{1}{48}z^2 + \frac{7}{96}z^4$ in case of h_t^2, are equal to those obtained from [58]. Regarding the numerical result of Figure 3.15, those coefficients may be verified by a fit. The best fit value for the sum of all thermal contributions, i.e. Equations (3.325)-(3.330), compared to the numerical data within $m_N = (10^{1.5}\ldots10^2)T$ at $|\vec{p}| = 10^{-3}T$ is

$$\approx AG\left(1.00 \times \frac{1}{48\pi}z^2 + 1.06 \times \frac{37}{720}z^4\right). \tag{3.332}$$

---

[62] Factors of $e^{-\frac{m_N}{T}}$ are encountered during integration. Those spoil a pure series expansion in $\frac{m_N}{T}$. Nevertheless, expanding in powers of $e^{-\frac{m_N}{T}}$ at ∞ is possible. In this sense, the upper expansion bound $O\left(e^{-\frac{m_N}{2T}}\right)$ reflects that such exponential suppressed terms are neglected completely. Afterwards, the remainder is a pure series expansion into $\frac{m_N}{T}$.

The vacuum terms given by Equations (3.322) - (3.324) are logarithmic enhanced, which is why they are excluded from the fit (3.332). These give approximately

$$\approx AG\left(0.998 \times \frac{3}{128} + 1.000 \times \frac{1}{32}\ln\left(\frac{T}{m_N}\right)\right) \tag{3.333}$$

when fitted to the same range with $\Lambda = 1T$.

3.5.7.2 Expansion Coefficients of $\mathcal{F}^{O(G)}$

The non-relativistic series expansion of $\mathcal{F}^{O(G)}$ can be obtained from the following expressions. For simplicity, several contributions are added in the usual fashion:

$$\mathcal{F}^{vac,col,vac} = AG\left(-\frac{1}{128} + \frac{1}{64}\ln\left(\frac{m_N}{T}\right)\right) \tag{3.334}$$

$$\mathcal{F}^{vac,col,T\neq 0} = AG\left(\frac{1}{96}z^2 + \frac{1}{60}z^4\right) \tag{3.335}$$

$$\mathcal{F}^{vac,fin,vac} = AG\left(\frac{1}{256} - \frac{1}{64}\ln\left(\frac{\Lambda}{T}\right)\right) \tag{3.336}$$

$$\mathcal{F}^{vac,fin,T\neq 0} = AG\frac{1}{96}z^2 \tag{3.337}$$

$$\mathcal{F}^{HTL,col,vac} = AG\left(-\frac{1}{32}z^2\ln\left(\frac{m_N}{T}\right) + \frac{1}{48}z^2\right) \tag{3.338}$$

$$\mathcal{F}^{HTL,col,T\neq 0} = AG\left(+\frac{1}{32}z^2\ln\left(\frac{m_N}{T}\right) - \frac{1}{48}z^2 - \frac{1}{48}z^4\right) \tag{3.339}$$

$$\mathcal{F}^{HTL,fin,vac} = 0 \tag{3.340}$$

$$\mathcal{F}^{HTL,fin,T\neq 0} = 0 \tag{3.341}$$

$$\mathcal{F}^{\overline{T\neq 0}} = -AG\frac{1}{1440}z^4 \,. \tag{3.342}$$

Altogether, the non-relativistic limit of $\mathcal{F}^{O(G)}$ is

$$\mathcal{F}^{O(G)NR} = \frac{g_w|Y|^2 m_N^2}{\pi^3}G\left(-\frac{1}{256} - \frac{1}{64}\ln\left(\frac{\Lambda}{m_N}\right) + \frac{1}{48}z^2 - \frac{7}{1440}z^4\right) + m_N^2 O(z^5, s^2, e^{-\frac{m_N}{2T}})\,. \tag{3.343}$$

The thermal coefficients $\frac{1}{48}z^2 - \frac{7}{1440}z^4$ may be compared to [58] and by a fit within $M = (10^{1.7}\ldots 10^2)T$ at $|\vec{p}| = 10^{-3}T$ and $\Lambda = 1T$. Due to large cancellations, the best fit is stable only if applied to each contribution

separately:

$$\mathcal{F}^{vac,col,vac} \approx AG\left(-\frac{1}{128}\times 1.128 + \frac{1}{64}\ln\left(\frac{m_N}{T}\right)\times 1.015\right) \tag{3.344}$$

$$\mathcal{F}^{vac,col,T\neq 0} \approx AG\left(\frac{1}{96}z^2\times 1.000 + \frac{1}{60}z^4\times 1.038\right) \tag{3.345}$$

$$\mathcal{F}^{vac,fin,vac} \approx AG\frac{1}{256}\times 1.000 \tag{3.346}$$

$$\mathcal{F}^{vac,fin,T\neq 0} \approx AG\frac{1}{96}z^2\times 1.000 \tag{3.347}$$

$$\mathcal{F}^{HTL,col,vac} \approx AG\left(-\frac{1}{32}z^2\ln\left(\frac{m_N}{T}\right)\times 1.000 + \frac{1}{48}z^2\times 1.040\right) \tag{3.348}$$

$$\mathcal{F}^{HTL,col,T\neq 0} \approx AG\left(+\frac{1}{32}z^2\ln\left(\frac{m_N}{T}\right)\times 1.003 - \frac{1}{48}z^2\times 1.061 - \frac{1}{48}z^4\times 0.937\right) \tag{3.349}$$

$$\mathcal{F}^{HTL,fin,vac} \approx 0.000 \tag{3.350}$$

$$\mathcal{F}^{HTL,fin,T\neq 0} \approx 0.000 \tag{3.351}$$

$$\mathcal{F}^{\overline{T\neq 0}} \approx -AG\frac{1}{1440}z^4\times 1.056\,. \tag{3.352}$$

This verifies the numerics in the non-relativistic limit.

3.5.7.3 Expansion Coefficients of $\mathcal{J}$

The non-relativistic expansion of the vertex corrections involve the cancellation of IR divergences. Therefore, these contributions need to be summed up. In total, the expansions

$$\mathcal{J}^{T\neq 0,NR} = \frac{g_w|Y|^2 m_N^2}{\pi^3}G\left(\frac{1}{24}z^2 + \frac{19}{360}z^4\right) + m_N^2 O(z^6, s^2, e^{-\frac{m_N}{2T}}) \tag{3.353}$$

$$\mathcal{J}^{vac,NR} = -\frac{g_w|Y|^2 m_N^2}{\pi^3}G\frac{1}{32}\left(\frac{9}{4} + \ln\left(\frac{2\Lambda}{m_N}\right)\right) + m_N^2 O(s^2, e^{-\frac{m_N}{2T}}) \tag{3.354}$$

can be obtained. The thermal coefficients agree with those obtained in [58]. By using the numerical data from Section 3.5.6.7 within $M = (10^{1.5}\ldots 10^2)T$ at $|\vec{p}| = 10^{-3}T$, the fit coefficients are

$$\mathcal{J}^{T\neq 0,NR} \approx \frac{g_w|Y|^2 m_N^2}{\pi^3}G\left(0.998\times\frac{1}{24}z^2 + 1.01\times\frac{19}{360}z^4\right)\,. \tag{3.355}$$

To obtain the correct fit of the second coefficient, $\mathcal{J}^{T\neq 0}$ is evaluated with a relative error of 10^{-5}.

4

Numerics

Within this chapter, details on the numerical treatment of the integrals is provided.[63] Since a huge parameter range spanning over certain physically distinct processes is incorporated, several considerations are required. These are described in the following sections.

However, the remaining unsolved integrals used for the Higgs and lepton self-energies have to be evaluated first.

4.1 Notes on $I_{2\pm}$ and $\bar{I}_3^{T \neq 0}$

The integrals $I_{2\pm}$ and $\bar{I}_3^{T \neq 0}$ are obtained during the derivation of the lepton and Higgs self-energies. They are used particularly within the resummed propagators and hence are evaluated several times during integration of the $\mathcal{B}$ and $\mathcal{F}$ terms. In order to save CPU time, $I_{2\pm}$ and $\bar{I}_3^{T \neq 0}$ are precisely solved and saved for later usage.

$I_{2\pm}$ is defined in (2.80). It depends on the two parameters p^0 and $|\vec{p}|$ and can be written as a function of $p_+ \equiv p^0 + |\vec{p}|$ and $p_- \equiv p^0 - |\vec{p}|$.

$$I_{2\pm}(p^0, |\vec{p}|) = T \int_0^\infty \mathrm{d}x \frac{1}{e^x \pm 1} \ln \left| \frac{(2x + \beta p_+)(2x - \beta p_-)}{(2x - \beta p_+)(2x + \beta p_-)} \right| \tag{4.1}$$

The advantage of this reparametrization is that the two-dimensional $I_{2\pm}(p^0, |\vec{p}|)$ can be written in terms of a one-dimensional function a:

$$I_{2\pm}(p^0, |\vec{p}|) = T(a_\pm(\beta p_+) - a_\pm(\beta p_-)). \tag{4.2}$$

Furthermore, the symmetry $a(-y) = -a(y)$ allows the restriction to positive arguments $y \geq 0$:

$$a_\pm(y) = \int_0^\infty \mathrm{d}x \frac{1}{e^x \pm 1} \ln \left| \frac{2x + y}{2x - y} \right| \qquad , \qquad a_\pm(0) = 0. \tag{4.3}$$

---

[63] All numerical integrals are done by Mathematica's *NIntegrate* command, with routines lasting from seconds up to roughly 10 minutes per integral value on a typical desktop computer with the aforementioned precision. However, for those timings *NIntegrate* should not output error messages. This can be achieved by the following methods, and otherwise by raising the number of digits, i.e. Mathematica's *WorkingPrecision*, to avoid numerical noise from large cancellations. In special cases, the routines have to be optimized such that the integrands' evaluation time is less than $\sim 0.01 s$. Nevertheless, due to the parameter scans' sheer number of integrals, parallelization on a computer cluster is suggested.

In the end, however, the numerically better behaved function b may be utilized:

$$b_\pm(y) = \int_0^\infty dx \frac{1}{e^{x\frac{y}{2}} \pm 1} \ln\left|\frac{x+1}{x-1}\right| \qquad , \qquad a_\pm(y) = \frac{y}{2} b_\pm(y). \qquad (4.4)$$

$b_\pm(y)$ is evaluated within a relative error of 10^{-10} in the range $-13.8149 \le \ln(y) \le 13.8151$ at 9839 points on a logarithmic scale. These values are interpolated and saved for later usage. For larger and smaller values of y, the asymptotic formulas

$$b_-(y \ge) \approx \frac{2\pi^2}{3y} \quad , \quad b_-(y \le) \approx \frac{\pi^2}{2} \quad , \quad b_+(y \ge) \approx \frac{\pi^2}{3y} \quad , \quad b_+(y \le) \approx 0 \qquad (4.5)$$

can be used.

The same approach applies to $\bar{I}_3^{T\neq0}$, which is needed for the lepton self-energy. It is defined in (2.93) and can be expressed using the auxiliary function c:

$$\bar{I}_3^{T\neq0}(p^0, |\vec{p}|) = T^2 \int_0^\infty dx \left(\frac{1}{e^x+1} + \frac{1}{e^x-1}\right) x \ln\left|\frac{\beta^2 p_-^2 - 4x^2}{\beta^2 p_+^2 - 4x^2}\right| = T^2 (c(\beta p_-) - c(\beta p_+)). \qquad (4.6)$$

$c(y)$ reads

$$c(y) = \int_0^\infty dx \left(\frac{1}{e^x+1} + \frac{1}{e^x-1}\right) x \ln\left|\frac{y^2 - 4x^2}{4x^2}\right|, \qquad (4.7)$$

and is evaluated in the range $-26.47 \le \ln(y) \le 13.8151$ at 14345 points on a logarithmic scale within a relative error of 10^{-10}. Again, those values are interpolated and saved. For a larger y, the expansion

$$c(y \ge) \approx \frac{\pi^2}{2} \ln(y) - \frac{\pi^2}{6} (3 + 7\ln(2) - 36\ln(A) + 3\ln(\pi)) \qquad (4.8)$$

can be used, while for smaller arguments c is quadratically suppressed and the numerical approximation

$$c(y \le) \approx \tilde{c} y^2 \qquad , \qquad \tilde{c} = \lim_{y \to 0} \frac{c(y)}{y^2} \approx \frac{c(e^{-26.47})}{e^{-2 \times 26.47}} \approx 0.17328679514 \qquad (4.9)$$

is sufficient. A is Glaisher's constant with the value $\ln(A) = \frac{1}{12} - \zeta'(-1)$.
The $4x^2$ in the numerator of (4.7) is important for a small y, since otherwise the numerical precision is spoiled due to a large cancellation in the difference $c(p_+) - c(p_-)$.
In this way, the final integrands for $\mathcal{B}$ and $\mathcal{F}$ evaluate at least 100 times faster.

4.2 IMT Transformation

Whenever one integrates over a pole of the type $x^{-\beta}$ with $\beta < 1$ numerically, Mathematica offers the possibility of applying several so called "singularity handlers". One of them is the IMT transformation, which appears to be useful in many cases in this study. In the case of a singular point at $x = 0$ and the integration region $0 < x \le 1$, the IMT transformation is defined via the substitution rule $x \to \phi(t, \omega)$, $0 < t < 1$, $\omega > 0$, with

$$\phi(t, p) = e^{1-t^{-\omega}}. \qquad (4.10)$$

ω is a parameter that is chosen appropriately to the width of the integrated pole. In the above example $x^{-\beta}$, ϕ removes the singular point and the new integrand goes to zero for $t \to 0$. The pole is replaced by a smooth function with a maximum at a certain point. ω is chosen such that this maximum is placed approximately at $t = 0.2$, but ω is at least in the range $0.1 < \omega < 1.6$ for numerical stability.

4.3 PV Transformation

Several perturbative contributions involve 1-dimensional Cauchy principal value (PV) integrations in n dimensions.[64] These may be evaluated along some suitable complex contours. However, this investigation aims to stay on the real axis and to use the direct evaluation rule. Principal values are evaluated in a symmetric fashion like

$$\fint_{-a}^{b} \frac{f(x)}{x} dx = \lim_{\varepsilon \to 0^+} \left(\int_{-a}^{-\varepsilon} + \int_{\varepsilon}^{b} \right) \frac{f(x)}{x} dx \tag{4.11}$$

for some positive reals a, b, and a real valued function f that is smooth in $[a, b]$. If Equation (4.11) is extended by $n - 1$ integrations, the whole expression becomes a n-dimensional integral with a singular hypersurface of dimension $n - 1$. Furthermore, this hypersurface may be curved by any smooth coordinate transformations.

In conclusion, a n-dimensional integral with a 1-dimensional Cauchy principal value can be evaluated via

$$\fint_{V} \frac{f(x)}{g(x)} d^n x = \lim_{\varepsilon \to 0^+} \int_{V_\varepsilon} \frac{f(x)}{g(x)} d^n x. \tag{4.12}$$

V is the real integration domain containing the smooth pole hypersurface $\Gamma = \{x | g(x) = 0\}$. The V_ε equals V minus a neighborhood of Γ with orthogonal size ε: $V_\varepsilon = V / B_\varepsilon(\Gamma)$. $B_\varepsilon(\Gamma)$ is the n-dimensional ε ball located at all points of Γ.

The numerical limit in Equation (4.12) can be circumvented by the following two possibilities:

(i) Find a coordinate transformation, such that Γ is plane. Fold along Γ symmetrically to obtain one or more separate finite integrals over a smooth function.
For example, Equation (4.11) with $0 < a < b$ can be split into

$$\left(\fint_{-a}^{a} + \int_{a}^{b} \right) \frac{f(x)}{x} dx = \int_{0}^{a} \frac{f(x) - f(-x)}{x} dx + \int_{a}^{b} \frac{f(x)}{x} dx. \tag{4.13}$$

The first integral on the right-hand side has no remaining pole, since $f(x) - f(-x)$ is of order $O(x)$ at $x = 0$.

(ii) Find a complete and disjunct splitting of V into sub-regions V_i, and a corresponding smooth map from each V_i to $[0, 1]^n$, such that the limit $\varepsilon \to 0^+$ in (4.12) is trivial. Sum each integrand i respective to V_i such that the PV pole cancels under the integral.

If there is only one PV pole in the integration area, and if Γ is plane, option (i) is clearly the better choice. However, as one may have to deal with multiple poles crossing each other, option (ii) should be mentioned. It is always possible to construct a bijective map $\Phi_\varepsilon : [0, 1] \to [\varepsilon, b]$ and $\Psi_\varepsilon : [0, 1] \to [-a, -\varepsilon]$, such that $\Phi_\varepsilon(0) = -\Psi_\varepsilon(0) = \varepsilon$, $\Phi_\varepsilon(1) = b$ and $\Psi_\varepsilon(1) = -a$. Equation (4.11) is then equal to

$$\fint_{-a}^{b} \frac{f(x)}{x} dx = \lim_{\varepsilon \to 0} \int_{0}^{1} \left(\frac{f(\Phi_\varepsilon(\tau))}{\Phi_\varepsilon(\tau)} \Phi'_\varepsilon(\tau) - \frac{f(\Psi_\varepsilon(\tau))}{\Psi_\varepsilon(\tau)} \Psi'_\varepsilon(\tau) \right) d\tau. \tag{4.14}$$

$'$ is the short notation for ∂_τ. The right-hand side integrand can be evaluated at $\tau = \varepsilon$. The series expansion at $\varepsilon = 0$ then results in

$$\frac{f(0)(\Phi'_0(0) + \Psi'_0(0))}{\varepsilon(1 - \Psi'_0(0))(1 + \Phi'_0(0))} + O(\varepsilon^0). \tag{4.15}$$

---

[64] A 1d PV in n dimensions is meant to be a 1d principal value integral which can be found by a suitable coordinate choice. After integrating in this direction, the remaining $n - 1$ dimensions are free of PV singularities and integrable at least close to the pole.

This pole in ε shows that limit and integration can only be exchanged in (4.14) if the connection condition $\Phi_0'(0) = -\Psi_0'(0)$ holds. In the case of a n-dimensional integral, for a PV pole of degree m, this condition reads

$$\partial_{n_1}^i \Phi(x) = \partial_{n_2}^i \Psi(x)\,,\ \forall x \in \Gamma\,,\ i = 1 \ldots m\,, \tag{4.16}$$

with n_1 and n_2 being the outward oriented normal vectors of the two domains that are separated by Γ. All poles in ε then vanish, and ε may be set to zero from the beginning. Hence, the subscript ε is dropped from Φ and Ψ in (4.16). The case $m > 1$ can be checked the same way.[65] However, additional conditions on the numerator f and the integration domain V appear for $m > 1$. Nevertheless, if f and V are such that the integral does exist, the corresponding number of normal derivatives of Ψ and Φ at Γ have to be equal.

4.3.1 Example

In the following equation, a non-trivial and analytically solvable example is considered:

$$\oint_V \frac{1}{x - \frac{1}{2}y^2}\, dx\, dy = \sqrt{2}\ln\!\big(3 + 2\sqrt{2}\big) + \sqrt{5}\ln\!\Big(\frac{5}{2}\big(7 - 3\sqrt{5}\big)\Big) + \ln\!\big(6 - 2\sqrt{5}\big)\,, \tag{4.17}$$

with $V = \{x, y\,|\,0 \le x \le \text{Min}(1, 2 - y) \wedge 0 \le y \le -1 + \sqrt{5}\}$ being the area plotted in Figure 4.1. There are two numerically problematic points, where procedure (i) is not applicable in a straightforward way without numerical limits. The point $(0, 0)$ is problematic, since Γ is adapting the boundary of V. At the other point $(3 - \sqrt{5}, \sqrt{5} - 1)$, Γ is hitting a corner. In order to apply method (ii), the following maps are constructed. They span $V = V_1 \oplus V_2$ in terms of functions that interpolate linearly between the boundaries, such that the PV pole at Γ is placed at the line $t_1 = 0$:

$$r_1 : [0,1]^2 \to V_1, (t_1, t_2) \mapsto \Big(\big(\sqrt{5} - 3\big)(t_1 - 1)\, t_2^2,\big(\sqrt{5} - 1\big) t_2\Big) \tag{4.18}$$

$$r_2 : [0,1]^2 \to V_2, (t_1, t_2) \mapsto \Big(\big(3 - \sqrt{5}\big) t_2^2 + t_1\big(\big(\sqrt{5} - 3\big) t_2^2 + 1\big)\,,$$

$$\big(\big(2 - \sqrt{5}\big) t_1 + \sqrt{5} - 1\big) t_2\Big)\,. \tag{4.19}$$

The functions Φ and Ψ are defined as

$$\Phi(r, s) = r_1(r, s) \tag{4.20}$$
$$\Psi(r, s) = r_2(r(1 + c(s)(r - 1)), s)\,. \tag{4.21}$$

$c(s)$ can be solved such that the condition (4.16) is fulfilled for all $s \in [0, 1]$.[66] In this way, the bijective maps

$$\Phi : [0,1]^2 \to V_1,(r, s) \mapsto \Big(\big(\sqrt{5} - 3\big)(r - 1)\, s^2,\big(\sqrt{5} - 1\big) s\Big) \tag{4.22}$$

$$\Psi : [0,1]^2 \to V_2,(r, s) \mapsto \Big(-\big(\sqrt{5} - 3\big) s^2 +$$

$$\frac{r\big(1 + \big(\sqrt{5} - 3\big) s^2\big)\big(4\big(\sqrt{5} - 2\big) s^2 + r\big(\sqrt{5} - 1 + 2\big(\sqrt{5} - 3\big) s^2\big)\big)}{\sqrt{5} - 1 + 2\big(3\sqrt{5} - 7\big) s^2}\,,$$

$$\frac{s\big(\big(6 - 2\sqrt{5} - 7r^2 + 3\sqrt{5}r^2 + 2\big(22 - 10\sqrt{5} + r\big(-18 + 8\sqrt{5} + \big(5\sqrt{5} - 11\big) r\big)\big) s^2\big)}{\sqrt{5} - 1 + 2\big(3\sqrt{5} - 7\big) s^2}\Big)$$

---

[65] Even though a principal value integral is typically not considered for an integral of a pole of degree 2 or higher, this can be integrated in the symmetric principal value scheme.

[66] The r-polynomial in Ψ is not mandatory. However, it appears to be the most flexible substitution by which this method can be implemented into Mathematica.
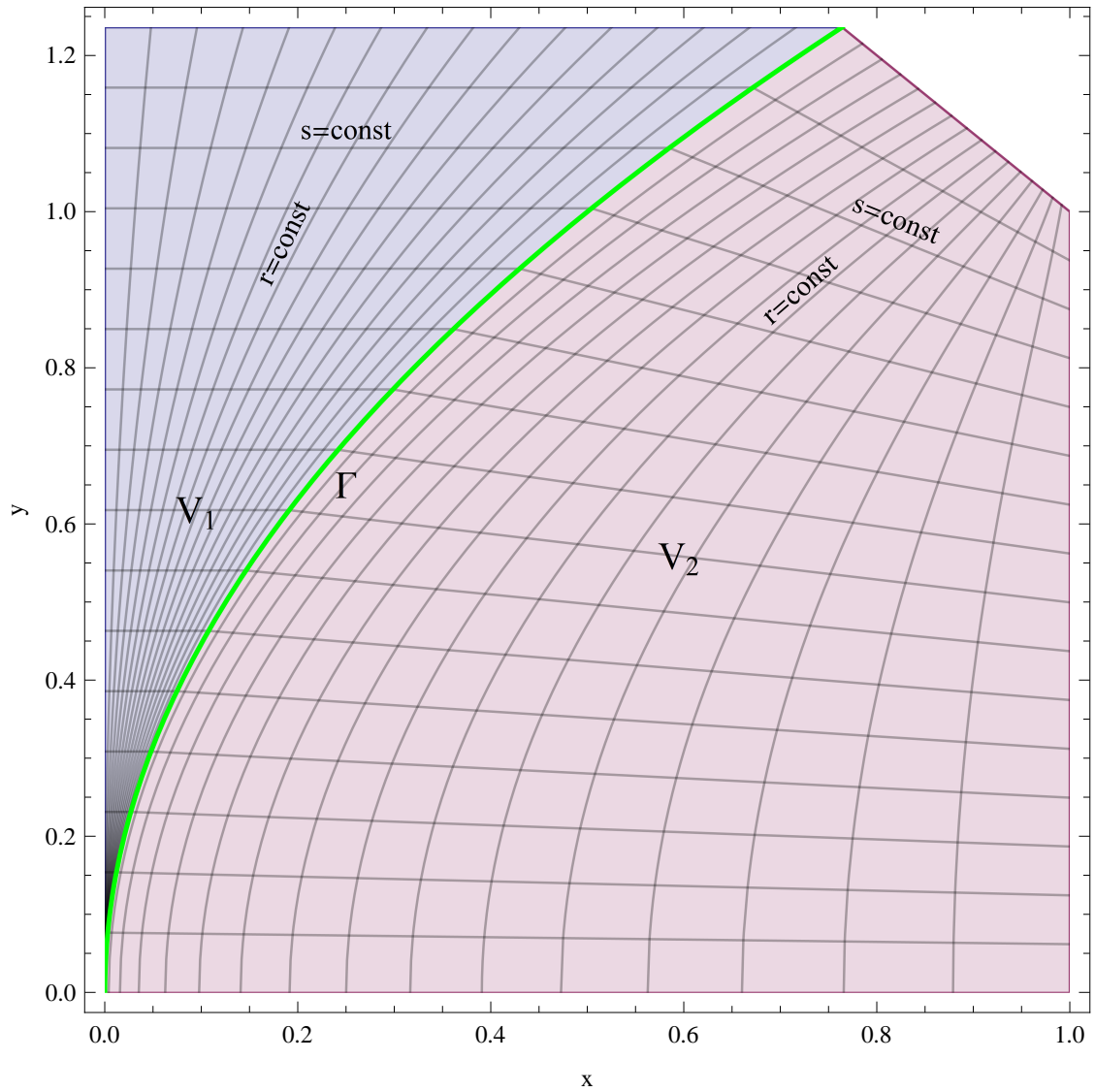
Figure 4.1: Plot of the (x, y) domain V in (4.17). The coloring shows the splitting into the two regions V_1 and V_2. The mesh lines represent the lines of constant r and s of the coordinate transformations (4.22). The PV hypersurface Γ is located at the green line.

are constructed. They are visualized in Figure 4.1. The mesh lines represent the lines of constant r and s, such that the smooth normal derivatives of Φ and Ψ can be observed at Γ.

Those variable substitutions are applied to the integrand of (4.17) and result, when added together, in a smooth $\mathrm{d}r\,\mathrm{d}s$ integrand that is free of poles. Consequently, a fast and convergent numerical solution of principal value integral (4.17) that fits to the analytic expectations is obtained.

4.4 Evaluation of $\mathcal{B}_0$

The wave-function type contribution $\mathcal{B}_0(p)$ for massless on-shell RHNs is defined in Chapter 3.4.1.2. It is expressed in the plasma frame for positive p^0: $p^0 = +|\vec{p}|$. The integration variables are $\cos \angle(k, p)$ and $|\vec{k}|$. k is the 4-momentum of the lepton.

The coupling expanded form in Equation (3.44) contains the sum of the two branches $k^0 = \pm|\vec{k}|$. For $k^0 = -|\vec{k}|$ the integrand

$$\mathrm{d}\cos\angle(k,p)\,\mathrm{d}|\vec{k}|\,\frac{\Pi_\phi^{\mathcal{A}}(p-k)}{(p-k)^2}|\vec{k}|\Big(f_+(-k^0)+f_-(p^0-k^0)\Big)\Big|_{k^0=-|\vec{k}|} \tag{4.23}$$

is free of singularities, because $\Pi_\phi^{\mathcal{A}}(p-k)$ is proportional to $(p-k)^2$. This case can be integrated numerically without further considerations. However, $\mathcal{B}^0$ can be separated into a vacuum and a thermal part according to $\Pi_\phi^{\mathcal{A}}$. The vacuum part can be solved analytically.

For $k^0 = +|\vec{k}|$ the integrand has a singularity at $|\vec{p}| = |\vec{k}|$ in the Higgs's Bose-Einstein-distribution. However, this is flattened by the Higgs self-energy $\Pi^{\mathcal{A}}$ such that only an integrable peak remains. For numerical stability, this is integrated by splitting the $\mathrm{d}|\vec{k}|$ integration range into $0 < |\vec{k}| < |\vec{p}|$, $|\vec{p}| < |\vec{k}| < 2|\vec{p}|$, and the remaining range $2|\vec{p}| < |\vec{k}|$. The IMT transformation is then utilized to flatten the peak. Those three parts are integrated separately and add to the final result in (3.46).

For the resummed case using the Higgs propagator (3.48) without Π_ϕ^H, the pole structure does not change. Only the integrand becomes more complicated, and the vacuum part needs to be calculated numerically. Otherwise, the same method can be used.

If Π_ϕ^H is included, $\Pi_\phi^{\mathcal{A}}$ cannot cancel the pole at the Higgs mass shell $(p-k)^2 = \Pi_\phi^H$. This leads to a peak that is hit during integration within the $k^0 = -|\vec{k}|$ branch.[67] This term has to be split in order to flatten the peak using the IMT transformation. Hence, the peak position and its width should be known analytically. Since Π_ϕ^H is well approximated by the thermal mass $m_\phi^{th2} = \frac{1}{4}G + \frac{1}{4}h_t^2 + \frac{1}{4}\lambda_\phi$ in the ultra-relativistic regime, the peak position is approximated by

$$|\vec{k}|_{peak} = \frac{m_\phi^{th2}}{|\vec{p}|(1-\cos\angle(k,p))}\,. \tag{4.24}$$

Furthermore, the propagator width along the line $|\vec{k}| = |\vec{p}|$ is modeled by the constant[68]

$$\delta|\vec{k}| = \frac{\left|\Pi_\phi^{\mathcal{A}}\right|}{1-\cos\angle(k,p)}\Bigg|_{\substack{|\vec{k}|^2=|\vec{p}||\vec{k}|_{peak}\\ \cos\angle(k,p)=1-10^{-3}}} \,. \tag{4.25}$$

The splitting of the integration region is done using those approximations, however the integrand takes the full Π_ϕ^H and $\Pi_\phi^{\mathcal{A}}$.

This strategy works in particular when the $\mathrm{d}|\vec{p}|$ integral for γ_N is included. The integrand can then be symmetrized in $|\vec{k}| \leftrightarrow |\vec{p}|$, and the whole integration area shown in Figure 4.2 is parameterized by the three

---

[67] For the $k^0 = +|\vec{k}|$ branch, the evaluation strategy does not need to be modified.

[68] The IMT transformation can of course tolerate a dynamic varying width. However, it is numerically preferable to have some constant width that applies for the whole integration at once.

functions $(|\vec{p}|, |\vec{k}|) = r_i(t_1, t_2)$, $(t_1, t_2) \in (0, 1)^2$:

$$r_1 = \left(\frac{a(1 - t_2)}{-1 + \sqrt{a} + \frac{1}{t_1}}, -1 + \frac{1}{t_1} - \sqrt{a}(t_2 - 1) \right) \tag{4.26}$$

$$r_2 = \left(\frac{at_1(1 - t_2)}{1 + (-1 + \sqrt{a})t_1} + \frac{bt_2}{-1 + \sqrt{b} + \frac{1}{t_1}}, -1 + \frac{1}{t_1} - \sqrt{a}(-1 + t_2) + \sqrt{b}t_2 \right) \tag{4.27}$$

$$r_3 = \left(\frac{b}{-1 + \sqrt{b} + \frac{1}{t_1}} + \frac{t_2}{1 - t_2}, -2 + \sqrt{b} + \frac{1}{t_1} + \frac{1}{1 - t_2} \right). \tag{4.28}$$
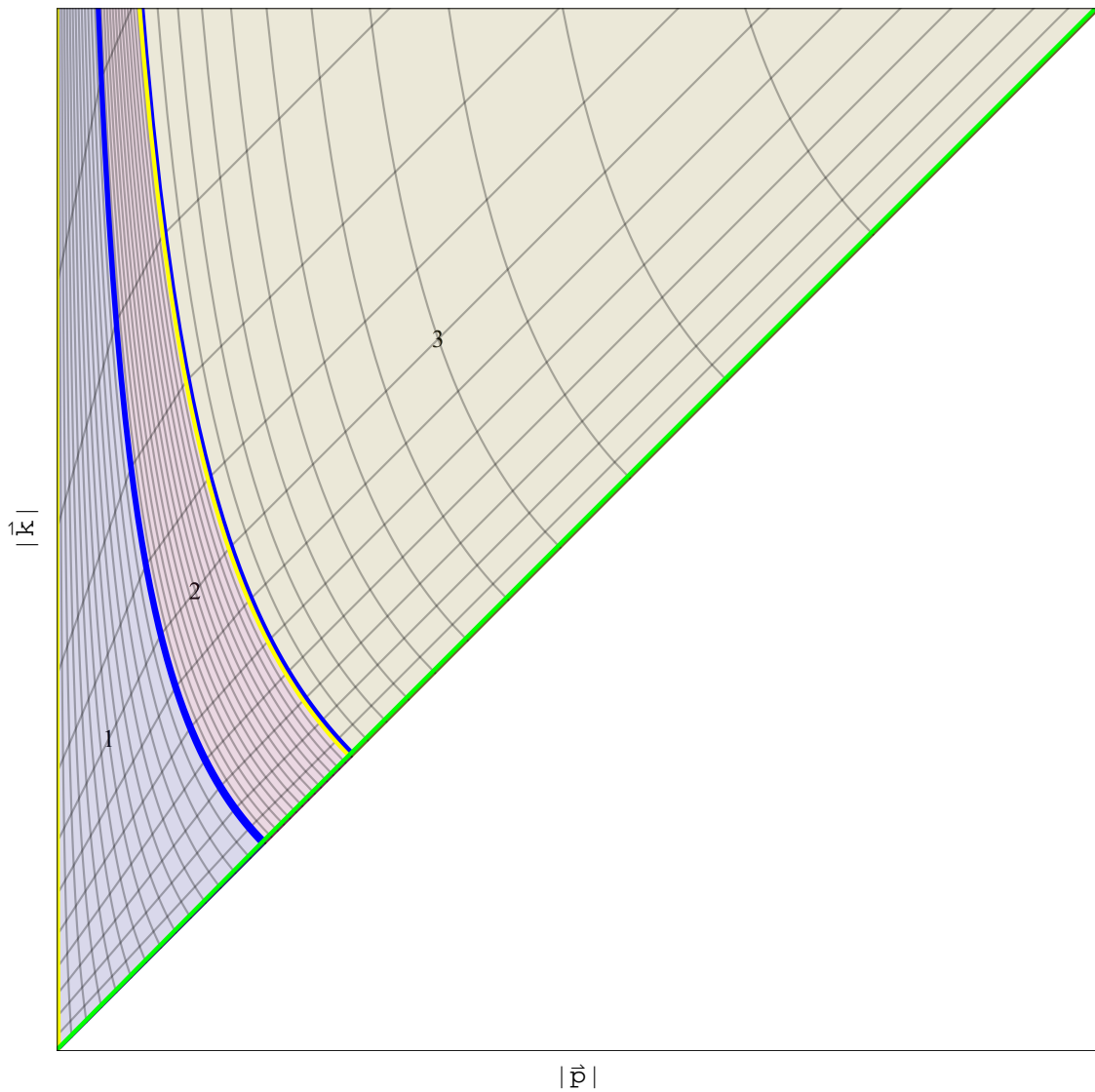
Figure 4.2: This is a plot of the parametrisations r_1, r_2 and r_3 for some arbitrary numbers $0 < a < b$. The mesh lines correspond to lines of constant t_1 and t_2. The green, blue and yellow lines correspond to $t_1 = 1$, $t_2 = 0$ and $t_2 = 1$ respectively.

The r_i are derived according to the cutting lines

$$|\vec{p}| = 0 \qquad\qquad |\vec{k}| = \infty \qquad\qquad |\vec{k}| = |\vec{p}| \qquad\qquad (4.29)$$

$$|\vec{k}| = \frac{a}{|\vec{p}|} \qquad\qquad |\vec{k}| = \frac{b}{|\vec{p}|} \qquad\qquad\qquad\qquad\qquad (4.30)$$

for some fixed numbers $0 < a < b$. a and b are chosen to be $a = \frac{m_\phi^{th2}}{1-\cos \measuredangle(k,p)}$ and $b = 2a$, such that r_1 parametrizes the interval $0 < |\vec{p}| < |\vec{k}|_{peak}$ and r_2 is the range $|\vec{k}|_{peak} < |\vec{p}| < \sqrt{2}|\vec{k}|_{peak}$. Therefore, r_1 and r_2 correspond to the aforementioned "pole" part while r_3 is the "medium" or "non-pole" contribution. For the actual numerics, the IMT transformation is applied in all three regions with respect to t_2 and the width $\omega = 10\delta|\vec{k}|$. Furthermore, in the regions r_1 and r_2 the IMT transformation with respect to $t_3 \equiv 2 - 2\cos\measuredangle(k,p)$ with $\omega = 10^{-6}$ is utilized.

All in all, this method yields the aforementioned results. Additionally, this is the general strategy for the numerical integrals in this work. It can deal with arbitrary widths and is only restricted by the number of digits used when evaluating the integrand.

4.5 Evaluation of $\mathcal{B}^{O(G)}$ and $\mathcal{F}^{O(G)}$

The perturbatively calculated wave-function type contributions $\mathcal{B}^{O(G)}$ and $\mathcal{F}^{O(G)}$ are integrated along the same lines. Both are expressed in Chapter 3.5.1 in the p-frame and consist of one- and two-dimensional integrals in $d\cos\angle(k,p)$ and $d|\vec{k}|$. The two-dimensional integrals typically feature a principal value integral at $|\vec{k}| = \frac{m_N}{2}$, a discontinuity at $|\vec{k}| = m_N$, and a peak at the Bose-Einstein distribution of the internal Higgs at $(|\vec{k}| - m_N)\tilde{p}^0 - |\vec{k}||\vec{p}|\cos\angle(k,p) = 0$. The peak is regulated by the RHN mass and becomes important for approximately $m_N < 0.1T$. Furthermore, the (HTL, col) contribution of $\mathcal{F}^{O(G)}$ contains a peak that may ultimately end up in a principal value type integral in the limit $m_N \to 0$. Even if $\mathcal{F}^{O(G)}$ is not evaluated at $m_N = 0$, this limit should be respected for $m_N < 0.1T$ to obtain stable numerics. On top of that, some contributions serve a sign change in $\cos\angle(k,p) \leftrightarrow -\cos\angle(k,p)$. Those may result in large cancellations within the integrand of contributions coming from $\cos\angle(k,p) = \pm 1$.

The integration strategy is to parametrize the integration domain by functions incorporating those special lines, and to apply the IMT and PV transformations afterwards. For the PV transformation, a maximal pole degree of 1 is assumed. For simplicity, the reparametrizations are applied to all two-dimensional integrals, regardless of whether the corresponding transformation is needed or not. Furthermore, the one-dimensional integrals are easily extended to two dimensions. Hence, one does not need to analyze each term separately to find the corresponding parametrization.

After the symmetrization in $\pm\cos\angle(k,p) \equiv \cos$, the remaining integration area is $0 < \cos < 1$ and $0 < |\vec{k}| < \infty$. The special lines are

$$|\vec{k}| = 0 \qquad\qquad |\vec{k}| = \frac{m_N}{2} \qquad\qquad |\vec{k}| = m_N \tag{4.31}$$

$$|\vec{k}| = \infty \qquad\qquad |\vec{k}| = \frac{m_N\tilde{p}^0}{\tilde{p}^0 \pm \cos|\vec{p}|} \qquad\qquad |\vec{k}| = \kappa\frac{m_N\tilde{p}^0}{\tilde{p}^0 - \cos|\vec{p}|} \tag{4.32}$$

with $\kappa \geq 2$. For technical reasons[69]

$$|\vec{k}| = \frac{1}{2}\left(\frac{m_N\tilde{p}^0}{\tilde{p}^0 + \cos|\vec{p}|} + \frac{m_N}{2}\right) \qquad |\vec{k}| = \frac{\kappa\, m_N\tilde{p}^0}{\tilde{p}^0 - \cos|\vec{p}|} \qquad \cos = \frac{\tilde{p}^0}{5|\vec{p}|} \text{ for } \tilde{p}^0 < 5|\vec{p}| \tag{4.33}$$

are included too. The full domain is parametrized by the following 11 functions $(\cos, |\vec{k}|) = r_i(t_1, t_2)$ with $(t_1, t_2) \in (0,1)^2$:

$$r_1 = \left(\; 1 - t_1 \quad,\quad -\frac{m_N(t_2-1)\left(\tilde{p}^0(t_2+2)-|\vec{p}|(t_1-1)(3t_2+2)\right)}{4\left(\tilde{p}^0+|\vec{p}|-|\vec{p}|t_1\right)} \;\right) \tag{4.34}$$

$$r_2 = \left(\; 1 - t_1 \quad,\quad \frac{m_N\left(|\vec{p}|(t_1-1)(t_2-2)+\tilde{p}^0(t_2+2)\right)}{4\left(\tilde{p}^0+|\vec{p}|-|\vec{p}|t_1\right)} \;\right) \tag{4.35}$$

$$r_3 = \left(\; 1 - t_1 \quad,\quad -\frac{m_N\left(|\vec{p}|(t_1-1)t_2(5t_2-4)+\tilde{p}^0(t_2^2-4)\right)}{4\left(\tilde{p}^0+|\vec{p}|-|\vec{p}|t_1\right)} \;\right) \tag{4.36}$$

$$r_4 = \left(\; 1 - t_1 \quad,\quad \frac{m_N\left(\tilde{p}^0-|\vec{p}|(t_1-1)t_2\right)}{\tilde{p}^0+|\vec{p}|-|\vec{p}|t_1} \;\right) \tag{4.37}$$

$$r_5 = \left(\; -\frac{\tilde{p}^0(t_1-1)}{5|\vec{p}|} \quad,\quad \frac{m_N(t_2(t_1(5t_2-4)+4)-20)}{4(t_1-6)} \;\right) \tag{4.38}$$

$$r_6 = \left(\; -\frac{\tilde{p}^0(t_1-1)}{5|\vec{p}|} \quad,\quad \frac{m_N((t_1-1)t_2-5)}{t_1-6} \;\right) \tag{4.39}$$

$$r_7 = \left(\; \frac{-t_1\tilde{p}^0+\tilde{p}^0+5|\vec{p}|t_1}{5|\vec{p}|} \quad,\quad \frac{m_N\left(\tilde{p}^0((t_1+4)t_2-20)-5|\vec{p}|t_1t_2\right)}{4\left(\tilde{p}^0(t_1-6)-5|\vec{p}|t_1\right)} \;\right) \tag{4.40}$$

---

[69] The PV transformation is applied using an automated Mathematica code. This code demands those extra lines.

$$r_8 = \left(\quad \frac{-t_1\tilde{p}^0 + \tilde{p}^0 + 5|\vec{p}|t_1}{5|\vec{p}|} \quad , \quad \frac{m_N\left(5|\vec{p}|t_1\left(1-5t_2\right)t_2 + \tilde{p}^0\left(5t_1t_2^2 - (t_1+4)t_2 - 20\right)\right)}{4\left(\tilde{p}^0(t_1-6) - 5|\vec{p}|t_1\right)} \quad \right) \tag{4.41}$$

$$r_9 = \left(\quad \frac{-t_1\tilde{p}^0 + t_1t_2\tilde{p}^0 + \tilde{p}^0 - |\vec{p}|t_1t_2}{\tilde{p}^0 - |\vec{p}|t_1} \quad , \quad \frac{m_N\left(\tilde{p}^0 - |\vec{p}|t_1 + |\vec{p}|(t_1-1)t_2\right)}{\tilde{p}^0 - |\vec{p}|} \quad \right) \tag{4.42}$$

$$r_{10} = \left(\quad \frac{\tilde{p}^0 - \tilde{p}^0 t_1}{\tilde{p}^0 - |\vec{p}|t_1} \quad , \quad \frac{m_N\left(-|\vec{p}|t_2\left(|\vec{p}|t_1^2 + \tilde{p}^0 t_2\right) + |\vec{p}|t_2\left(|\vec{p}|t_2t_1^2 + \tilde{p}^0\right) + \tilde{p}^0\left(\tilde{p}^0 - |\vec{p}|t_1\right)\left((\kappa-1)t_2^2 + 1\right)\right)}{\tilde{p}^0\left(\tilde{p}^0 - |\vec{p}|\right)} \quad \right) \tag{4.43}$$

$$r_{11} = \left(\quad \frac{(t_1-1)\left(\tilde{p}^0 - |\vec{p}|t_1t_2\right)}{|\vec{p}|t_1 - \tilde{p}^0} \quad , \quad \frac{\kappa m_N\left(\tilde{p}^0 - |\vec{p}|t_1\right)}{\tilde{p}^0 - |\vec{p}|} + \frac{t_2}{1-t_2} \quad \right). \tag{4.44}$$

These expressions already include the PV transformation at the matching boundaries of r_1 and r_2, r_3 and r_4, r_5 and r_6, r_7 and r_8, and r_9 and r_{10}. See Figure 4.3 for a parametric plot of the r_i.
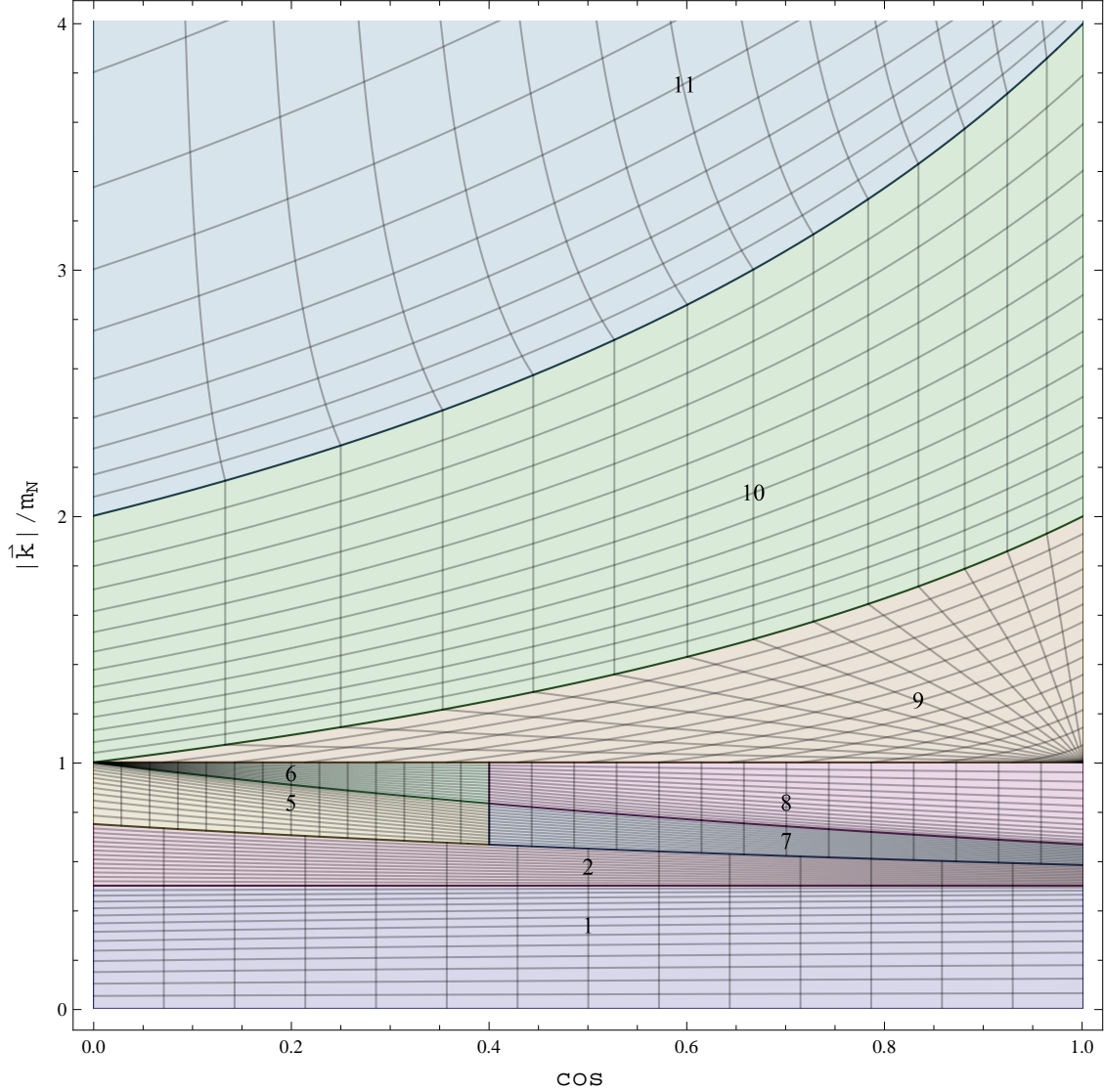
Figure 4.3: This is a plot of the parametrizations r_i using $\tilde{p}^0 = 2|\vec{p}|$ and $\kappa = 2$. The mesh lines are lines of constant t_1 and t_2.

If $\tilde{p}^0 < 5|\vec{p}|$, the parameterizations $r_5, \ldots, r_8$ have to be used instead of $r_3, \ldots, r_4$. With the help of κ, the principal value type pole at $|\vec{k}| = \frac{m_N\tilde{p}^0}{\tilde{p}^0 - \cos|\vec{p}|}$, i.e. the sum of r_9 and r_{10}, is separated from the continuum integral r_{11} in $\mathrm{d}|\vec{k}|$ up to infinity. For the actual numerics, a fixed $\kappa = 2$ is used. Furthermore, t_1 and t_2 are chosen such that the peaks and poles are all placed at $t_2 = 0$.

112

The r_i are applied to the symmetrized $\mathcal{B}^{O(G)}$ and $\mathcal{F}^{O(G)}$ terms. After summing over all i, the IMT transformation is applied at $t_2 = 0$, and the integrals over t_1 and t_2 are evaluated. In this way, the results of the Figures 3.15 and 3.17 are produced.

4.6   Evaluation of $\mathcal{B}$

The wave-function type correction to the neutrino production rate using a resummed Higgs boson propagator is formulated in Section 3.5.2. Here, some remarks are provided on how the results in the Figures 3.19 and 3.20 are derived. The method itself is the same as in the last sections. Only a different parametrization is encountered.

The parametrization from the Equations (4.34) - (4.44) cannot be used, because the Higgs obtains a thermal mass m_ϕ^{th}. The following approach appears to be more appropriate. First, the integration variable $|\vec{k}|$ is redefined. Equation (3.161) contains the sum of two terms with $k^0 = -m_N \pm |\vec{k}|$. However, $|\vec{k}|$ only appears in squared form, or multiplied by $\cos \angle(k, u)$ within $k \cdot u$. Hence, $|\vec{k}|$ can be redefined to be some abstract variable running from $-\infty$ to ∞. In the same step, the sum of the two k^0 cases is absorbed. For notational simplicity, cos is defined as $\cos \equiv \cos \angle(k, u)$. Hence, the $\mathcal{B}$ integral becomes

$$\mathcal{B}(\tilde{p}) = \quad = g_w |Y|^2 \frac{2}{(2\pi)^2} m_N \int_{-\infty}^{\infty} d|\vec{k}| \, |\vec{k}|^2 \frac{\Pi_\phi^{\mathcal{A}}}{\left(k^2 - \Pi_\phi^H\right)^2 + \left(\Pi_\phi^{\mathcal{A}}\right)^2} dF^{\mathcal{B}}(\tilde{p}, k^0, |\vec{k}|) \Bigg|_{k^0 = -m_N - |\vec{k}|} . \tag{4.45}$$

Within this definition, the propagator has its maximum approximately at $|\vec{k}| = |\vec{k}|_1 \equiv \frac{m_N^2 - (m_\phi^{th})^2}{2m_N}$. This value can be positive or negative. In particular, during variation of m_N and the couplings, a smooth crossover is encountered. Without the $|\vec{k}|$-redefinition in (4.45), the crossover is numerically much more challenging. With the redefinition, some reparametrizations that also cross $|\vec{k}| = 0$ smoothly can be found. Of course, a more precise $|\vec{k}|_1$ can be found numerically. However, within the used parameter range the small deviation of the approximated pole maximum from the true one is much smaller than the pole width. Furthermore, the additional symmetrization in cos as applied in Section 4.5 is not needed due to the redefinition. In the limit of small m_N, the peak of the Higgs Bose-Einstein distribution is encountered at $|\vec{k}| = |\vec{k}|_2 \equiv \frac{m_N \tilde{p}^0}{\tilde{p}^0 + \cos |\vec{p}|}$. Because $|\vec{k}|_2$ here is always larger than $|\vec{k}|_1$, those peaks do not cross.

The following reparametrizations $(\cos, |\vec{k}|) = r_i(t_1, t_2)$, $t_1, t_2 \in (0, 1)^2$, are found such that the peaks can be integrated in the simplest way:

$$r_1 = \left(\ 2t_1 - 1 \quad , \quad |\vec{k}|_1 + \tfrac{1}{2}(|\vec{k}|_1 - |\vec{k}|_2)t_2 \ \right) \tag{4.46}$$

$$r_2 = \left(\ 2t_1 - 1 \quad , \quad |\vec{k}|_1 + \tfrac{1}{2}(|\vec{k}|_2 - |\vec{k}|_1)t_2 \ \right) \tag{4.47}$$

$$r_3 = \left(\ 2t_1 - 1 \quad , \quad |\vec{k}|_2 + \tfrac{1}{2}(|\vec{k}|_1 - |\vec{k}|_2)t_2 \ \right) \tag{4.48}$$

$$r_4 = \left(\ 2t_1 - 1 \quad , \quad |\vec{k}|_2 + \tfrac{1}{2}(|\vec{k}|_2 - |\vec{k}|_1)t_2 \ \right) \tag{4.49}$$

$$r_5 = \left(\ 2t_1 - 1 \quad , \quad \tfrac{3|\vec{k}|_1}{2} - \tfrac{|\vec{k}|_2}{2} - \tfrac{1}{t_2} + 1 \ \right) \tag{4.50}$$

$$r_6 = \left(\ 2t_1 - 1 \quad , \quad -\tfrac{|\vec{k}|_1}{2} + \tfrac{3|\vec{k}|_2}{2} + \tfrac{1}{t_2} - 1 \ \right) . \tag{4.51}$$

$r_1, \ldots, r_4$ split the integration domain into symmetric parts around the peaks at $|\vec{k}|_1$ and $|\vec{k}|_2$. $r_5, \ldots, r_6$ deal with the remaining domains up to $|\vec{k}| = \pm\infty$. Figure 4.4 shows the reparametrizations exemplary.
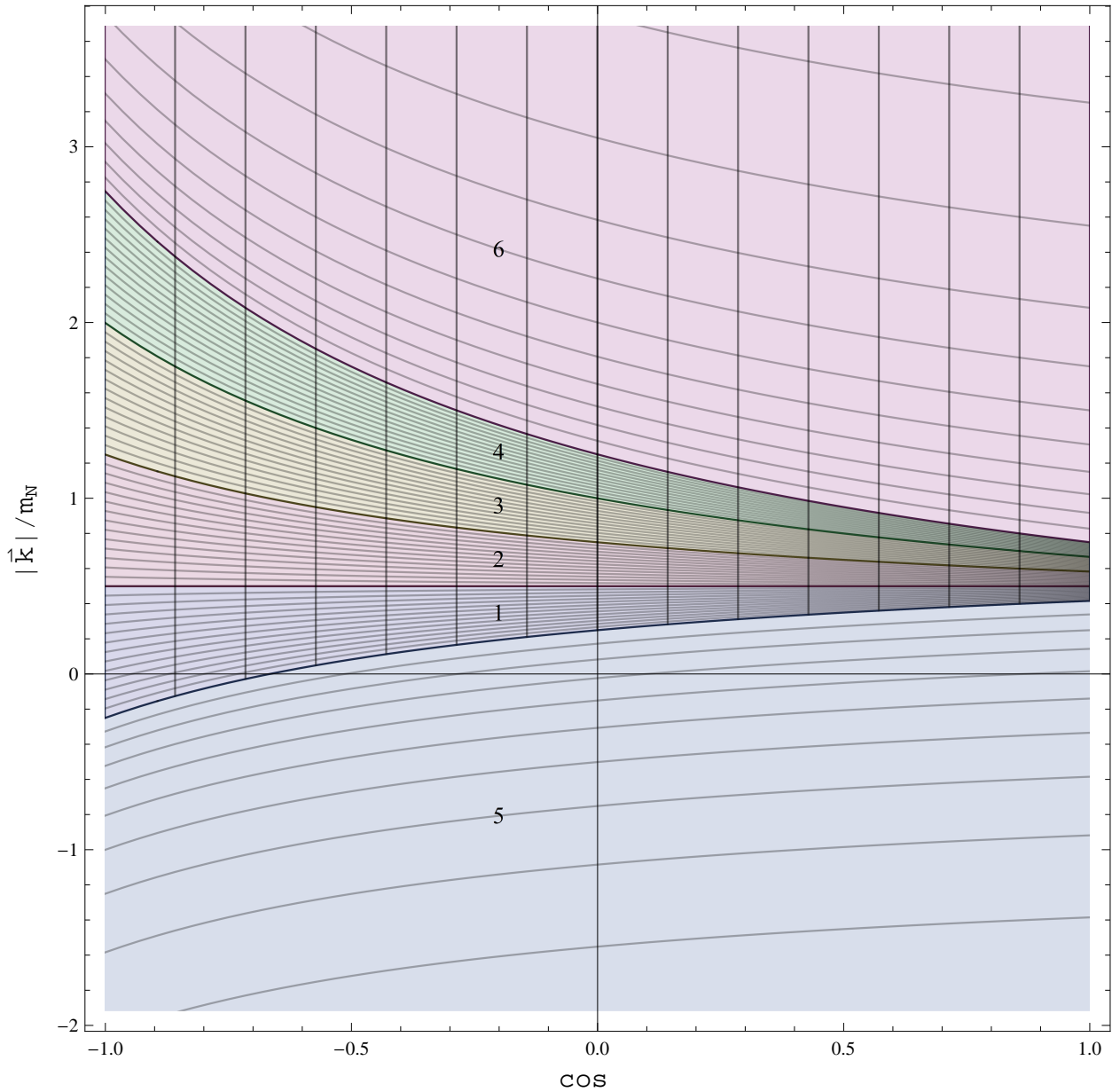
Figure 4.4: This is a parametric plot of the parametrizations r_i using $m_\phi^{th} = 0$. The mesh lines are lines of constant t_1 and t_2.

The variable transformations r_i are applied to the integrand of (4.45) and summed up. Afterwards, the IMT transformation is used at $t_2 = 0$ to deal with small pole widths, and at $t_1 = 0$ to account for the collinear effects at $\cos = -1$.

4.7 Evaluation of $\mathcal{F}$ and $\mathcal{F}_0$

This section provides remarks on how the wave-function type correction to the neutrino production rate using a resummed lepton propagator can be evaluated. The massive RHN $\mathcal{F}$ term is formulated in Section 3.5.2. Likewise, the massless case $\mathcal{F}_0$ can be found in Section 3.4.1.3.

The term $\mathcal{F}_0$ is expressed in the u-frame, since this is the only available frame. Otherwise, one may expect that $\mathcal{F}$ is better formulated and numerically evaluated in the frame of the massive RHN, i.e. the p-frame, because m_N is the relevant scale. Nevertheless, a lepton in a thermal plasma of gauge bosons has a complex dispersion relation that spoils the simple treatment of $\mathcal{F}$ within the p-frame – as it was done for $\mathcal{B}$ in Section 4.6. Even though the position of the lepton poles can be solved numerically, knowing them analytically results in a much more stable numerics and is therefore favorable. The lepton dispersion relation can be solved analytically in the HTL approximation with respect to u-frame variables, as it can be found in [82]. Therefore, $\mathcal{F}$ is better evaluated in the u-frame. In addition, the method can be copied for $\mathcal{F}_0$. In the following pages, the lepton dispersion relation is derived for the present case following the steps of [82].

lepton dispersion relation: According to Equation (3.50) the spectral lepton propagator is

$$P_L \slashed{S}_l^{\mathcal{A}}(p) = P_L \frac{\gamma \cdot a\, 2a \cdot b - \gamma \cdot b\left(a^2 - b^2\right)}{\left(a^2 - b^2\right)^2 + \left(2a \cdot b\right)^2} P_R \quad , \quad a^\mu = p^\mu - \Sigma_l^{H\mu} \quad , \quad b^\mu = \Sigma_l^{\mathcal{A}\mu} . \tag{4.52}$$

The dispersion relation of $\slashed{S}_l(q)$ in the HTL approximation is given by the zeros of

$$\left(q - \Sigma_l^{H,HTL}(q)\right)^2 - \left(\Sigma_l^{\mathcal{A},HTL}(q)\right)^2 = \tag{4.53}$$

$$\frac{G^2 T^4 \ln\left(\frac{(q^0+|\vec{q}|)^2}{(q^0-|\vec{q}|)^2}\right)\left(-q^2\ln\left(\frac{(q^0+|\vec{q}|)^2}{(q^0-|\vec{q}|)^2}\right) + 8q^0|\vec{q}|\right) - 16\left(\left(G|\vec{q}|T^2 + 8|\vec{q}|^3\right)^2 - 64\left(q^0\right)^2|\vec{q}|^4\right)}{1024|\vec{q}|^4} . \tag{4.54}$$

In line (4.54), the assumption to find a solution only for $q^2 > 0$ is used. In fact, Equation (4.53) also has a zero for $q^2 < 0$. Nevertheless, this cancels with the numerator of the propagator such that in total there is no tachyonic pole. This cancellation works only if the propagator numerator is not expanded in the couplings.

With help of the substitution $x = \frac{q^0+|\vec{q}|}{q^0-|\vec{q}|}$, i.e. $q^0 = |\vec{q}|\frac{x+1}{x-1}$, and $|\vec{q}| = \frac{1}{4}\sqrt{GT^2 y}$, the zeros of (4.54) are given by

$$0 = \left(\ln|x| - x + y + 1\right)\left(xy + x - 1 - x\ln|x|\right) . \tag{4.55}$$

In choosing $q^0 > |\vec{q}| > 0$, i.e. $x > 1$, the two solutions

$$x_+ = -W_{-1}\left(-e^{-\frac{16|\vec{q}|^2}{GT^2} - 1}\right) \tag{4.56}$$

$$x_- = -W_0^{-1}\left(-e^{-\frac{16|\vec{q}|^2}{GT^2} - 1}\right) \tag{4.57}$$

are obtained. W is the Lambert W-function, and $W_0(z)$ and $W_{-1}(z)$ are the two real solutions of $z = We^W$. x_+ and x_- are the two "HTL" branches of the dispersion relation that are plotted in Figure 4.5.
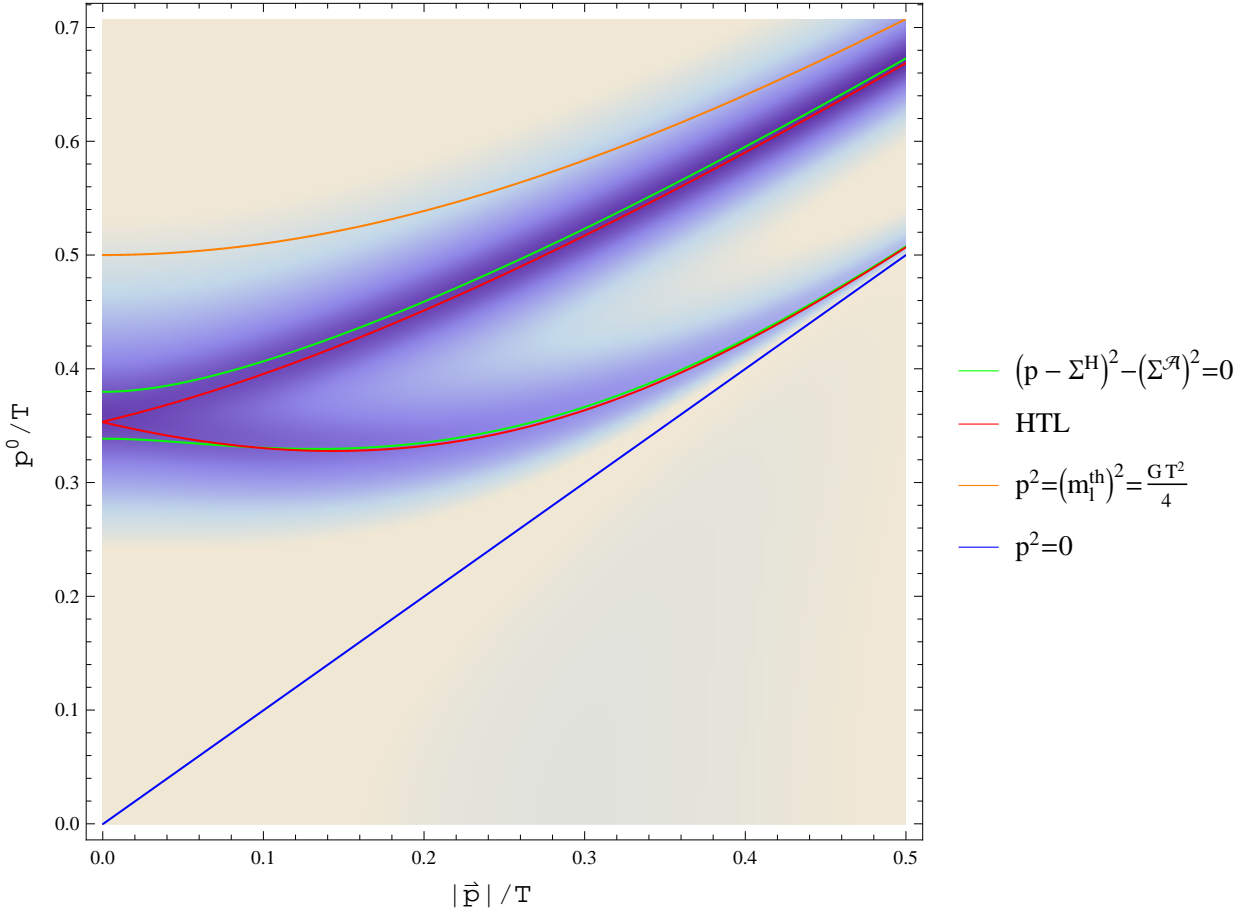
Figure 4.5: Dispersion relation of the resummed lepton plotted in the case of $G = 1$. The density plot in the background shows $u \cdot \Sigma_l^{\mathcal{A}}(p)$, and visualizes the true dispersion relation given by the maxima of the propagator.

The green lines are the zeros of Equation (4.53) without the HTL approximation, and the background density plot shows logarithmically the full propagator.[70] Hence, in the present case, the dispersion relation is better modeled by the HTL approximated form than by the expected maxima of the Breit-Wigner form in Equation (4.52). Nevertheless, regarding the numerics the HTL approximated dispersion relation

$$q_+^0 = +|\vec{q}| \frac{W_{-1}\left(-e^{-\frac{16|\vec{q}|^2}{GT^2}-1}\right) - 1}{W_{-1}\left(-e^{-\frac{16|\vec{q}|^2}{GT^2}-1}\right) + 1} \tag{4.58}$$

$$q_-^0 = -|\vec{q}| \frac{W_0\left(-e^{-\frac{16|\vec{q}|^2}{GT^2}-1}\right) - 1}{W_0\left(-e^{-\frac{16|\vec{q}|^2}{GT^2}-1}\right) + 1} \tag{4.59}$$

is enough for the analysis and also the most advantageous analytically. Figure 4.5 also shows the asymptotic dispersion relation branches for $|\vec{p}| \gg T$. In particular, the thermal lepton mass $(m_l^{th})^2 = \frac{1}{4}GT^2$ can be verified by first expanding $x_+(q)$ in $e^{-\frac{16|\vec{q}|^2}{GT^2}}$ at 0 up to the leading order, and afterwards expanding the resulting q^2 in $\frac{|\vec{q}|}{T}$ at ∞ to the leading order.

---

[70] The vacuum self-energy is dropped according to Section 3.5.2.1.

116

The integration domain B for the $dk^0 \, d|\vec{k}|$ integral in $\mathcal{F}$ is determined by

$$0 < \mathrm{gd}(u, p, k) - \frac{1}{4} \Big((k^0 + |\vec{k}|)(k^0 + |\vec{k}| - 2p^0) + m_N^2 \Big) \Big(k^{0^2} - 2k^0(|\vec{k}| + p^0) + |\vec{k}|^2 + 2|\vec{k}|p^0 + m_N^2 \Big). \quad (4.60)$$

The maximum of the Bose-Einstein distribution of the internal Higgs particle is located at $k^0 = p^0$. This peak should be evaluated symmetrically[71] even if it is regulated by m_N. The domain B, together with the peak position of the Bose-Einstein distribution, and the peaks $k_\pm^0$ of the lepton propagator given by the above dispersion relation are used to parametrize the integration domain in terms of functions $(k^0|\vec{k}|) = r_i(t_1, t_2)$ with $t_1, t_2 \in (0, 1)$. Under the variation of the parameters m_N, $|\vec{p}|$ and G, the peaks $k_\pm^0$ move across the domain B. Therefore, B needs to be parametrized case by case. This is done automatically during evaluation for each parameter choice independently. Consequently, those r_i cannot be shown here. However, there are at least 5 different cases that need to be considered. They are sketched in Figure 4.7. Figure 4.6 shows the parameter space for each case. I-V are relevant for $m_N \neq 0$, and for $m_N = 0$ only IV and V need to be considered. Finally, the results for a massive RHN can be found in the Figure 3.21, and massless neutrinos are shown in Figure 3.10.
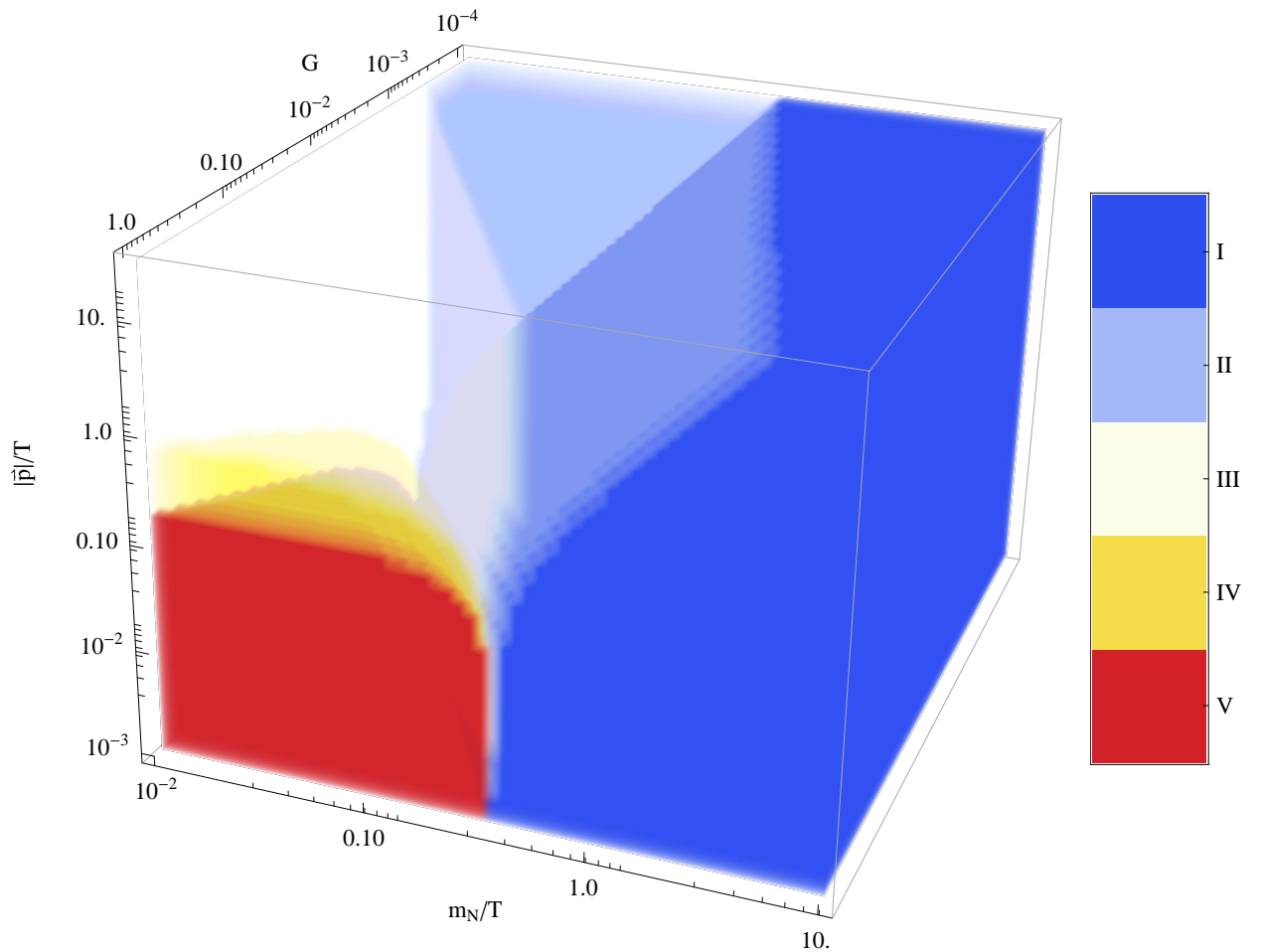
Figure 4.6: The plot relates the cases I-V to the corresponding parameters m_N, $|\vec{p}|$ and G relevant for $\mathcal{F}$.

---

[71] i.e. in the principal value scheme, to optimize the numerical cancellation of large contributions.
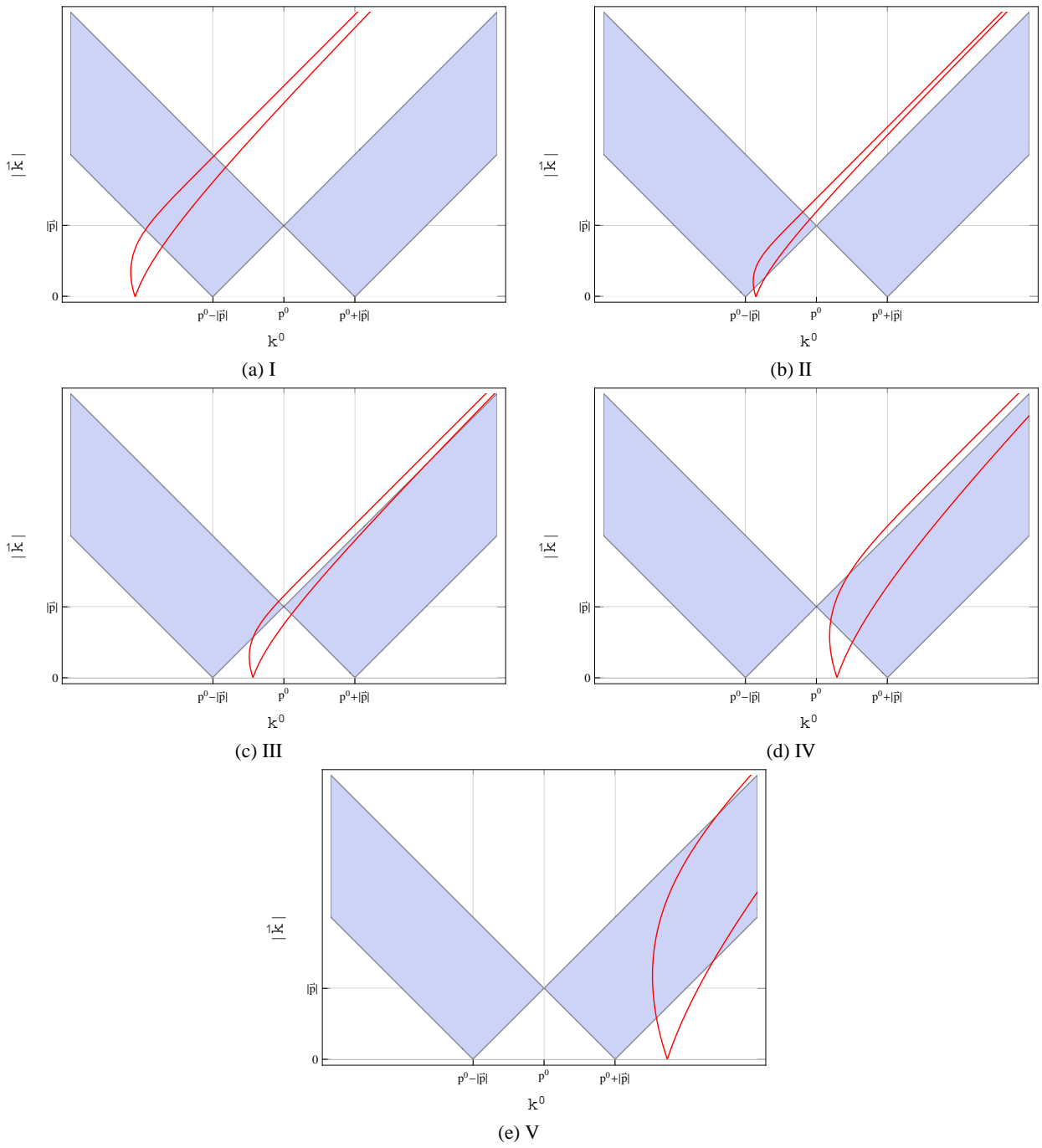
Figure 4.7: The figures sketch the five different cases that need to be considered during the integral parametrization for numerical evaluation of $\mathcal{F}$ and $\mathcal{F}_0$. The blue region is the integration domain given by (4.60). The propagator peaks of $S_l^{\mathcal{A}}(k)$ are located at the red lines.

4.8 Evaluation of $\mathcal{J}^{O(G)}$

The final numerics chapter provides further remarks on the evaluation routines for $\mathcal{J}$. $\mathcal{J}$ is the sum of $\mathcal{J}^{vac} + \mathcal{J}^{T\neq0,\lambda=0} + \mathcal{J}^{T\neq0,corr}$. $\mathcal{J}^{vac}$ is already solved analytically in (3.317). However, $\mathcal{J}^{T\neq0,\lambda=0}$ and $\mathcal{J}^{T\neq0,corr}$ need to be evaluated numerically.

The first one is obtained by the symmetrization according to Equation (3.301) and by setting $\lambda = 0$. The integration domain of $\mathcal{J}^{T\neq0,\lambda=0}$ and its splitting are plotted in Figure 3.31. The boundaries of those sub-regions fit to the propagator poles at $x, y = 0$ and to the discontinuities which are generated by adding several contributions of different support.
Even after the symmetrization (3.301) is done, there are still integrable poles from the Bose-Einstein distributions of the internal bosons at $(x, y) = (0, 0)$ and $(x, y) = \left(\frac{m_N}{2}, 0\right)$. They are only located in regions I...III, but not in IV...VII. Those poles are evaluated numerically using the IMT transformation.
For technical reasons, the polynomial part of the integrand of $\mathcal{J}^{T\neq0,\lambda=0}$ is separated by a partial fractioning into terms proportional to $\frac{1}{xy}$, $\frac{1}{x}$ and $\frac{1}{y}$, and the 1 remainder. Those 28 integrals, i.e. 4 fractions multiplied by 7 regions, are evaluated separately.
In regions I, II and III, the $\frac{1}{xy}$ and $\frac{1}{y}$ terms have an opposite sign. This results in a large cancellation for $m_N < 0.1T$, such that the $\frac{1}{xy}$ and $\frac{1}{y}$ terms have to be evaluated within one integral. The $\frac{1}{xy}$ and $\frac{1}{y}$ terms in regions I...III plus the 1 term at region VII form the dominant and non-vanishing contributions in the ultra-relativistic limit.
For the case of small m_N, there are several other peaks in the integrand from the Bose-Einstein distributions. For a well-behaved numeric, their positions should be obtained from the symmetrizations. Depending on the parameter choice, the peaks cross each other in different formations such that one should again analyze each case in order to find an appropriate parametrization, as is done for $\mathcal{F}$. In fact, by utilizing a large enough value for Mathematica's *NIntegrate* options *MinRecursion* and *MaxRecursion*, the integrals can be solved with a relative error of about 10^{-3} in the small m_N range in exchange for CPU time.

The other part, $\mathcal{J}^{T\neq0,corr}$, is derived in Equation (3.308). It accounts for the error that is done by switching from the $\lambda \to 0$ prescription to the principal value type prescription. It is a three-dimensional integral with two integrable poles at $x = \frac{m_N}{2}$ and $x = 0$, that are related to those at $(x, y) = \left(\frac{m_N}{2}, 0\right)$ and $(x, y) = (0, 0)$ of $\mathcal{J}^{T\neq0,\lambda=0}$. Depending on the parameter choice, a large cancellation of the contributions above and below $x = \frac{m_N}{2}$ occurs. Hence, this pole is integrated symmetrically even though it is not a principal value. Both poles, $x = \frac{m_N}{2}$ and $x = 0$, are integrated using the IMT transformation.

The final results can be found in Chapter 3.5.6.7.

CHAPTER

5

Conclusions and Outlook

5.1 Summary

The aim of the present investigation was to formulate an approach to obtain the differential production rate of massive and massless singlet right-handed neutrinos relevant for leptogenesis. Previous attempts were only able to account for the non-relativistic regime, where the neutrino mass is much larger than the temperature. Here, several approaches were formulated and analyzed in order to obtain the differential production rate of massive right-handed neutrinos. In combination, they covered the full mass range from the non-relativistic up to the ultra-relativistic regime.

The study was based on the Closed-Time-Path formalism, since this is a first-principle approach to thermal non-equilibrium Quantum Field Theory. Furthermore, the neutrino production rate was derived in the 2PI approach from the 1- and 2-loop spectral neutrino self-energy. The 2PI approach was relevant for a consistent description of the screening effects in the intermediate and ultra-relativistic regime. However, the 2PI diagrams were expanded in the Standard Model couplings for calculational simplicity, until the *NLO* of ordinary perturbation theory was reached. In this way, the improvement of a gradual inclusion of resummation effects was analyzed up to the point where all soft and collinear divergences were screened by the thermal plasma.

Up to the 2-loop 2PI order, the neutrino rate is determined by wave-function and vertex type contributions. It was pointed out that the wave-function type contributions involved infrared divergences from massless particle exchanges within the thermal plasma. Those radiative corrections spoiled the perturbation theory and therefore had to be resummed. Consequently, the wave-function type contributions could only be perturbatively described in the non-relativistic regime. This approach was called the "perturbative thermal mass insertion". Within the perturbative approach, the cancellation of intermediate infrared divergences of the real and virtual contributions was confirmed for thermal corrections too.

However, the vertex type contributions behaved much less divergently. Their infrared divergences canceled out under the integral at the perturbative level. Therefore, the finiteness of the perturbative approach was checked numerically for neutrino masses up to the ultra-relativistic regime. No need for a resummation was found.

Those numerical results of the wave-function type and vertex type contributions were verified by a fit to non-relativistic expansion coefficients. In addition, the coefficients were obtained analytically and verified by the literature.

121

In the ultra-relativistic regime, the perturbative wave-function and vertex type contributions possessed an enhancement that was not found in the ultra-relativistic limit. This discrepancy was thought to be a physical effect due to interferences of Bose-Einstein distributions. It was not interpreted as the breakdown of the perturbation theory and the call for resummation, however, this just meant that the massless limit $m_N \to 0$ and integration was not exchangeable. This effect enhanced the RHN rate of the vertex type contributions in the ultra-relativistic limit by a factor of two.

In the intermediate and the ultra-relativistic regime, the full propagators, which are demanded by the 2PI formalism, had to be used to describe the wave-function type contributions. Those propagators were obtained by the resummation of the 1-loop lepton and Higgs self-energies. Since those self-energies were obtained perturbatively, the IR divergences of the hermitian self-energies had to be absorbed by a vacuum counter term in addition to the UV renormalization counter terms. The IR counter term was justified to provide the correct NLO rate in the ultra-relativistic regime up to some RHN mass scale in the intermediate regime. Furthermore, a region of congruence of this resummed approach to the perturbative one was found in the intermediate regime. Consequently, this region was utilized to switch between both approaches in order to describe the NLO RHN rate in the full mass range.

Furthermore, a subtlety of the Higgs resummed spectral propagator was found. The resummation of the perturbatively obtained Higgs self-energy led to a causality violating resummed function due to the neglection of back reaction effects. In order to obtain the correct resummed Higgs propagator, the Higgs self-energy itself had to be derived using the resummed Higgs propagator. This kind of Schwinger-Dyson equation was solved in the vacuum limit, and the solution was found to be causal. As a consequence, an improvement of the resummed Higgs function relevant for finite temperature was derived.

Finally, a method using gram determinants to easily provide integration domains for massless and massive loop integrals, and several tools numerically dealing with multi-dimensional integrals having one-dimensional principal values and poles of the resummed and the distribution functions with arbitrary widths were investigated. Those contribute to the CTP formalism and theories described by nPI effective actions, since the particle distribution functions and the resummed functions spoil the direct analytic evaluation that is usually applied to loop integrals at zero temperature in perturbation theory.

Some of the results are published in [75, 80] – as mentioned in the present text.

5.2 Outlook

There are several aspects in this work that can be investigated further.

First, the renormalization scheme for all relevant particles may be fixed to get well-defined mass and coupling parameters. Furthermore, the effect of resummed gauge bosons and their thermal masses should be investigated. In this context, the IR counter term may be removed, such that the resummed approach becomes valid in the non-relativistic regime too.

Second, a numerical solution of the causal and resummed thermal Higgs propagator may be found to explain the validity range of the mentioned analytic improvement in detail.

Third, the NLO right-handed neutrino rate may be evaluated from the wave-function and vertex diagrams using 2PI functions for all propagators. Hence, one should check whether interferences of the continuum parts of those propagators give sizable contributions. Even though the vertex diagram was numerically IR finite in the ultra-relativistic limit, the effects of resummed functions may be investigated. In this context, the physical correctness of the Bose-Einstein interferences and the resulting rate enhancement of the vertex type contributions may be confirmed in the massless limit as well.

If those tasks are completed, a major step forward in clarity and understanding of the propagator resummation may be achieved.

Furthermore, as previously mentioned, the 3PI formalism should be considered for a self-consistent description of an effective action up to 3-loop order. The vertex type contributions then involve resummed vertex

functions. The size of such vertex resummation effects should be analyzed.

In addition, flavor effects like the flavor resonant enhancement may be investigated using the presented re-summed functions. In particular, if several bosonic particles are involved, the interferences of Bose-Einstein distributions may provide additional contributions.

Finally, the mentioned approach can be used to derive production rates and transport coefficients for other scenarios that physically happen on non-relativistic up to ultra-relativistic scales.

Bibliography

[1] Georges Aad et al. Observation of a new particle in the search for the Standard Model Higgs boson with the ATLAS detector at the LHC. *Phys.Lett.*, B716:1–29, 2012.

[2] Serguei Chatrchyan et al. Observation of a new boson at a mass of 125 GeV with the CMS experiment at the LHC. *Phys.Lett.*, B716:30–61, 2012.

[3] P.A.R. Ade et al. Planck 2013 results. XVI. Cosmological parameters. 2013.

[4] W. M. Yao et al. Review of particle physics. *J. Phys.*, G33:1–1232, 2006.

[5] E. Komatsu et al. Five-Year Wilkinson Microwave Anisotropy Probe (WMAP) Observations: Cosmological Interpretation. 2008.

[6] E. Komatsu et al. Seven-Year Wilkinson Microwave Anisotropy Probe (WMAP) Observations: Cosmological Interpretation. *Astrophys.J.Suppl.*, 192:18, 2011.

[7] Gary Steigman. Primordial Nucleosynthesis: The Predicted and Observed Abundances and Their Consequences. 2010.

[8] G. Hinshaw, D. Larson, E. Komatsu, D.N. Spergel, C.L. Bennett, et al. Nine-Year Wilkinson Microwave Anisotropy Probe (WMAP) Observations: Cosmological Parameter Results. 2012.

[9] Antonio Riotto. Theories of baryogenesis. pages 326–436, 1998.

[10] A. D. Sakharov. Violation of CP Invariance, c Asymmetry, and Baryon Asymmetry of the Universe. *Pisma Zh. Eksp. Teor. Fiz.*, 5:32–35, 1967.

[11] V. A. Kuzmin, V. A. Rubakov, and M. E. Shaposhnikov. On the anomalous electroweak baryon number nonconservation in the early universe. *Phys. Lett.*, B155:36, 1985.

[12] M. Fukugita and T. Yanagida. Baryogenesis Without Grand Unification. *Phys. Lett.*, B174:45, 1986.

[13] W. Buchmuller. Leptogenesis: Theory and neutrino masses. 2012.

[14] Steve Blanchet and Pasquale Di Bari. The minimal scenario of leptogenesis. *New J.Phys.*, 14:125012, 2012.

[15] Chee Sheng Fong, Enrico Nardi, and Antonio Riotto. Leptogenesis in the Universe. *Adv.High Energy Phys.*, 2012:158303, 2012.

[16] J. S. Schwinger. Brownian motion of a quantum oscillator. *J. Math. Phys.*, 2(407), 1961.

[17] L. V. Keldysh. Diagram technique for nonequilibrium processes. *Zh. Eksp. Teor. Fiz.*, 47(1515), 1964.

[18] P. M. Bakshi and K. T. Mahanthappa. Expectation value formalism in quantum field theory 1. *J. Math. Phys.*, 4(1), 1963.

[19] P. M. Bakshi and K. T. Mahanthappa. Expectation value formalism in quantum field theory 2. *J. Math. Phys.*, 4(12), 1963.

[20] Wilfried Buchmuller and Stefan Fredenhagen. Quantum mechanics of baryogenesis. *Phys.Lett.*, B483:217–224, 2000.

[21] Tomislav Prokopec, Michael G. Schmidt, and Steffen Weinstock. Transport equations for chiral fermions to order h bar and electroweak baryogenesis. Part 1. *Annals Phys.*, 314:208–265, 2004.

[22] Tomislav Prokopec, Michael G. Schmidt, and Steffen Weinstock. Transport equations for chiral fermions to order h-bar and electroweak baryogenesis. Part II. *Annals Phys.*, 314:267–320, 2004.

[23] D. Boyanovsky, K. Davey, and C.M. Ho. Particle abundance in a thermal plasma: Quantum kinetics vs. Boltzmann equation. *Phys.Rev.*, D71:023523, 2005.

[24] Andrea De Simone and Antonio Riotto. Quantum Boltzmann Equations and Leptogenesis. *JCAP*, 0708:002, 2007.

[25] Vincenzo Cirigliano, Christopher Lee, Michael J. Ramsey-Musolf, and Sean Tulin. Flavored Quantum Boltzmann Equations. *Phys.Rev.*, D81:103503, 2010.

[26] Martin Beneke, Bjorn Garbrecht, Christian Fidler, Matti Herranen, and Pedro Schwaller. Flavoured Leptogenesis in the CTP Formalism. *Nucl.Phys.*, B843:177–212, 2011.

[27] A. Anisimov, W. Buchmuller, M. Drewes, and S. Mendizabal. Quantum Leptogenesis I. *Annals Phys.*, 326:1998–2038, 2011.

[28] Florian Gautier and Julien Serreau. On the Langevin description of nonequilibrium quantum fields. *Phys.Rev.*, D86:125002, 2012.

[29] Laura Covi, Nuria Rius, Esteban Roulet, and Francesco Vissani. Finite temperature effects on CP violating asymmetries. *Phys.Rev.*, D57:93–99, 1998.

[30] G.F. Giudice, A. Notari, M. Raidal, A. Riotto, and A. Strumia. Towards a complete theory of thermal leptogenesis in the SM and MSSM. *Nucl.Phys.*, B685:89–149, 2004.

[31] M. Garny, A. Hohenegger, A. Kartavtsev, and M. Lindner. Systematic approach to leptogenesis in nonequilibrium QFT: Vertex contribution to the CP-violating parameter. *Phys.Rev.*, D80:125027, 2009.

[32] M. Garny, A. Hohenegger, A. Kartavtsev, and M. Lindner. Systematic approach to leptogenesis in nonequilibrium QFT: Self-energy contribution to the CP-violating parameter. *Phys.Rev.*, D81:085027, 2010.

[33] A. Anisimov, W. Buchmuller, M. Drewes, and S. Mendizabal. Leptogenesis from Quantum Interference in a Thermal Bath. *Phys.Rev.Lett.*, 104:121102, 2010.

[34] M. Garny, A. Hohenegger, and A. Kartavtsev. Medium corrections to the CP-violating parameter in leptogenesis. *Phys.Rev.*, D81:085028, 2010.

[35] Martin Beneke, Bjorn Garbrecht, Matti Herranen, and Pedro Schwaller. Finite Number Density Corrections to Leptogenesis. *Nucl.Phys.*, B838:1–27, 2010.

[36] Bjorn Garbrecht. Leptogenesis: The Other Cuts. *Nucl.Phys.*, B847:350–366, 2011.

126

[37] Marco Drewes. On the Role of Quasiparticles and thermal Masses in Nonequilibrium Processes in a Plasma. 2010.

[38] Bjorn Garbrecht and Matti Herranen. Effective Theory of Resonant Leptogenesis in the Closed-Time-Path Approach. *Nucl.Phys.*, B861:17–52, 2012.

[39] Mathias Garny, Alexander Kartavtsev, and Andreas Hohenegger. Leptogenesis from first principles in the resonant regime. *Annals Phys.*, 328:26–63, 2013.

[40] Bjorn Garbrecht. Leptogenesis from Additional Higgs Doublets. *Phys.Rev.*, D85:123509, 2012.

[41] Marco Drewes and Bjorn Garbrecht. Leptogenesis from a GeV Seesaw without Mass Degeneracy. *JHEP*, 1303:096, 2013.

[42] Björn Garbrecht. Baryogenesis from Mixing of Lepton Doublets. *Nucl.Phys.*, B868:557–576, 2013.

[43] T. Frossard, M. Garny, A. Hohenegger, A. Kartavtsev, and D. Mitrouskas. Systematic approach to thermal leptogenesis. *Phys.Rev.*, D87:085009, 2013.

[44] Peter Millington and Apostolos Pilaftsis. Perturbative Non-Equilibrium Thermal Field Theory. 2012.

[45] Marco Drewes. The Phenomenology of Right Handed Neutrinos. *International Journal of Modern Physics E, Vol.*, 22:1330019, 2013.

[46] Peter Minkowski. mu → e gamma at a rate of one out of 1-billion muon decays? *Phys. Lett.*, B67:421, 1977.

[47] Murray Gell-Mann, Pierre Ramond, and Richard Slansky. Complex Spinors and Unified Theories. *Conf.Proc.*, C790927:315–321, 1979.

[48] Rabindra N. Mohapatra and Goran Senjanovic. Neutrino mass and spontaneous parity nonconservation. *Phys. Rev. Lett.*, 44:912, 1980.

[49] Tsutomu Yanagida. Horizontal Symmetry and Masses of Neutrinos. *Prog.Theor.Phys.*, 64:1103, 1980.

[50] Piotr H. Chankowski and Zbigniew Pluciennik. Renormalization group equations for seesaw neutrino masses. *Phys.Lett.*, B316:312–317, 1993.

[51] Harald Fritzsch and Peter Minkowski. Unified Interactions of Leptons and Hadrons. *Annals Phys.*, 93:193–266, 1975.

[52] W. Buchmuller and M. Plumacher. Baryon asymmetry and neutrino mixing. *Phys.Lett.*, B389:73–77, 1996.

[53] Yasunori Nomura and T. Yanagida. Bimaximal neutrino mixing in SO(10)(GUT). *Phys.Rev.*, D59:017303, 1999.

[54] Scott Dodelson and Lawrence M. Widrow. Sterile-neutrinos as dark matter. *Phys. Rev. Lett.*, 72:17–20, 1994.

[55] Xiang-Dong Shi and George M. Fuller. A new dark matter candidate: Non-thermal sterile neutrinos. *Phys. Rev. Lett.*, 82:2832–2835, 1999.

[56] Laurent Canetti, Marco Drewes, Tibor Frossard, and Mikhail Shaposhnikov. Dark Matter, Baryogenesis and Neutrino Oscillations from Right Handed Neutrinos. *Phys.Rev.*, D87(9):093006, 2013.

[57] Alberto Salvio, Paolo Lodone, and Alessandro Strumia. Towards leptogenesis at NLO: the right-handed neutrino interaction rate. *JHEP*, 1108:116, 2011.

[58] M. Laine and Y. Schroder. Thermal right-handed neutrino production rate in the non-relativistic regime. *JHEP*, 1202:068, 2012.

[59] Alexey Anisimov, Denis Besak, and Dietrich Bodeker. Thermal production of relativistic Majorana neutrinos: Strong enhancement by multiple soft scattering. *JCAP*, 1103:042, 2011.

[60] Denis Besak and Dietrich Bodeker. Thermal production of ultrarelativistic right-handed neutrinos: Complete leading-order results. *JCAP*, 1203:029, 2012.

[61] Clemens P. Kiessig, Michael Plumacher, and Markus H. Thoma. Decay of a Yukawa fermion at finite temperature and applications to leptogenesis. *Phys.Rev.*, D82:036007, 2010.

[62] Clemens Kiessig and Michael Plumacher. Hard-Thermal-Loop Corrections in Leptogenesis I: CP-Asymmetries. *JCAP*, 1207:014, 2012.

[63] Clemens Kiessig and Michael Plumacher. Hard-Thermal-Loop Corrections in Leptogenesis II: Solving the Boltzmann Equations. 2011.

[64] M. Laine. Thermal right-handed neutrino production rate in the relativistic regime. *JHEP*, 1308:138, 2013.

[65] Tomohiro Endoh, Takuya Morozumi, and Zhao-hua Xiong. Primordial lepton family asymmetries in seesaw model. *Prog.Theor.Phys.*, 111:123–149, 2004.

[66] Asmaa Abada, Sacha Davidson, Francois-Xavier Josse-Michaux, Marta Losada, and Antonio Riotto. Flavor issues in leptogenesis. *JCAP*, 0604:004, 2006.

[67] Enrico Nardi, Yosef Nir, Esteban Roulet, and Juan Racker. The importance of flavor in leptogenesis. *JHEP*, 0601:164, 2006.

[68] Peter Brockway Arnold, Guy D. Moore, and Laurence G. Yaffe. Transport coefficients in high temperature gauge theories. 1. Leading log results. *JHEP*, 0011:001, 2000.

[69] Peter Brockway Arnold, Guy D. Moore, and Laurence G. Yaffe. Photon emission from quark gluon plasma: Complete leading order results. *JHEP*, 0112:009, 2001.

[70] I. Ghisoiu and M. Laine. Right-handed neutrino production rate at T > 160 GeV. *JCAP*, 1412(12):032, 2014.

[71] J. Berges. Introduction to nonequilibrium quantum field theory. *AIP Conf. Proc.*, 739(3), 2005.

[72] Chou, Kuang-chao and Su, Zhao-bin and Hao, Bai-lin and Yu, Lu. Equilibrium and Nonequilibrium Formalisms Made Unified. *Phys.Rept.*, 118:1, 1985.

[73] B. Garbrecht and M. Garny. Finite width in out-of-equilibrium propagators and kinetic theory. *Annals Phys.*, 327(914), 2012.

[74] M. Le Bellac. *Thermal Field Theory*. Cambridge University Press, 1996.

[75] B. Garbrecht, F. Glowna and P. Schwaller. Scattering rates for leptogenesis: Damping of lepton flavour coherence and production of singlet neutrinos. *Nucl.Phys. B*, 877, 2013.

[76] M.E. Peskin and D.V. Schroeder. *An Introduction to Quantum Field Theory*. Advanced book classics. Addison-Wesley Publishing Company, 1995.

[77] A. Gehrmann-De Ridder, T. Gehrmann, and G. Heinrich. Four particle phase space integrals in massless QCD. *Nucl.Phys.*, B682:265–288, 2004.

[78] T. Binoth and G. Heinrich. Numerical evaluation of phase space integrals by sector decomposition. *Nucl.Phys.*, B693:134–148, 2004.

[79] Juergen Berges. N-particle irreducible effective action techniques for gauge theories. *Phys.Rev.*, D70:105010, 2004.

[80] B. Garbrecht, F. Glowna and M. Herranen. Right-handed neutrino production at finite temperature: Radiative corrections, soft and collinear divergences. *JHEP*, 1304, 2013.

[81] T. Altherr. Resummation of perturbation series in nonequilibrium scalar field theory. *Phys. Lett. B*, 341(325), 1995.

[82] Clemens Paul Kiessig. Quasiparticles in Leptogenesis: A Hard-thermal-loop study. 2011.

List of Figures

List of Tables